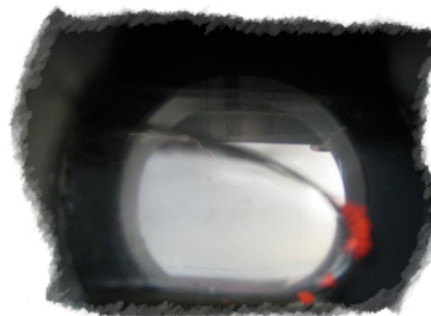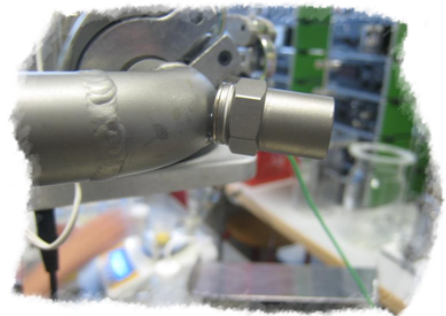# Evaluation of Sampling Facilities and Process Analytical Technologies in Applied Biotechnology:

Process Sampling, Representativeness, and Acoustic Chemometrics

Ludovic Boland

July 3, 2008

Master of Science in Engineering Thesis

Department of Chemical Engineering and Biotechnology
Esbjerg Institute of Technology – Aalborg University – Denmark

Title

Evaluation of Sampling Facilities and Process Analytical Technologies in Applied Biotechnology: Process Sampling, Representativeness, and Acoustic Chemometrics

University

Aalborg University, Esbjerg Institute of Technology

Niels Bohrs Vej 8, 6700 Esbjerg, Denmark – http://www.aaue.dk/

Project period

From the 1st of February 2008 to the 3rd of July 2008.

Candidate

Ludovic BOLAND

_____

Academic supervisors

Professor Kim H. ESBENSEN, Ph.D. – kes@aaue.dk

Ph.D. Student Carina J. LOMBORG, M.Sc. Eng. – cjp@aaue.dk

Ph.D. Student Michael MADSEN, M.Sc. Eng. – mima@aaue.dk

Esbjerg Institute of Technology, ACABS Research Group – http://www.acabs.dk/

To my mother,
*30th of March 1948
– 19th of April 2002.*

Abstract

A comprehensive evaluation of sampling systems and sampling efficiencies of lab-scale applied biotechnology systems has been performed. A planned evaluation of ACABS' bioreactor system was completely defaulted due to Force Majeure; the international TENIRS system could however be evaluated in full.

Surprising results ensued: the TENIRS sampling devise is inaccurate and highly sensitive to operating conditions – while showing an almost constant reproducibility. This sampler is in point of fact *precisely wrong*.

The evaluation comprised three kinds of model-systems composed by polymer/water: light particles, heavy particles, and a mixture of both, concluding with a synthetic manure, all spanning realistic dry matter concentrations.

The bias increases with complexity of the multi-phase system, but decreases with respect to the circulation speed in the TENIRS measuring loop. Composite samples of synthetic manure – the most realistic model-systems evaluated – composed of 10 increments extracted at low speed (20% of the top circulation speed) can present a bias as high as 320% whereas composite samples of light pellets extracted in the same conditions reaches some 85%.

At higher speed (60% of the top circulation speed), the bias observed for the synthetic manure was 15% while being significantly negative, -70% for model-systems based on the heavy model system particles. These findings have severe implications regarding the necessity of redesigning the TENIRS reference sampling system completely.

Acoustic chemometrics was used to model the dry matter concentration of these lots. All models were *test set validated*. Promising results were obtained: synthetic manure displays a prediction vs. reference slope of 0.89 and a correlation coefficient, r^2 of 0.89 – demonstrating acoustic chemometrics as a powerful potential PAT modality concerning physical Y-variables. Much work on acoustic chemometrics on this type of applied biotechnological systems remains.

A review of PAT modalities is also given with special focus on applied biotechnological system.

Keywords: Process Analytical Technology, PAT, Process Analytical Chemometrics, PAC, Theory of Sampling, Process sampling, Representative sampling, ACABS' recurrent sampling loop, Acoustic chemometrics, TENIRS system.

i

Acknowledgments

This is the end of a long challenging journey. It is now time to cheer up and thank several people for their help and support even when everything collapsed.

Among them, Professor Kim H. Esbensen, the head of ACABS Research Group at Aalborg University-Esbjerg (AAUE), Ph.D students Carina J. Lomborg and Michael Madsen also associated with ACABS Research Group are warmly thanked for many valuable comments and hints they gave me during the whole thesis work.

Even when everything seems to collapse, Kim's ability to always see the glass as half full – while anyone else would have seen it as half empty – was greatly appreciate. In fact, this helped me to keep on working and trying to solve all the issues encountered during the first part of the practical work.

Associate Professor Birgit K. Storm, the head of POeM Research Group at Aalborg University-Esbjerg (AAUE), is acknowledged for her kind help when we were trying to find the plastic particles.

Thanks also go to my good friend, Johan Haitel, an exchange student from Hanze University in the Netherlands, for the enthusiasm he showed to help me with the practical work when I started the TENIRS sampling evaluation and I was running out of time and . . . energy. In fact, it would not have been possible to perform so many experiments without his kind help.

I could never have completed this long journey without the permanent help and support of everyone around me. Special thanks go to my friends, family, and in particular to my wonderful fiancée, Annelise Bette.

Foreword

The present thesis documents the work done in partial fulfilment of the requirements for obtaining the degree Master of Science in Engineering in Industrial Biotechnology and Bioenergy at Aalborg University, Esbjerg Institute of Technology, Denmark.

It is divided into five parts:

The first part starts on page and gives a literature review of the *Process Analytical Technology* approach, the *Theory of Sampling – TOS* and some sensors technologies as *Acoustic Chemometrics* and *Near Infrared Spectroscopy*.

The second part starts on page and concerns practical work done regarding the representativeness evaluation of the Applikon® standard sampling system v.s. the ACABS' recurrent sampling loop. The study was carried out on a laboratory scale reactor.

The third part starts on page and concerns the practical work done regarding the representativeness evaluation of the TENIRS sampling valve facility and the application of acoustic chemometrics in order to quantify the dry mater content of the flow.

The fourth part starts on page and concerns the overall perspectives and conclusions to the practical work including suggestion for further development of acoustic chemometrics.

The fifth part starts on page and contains additional information and documentation. References to relevant appendices have been provided in the report, where appropriate.

Throughout the thesis figures and table are numbered Figure # and Table #, respectively. Their numbering consists of two digits. The first refers to the chapter

number and the second to the consecutive number of object in that particular chapter. If no source is cited along with a figure or table, it is a personal production of the author. After the table of contents, the list of Figures and Tables have been placed, which should help finding appropriate object in the thesis. Equations are numbered with the same logic.

The reference numbers are given in brackets [#] and refer to the list of literature found on page 157 where a detailed description of the sources used can be found.

A CD is available at the end of the manuscript. It contains the laboratory results and the electronic version of this thesis.

Contents

List of Figures

List of Tables

Chapter 1

Introduction

The quest for robust, reliable, fast, and technically simple at-, on-line monitoring and control technology has radically gained attention during the past few years, aiming to gain new knowledge about the process in order to decrease production costs and increase quality of the final product, including minimizing waste of energy and environmental impacts. The objectives of this quest can be fulfilled by applying the principles of *Process Analytical Technologies*, abbreviated ***PAT***, to the process.

Process Analytical Technology initiative provides guidance and tools for real-time monitoring, quality assurance and risk management. It also acknowledges the need of representative samples to ensure reliable information to be extracted from the process. However, it never explained how such representative samples can be taken out of process stream.

Generally, all the scientific and financial attention is given to the technology used to monitor and control the process i.e. process sensors must be accurate and precise, computer softwares for automation must be fast and reliable, etc. Whereas little or no attention is given to the extraction of the samples, which is always, erroneously, considered as an easy task. Indeed, grab sampling is the most often used method in practice. Grab sampling consists of obtaining the sample by simply scooping *from the top of the lot* or similar. This is the worst method that could ever be used; too much focused on the final sample volume needed for the analysis, it *always* generates sampling error that can be up to hundredfold larger, than those produced in the analytical instruments!

Hence, it is **impossible** to obtain reliable information on the process state if the extracted sample is not representative of the process state. The ***Theory of Sampling***

($\boldsymbol{TOS}$), which defines tools and rules which lead to a truly representative sample, is therefore revealed to be the *missing link* between the process and the monitoring tools.

Acoustic chemometrics is a new technique used in many technological and industrial sectors. It is particularly useful for real-time characterization of multiphase fluid flow rate and physical composition. In this new approach, vibrations generated in a transportation process or as a results of manufacturing of a product are used to quantify physical process parameters such as particle size distribution, flow velocity, concentration of solids, density, and viscosity.

Nonetheless, in most cases, acoustic signals from complex system are useless by themselves and multivariate analysis techniques must be used to unscramble the relevant information from this apparent noise spectra. In fact, during the calibration, multivariate analysis i.e. chemometrics is used to create a model between the reference value and the corresponding acoustic spectra. Once calibrated the model can be used to predict future value of the parameter modeled. Careful attention should be given to the validation technique used to validate the model. Indeed only proper validation can ensure reliable future predictions. Test set validation constitutes the **best** approach to validate a model. The test set is not, in any way, associated with the calibration data set. Furthermore, ensuring that the samples of both sets are true representatives of the future population span increases the validity of validating a model.

1.1   Project objectives

At the beginning, the primary objective of the project was to contribute to the development of a laboratory scale sampling facility, followed by an evaluation of the representativeness of the sampling extracted. Due to unexpected events and difficulties[1], the objective of the thesis changed to evaluating the representativeness of the sampling system mounted on the TENIRS system owned by the university and which has been used many times in scientific researches without quantification of its bias and reproducibility.

The second objective is to demonstrate the ability of passive acoustic chemometrics to monitor dry matter content of biochemical processes.

The most important parameter when evaluating the quality of a sampling device is its representativeness r_e^2 which is a synthesis of accuracy m_e^2 and reproducibility σ_e^2 of the sampler. The accuracy is defined as the absence of bias or systematic error. It is a property of the mean of the sampling errors and should less than a small predefined

---

[1]They are summarized in section 1.2 and explained in detail in section 10.3.

acceptable value. Whereas the reproducibility is defined as a low dispersion of the sample values about their mean. It is a property of the variance of the sampling errors and should be less than a low predefined acceptable value. The sum of the accuracy and the reproducibility gives the representativeness of the sampling process.
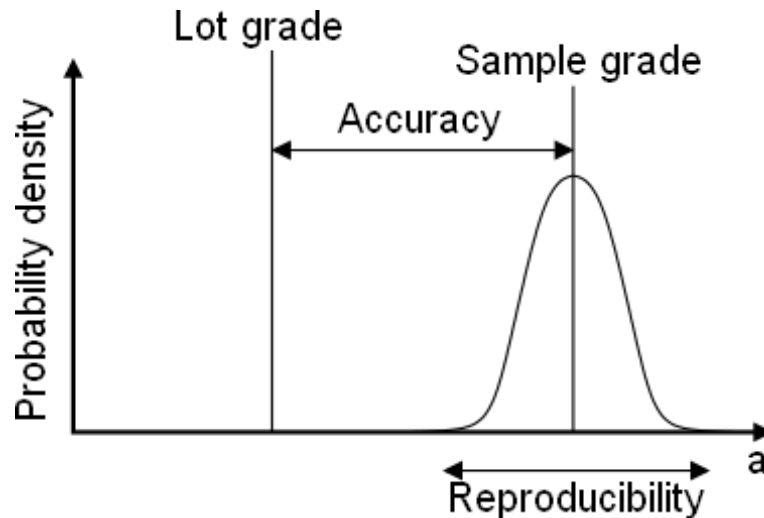
Figure 1.1: Accuracy v.s. Reproducibility.

The most critical parameter when using passive acoustic chemometrics to quantify physical properties of the flow is to find the optimal position of the acoustic sensor. In the particular case of determining the dry matter content, the sensor should be deployed where the most important vibrations are produced by the particles moving in the flow. From a mechanical point of view, the best location would be where the particles are stopped or where they loose a most of their velocity in a very short period. Thus, deploying the sensor in a bend should ensure to register the highest frequency possible that the particles can produce.

1.2 Story of a cursed thesis

This section tries to explain why I felt that I was doing my practical work together with Marvin, the Paranoid Android, the depressed robot of *The Hitchhiker's Guide to the Galaxy.*

The story began at the end of January, when I went to Prof. Esbensen to have a final project in the area of sampling and chemometrics. He told me that he had a project on a shelf which can be my master thesis. We discussed it together and he asked me to take a decision within two hours. At that time I did not hear the *Mission*[2]*: Impossible* theme being played in my mind, and I accepted this thesis full of challenges i.e. traps.

---

[2]In this particular case, it can be renamed in *Thesis: Impossible.*

The first challenge was to find plastic particles that no one could find before. Prof. Esbensen was confident, *the particles exist and we will find them somewhere.* Nevertheless, it was not possible to find them, they were too small, and none of the 35 chemical companies contacted within the first month and a half of the thesis could help us.

The second challenge was to redesign the recurrent sampling loop of the laboratory scale reactor. It was decided to used solenoid valves to extract the samples, so we ordered the valves needed according to the catalogue of the suppliers. However, when we received the order after 6 weeks, we found out that the valve did not correspond to what is written in the catalogue. We had to order new valves.

Finally, at the end of April we had the valve, but the pellets were still missing. Therefore, we took the bag of pellets used in the first screening experiments – which revealed that they were too big – and we all sat at the same table, to cut them using razor blade. A few hours later, we gave up, and decided to try the find the ultimate clogging concentration to perform the experiments with them.

The clogging concentration found, the experiments were started, and ... after a few minutes of circulation, a clog was formed at the in-let of the sampling valve, and when I closed the flow of the loop to take out a sample, the pressure blew up the pipes, flooding the lab. It was on May 17th, a few seconds after the incident I felt like Marvin, I was almost as depressed as he is. Even the lowest concentration of the experimental design clog the entire system. The conclusion was popping in my mind ... it is not possible to perform the experiments with this kind of pellets, and we do not have time to cut them either.

In parallel, a design of an up-scaled reactor allowing to use plastic pellets of normal size was started. The reactor will only be used for sampling study, therefore we decided to order a PMMA pipe as body at the beginning of May. The company lost our order, and we had to sent it again, in the middle of May. They could not produce the pipe within the dimensions asked, so we told them to ship a pipe with a standard diameter ... it was what they did but they did not cut it so we received during the first week of June a pipe of $2m$ height instead of $0.60m$.

Prof. Esbensen was in the US, and I wrote him a email to find a emergency solution to work with. Fortunately, he came back with the idea to transfer the objectives of the thesis to the TENIRS system the university owns. That was fine by me and I started the experiments at the end of May ... two weeks of intensive experiments[3] to produce all the results needed. Of course, I was helped by Marvin, since after the first experiments, the sampling device broke down, and needed to be fixed.

Owing to all those reasons this thesis has been delayed and the practical work could not be started before the first of June.

Figure 1.2 perfectly summarized what I had in mind during the practical work ... *Don't*

---

[3]7 days a week, 15 hours a day ...

panic ... it could be worse ... I could be much more depressed than Marvin.

Figure 1.2: Don't Panic – Summary of the practical work. [13]

Part I

Literature review

Process Analytical Strategies

This chapter introduces and compare the Centralized laboratory, the Process Analytical Chemistry/Chemometrics (PAC), and the Process Analytical Technology (PAT) approaches for process monitoring and quality control.

Effective monitoring and control of production processes are necessary in order to enhance process performance. This includes increasing the product quality, reducing the energy consumption, enhancing the productivity, etc. In other words, this leads to ensure a higher economic viability of the process.

This can be done by applying process analytical strategies, to the process. [38]

The traditional way of monitoring and assessing the quality of a production process is based on the *centralized laboratory* approach. Samples are taken out from a process stream and transported to a centralized analytical laboratory where the sub-sampling, sample preparations, and chemical analysis are carried out by highly qualified technical staff using state-of-art equipment. Hence, the time elapsed from the primary sampling takes place at the process stream and until the analytical result had been produced and approved could vary from hours to several days depending on the laboratory infrastructure and routine. [41, 42, 44]

Unless if the process was designed to accommodate this time delay, this centralized strategy is almost useless in terms of process control. For instance, a fast changing process would require an immediate detection and thus, a short combined analysis time, if the analytical result was to be used as an efficient process regulating tool.

Therefore, in most cases, the centralized laboratory approach can only be used as
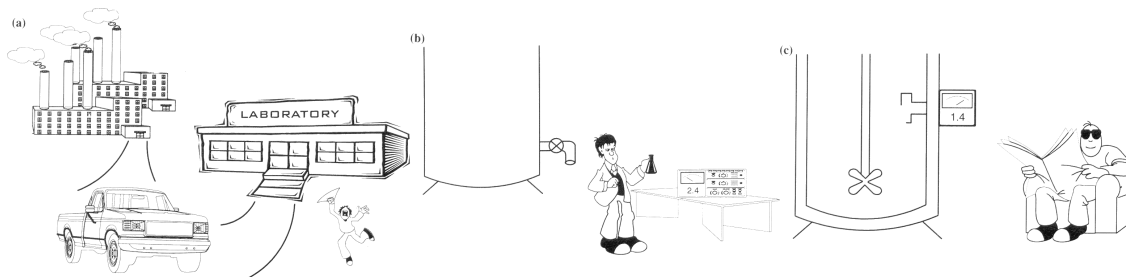
Figure 2.1: (a) Off-line, (b) At-line, (c) On-line analysis. Adapted from [42]

a quality control assessment in order to document that the final product is within its specifications.

As an alternative to this traditional approach, the process analytical strategy or **Process Analytical Chemistry** (**PAC**). Introduced in the beginning of the last century (1911), it has been applied in the petroleum and petrochemical industries since the early 1950's. Nowadays, it is going through a reincarnation and becoming a fast developing field in all areas of chemical production (e.g. fine chemicals, commodity chemicals, pharmaceutical, biotechnology, etc). [42]
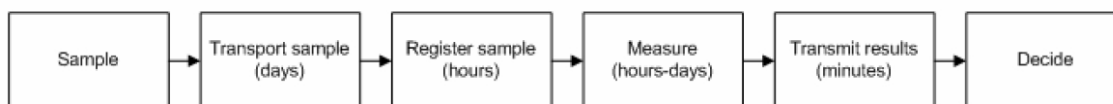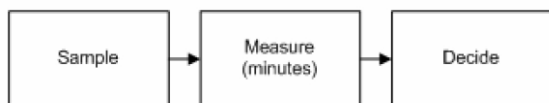
Figure 2.2: Comparison of analytical strategies for process monitoring [42, 44]

The most obvious differences between the centralized laboratory strategy and the process analytical strategy are location and speed. Indeed, process analyzers are placed right next to the process (at-line[1]) or in the process (on-line[2]) and are often abe to produce a result within minutes (See Figures 2.1 and 2.2). [44]

Analysis speed is critical in order to monitor a process in real time. Actually, a

---

[1]This involves manual sampling but in this case the measurement is carried out on a dedicated analyzer by the process operative. Usually accompanied by significant method development work to simplify the sample preparation and to modify the measurement technique to permit the use of robust, reliable instrumentation. [42]

[2]This includes all examples of fully automated analyzer system. [42]

rapid analyzer feedback allows to learn from the process and to know what is really going on. It also brings the possibility to react to unusual process variations and will therefore, increase the chances to keep the process under control.

The American **F**ood and **D**rugs **A**dministration (**FDA**) describes process understanding in their new **P**rocess **A**nalytical **T**echnology (**PAT**) initiative, which essentially is a re-compilation of the earlier PAC-process analytical strategy. [44]

According to FDA, process is generally considered well understood when: [5]

 i. all critical sources of variability are identified and explained;

 ii. variability is managed by the process;

iii. product quality attributes can be accurately and reliably predicted over the design space established for materials used, process parameters, manufacturing, environmental, and other conditions.

Nevertheless, the centralized laboratory strategy is still widely used owing to the fact that the process analytical strategy is far from trivial, and must not be considered as an easy task. In fact, the strategy lies on several key technologies which must be mastered prior to any PAT deployment.

Figure 2.3 depicts the pyramid of the fundamental technologies behind PAC [41, 44].
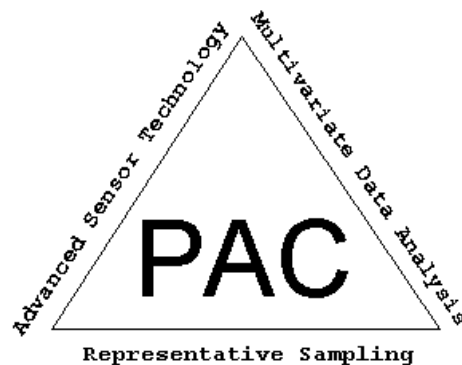
Figure 2.3: Fundamental disciplines behind Process Analytical Chemistry [41]

 i. *Representative sampling* is the basis of the pyramid which means that the sample analyzed should faithfully represent the process. Most of the time, sampling is not considered important; however, only correct sampling will lead to representative

samples. The ***Theory of Sampling*** (***TOS***) explains the general principles behind representative sampling and correct sampling. Chapter 3 on page 13 discusses the principles of TOS.

ii. *Advanced sensor technology* covers a considerable suite of different analytical techniques. In fact, the general trend for analyzers is that they are becoming smaller and the research is focused on improving the response time in order to carry on real-time measurements for both biological and chemical phenomena. Within the field of sensor technology, this thesis is focussed on Acoustic Chemometrics where the sensor used is an 1-axis piezoelectric accelerometer. Chapter 4 on page 37 introduces the theory and the principles behind the technology.

iii. *Multivariate data analysis* extracts the relevant information from the process analyzer. The results can be used for process monitoring purposes by plant operators. Within the field of data analysis, this thesis is focussed on Chemometrics techniques. Chapter 5 on page 57 describes its principles.

A few years ago, PAC converged to what is known as Process Analytical Technology (PAT). The American ***Food and Drugs Administration*** (***FDA***) has been one of the key actors in defining the concept of PAT [41]. The FDA issued its so-called PAT-Initiative which defines PAT as [57] :

> *A system for designing, analyzing, and controlling manufacturing through timely measurements (i.e. during processing) of critical quality and performance attributes of raw and in-process materials and processes with the goal of ensuring final product quality.*

PAT is largely directed towards the pharmaceutical industry but there is no restriction to use PAT principles in other industries [44].

PAT and PAC may look to be the same strategy. However, PAT differs from PAC in the sense that it also provides guidance and tools for quality assurance and risk management, whereas the PAC strategy is solely technology driven. Therefore, PAC is more oriented towards real-time monitoring.[39, 42, 44]

Moreover, even though the PAT framework acknowledges the sampling aspect by mentioning the need of representative samples to ensure reliable information to be extracted from the process, but unlike PAC, it does not explain how such representative samples can be taken out of a process stream. [44]

Chapter 3

Theory of Sampling – TOS

This chapter presents Pierre Gy's Theory of Sampling and its importance to ensure reliable, accurate, and precise quantification of parameters of interest, i.e representative sampling. First, it introduces the seven sampling errors, and the theory of zero dimensional sampling, followed by one dimensional sampling, or process sampling ending with variographic analysis. Applying principles of the Theory of Sampling will lead to extraction of truly representative samples from any lot.

3.1 Introduction

We may want to sample because of many different reasons. For instance, if we do not have the time, money, or personnel to examine an entire *population* or *lot* or if measuring a property of interest may require destroying the lot. Sampling can also be used to characterize the spatial contaminant in soil, air or water in an environmental situation, or to characterize industrial process variation over time. Extracted samples can thus be used as process control, environmental monitoring, etc. [59]

The ***T**heory **o**f **S**ampling* (**TOS**) can be applied in many fields and to many materials. In fact the theory stays equally valid either for sampling of solids, liquids or gases and at all scales from the largest lot dimensions to any relevant collection of molecules! [27, 48, 59]

Pierre Gy's Theory of Sampling provides a structured approach from which it is possible to break down a sampling problem into its component parts and the basic principles (***S**ampling **U**nit **O**perations*, abbreviated **SUO**) that should be applied to

13

any sampling situations.

Table 3.1 provides a minimum of basic definitions used in the Theory of Sampling:

Terms	Definitions
Lot	The original material subject to the sampling procedure, e.g. a truckload, all the material in a reactor, or flowing through a pipeline.
Sample	The *correctly* extracted material from the lot.
Specimen	A material extracted from the lot in an *incorrect* fashion.
Increment	A partial sample unit, which combined with other increments form a *composite sample*.
Composite sample	A sample made by the reunion of several distinct increments.
Fragment	The smallest separable unit of the lot. Physically, this could be a molecule, a granule or grain.
Group of fragments	consists of spatially correlated fragments, which act as a coherent unit during sampling.
Analytical grade a_L	The lot is the mass of analyte divided by the total mass of the lot.
Analytical grade a_S	The sample is the mass of analyte divided by the total mass of the sample.

Table 3.1: Basic definitions used in TOS. [18, 26, 27, 31, 48–50, 52]

3.2   Correct sampling

The purpose of a sampling procedure is to extract material with the same properties as the lot i.e. securing a *representative sample*. The **F**undamental **S**ampling **P**rinciple, abbreviated **FSP**, sets the basic prerequisite for a correct sampling procedure which is that all elements[1] in the lot should have the same *non-zero* probability P of ending up in the final sample.

Obtaining a representative sample is far from trivial and it can not be guaranteed without professional consideration. The Theory of Sampling defines tools and rules which shall lead to a truly representative sample. Furthermore, the quality of the extracted sample should be constant over time. This is done by reducing the *bias* as much as possible, preferentially eliminating it.

---

[1]Particles, molecules, impurities, etc. at the fragment level or all increments.

Moreover, all elements that do not belong to the lot must have a zero probability of being selected [26, 27, 52, 59], or in other words, leftovers in the sampling equipment from previous increments/batches may not pollute new increments. A sample is preferably materialized through several increments from the lot, this is called composite sampling.

The relative sampling error is defined as:

$$e = \frac{a_S - a_L}{a_L} \tag{3.1}$$

A sampling process is said to be *accurate* if the average error m_e equals zero, or practically when $|m_e| \leq m_0$, where m_0 is a predetermined low acceptable value. Likewise the sampling process is said to be *reproducible* or *precise* if the variance of the sampling error is less than a small predetermined value, i.e. $\sigma_e^2 \leq \sigma_0^2$. A contrario, a sampling process is said *biased* when it is not accurate or, mathematically speaking, when $|m_e| > m_0$.

The sampling procedure is said *representative* when $r_e^2 \leq r_0^2$ in which, by definition

$$r_0^2 = m_0^2 + \sigma_0^2 \tag{3.2}$$

In other words, a sample is representative when it is taken by a selection method that is both *accurate* (property of the mean) and *reproducible* or *precise* (property of the variance) [27]. However, any specific analytic results, a_S, will always only be an estimate of the true (average) a_L.

Grab sampling is the most often used method in practice. Grab sampling consists of obtaining the sample by simply scooping from the top of the lot. This is the worst method that could ever be used. Indeed, it is too much focused on the final sample volume needed for the analysis and it *always* generates sampling error that can be up to hundredfold bigger, than those produced in the analytical laboratory.

TOS defines a set of seven **S**ampling **U**nit **O**perations, abbreviated **SUO** (Table 3.2). They represent a toolbox of operations that must be used to ensure a correct sampling.

The SUO's # 1 and 2 are applied prior designing a new sampling situation. [49]

The last SUO # 3, states that 2-D or 3-D lots should, whenever possible, transformed into 1-D situations. [49]

SUO #	Operation
1	Perform heterogeneity characterization of new materials
2	Characterize 1-D heterogeneity using variographic analysis
3	Transform 2-D and 3-D lots into 1-D cases, whenever possible
4	Apply composite sampling wherever possible
5	Reduce particle size, whenever necessary
6	Mix well before sub-sampling
7	Mass reduce using representative techniques

Table 3.2: Sampling Unit Operations (SUO). Adapted in a modified form from [49]

The SUO's # 4, 6 are the most commonly used in every sampling situations. Mixing of a smaller lot before sub-sampling is common practice before mass reduction in most analytical laboratories. Combining a number of increments in order to make a composite sampling is naturally also encountered frequently. [49]

SUO # 5 makes representative sampling of a highly heterogeneous material with particles of different size easier. [49]

SUO # 7 is one of the most critical issues at all sampling scales. [49]

During elaboration of a sampling procedure, it is important the be aware that when a given sample has reached the analytical laboratory, it is impossible to determine if it is representative of the lot it was extracted from. Therefore, representative sampling is a necessary pre-requisite in order to ensure reliable data. [50]

3.3   Lot dimensionalities

A sampling situation classifies according to the specific nature of the material i.e. lot being sampled; TOS deals with 0-, 1-, 2-, and 3-dimensional sampling lots (0-D, 1-D, 2-D, 3-D).

The four sampling dimensions are depicted in Figure 3.1, where gray boxes represent extracted increments and white boxes the remaining lot i.e. the stock.

In case of 0-D sampling, the lot (heap of material) sampled is definite in space. The 0-D lot can be manipulated – at least in theory – by using SUO#2 previously defined. Examples of a 0-D lot could be a container, a big bag or a truckload of material. [44]

For 1-D sampling, one dimension in space dominates the lot and there is a natural order between groups. A conveyor belt or a process stream, where material is flowing by continuously are examples of 1-D lots. [44]

In 2-D and 3-D sampling, respectively two or three dimensions are dominating. These sampling techniques are used especially within the field of geostatistics. [44]
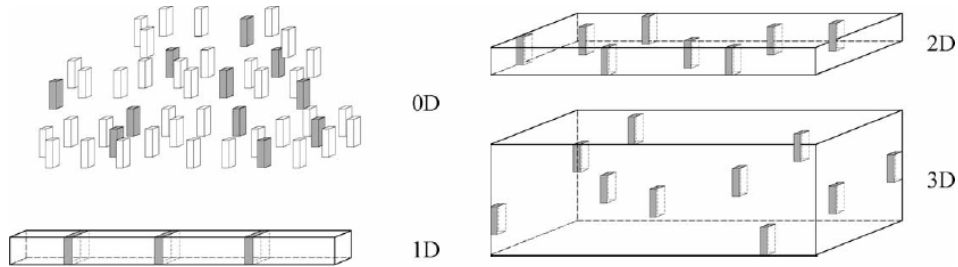
Figure 3.1: Lot dimensionalities [49]

3.4 The seven sampling errors
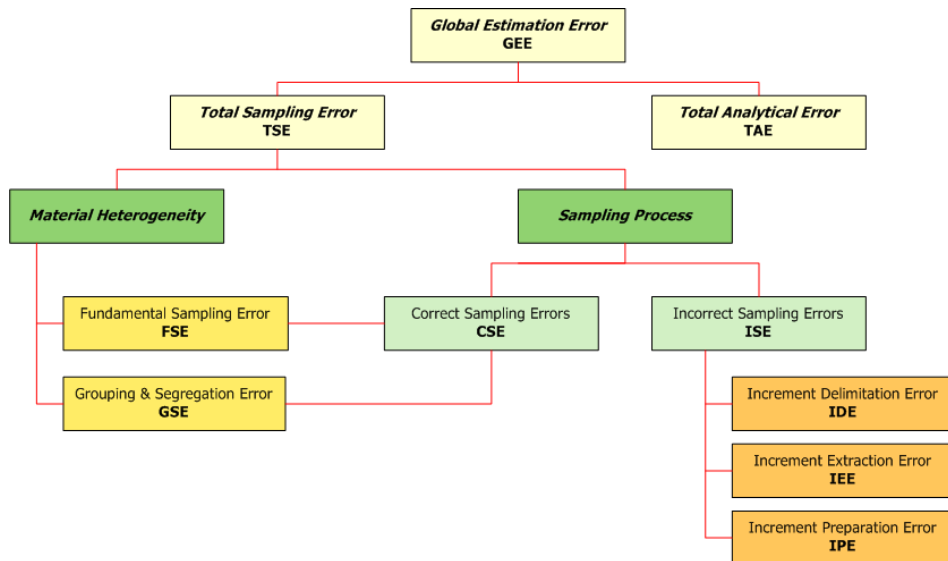
Figure 3.2: Sampling errors in 0-D and 1-D sampling and their relations.

Uncertainties are everywhere, especially when dealing with measurements. In a sampling process, it is a consequence of variabilities at all events from the moment the increment is extracted until the analytical procedure is completed. Therefore, the analytical result is just an **estimate** of the parameter of interest in lot and the *Global Error Estimate*, abbreviated *GEE* is the sum of all sampling and analytical errors

AALBORG UNIVERSITY ESBJERG

(see Figure 3.2 and Equation 3.3). It is composed of the **Total Analytical Error**, abbreviated **TAE** and the **Total Sampling Error**, abbreviated **TSE**.

$$GEE = TSE + TAE \tag{3.3}$$

TAE is due to the analytical procedure, it has often been optimized through well-documented analytical routines. Modern analytical equipments are capable of delivering results that are reproducible to a large extent. TAE is very nearly always negligible compared to TSE, except in special circumstances.

In TOS the total sampling error (TSE) splits into seven error components, some of which characterize the material sampled and some the sampling procedure itself. Five errors are, in principle, present at every sampling stage (n).

$$TSE = \sum[\text{Material Heterogeneity Errors}] + \sum[\text{Sampling Process Errors}] \tag{3.4}$$

$$GEE = TAE + \sum_{n=1}^{N} (FSE_n + GSE_n + IDE_n + IEE_n + IPE_n) \tag{3.5}$$

There are two basic sampling errors encountered in all sampling operations; the **Fundamental Sampling Error** (**FSE**) and the **Grouping and Segregation Error** (**GSE**). FSE and GSE are present in all sampling operations, but can be minimized by application of the principles of TOS during the design of the sampling procedure.

The **Time Fluctuation Error** (**TFE**) and the **Cyclic Fluctuation Error** (**CFE**) comprise the two additional sampling errors, they relate only to 1-D sampling.

3.4.1   Fundamental Sampling Error (FSE)

The fundamental sampling error is due to the fact that the composition of a lot is never homogenous and result indeed in an assembly of fragments which are not equally the same for each increments

FSE is the smallest possible sampling error made during the sampling process, it is always present and is impossible to cancel. However, it can be lowered significantly by physical manipulations of the lot, i.e. particle size reduction.

The theory of sampling describes the compositional distribution of a lot by the constitutional heterogeneity (CH_L). The **Constitutional Heterogeneity** (**CH**) describes the heterogeneity dependent on the physical and/or chemical *differences* between the individual fragments. It increases when the compositional differences between the fragments increases. It is defined as follows: [27]

$$CH_L = \sigma^2(h_i) = \frac{1}{N_F} \sum_i h_i^2 \tag{3.6}$$

Where N_F is the number of fragments in the population (lot), h_i is the heterogeneity contribution from fragment i, defined in this way:

$$h_i = \frac{a_i - a_L}{a_L} \frac{M_i}{\overline{M}_i} = N_F \frac{a_i - a_L}{a_L} \frac{M_i}{M_L} \tag{3.7}$$

Where a_i is the mass proportion of the analyte in fragment i, M_i is the weight of fragment i, $\overline{M}_i$ is the average fragment weight, M_L is the lot mass and a_L is the proportion of analyte in the lot:

$$a_L = \frac{\sum\limits_i a_i M_i}{\sum\limits_i M_i} \tag{3.8}$$

Owing to its mathematical definition, the heterogeneity contribution is dimensionless and has a mean equal to zero.

The relation between the constitutional heterogeneity and the variance of the fundamental error $\sigma^2(FSE)$ is defined as follows:

$$\sigma^2(FSE) = \frac{1-P}{N_F P} CH_L \tag{3.9}$$

where P is the constant non-zero probability of selection.

Calculation of CH_L involves knowing the total number of fragment in the lot, N_F. Obviously, this is never a known quantity in practical situation. Instead, at the cost of some approximations, the *constant factor of the constitution heterogeneity, HI_L*, can be used. Pierre Gy defines HI_L as [26, 27]:

$$HI_L = CH_L\overline{M}_i = \frac{CH_L M_L}{N_F} = \frac{1}{M_L}\sum_i \left(M_i \frac{a_i - a_L}{a_L}\right)^2 = c\beta f g d_{95}^3 \qquad (3.10)$$

Where c, f, g, and β are material characteristics, and d_{95} is a measure of the coarsest fragment size[2] [19, 26, 27, 50].

HI_L has the unit dimension of mass and can be calculated via an approximate material's parameter approach, according to Gy's formula[3] or estimated experimentally.

When we deal with particulate materials, Equation 3.10 is always able to provide an estimate of HI_L. The reliability of the estimate highly depends on the quality of the estimates for the material parameters, of which the composition factor (also called the mineralogical factor), c, and the top particle size, d_{95} are the most influential since c can vary between one and infinity (but is constant for any material in a specific state) and the particle size d_{95} is to the third exponent. [49]

The remaining factors may often be used at default values, or estimated more precisely for higher overall estimate quality. It is noteworthy that this famous formula generates an estimate to an order-of-magnitude only, which is most often all that is needed in practice. [26, 27, 50]

The relation (Gy's formula) between the heterogeneity invariant and the variance of the fundamental sampling error is defined as follows; M_S is the mass of the sample and M_L is the mass of the lot:

$$\sigma^2(FSE) \;=\; \frac{1-P}{N_F P}CH_L = \left(\frac{1}{M_S} - \frac{1}{M_L}\right)HI_L \qquad (3.11)$$

$$=\; c\beta f g d_{95}^3 \left(\frac{1}{M_S} - \frac{1}{M_L}\right) \approx \frac{C d_{95}^3}{M_S} \qquad (3.12)$$

The last expression is valid when $M_S \ll M_L$ and $C = c\beta f g$.

---

[2]d_{95} is the *top particle size*, defined as the square-mesh screen that retains 5% of the material i.e. upper 95% average grain size diameter.

[3]A complete development of Gy's Formula can be found in Appendix A on page 165.

3.4.2   Grouping and Segregation Error (GSE)

The Grouping and Segregation Error is due to the inherent tendency for particles to segregate and group in a lot, not only over the whole lot but especially also locally. Unlike for CH_L, which is a function of the material properties only, the **D**istributional **H**eterogeneity (**DH**) describes the heterogeneity dependent on the *spatial distribution* of the individual fragments and groups-of-fragments in the lot (stratification of fragments with a significant high/low concentration of the critical element). DH_L can actively be modified, for instance by choosing a smaller volume of observation, i.e. a smaller sampling tool volume, and in this way reduce it, or the lot can be **mixed**. [26, 27, 49, 52, 59].

As CH_L is defined in relation to $\sigma^2(FSE)$, the distributional heterogeneity of the lot DH_L is defined in relation to $\sigma^2(GSE)$

$$DH_L = \sigma^2(h_n) = \frac{1}{N_G} \sum_n h_n^2 = N_G \sum_n \left(\frac{a_n - a_L}{a_L} \frac{M_n}{M_L} \right)^2 \tag{3.13}$$

N_G is the number of groups of fragments in the population, h_n is the contribution to the heterogeneity as defined by Equation 3.7 but now on a different scale, the index n represents a group of neighboring fragments instead of a single fragment.

From its definition it can be noticed that DH_L can be, indeed, easily estimated in practice by extracting and analyzing a number of group *covering the lot* and calculating the resulting empirical variance. Often a relatively small number of groups are required [49], but this is of course not a universal rule.

The distributional heterogeneity of a given lot L is an expression of the way different groups are spatially distributed inside it. DH_L is a function of the composition (CH_L), the tendency for particles to group together (grouping factor γ) and the tendency for particles to segregate (segregation factor ξ). The greater the difference in composition, particle size, and weight, the greater DH_L is possible.

$$DH_L = \frac{1 + \gamma\xi}{1 + \gamma} CH_L \tag{3.14}$$

Where γ is the grouping factor ($\gamma \geq 0$), it characterizes the increment size. When the increment size is equal to a particle, the grouping factor is equal to zero and DH_L equals CH_L. ξ is the segregation factor ($0 \leq \xi \leq 1$), it characterizes the distribution of the constituents within the lot. A perfectly mixed lot results in ξ being close to zero

AALBORG UNIVERSITY ESBJERG

while a perfectly layered leads in ξ close to one (This phenomena is depicted in Figure 3.3).
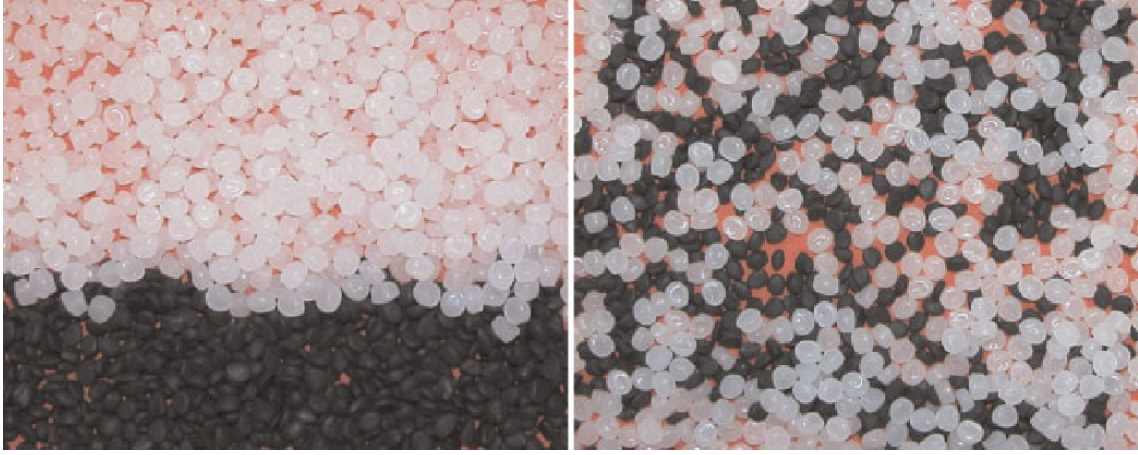
Figure 3.3: Material of same composition in two different segregation states. [49]

The grouping factor γ describes the size of increments taken from the lot in relation to the size of the lot. It is defined as follows:

$$\gamma = \frac{N_F - N_G}{N_G - 1} \Leftrightarrow \frac{1}{1 + \gamma} = \frac{N_G - 1}{N_F - 1} \tag{3.15}$$

N_F is the number of particles (fragments) in the lot and N_G is the number of groups in the lot.

For big lots $(N_F \gg N_G)$ this equation approximates well to [27, 52]

$$\gamma \approx \frac{N_F}{N_G} \tag{3.16}$$

The variance of the grouping and segregation error $\sigma^2(GSE)$ is defined by [52]

$$\begin{aligned}
\sigma^2(GSE) &= \gamma\xi\sigma^2(FSE) = \gamma\xi\frac{1-P}{N_F P}CH_L \\
&= \gamma\xi\frac{1-P}{N_F P}\frac{1+\gamma}{1+\gamma\xi}DH_L
\end{aligned} \tag{3.17}$$

Therefore, $\sigma^2(GSE)$ is proportional to DH_L, which in turn is proportional to CH_L.

3.4.3 Incorrect Sampling Errors

The remainder of errors (IDE, IPE, IEE) concerns the sampling equipment and procedures. Together they are termed the *Incorrect Sampling Errors*, (**ISE**'s), and they can all be eliminated from a sampling scheme, although this is not necessarily an easy task.

The *Increment Delimitation Error*, (**IDE**), relates to the physical extraction of the sample. The cutting lines that define the sample must be strictly parallel in both transversal and vertical dimensions, perpendicular to the process dimension.

The *Increment Extraction Error*, (**IEE**), concerns the center-of-gravity rule.

The *Increment Preparation Error*, (**IPE**), deals with incidents that occur after the sample extraction until the analytical result has been produced. For instance, contamination, evaporation, deliberate manipulation, spillage, loss of sample to containers etc. represent a few of the events that can happen during transport and storage of the sample.

Figure 3.4 depicts three different situations in a 1-D sampling case. Fragments having their center of gravity within the dot-and-dash line belong to the geometrically correctly extracted sample. The upper illustration shows the theoretical ideal case. The center illustration shows a practically correctly delimitated and extracted sample, the lower illustration shows a practically incorrectly extracted sample.

With exception of IPE all errors are regarded as random variables with a given average (might be zero) and variance (never zero).
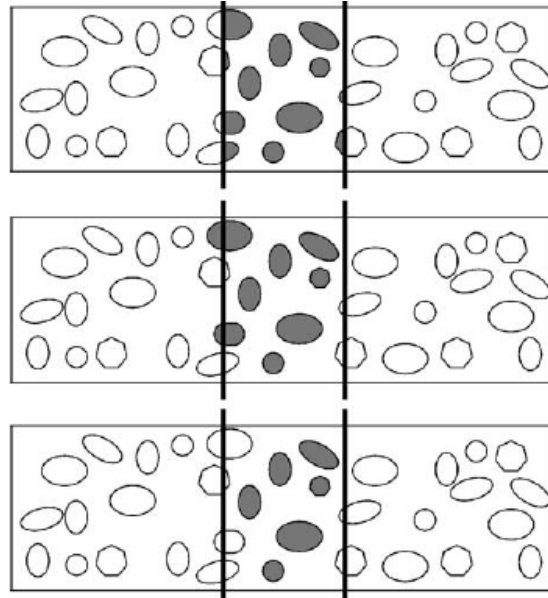
Figure 3.4: Examples of correct and incorrect delimitation and extraction in a 1-D situation [49]

3.5 Process Sampling (1-D) – Variography

There are principally three different kinds of 1-D lots: [26, 27, 49, 52, 59]

  i. A moving or stationary, stream of particulate material. Examples: conveyor belts transporting fragmental materials or powders, slurries in ducts etc.

 ii. A moving or stationary string of fluids (i.e. gasses, liquids). Examples: rivers or produced/manufactured fluids in pipelines.

iii. A moving or stationary stream made of discrete chronological units. Examples: railroad cars, truck loads, *units* (bags, drums, packages ...) from a production or a manufacturing line.

3.5.1 Heterogeneity of 1-D lots

For 1-D lot sampling, it is necessary to characterize further the heterogeneity of the material i.e. understanding the nature of the non-random heterogeneity fluctuations along elongated or moving lots. Interest is now no longer in the heterogeneity within the units of observation (as treated above) but in the heterogeneity related to the differences between them in the process stream direction. [49]

Focus is now placed on a new set of N_U discrete units, U_q ($q \in \mathbb{N} \subset [1, N_U]$), making up the 1-D lot. The units are discrete (complete cross-stream) collections/materializations of material or similar, these unites are called increments.

The heterogeneity contribution, h_q, of unit U_q, is defined as follow:

$$h_q = \frac{a_q - a_L}{a_L} \frac{M_q}{\overline{M}_q} = N_U \frac{a_q - a_L}{a_L} \frac{M_q}{M_L} \qquad (3.18)$$

Where M_q is the unit mass, $\overline{M}_q$ the average unit mass, a_q is the grade of the unit and N_U the number of units in the lot.

The heterogeneity contribution, h_q, from a unit is composed of four parts when dealing with 1-D processes: [49]

1. A random, discontinuous, short range fluctuation term, h_{1q}, describing the natural randomness of the CH. This is equal to $FSE + GSE$ with the unit

2. A non-random, continuous, long range fluctuation term, h_{2q}, describing trends in the process/lot (between units) over time/distance.

3. A non-random, continuous, cyclic term, h_{3q}, describing cyclic or periodic behavior of the process/lot.

4. A random fluctuation term, h_{4q}, taking into account all measurement errors stemming from weighing, sample processing and analysis. This is also named the TAE.

Therefore,

$$h_q = \sum_{i=1}^{4} h_{iq} \qquad (3.19)$$

Heterogeneity characterization of a 1-D lot must contain information on the *chronological order* of the units. If this information is not included, only 0-D lot relations can be used to determined heterogeneity parameters, such as DH, DH_L, and HI_L. When it is necessary to include the correlation information, the so-called variogram[4] is utilized.

---

[4]Technically known as a semi-variogram.

3.5.2   The variogram

Plotting process data is a necessary and important step in understanding process variations. As stated before, two sources of sampling error are the variation of the material as a short-range or localized phenomenon, FSE and GSE. [59]

Variation, such as cycles, long-range trends, and non-random changes, result from differences in the material over time. Changes in the process result in variation, and increments taken sufficiently far apart in time may differ greatly from each other in the properties of interest. [59]

The exact concentration of an analyte in a material stream is always unknown and will vary over time. The conceptual series of successive concentrations (or heterogeneity) of component A along the 1-D is in theory a continuous function of time, $a(t)$ (or $h(t)$), or more generally $x(t)$ standing either for $a(t)$ or $h(t)$. The function $x(t)$ is always evaluated as a discrete function over time since discrete since only increments are extracted and analyzed at several points in time, for practical reasons

To highlight process variations performing a variographic analysis is usually required. A variogram is plot of the average squared difference in a characteristic, such as the values of the various h_q, between pairs of units selected as a function of time or distance [52], or in other words, it is a graph of the variation of units (increments) taken at regular frequencies plotted against the time lag j between them [59]. The lag is a dimensionless parameter reflecting the distance between two increments.

Figure 3.5 shows an example of unit pairs in a variographic experiment; only eight units are extracted at 2 min intervals. Then seven unit pairs that are spaced by 2 min (A), six unit pairs spaced by 4 min (B), five unit pairs spaced by 6 min (C) and this continues until finally 1 unit pair spaced by 14 min (D) exist. The units shown in the figure are the same physically extracted units in A, B, C and D, only the calculation of intervals is different. [49]

3.5.2.1   Mathematical definition

To calculate the variogram a sufficient number of units, which spans the process interval of interest, has to be extracted *equidistantly*. A dimensionless and relative lag parameter j describing the distance between two extracted units is defined:

$$j = \frac{\theta}{\theta_{\min}} \tag{3.20}$$
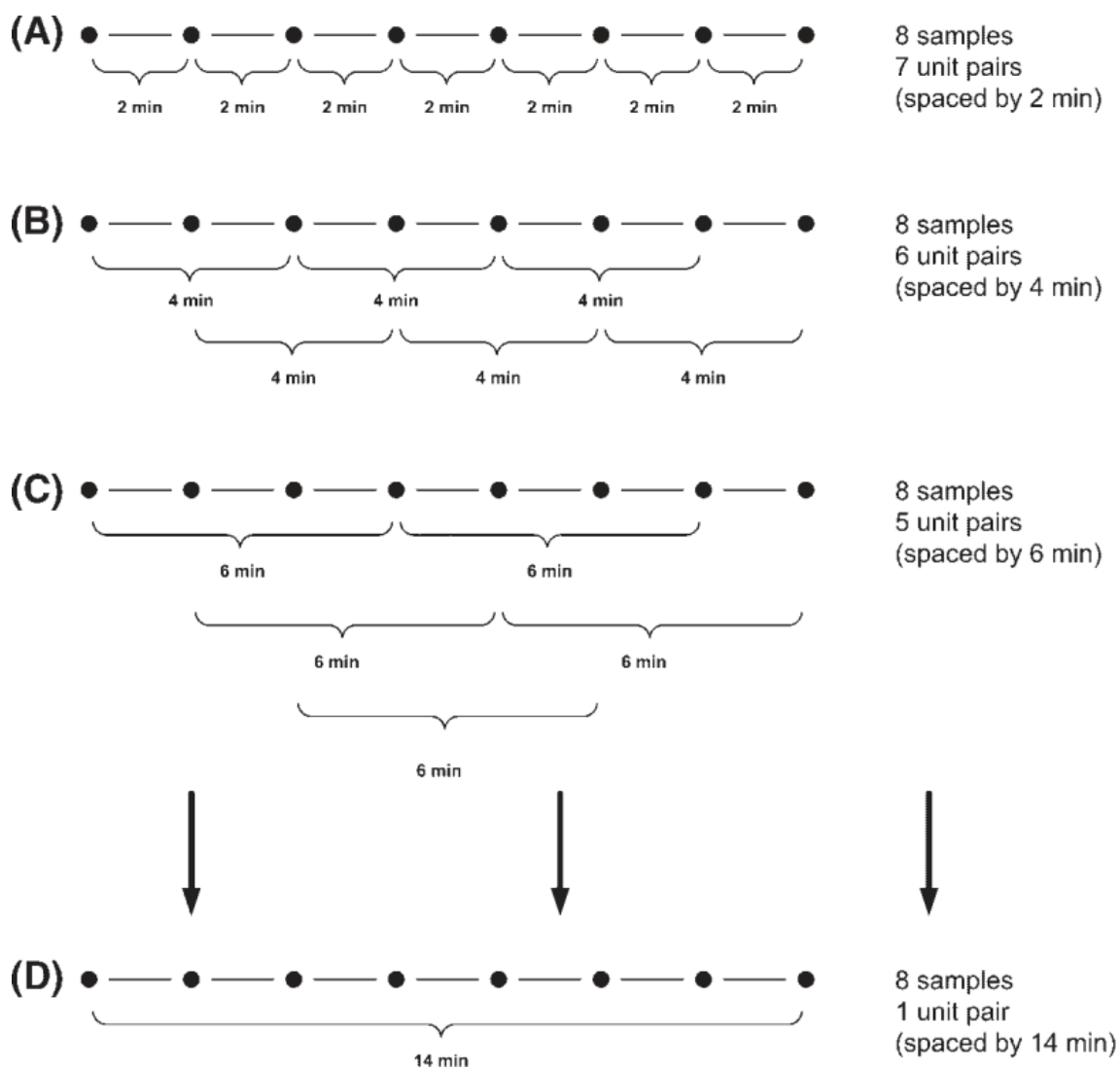
Figure 3.5: Example of unit pairs in a variographic experiment. [49]

where θ is the inter-sample distance and $\theta_{\min}$ the smallest interval sampled, also known as T_0. θ can be measured in units of minutes, hours, meters, kilometers, product number, and so on, depending on the given situation.

If N_U units are extracted and analyzed, $N_U - 1$ pairs of units with space θ, $N_U - 2$ pairs of units with space 2θ are available, etc. In practice, it is not necessary to go higher than half of measured series, $\frac{1}{2}N_U$ for the different pairs of units. [49]

The most intuitive ways to compare two values such as x_{q+j}, and x_q representing, respectively a given characteristic of unit U_{q+j} relative to that of unit U_q separated by a given lag j, is to consider their difference. [52]

For each value of $q + j < N_U$, the difference $\Delta x(q + j, q)$ is a given characteristic x_q between the final observation at time t_{q+j} and the instant t_q at which the observation started is defined as:

$$\Delta x(q + j, q) = x_{q+j} - x_q \tag{3.21}$$

These two points are separated on the time axis by an interval of $[t_{q+j} - t_q] = jT_0$ called the lag. What is important is not the value or sign for each individual $\Delta x(q+j, q)$; it is instead their quadratic mean at each lag.

This function called the variogram $v(jT_0)$, or more simply $v(j)$, is defined as the semi-mean square of the increment differences :

$$v(j) = \frac{1}{2(N_U - j)} \sum_{q=1}^{N_U - j} (x_{q+j} - x_q)^2 \tag{3.22}$$

Where N_U is the number of equidistantly distributed units in the time series $x(t)$ and j is the lag. If the descriptor x has a relative and dimensionless value, therefore the variogram is absolute.

The variograms of non-dimensionless descriptors are easier to compare if they are relative and dimensionless. Therefore, if a_n is a non-dimensionless descriptors (the grade for instance), it is possible to keep the variogram absolute and dimensionless by modifying Equation 3.22 as follow:

$$v(j) = \frac{1}{2(N_U - j)} \frac{1}{a_L^2} \sum_{q=1}^{N_U - j} (a_{q+j} - a_q)^2 \tag{3.23}$$

3.5.2.2   Interpretation

A variogram can be used to identify the presence of patterns in the process data structure. For instance it may reveal trends in the variation, asses the periodicity of cycles, and determine optimal sampling frequency.

Variograms have different appearances, depending on the information it carries, however the three more important features are: (see Figure 3.6)

1. The sill: it represents the average overall variance between the units.

2. The range: it indicates the lag (j) above which autocorrelation[5] is no longer discernable.

3. The nugget effect: it is an indication of the **M**inimum **P**ractical **E**rror.
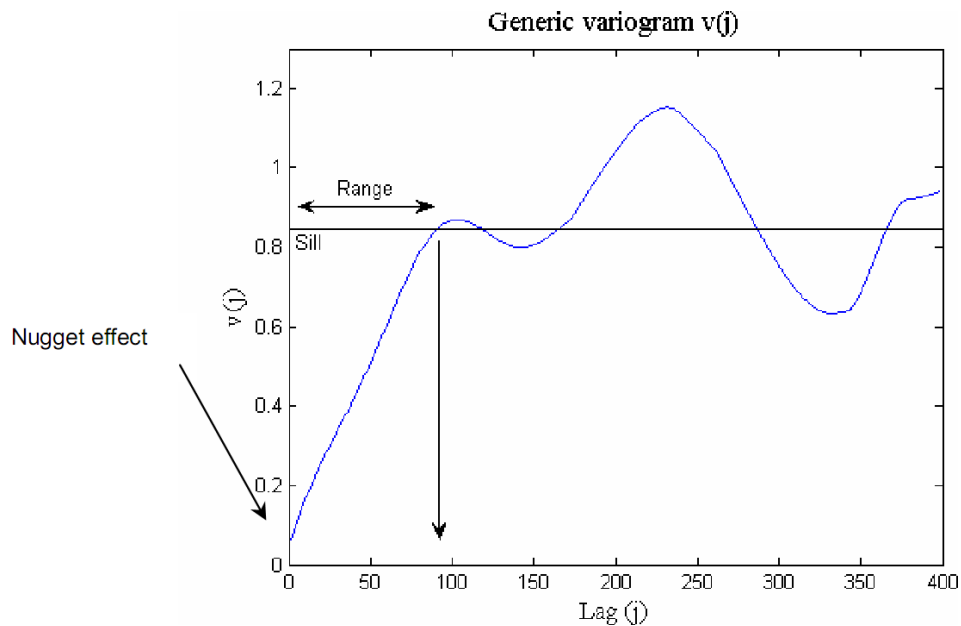
Figure 3.6: Generic variogram $v(j)$, illustrating the three key parameters: the nugget effect, the range and the sill. [44]

The sill is an important feature since it represents the maximum variation within a time series and is an indicator for spatial randomness. In other words, when the variogram converges towards the sill, points in the time series $x(t)$ are no longer correlated.

---

[5]Autocorrelation is a mathematical tool for finding repeating patterns, such as the presence of a periodic signal which has been buried under noise, or identifying the missing fundamental frequency in a signal implied by its harmonic frequencies.

The range is the part of the variogram function is below the sill. Sampling within these increment distances will be able to reveal variation in the process.

Finally, the nugget effect is estimated by extrapolating the variogram to $v(0)$. A time lag of zero signifies that the units have been extracted at the same time which collapse the 1-D sampling situation to a 0-D sampling. In 0-D sampling, the nugget effect represents the smallest error made by sampling twice in the same material at the same localization. It is also called the variance of the minimum practical error $\sigma^2(MPE)$. In fact, the nugget effect is the sum of all variances in the 0-D sampling situation including the total analytical error. [18]

In practice, often one of three primary types of variograms is encountered (see Figure 3.7):

1. The increasing variogram (top-left);

2. The flat variogram (top-right);

3. The cyclic variogram (bottom);
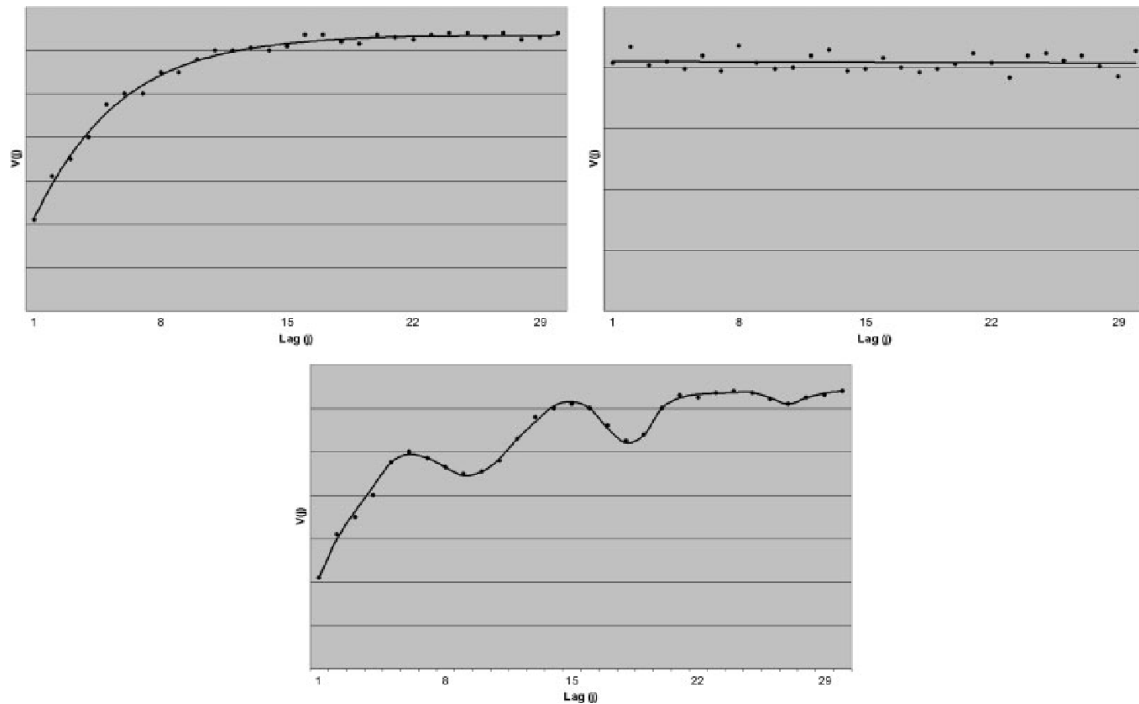
Figure 3.7: The three basic shapes of a variogram. Adapted in a modified form from [49]

3.5.2.3 Auxiliary functions

The variogram only provides a set of limited integer values of the lag j. To avoid this, and in order to estimate the **Continuous Selection Error** (**CSE**), a set of so-called auxiliary functions and error generating functions is needed. [49]

The generation of these functions can be performed through a simple point-by-point calculation based directly on the individual points of the variogram or by an algebraic modeling.

The variogram can be broken down into four component parts-corresponding to the description of the four heterogeneity components above:

$$v(j) = \sum_{i=1}^{4} v_i(j) \tag{3.24}$$

where

i. $v_1(j)$ is the discontinuous random part of $v(j)$ or the variogram of the discontinuous short range fluctuation term h_{1m}. It describes the random fluctuations of the constitutional and distributional heterogeneities within each unit of the total set of units. As these fluctuations are random, the mean would normally be approximately zero and their variance $\sigma^2(h_{1m})$ is a constant. [49]

ii. $v_2(j)$ is the non-random continuous part of $v(j)$ or the variogram of the continuous long rage fluctuation term h_{2m}. It describes trends in the process/lot. [49]

iii. $v_3(j)$ is the non-random, continuous, cyclic part of $v(j)$ or the variogram of the cyclic term h_{3m}. [49]

iv. $v_4(j)$ is the residual part of $v(j)$ not described by any of the others $v_i(j)$. Usually this term is equal to zero or is very close to zero. The variance of the fluctuations $\sigma^2(h_{4m})$ is a constant. [49]

The nugget effect, equal to the intercept of the variogram with the ordinate axis, termed $v(0)$, actually involves two of the above four parts: $v(0) = v_1(0) + v_4(0)$.

After calculation and interpretation of the variogram a set of so-called auxiliary functions, that are helpful in expressing the sampling variance, can be calculated or derived.

Four of these auxiliary functions exist:

i. The single integral $S(j)$ of the variogram $v(j)$.

ii. The average integral $\omega(j)$ of $S(j)$.

iii. The double integral $S'(j)$ of the variogram $v(j)$.

iv. The average double integral $\omega'(j)$ of $S'(j)$.

The first order average integral of the variogram is defined as follow

$$\omega(j) = \frac{1}{j} \int_0^j v(\vartheta)d\vartheta \tag{3.25}$$

Which applied to Equation 3.24 gives [52]

$$\omega(j) = \sum_{i=1}^4 \left\{ \frac{1}{j} \int_0^j v(\vartheta)d\vartheta \right\}_i = \sum_{i=1}^4 \omega_i(j) \tag{3.26}$$

The second order average integral of the variogram is defined as follow

$$\omega'(j) = \frac{2}{j^2} \int_0^j d\vartheta \int_0^\vartheta v(\zeta)d\zeta \tag{3.27}$$

Which applied to Equation 3.24 gives [52]

$$\omega'(j) = \sum_{i=1}^4 \left\{ \frac{2}{j^2} \int_0^j d\vartheta \int_0^\vartheta v(\zeta)d\zeta \right\}_i = \sum_{i=1}^4 \omega'_i(j) \tag{3.28}$$

Point-by-point calculation of auxiliary functions

Before going further into details, it is necessary to elaborate a method of variogram integration. As recommended by Gy and Pitard, a point-by-point modeling will be used instead of a mathematical modeling as indicated in Figure 3.8, where the hatched area is approximately equal to the area between the curve and the abscissa axis, which is

approximately equal to the area under an algebraically fitted, integrated mathematical model through the points. The value of $v(0)$ is estimated by backward extrapolation, since it is not experimentally known. [49]
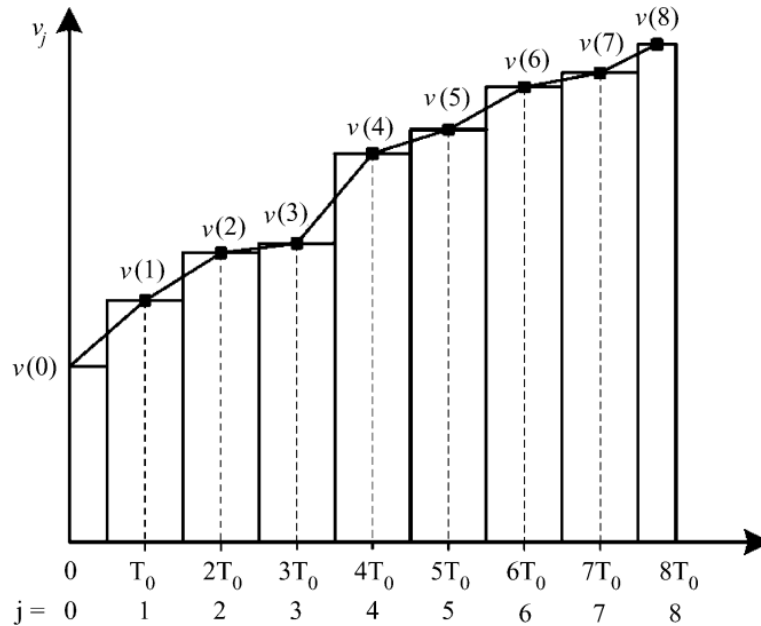
Figure 3.8: Point-by-point integration of a variogram (or any other function). [23]

The point-by-point approach is preferred owing to the fact that oftentimes mathematical models are unable to capture and satisfactory describe periodic phenomena; they also provide greater demands to the computer and programming. [49]

According to Gy and Pitard, the point-by-point calculations can be done by following this procedure

i. Estimation of $v(0)$, either by backward extrapolation or through an added experiment of very closely spaced increment extractions, called a short-term variogram.

ii. Calculation of the variogram's single integral:

$$S(j) = S(j-1) + \frac{1}{2}v(j-1) + \frac{1}{2}v(j) \quad \text{for } j \geq 1 \tag{3.29}$$

$$S(0) = 0 \quad \text{for } j = 0 \tag{3.30}$$

iii. Calculation of the average integral:

$$\omega(j) = \frac{S(j)}{j} \quad \text{for } j \geq 1 \tag{3.31}$$

$$\omega(0) = v(0) \quad \text{for } j = 0 \tag{3.32}$$

iv. Calculation of the variogram's double integral:

$$S'(j) = S'(j-1) + \frac{1}{2}S(j-1) + \frac{1}{2}S(j) \quad \text{for } j \geq 1 \tag{3.33}$$

$$S'(0) = 0 \quad \text{for } j = 0 \tag{3.34}$$

v. Calculation of the average double integral:

$$\omega'(j) = 2\frac{S'(j)}{j^2} \quad \text{for } j \geq 1 \tag{3.35}$$

$$\omega'(0) = 0 \quad \text{for } j = 0 \tag{3.36}$$

The auxiliary functions are used to estimate the so-called continuous selection error (CSE). CSE is comprised of three error parts, CSE_1 stemming from the short-range random (stochastic) variation of the process, CSE_2 stemming from the long-range trend development of the process and CSE_3 stemming from cyclic variations of the process. More on the estimation of CSE in the section on error generating functions is described below. [49]

3.5.2.4 The error generating functions and calculation of the Continuous Selection Error (CSE)

In practice, a sample, S, describing a lot, L, is typically made up by a number, N_U, of increments. The objective of the sample is to characterize the lot with regard to the average of the critical component (the analyte).

This is not the same scenario if the main purpose is, for example to map the 1-D variance or map the internal heterogeneity variance of the lot-in which case the increments are analyzed individually.

For typical process sampling purposes increments can be extracted according to basically three different sampling schemes: [49]

i. Systematic sampling, denoted sy, where increments are extracted equidistant over the runtime of the process (lot)-perhaps with a random starting point;

ii. Stratified random sampling, denoted st, where the run-time of the process is divided into a number of equally sized intervals, and an increment is extracted at random within each of these intervals;

iii. Totally random selection, denoted ra, of the increments over the runtime of the process.

The variogram and its auxiliary functions provide a lot of information on the sampling error as a function of the distance between selected increments. This information can be used at a great advantage, and this can be seen directly from the so-called error generating functions. The sampling variance is a function of the number of increments making up the sample and the sampling scheme chosen.

The error generating functions, denoted W, are the following:

$$W(j)_{\text{sy}} = 2\omega(\tfrac{j}{2}) - \omega'(j) \quad \text{and} \quad \sigma^2(CE)_{\text{sy}} = \frac{1}{N_U} W(j)_{\text{sy}} \qquad (3.37)$$

$$W(j)_{\text{st}} = \omega'(j) \quad \text{and} \quad \sigma^2(CE)_{\text{st}} = \frac{1}{N_U} W(j)_{\text{st}} \qquad (3.38)$$

$$W(j)_{\text{ra}} = \sigma^2(h_m) = CH_L = \text{constant} \quad \text{and} \quad \sigma^2(CE)_{\text{ra}} = \frac{1}{N_U} W(j)_{\text{ra}} \qquad (3.39)$$

The value $2\omega(\tfrac{j}{2})$ is also needed to calculate $W(j)_{\text{sy}}$. If j_0 is an integer then

i. if j is even, then $j = 2j_0$ and $2\omega(\tfrac{j}{2}) = 2\omega(j_0)$;

ii. if j is odd, then $j = 2j_0 + 1$ and $2\omega(\tfrac{j}{2}) = 2\frac{S(j_0+\frac{1}{2})}{j_0+\frac{1}{2}}$

where

$$S(j_0 + \frac{1}{2}) = S(j_0) + \frac{1}{4}v(j_0) + \frac{1}{4}v(j_0 + \frac{1}{2}) \qquad (3.40)$$

The values of $v(j_0 + \frac{1}{2})$ and $S(j_0 + \frac{1}{2})$ are estimated by linear interpolation.

3.5.3   Designing a variographic experiment

For all practical situation the following procedure can be applied in order to extract the most reliable information on the process/lot. [26, 27, 49, 52, 59]

i. In accordance with TOS, extract 60-100 units (increments) at a constant interval designed to span the expected autocorrelation or cyclic behaviors of the process or lot.

ii. Prepare and analyze all these units according to the existing sample preparation and analysis protocol.

iii. Calculate the individual heterogeneity contributions, h_m, for all units.

iv. Calculate a variogram $v(j)$ of lag j up to 30 or 50 of the heterogeneity contributions (depending on the number of original units).

v. In accordance with TOS, also extract 30-50 units (increments) as closely together as possible to make an accurate estimate of the ordinate $v(0)$ or nugget effect and thus the MPE.

vi. Calculate the error generating functions.

Real life examples of variographic analysis can be found in the literature. [18, 26, 27, 49].

Chapter 4

Sensor technologies

This chapter concerns sensors technologies in a frame of real time or nearly real time analysis. Acoustic chemometrics and near infrared spectroscopy including their applications for process monitoring and quantification of process parameters are detailed. It also reviews some recent studies in which both technologies are used as process monitoring tool. Other sensors technology are quickly introduced at the end of the chapter.

4.1   Acoustic chemometrics

A*coustic* **C***hemometrics* (**AC**) is a multivariate data analysis technique, which can be used for on-line process monitoring. It is a new approach in which vibrations generated in a transportation process or as a result of manufacturing of a product, erroneously often considered as simple noise, can be used to quantify physical process parameters such as particle size distribution, flow velocity, concentration of solids, density, and viscosity [7].

Since the acoustic sensor is welded directly on the pipeline, acoustic chemometrics is said to be a **passive** approach as all of the parameters can be accessed by non-intrusive data-acquisition. Therefore, no interaction with the process stream takes place and the parameters can be monitored on-line in real-time for harsh environments such as microbiological process, corrosive chemical, etc. [2]

This approach requires multivariate calibration and representatively extracted reference samples in order for the multivariate calibration to be reliable. It is imperative to apply the most rigorous validation to all established prediction models, test set val-

idation should be hence preferred, relevant and acceptable cross validation could also be used if there is not possibilities to extract a test set.

However, acoustic patterns could be very complex and therefore difficult to interpret without adequate mathematical tools and theoretical background. Moreover, the deployment of acoustic sensors is not easy and its location has to be determined carefully since the vibrations that are being recorded must reflect actual information about the process and not just noise from the plant.

Table 4.1 presents an overview of the advantages and disadvantages of the acoustic chemometrics approach.

Advantages	Disadvantages
i. Clamp-on, non-intrusive sensors.	i. Calibration must be based on representative, problem-dependent signals and reference samples. It is a empirical approach.
ii. On-line, virtually real-time approach.	
iii. A single sensor may predict several process parameters.	ii. Generally not as ultimately accurate and precise as laboratory methods.
iv. Relatively inexpensive equipment.	
v. Acoustic sensors have many positioning options.	iii. Calibrated models are not necessarily robust with respect to drifts, upsets, interferences, transient phenomena-prediction models must be re-calibrated and updated.
vi. Applicable to all systems which generates acoustic energy.	

Table 4.1: Advantages and disadvantages of the acoustic chemometrics approach. [2, 17, 29, 41]

4.1.1 Principle

The physical explanation behind acoustic measurements is as follow: whenever a particle hits a pipe wall, it transfers a certain amount of its kinetic energy to the pipe, this kinetic energy is absorb by the pipe and released as vibrating energy. Thereby, a vibration wave is created inside the pipe wall, the magnitude of this vibration can

be measured and recorded by an acoustic sensor. A simple illustration of compression waves caused by different particle sizes and kinetic energy is given in Figure 4.1.
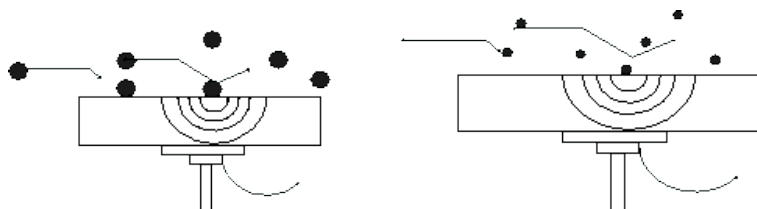
Figure 4.1: Mono-phase particles causing different kinetic impact (caused by different sizes and/or densities) leading to vibrations with different frequency characteristics in the sensor-head. [2]

In case of acoustic chemometrics, the acoustic sensor can be a well chosen piezo-electric accelerometer[1]. An accelerometer is an electronic sensor delivering an output directly proportional to the accelerations experienced. The signal is produced by a force that vibrates or excites a piezoelectric crystal which generates an electric charge proportional to the applied force. This charge is converted to a voltage or to a current which can measured and registered by a computer. [9, 15, 35, 36, 40, 55, 60]

However, prior to being recorded, the electrical signal generated by the piezoelectric crystal needs to be filtrated, adjusted and converted. When the signal is recorded it can be analyzed by multivariate data analysis techniques, also known as chemometrics.

It is common to transform the time series to a power spectrum by use of the **Fast Fourier Transform** (**FTT**) algorithm[2]. The result of this step is a frequency spectrum, which is used directly as a X-spectrum in the chemometrics calibration, seen as the last step in the data path in Figure 4.2. Multivariate calibration (PLS-regression modeling) is where the acoustic frequency spectra are calibrated versus reference values Y, representing the parameter-of-interest.

4.1.1.1 Signal adaptation

In order to get the highest possible resolution out of an acoustic signal, its amplitude should be as close as possible to the input range of the Data Acquisition board (DAQ). This can be done by amplifying the acoustic signal.

For an input range of $\pm\alpha V$, the amplitude should be as close as possible to $\pm\alpha V$ to extract the highest possible *resolution*. A resolution R of β bits leads to 2^{β} discrete

---

[1]The theory behind piezoelectric accelerometers can be found in Appendix B on page 167.

[2]Fourier Transform transforms signals from the time domain to the frequency domain. See Appendix C on page 181 for basic understanding of Fourier Transform.
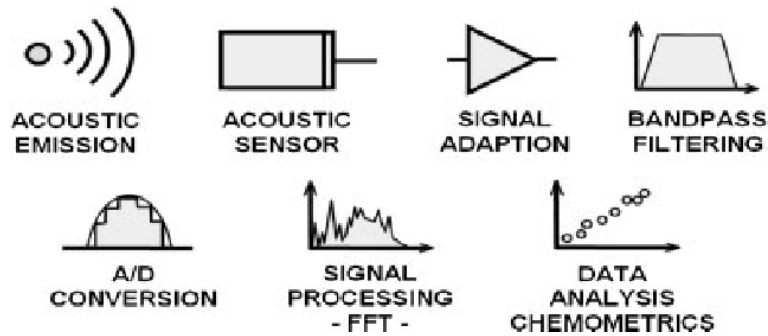
Figure 4.2: General acoustic chemometrics signal pathway, showing all principal steps towards final predicted parameter-of-interest. [17]

levels. However, if the signal amplitude is in a range of $\pm\frac{1}{2}\alpha V$, the resolution will only be $2^{(\beta-1)}$ discrete levels[3].

4.1.1.2   Band-pass filter

A pass-band filter is an analog electronic filter which passes frequencies within a certain range[4], and rejects (attenuates) frequencies outside its bandwidth [37]. Therefore, a well designed pass-band filter allows to record only the frequencies of interest, excluding most of the noise registered by the accelerometer.

In fact a band-pass filter can be decomposed into a low-pass filter[5] and a high pass-filter.

The role of the low-pass filter is to reduce/eliminate all the frequencies *higher* than the so-called cut-off frequency f_c whereas the role of the high-pass filter is to reduce/e-limate all the frequencies *lower* than its cut-off frequency. Therefore, a band-pass filter composed by a low-pass filter with a cut-off frequency of $f_c^{\text{low-pass}}$ and a high-pass filter with a cut-off frequency of $f_c^{\text{high-pass}}$, has a bandwidth of $[f_c^{\text{high}}; f_c^{\text{low-pass}}]$.

In practice the cut-off frequency of the low-pass filter is set either by the frequency of the upper sensor stability limit F_L or by the sampling rate of the DAQ board. In fact, in order to avoid aliasing error, the frequencies above half of the sampling rate (F_s) of the DAQ board must be eliminated. If it is not done, according to Nyquist-

---

[3]Since the signal amplitude is half of the maximum amplitude of the DAQ, the resolution is as follow:

$$R = \frac{1}{2}2^{\beta} = 2^{(\beta-1)}$$

[4]Generally called bandwidth.

[5]Further developments about low-pass filter can be found in Appendix D on page 187.

Shannon sampling theorem, the frequency is folded down into the frequency range $[0; \frac{1}{2}F_s]$ resulting in errors in the frequency range of interest, $\frac{1}{2}F_s$ is called the *Nyquist frequency*[6]. The cut-off frequency of the low-pass filter be chosen in accordance with the following equation:

$$f_c^{\text{low-pass}} < \min(\frac{1}{2}F_s, F_L) \tag{4.1}$$

The cut-off frequency of the high-pass filter is more difficult to determine since it is highly problem dependent. However, after many experiments for one given situation it is possible to determine wether a high-pass filter should be used or not, and then employ a full band-pass filter.

To conclude, a low-pass filter must be used in any case whereas the utility of a high-pass filter is revealed by the experience.

4.1.1.3 Analog to Digital conversion

When the signal is properly conditioned, its amplitude should be close to the optimal input voltage range and all frequencies above the Nyquist frequency. The resolution of the acoustic signal in digital form is then $\pm\alpha\frac{V}{A}$ bit, where A is the resolution of the A/D converter. The voltage resolution is given by Equation 4.2.

$$A = \frac{E_{FSR}}{2^M} = \frac{V_{RefHi} - V_{RefLo}}{2^M} \tag{4.2}$$

Where A is resolution in volts per step (volts per output code), E_{FSR} is the full scale voltage range, and M is the ADC's resolution in bits.

For an input range of $\pm\alpha V$ and a resolution of β bits, the resolution A of the A/D converter is

$$A = \frac{2\alpha}{2^\beta} = \frac{\alpha}{2^{(\beta-1)}} \tag{4.3}$$

The A/D converter is physically integrated in the DAQ board.

---

[6]The Nyquist frequency is an absolute maximum frequency limit for an ADC, and does not represent the highest practical frequency measurable. To be safe, it should not be expected that an ADC can successfully resolve any frequency greater than one-fifth to one-tenth of its sample frequency.

4.1.1.4   Signal conditioning

Now in a suitable digital form, the acoustic signal can be stored in a computer. In order to calculate the *power spectrum* of the signal, it is necessary to select where to start the calculation. In other words, determine the lowest practical frequency[7] under which the signal mainly contains noise.

The signal has now to be transformed from the time domain into the frequency domain by application of the Fourier transform theorem. However, since the signal is on a digital form, **D**iscrete **F**ourier **T**ransform (**DFT**) algorithm can be used advantageously. The DFT algorithm can be speeded up considerably by using the powerful **F**ast **F**ourier **T**ransform (**FTT**) algorithm. In fact, if there is n samples in the time domain, the DFT algorithm uses n^2 computer operation to calculate the spectrum whereas the FFT algorithm uses only $n \log_2 n$ operations. [29, 53]

4.1.2   Practical applications of Acoustic chemometrics

A series of articles published during the last decade by a Norwegian research group[8], introduces many new applications where passive acoustic chemometrics can be used. Their investigations have shown that acoustic chemometrics can be used, for instance, to quantify the concentration of oil in water due to changes in the surface tension. [14, 16, 28, 30]

The following paragraphs present some studies from the past decade involving acoustic chemometrics as passive prediction tool for in-line or on-line measurements.

i. An English study from 1999 [35] investigated the feasibility of extracting information from power spectra recorded with an acoustic sensor mounted onto a pipeline that was transporting fine-grained silica particles materialized in dense slurries. Relatively good regression models were established for parameters such as solid concentration (model $r^2 = 0.987$), mass flow rate (model $r^2 = 0.973$), and volumetric flow rate (model $r^2 = 0.989$). [35]

ii. A Norwegian study from 2000 [28] presents a new prototype acoustic chemometrics approach for in-line prediction of powder particle size distributions. The standard approach demand to carry out the calibration on representative *non-segregated* reference powder samples.

---

[7]This lowest practical frequency can be used as cut-off frequency for a high-pass filter.

[8]Applied Chemometrics Research Group ACRG, Telemark Institute of Technology Tel-Tek Institute of Process Technology, Porsgrunn, Norway

Nevertheless, in practice, powder flow with no segregation represent a highly difficult challenge to fulfill with the precision needed for calibration, there will always be a significant uncertainty in the reference values relative to what is measured. The problem encountered here is the flow segregation, which will be revealed to be also the solution by the study in question.

In fact, they have designed a completely new approach in which the flowing powder mass is forced to segregate as much as possible by various mechanical means. Their prototype measures the acoustic signals from an integrated series of segregated, part-sample characteristics.

The three way X-data matrix generated demands a three-way calibration to reveal the latent information on the segregated powder sample (see Figure 4.3). The study concludes that maximum segregation three-way decomposition (MS3WD) approach is a promising way to handle samples where the size ratio between the coarse and fine particles, D/d, was earlier significantly large.

But the most important discovery in this study is that phenomenons such as flow segregation and contrast ratio are no longer seen as problems but as solution to the problem. [28]
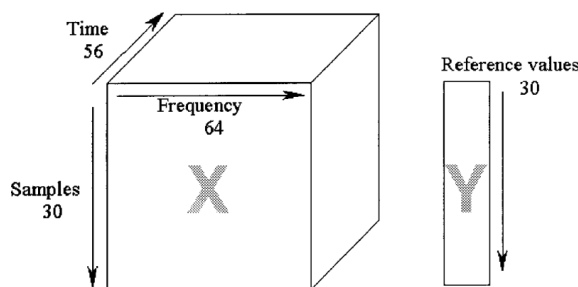
Figure 4.3: Data array configuration of the three-way PLS calibration experiments. [28]

iii. A Norwegian, Dutch, and Danish study from 2006 [30] investigates the potential of applying acoustic chemometrics as an on-line monitoring and control tool to a pilot plant producing urea fertilizer granules.

The granulation process was monitored both with traditional sensors and passive acoustic sensors.

The authors concluded that acoustic monitoring was able to provide very early warnings of upcoming process disturbances which could lead to process failure. Figure 4.4 depicts an example of such an early warning. [30]

iv. A Danish and Norwegian study from 2007 [17] investigated the feasibility of developing a robust acoustic chemometrics facility on bed-load mass flux quantification for deployment in rivers and hydroelectric power plant inlet canal system.
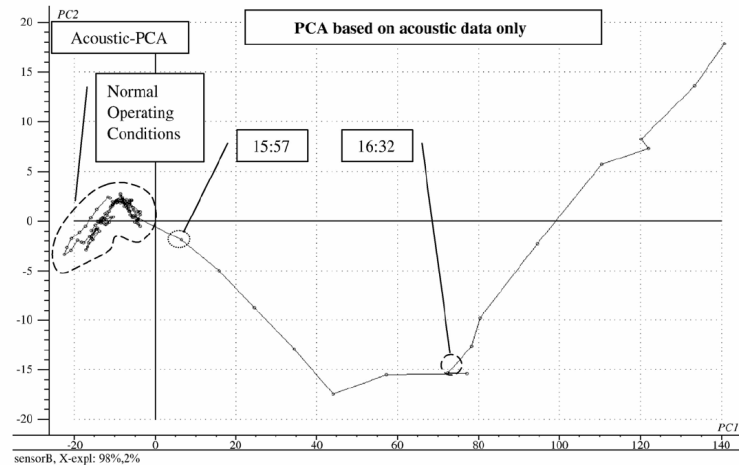
Figure 4.4: Score plot giving early warnings of upcoming process failure (PCA Analysis). [30]

The authors used a test rig equipped with an acoustic sensor attached to a steel plate flush at the flume bottom (see Figure 4.5), in order to reproduce natural sedimentary bed-load transportation characteristics.

Sensor signals were pre-treated by Fast Fourier Transform and subjected to PLS1 regression, enabling prediction of sediment bed-load transport interacting with carrying sedimentary characteristics.

The investigation was based on a comprehensive experimental design of two major factors, the mass flux and the grain-size distribution. It was was concluded that reliable, test set validated PLS-prediction models can be obtained for bed-load mass fluxes with effective compensation for widely varying sediment size. [17]
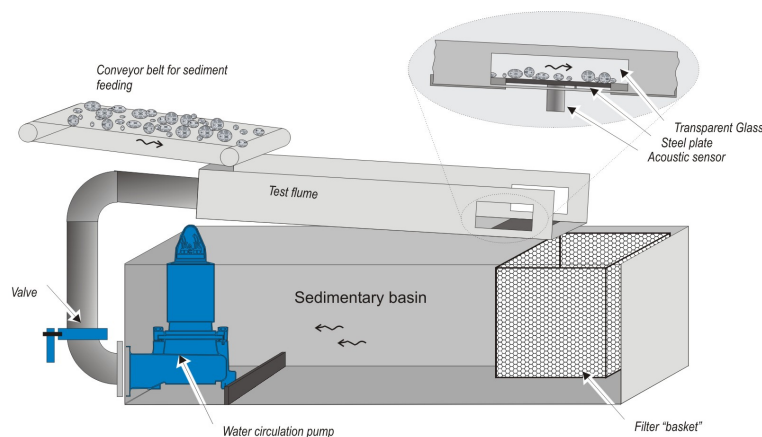
Figure 4.5: Schematic illustration of the test flume rig used in the study. [17]

Acoustic chemometrics is revealed to be a powerful on-line monitoring and control tool [30]. Applications of acoustic measurements to biotechnological process can serve several purposes such as monitoring the concentration of total solids, water, oil, and particle size distribution can be used to optimize the process strategy.

4.2 Near Infrared Spectroscopy

Near Infrared Spectroscopy (***NIRS***) is classified as molecular spectroscopy, and can be described as the study of the interaction of electromagnetic waves and matter [6, 54].

NIRS is said to be a non-invasive approach as the parameters of interest can be accessed by non-destructive data-acquisition. Therefore, no interaction with the process stream takes place and the parameters can be monitored on-line in real-time for harsh environments such as microbiological process, corrosive chemical, etc.

This approach requires multivariate calibration and representatively extracted reference samples in order to build a reliable model. It is imperative to apply the most rigorous validation to all established prediction models, test set validation should be hence preferred, relevant and acceptable cross validation could also be used if there is not possibilities to extract a test set.

Table 4.2 presents an overview of the advantages and disadvantages of the Near Infrared Spectroscopy approach.

4.2.1 Principle

The near infrared region of the electromagnetic spectrum spans from around 700 and $2500nm$ (Figure 4.6), lying between the visible and MIR regions. Most practical applications are based on the region between 1100 and $2500nm$. [6, 42, 54, 61]

In order to perform NIRS measurement, infrared light is passed through (transmission) or reflected (reflection) from a sample, the amount of energy absorbed is recorded as a function of wavelength/frequency. This function is known as the infrared spectrum.

In fact near infrared absorptions are overtones and combinations of the fundamental vibrations of molecule seen in the mid IR. However, in order for a molecule to be *IR-active*, two important conditions must be met. The frequency of the radiation must be identical to one of the transitions between energy levels of a molecule and produce

Advantages	Disadvantages
i. little or no sample preparation.	i. Calibration must be based on representative, problem-dependent spectra and reference samples.
ii. rapid, non-invasive, inexpensive.	
iii. multi-parametric method.	ii. Generally not as ultimately accurate and precise as laboratory methods.
iv. can be used in laboratory or on industrial fields.	
v. On-line, virtually real-time approach.	iii. Calibrated models are not necessarily robust with respect to drifts, upsets, interferences, transient phenomena-prediction models must be re-calibrated and updated.
vi. A single sensor may predict several process parameters.	

Table 4.2: Advantages and disadvantages of the Near Infrared Spectroscopy approach. [6, 41, 61]

a change in dipole moment of the molecule [44]. Owing to these conditions, almost exclusively covalent bonds are influenced by infrared light. Therefore, IR-techniques are widely used to analyze organic matter. [6, 61]

4.2.2 Instrumentation

There is two distinct types of NIR spectrometers: dispersive and Fourier Transform (FT-NIR).

Originally, NIR instruments were of the dispersive type, using a prism or grating monochromator to separate visible light into its frequencies. Grating based spectrometer are generally preferred over prism based since they offer better separation of frequencies of IR radiation and hence a better resolution. [6, 42, 54, 61]

A typical dispersive NIR spectrometers uses a tungsten-halogen filament lamp as radiation source. As shown in Figure 4.7, the monochromator is an oscillating concave holographic grating consisting of a reflecting surface, which converts white light into discrete wavelengths across the visible/NIR spectrum as it oscillates. [54]
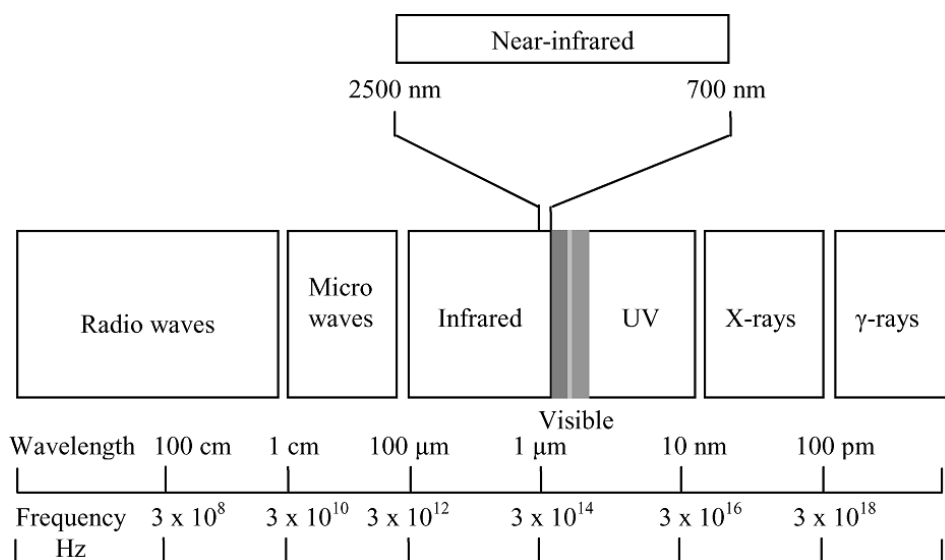
Figure 4.6: The Electromagnetic Spectrum showing near infrared region. [54]
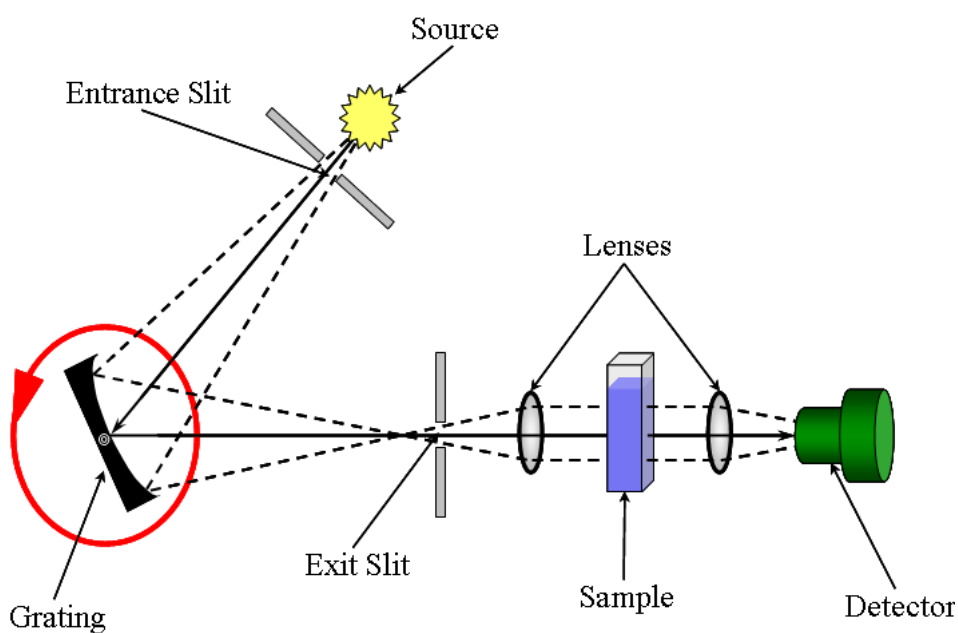
Figure 4.7: Schematic of NIR dispersive spectrometer. [56]

Due to its design, small movements in the optical components caused by vibrations or changes in the surrounding temperature can seriously affect the measurement of absorbance at each wavelength and potentially cause problems when developing multivariate calibration models. [6, 42, 54, 61]

Generally, FT-NIR instruments are build on the Michelson interferometer. The infrared light beam is divided and reflected off two mirrors, one fix and one mobile, prior being recombined (Figure 4.8). A modification in the light intensity at the detector occurs as the various light wavelengths interference with each other. The interferogram[9] is recorded and converted into the frequency domain by mean of Fourier Transform.
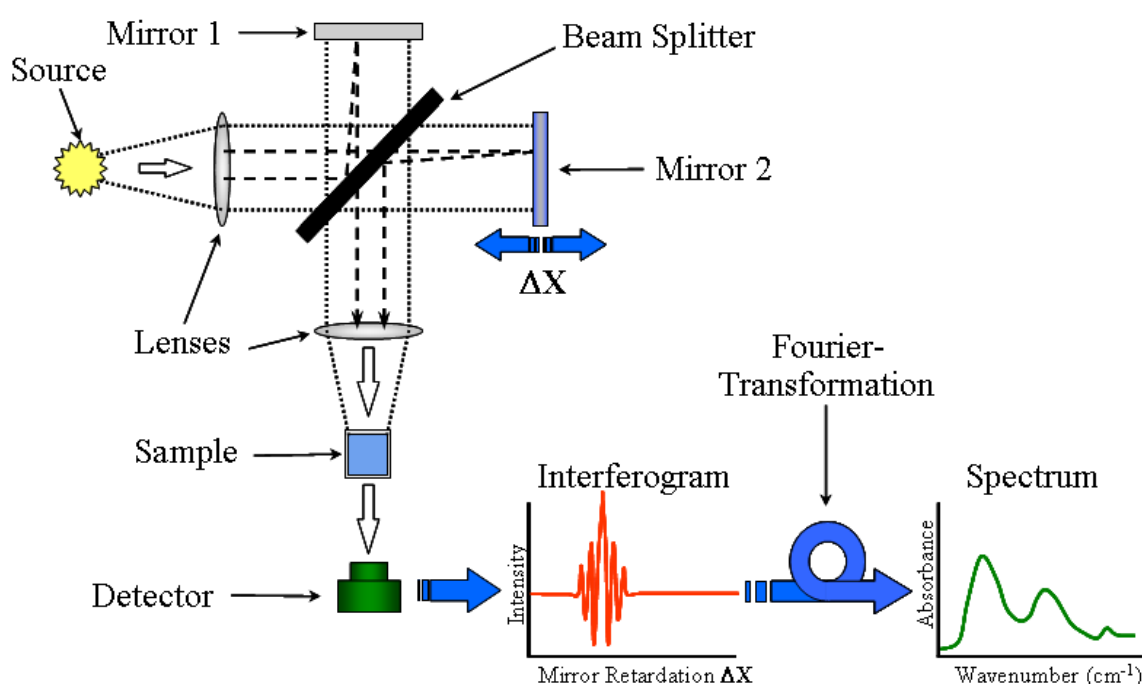
Figure 4.8: Schematic of NIR Fourier Transform spectrometer. [56]

FT-NIR based instruments have some distinct advantages over standard dispersive types: [54]

i. All frequencies are measured simultaneously which reduces the time required to generate a spectrum. Furthermore, the instrument is mechanically simpler than dispersive types there is less chance of changes occurring in spectra due to mechanical alignment during scanning process.

ii. The wavenumber accuracy is unaffected by changes in temperature or vibration since the instrument is wavelength calibrated during the scanning procedure.

---

[9]Plot of the light intensity vs. time.

iii. All light passed through the sample is measured at the same time.

4.2.3 Spectral acquisition

Two modes of spectral acquisition are possible in NIRS, transmission and reflection. In processes with a low cell density, it most common to use transmission spectroscopy, whereas in high cell density processes or when the analyte has a complex structure, resulting in an high risk of light dispersion by the sample, reflectance spectroscopy is often used.

However, if the particle size is sufficiently small, the instrument will not transmit enough energy through the sample for the detector to record a signal. To compensate, the ideal instrument would have both transmittance and reflectance capabilities. [10, 61]

4.2.3.1 Transmission

In transmittance measurements the entire pathlength ℓ of a sample is integrated into the spectral measurement (Figure 4.9), thereby reducing errors due to heterogeneity of samples.
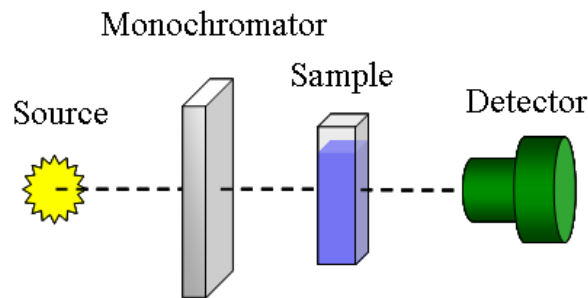
Figure 4.9: Near-infrared transmittance [56]

The reflection intensity is function of three factors. Transmittance T is defined as

$$T = \frac{I}{I_0} \tag{4.4}$$

Where I is the intensity of sample beam and I_0 is the intensity of reference beam.

When absorbance A is defined as

$$A = \log\left(\frac{1}{T}\right) \tag{4.5}$$

It follows from 4.4 and 4.5 that

$$A = \log\left(\frac{I_0}{I}\right) \tag{4.6}$$

A basis for quantification in absorption spectroscopy is the Beer-Lambert's equation, which relates concentration directly to the absorption:

$$A = \alpha_\lambda \mathcal{C} \ell \tag{4.7}$$

Where α_λ is the intrinsic constant of the material in question, or absorptivity coefficient, $\mathcal{C}$ is the concentration of the sample and ℓ is the thickness of the sample.

The absorptivity coefficient α_λ is an expression of the sensitivity of an absorption measurement at a particular wavelength. The thickness of the sample ℓ should be held as constant as possible. The concentration $\mathcal{C}$ is the number to be determined from this measurement.

4.2.3.2 Reflection

In reflectance measurements the light beam does not go through the sample but is reflected on it (Figure 4.10).

The Reflectance R is defined as

$$R = \frac{I}{I_0} \tag{4.8}$$

Where I is the intensity of sample beam and I_0 is the intensity of reference beam.
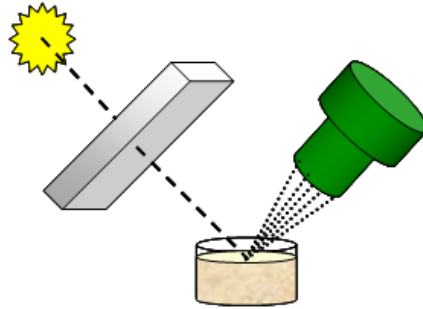
Figure 4.10: Near-infrared reflectance [56]

Several equations are used in reflectance spectrometry to relate the measured reflectance to absorbance so that quantification can be achieved, all resting on the assumptions underlying Beer's law. It is found that the sample transformation of

$$A = \log\left(\frac{1}{R}\right) \tag{4.9}$$

is a reasonable approximation. Nevertheless, in reflectance spectroscopy, the Beer-Lambert model ceases to be valid because of the changes in effective pathlength caused by light scattering. According to [56], equation 4.10 is also a good approximation.

$$A = \frac{\alpha_\lambda \mathcal{C}}{s} \tag{4.10}$$

Where α_λ is the intrinsic constant of the material in question, or absorptivity coefficient, $\mathcal{C}$ is the concentration of the sample and s is the sample scattering coefficient.

Kubelka-Munk (KM) transformation can also be used to relate the reflectance R to the absorption K and the scattering coefficient S: [10]

$$\frac{K}{S} = \frac{(1-R)^2}{2R} = f(R) \tag{4.11}$$

It may be stated that R is a function of the ratio $K/S = KM$ is proportional to the concentration.

4.2.4 Practical applications of Near Infrared Spectroscopy

Near infrared spectroscopy is of interest for on-line monitoring purposes since it is fast, inexpensive, simple, easy to automate, non-invasive, and remote sensing.

The following paragraphs present some recent studies involving NIRS as prediction tool on-line measurements.

i. A Danish study from 2007 [32] has evaluated the feasibility of applying transflexive embedded near infrared sensors (TENIRS) system for monitoring an anaerobic co-digestion process.

The purpose of the study was to simulate at-line conditions. However, the system can be configured as on-line, at-line, and off-line [32].

The manure samples were collected at two different Austrian biogas plant and analyzed with TENIRS system for volatile fatty acids, dry mater, volatile solids, total nitrogen, and ammonium content.

Acceptable models were obtained for the key parameters: total volatile fatty acids, acetic acid, ammonium and dry matter (Figure 4.11). [32]
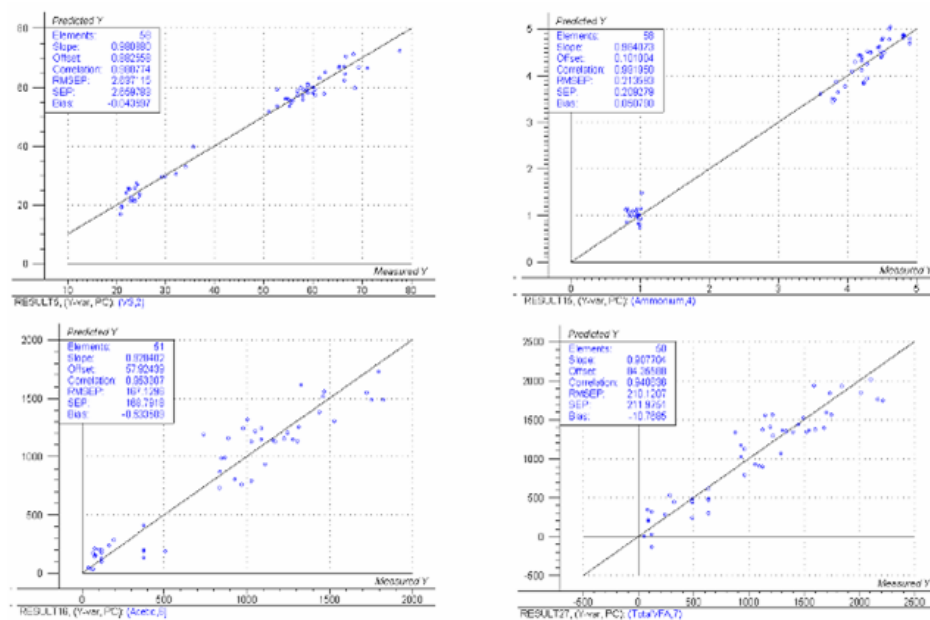
Figure 4.11: Calibration models for process parameters; spectra acquired at-line using TENIRS [32]

ii. A Danish study from 2007 [33] conducted on a laboratory scale glycerol boosted anaerobic digestion, has shown good perspectives for NIRS on-line monitoring of anaerobic digestion.

In fact, the PLS model for total VFA quantification leads to excellent measures of prediction, precision: $r^2 = 0.97$ and accuracy: $s = 1.04$. Similar results have been established for acetic acid and iso-butanoic acid. [33]

4.3 Other process analytical techniques

4.3.1 Acoustic-Resonance Spectrometry

Unlike Acoustic Chemometrics, **A**coustic-**R**esonance **S**pectrometry (**ARS**) is an active acoustic technique of measurements. Which means that an acoustic wave is emitted and it passes through the samples and then is recorded.

A acoustic wave is a longitudinal wave-one whose compressions and rarefaction oscillate parallel to the direction of propagation. When an acoustic wave is applied to a sample, the medium responds by locally contracting and expanding, with particles in the medium drawing closer together and moving farther apart. The degree to which a particular medium responds is a product of its incompressibility. For dense materials with very little compressibility, a sound wave propagates very rapidly, while for less dense samples, sound travels more slowly [43]. Once the spectra acquired the pathway of treatments is the same than for acoustic chemometrics.

It is still an under-utilized PAT tool that could become an analytical method of choice for the physical characterization of some analytes in pharmaceutical manufacturing. According to [43], the wide-ranging measurements that can be made by Acoustic-Resonance Spectrometry include sample compaction and axial strain, deformation, hydration and drying endpoint, elasticity, molecular stacking, and homogeneity, making ARS a very descriptive method of sample analysis. Furthermore, ARS provides a rapid and efficient noninvasive way to identify and quantify an analyte with no or little sample preparation.

4.3.1.1 Practical application of Acoustic-Resonance Spectrometry

This section analyze one of the application [43] of ARS in the pharmaceutical sector.

The US Food and Drug Administration frequently orders recalls of tablets because of labeling problems e.g. the wrong table appears in a bottle. A high-throughput, noninvasive method of online analysis and label comparison prior to shipment could limit the need for recall.

The study present ARS as an inexpensive and nondestructive method which is both accurate and precise for this purpose.

Figure 4.12 depicts the schematic of the AR spectrometer used by the authors of the study.

In the absence of a tablet at the vertex of the quartz rod, the applied acoustic signal received at the detector is a standing wave that is characteristic of the quartz wave guide. Whereas, when a tablet comes in contact with the rod, the acoustic waves propagate through the tablet/quartz interface and pass to the tablet holder[10]. Waves are reflected back or transmitted through the tablet, where they reenter the quartz rod. The two sound paths lead to a pattern of in-phase and out-of-phase interferences[11] that is characteristic of the tablet.
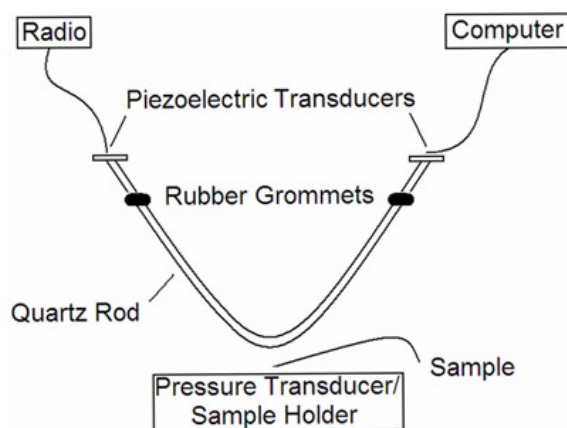
Figure 4.12: Acoustic-resonance spectrometer schematic illustrating the instrumentation. The piezoelectric transducer on the left receives the excitation signal from the radio, while the one on the right receives the transmitted signal through the quartz rod. [43]

To test the classification ability of ARS, the study analyzed five common household tablets of similar size and shape e.g. aspirin, ibuprofen, acetaminophen, vitamin C, and vitamin B12. Models giving the tablet mass ($r^2 = 0.977$), thickness ($r^2 = 0.977$), and density ($r^2 = 0.900$) were established using cross-validation (see Figure 4.13). The authors of the study concluded that the parameters were measured very accurately from the AR spectra, each with less than 10% error, demonstrating that ARS effectively identified and characterized the five types of tablets and could potentially serve as a rapid high-throughput online pharmaceutical sensor.

Thanks to chemometrics, ASR can now make his way into the pharmaceutical

---

[10]Which may contain a second transmitting transducer.

[11]Between the standing wave traveling through the quartz rod from piezoelectric transducer (PZT) to PZT with no tablet interaction, and the wave propagating through the tablet.
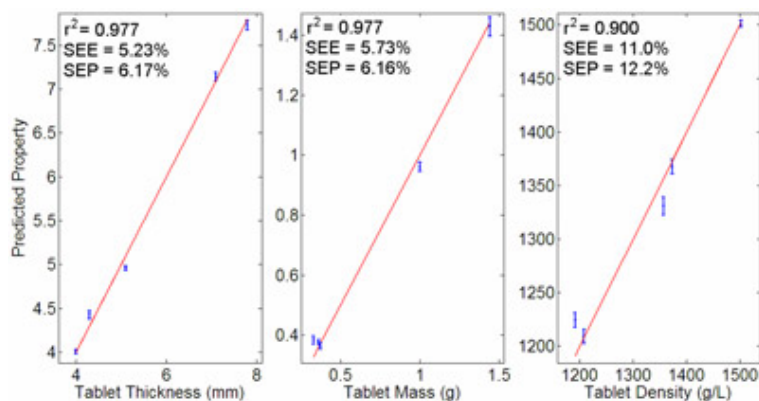
Figure 4.13: Cross-validation results demonstrating the ability of acoustic-resonance spectrometry to predict tablet thickness, mass, and density from the acoustic-resonance spectra of the tablets. [43]

industry as alternatives to traditional invasive testing[12] . ARS can easily be applied to the quantification of **A**ctive **P**harmaceutical **I**ngredient (**API**) or moisture in tablets because of the high correlation between AR spectral features and chemical composition. [43]

4.3.2 Process chromatography

Well-known technique in analytical chemistry, chromatography separates a sample, typically a mixture of different analytes, through a column, which retards the passage of the analytes in the sample. Each analyte ideally has a characteristic retention time, which is known in advance. This technique is an alternative to real time spectrophotometric techniques and it could e.g., be set up in e.g., the cultivation plant. A few multiplexed instruments will be able to serve several reactors. [44, 58]

Unlike laboratory chromatographs, process chromatographs have to be designed to withstand sometimes *harsh* environmental conditions, *hazardous* process areas, and *continuous* operation with *minimal* attention. Sample extraction, preparation, and injection are another important aspect.

Industrial end users expect an annual instrument up time in excess of 97% [42]. In other words, the instrument has to be on-line providing successive analyzes around the clock while requiring less than eleven days to calibrate and **maintain** the unit.

---

[12]Currently, the industry standard for tablet characterization and identification is high performance liquid chromatography (HPLC), which, in addition to requiring extensive preparation (tablet grinding, dissolution, and extraction), destroys the tablet during the analytical process. [43]

4.3.2.1   Practical application of Process Gas Chromatography

Gas chromatography is particulary useful for quantification of volatile compounds [42] and can thus be used for volatile fatty acids determination. In fact, process gas chromatography for VFA quantification has been investigated in a Danish study [51]. Concentrations from 6 to $3000 mgL^{-1}$ can be quantified [41, 51]. The study showed a good correlation ($r^2 = 0.9991$) between the samples extracted automatically and the samples extracted manually. [51]

However, the system can only analyze up to four samples per hour.
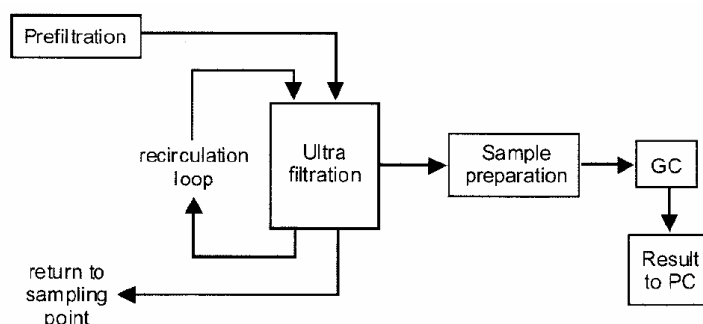
Figure 4.14: Schematic principle of on-line gas chromatography utilization for quantification of volatile fatty acids [51]

Compared to infrared spectroscopy, and as shown in Figure 4.14 the system is not easy to deploy, since a rotating pre-filtration unit has to be immersed into the reactor, the flow from the pre-filtration unit goes to an ultrafiltration unit, the flow is then pre-treated to removed gasses and precipitates the sample is prepared and injected into the GC for VFA quantification. PGC is also quite expensive compared to infrared spectroscopy.

4.3.3   Mass spectrometry

Mass spectrometry is a technique which determines the mass-to-charge (m/z) ratio of ions. It is generally used to find the composition of a compounds by generating a mass spectrum representing the masses of the components of a sample. [58]

The technique is being miniaturized leading to the possibility to clamp the instrument on any process pipe or vessel [44].

Chapter 5

Chemometrics

This chapter introduces the concepts and general mathematical overview of the elements of Multivariate Data Analysis techniques.

5.1 Introduction

The ***I***nternational ***C***hemometrics ***S***ociety (***ICS***) has formulated the present definition:

> *Chemometrics is the science of relating measurements made on a chemical system or process to the state of the system via application of mathematical or statistical methods.*

In other words, the essence of many chemometrics techniques is the production of an empirical model, derived from data, allowing to estimate one or more properties of a system from measurements.

However, *not even multivariate methods can help you if your data does not contain relevant information about the property that you are seeking.* [15]

Chemometrics based its *philosophy* on the following formal logic: [2]

  i. design or select optimal measurement procedures and experiments;

 ii. provide maximum relevant information by analyzing data.

5.2   Multivariate Data Analysis (MDA)

Multivariate Data Analysis (**MDA**) techniques assume that the measured data carry the information of interest.

Therefore, a quantitative relationship between the set of measured variables and the property of interest is compulsory to use MDA techniques. Mathematically speaking, the desired property called Y-Matrix, is a function of the measured variables, X-Matrix.

Generally, the property of interest Y represents an expensive or difficult type of analysis, whereas the X-Variables are variables which typically could be easier, less expensive, faster, automatic, instrumental methods like acoustic or spectroscopic measurements.

5.2.1   Purposes of Multivariate Data Analysis

Many multivariate data analysis techniques are available to reveal the relationship between the X- and Y-Matrix , however, the method to use depends on the type of structure to treat. When the problem and the data analysis objective are both well defined, the choice of technique is often obvious.

Multivariate data analysis is used for a number of distinct, different purposes and the objectives can be divided into three mains groups: [15]

i. Exploration and description of data including basic statistical analyzes and investigation of correlation between variables.

ii. Separation of groups of data by classification and discrimination. Discrimination involves deriving a quantitative data model in order to discriminate between groups of data. Classification has a somewhat similar purpose; prior to the analysis, we need to know a set of relevant groupings to determine which groups are relevant to model.

iii. Regression and Predication based on two data matrices (X and Y) focusing on interrelated explanation of one set of variables with the other. Regression is an approach for relating the two sets of variables to each other. It corresponds to determining one (or several) Y-Variables on the basis of a well-chosen relevant X-Variables set. Prediction means determining Y-Values from new X-Objects, based on a previously representative estimated (calibrated) $X - Y$ regression model.

5.2.2 Multivariate Data Analysis Techniques

Four basic Multivariate Data Analysis modeling techniques basically exist:

i. *Principal Component Analysis* (*PCA*). It consists in modeling the X-Matrix alone.

ii. *Multi-linear Regression* Analysis (*MLR*). With the assumption that it exist no linear relation in the X-Variables, MLR inter-relates several X-Variables to a single Y response variable.

iii. *Principal Component Regression* (*PCR*). It is similar to MLR but it can be applied in cases where X-variables are highly correlated or collinear.

iv. *Partial Least Squares Regression* (*PLS-R*) methods; PLS1 and PLS2. It comprises modeling the X-Matrix (several variables) in directions corresponding to maximum variation in the Y-Variable(s).

5.2.2.1 Principal Component Analysis (PCA)

Principal Components Analysis (*PCA*) is the basic weapon of all multivariate data analysis modeling techniques. It is used for data compression and information extraction. PCA finds combination of variable or factors that describe major trends in the data. Mathematically, PCA is defined as an orthogonal linear transformation which transforms the data to a new coordinate system such that the greatest variance by any projection of the data comes to lie on the first coordinate, called the first principal component, the second greatest variance on the second coordinate, and so on. PCA is based on an eigenvector decomposition and diagonalization of the covariance or correlation matrix of the process variables. [15, 42]

The objective is to find a unit vector, $\mathbf{p}_1$, called first loading vector, in the direction where the coordinates of the objects $\mathbf{t}_1$, called scores, have the largest variance.

For a given *data matrix* X with n rows and p columns, the covariance matrix of X is defined as

$$\text{cov}(X_c) = \frac{X_c^T X_c}{n-1} \tag{5.1}$$

$$= \frac{1}{n-1} \begin{pmatrix} x_{11} - \overline{x}_1 & \dots & x_{n1} - \overline{x}_1 \\ \vdots & \ddots & \vdots \\ x_{1p} - \overline{x}_p & \dots & x_{np} - \overline{x}_p \end{pmatrix} \begin{pmatrix} x_{11} - \overline{x}_1 & \dots & x_{1p} - \overline{x}_p \\ \vdots & \ddots & \vdots \\ x_{n1} - \overline{x}_1 & \dots & x_{np} - \overline{x}_p \end{pmatrix}$$

Owing to its definition, the covariance matrix is symmetrical.

Prior to the calculation of the covariance matrix, the columns of X have to be *mean centered*, i.e. adjusted to have a zero mean by subtracting off the original mean of each column. If the columns of X have been *auto-scaled*, i.e. adjusted to zero mean and unit variance by divided each column by its standard deviation, Equation 5.1 gives the correlation matrix of X[1].

PCA decomposes the data matrix X as the sum of the outer product or tensor product[2] of vectors $\mathbf{t}$ and $\mathbf{p}_i$, plus a residual matrix E

$$X = \mathbf{t}_1 \otimes \mathbf{p}_1 + \mathbf{t}_2 \otimes \mathbf{p}_2 + \dots + \mathbf{t}_k \otimes \mathbf{p}_k = \left(\sum_{i=1}^{k} \mathbf{t}_i \otimes \mathbf{p}_i \right) + E \tag{5.2}$$

Where k must be less than or equal to the smaller dimension of X, i.e. $k < \min(p, n)$. The $\mathbf{t}_i$ vectors are known as *scores* and contain information on how the samples or *objects* relate to each other, geometrically they represent the coordinates of the objects in the new PC axis system (See Figure 2.3). The $\mathbf{p}_i$ vectors are *eigenvectors* of the covariance matrix, i.e. for each $\mathbf{p}_i$

$$\text{cov}(X)\mathbf{p}_i = \lambda_i \mathbf{p}_i \tag{5.3}$$

---

[1]Unless otherwise noted, it is assumed that the data is either mean centered or auto-scaled prior to analysis.

[2]In linear algebra, the outer product or tensor product typically refers to the tensor product of two vectors. The result of applying the outer product to a pair of vectors is a matrix. For instance, the outer product of a $n \times 1$ column vector $\mathbf{a}$ and a $1 \times m$ row vector $\mathbf{b}$ is defined by

$$\mathbf{a} \otimes \mathbf{b} = \mathbf{a}\mathbf{b}^T = \mathbf{a}\mathbf{b} = \begin{pmatrix} a_1b_1 & \dots & a_1b_m \\ \vdots & \ddots & \vdots \\ a_nb_1 & \dots & a_nb_m \end{pmatrix} = A$$

Where A is a matrix $n \times m$.

Where λ_i is the *eigenvalue* associated with the eigenvector $\mathbf{p}_i$.

In PCA the $\mathbf{p}_i$ are known as loading-vectors and contain information on how the *variables* relate to each other. The $\mathbf{t}_i$ form an orthogonal set $((\mathbf{t}_i|\mathbf{t}_j) = 0$ for $i \neq j)$ while the $\mathbf{p}_i$ are orthogonal[3] $((\mathbf{p}_i|\mathbf{p}_j) = 0$ for $i \neq j$ and $(\mathbf{p}_i|\mathbf{p}_j) = 1$ for $i = j)$. For X and any $\mathbf{t}_i$, $\mathbf{p}_i$ pair

$$X\mathbf{p}_i = \mathbf{t}_i \tag{5.4}$$

i.e. the score vector $\mathbf{t}_i$ is the linear combination of the original X data defined by $\mathbf{p}_i$. The $\mathbf{t}_i$, $\mathbf{p}_i$ pairs are arranged in descending order according to the associated λ_i.

The λ_i are a measure of the amount of *variance* described by the $\mathbf{t}_i$, $\mathbf{p}_i$ pair. Therefore, we can think of variance as *information*.

Since the $\mathbf{t}_i$, $\mathbf{p}_i$ pair are in descending order of λ_i, the first pair captures the largest amount of information of any pair in the decomposition, and is called the first principal component PC_1. In fact, it can be shown that the $\mathbf{t}_i$, $\mathbf{p}_i$ pair captures the greatest amount of variation in the data that it is possible to capture with a linear factor, and each subsequent pair captures the greatest possible amount of variance remaining at that step.

Figure 2.3 depicts geometrically the PCA analysis for a 3-dimensional space. The upper left figure shows the objects, the upper right figure shows the first PC component PC_1, the lower left figure shows the second PC component $PC_2 \perp PC_1$, and the lower right figure shows the projects of some objects on the PC axes, or in other words shows the scores of a few objects.

Generally, the data can be adequately described using far fewer factors than original variables. Therefore, the data overload experienced in chemical process monitoring can be solved by monitoring fewer scores[4], with no significant loss of information. [42]

Also, PCA reveals combinations of variables that are useful descriptions, or even predictors, of particular process events. These combinations of variables are often more *robust* indicators of process conditions than individual variables due to the signal averaging aspects of PCA.

PCA is also a useful tool for classification purposes. In the case of very distinct separation between classes, a straightforward PCA might be sufficient. Nevertheless,

---

[3] The eigenvectors belonging to a symmetrical matrix are orthonormal.
[4] Weighted sum of the original variables.
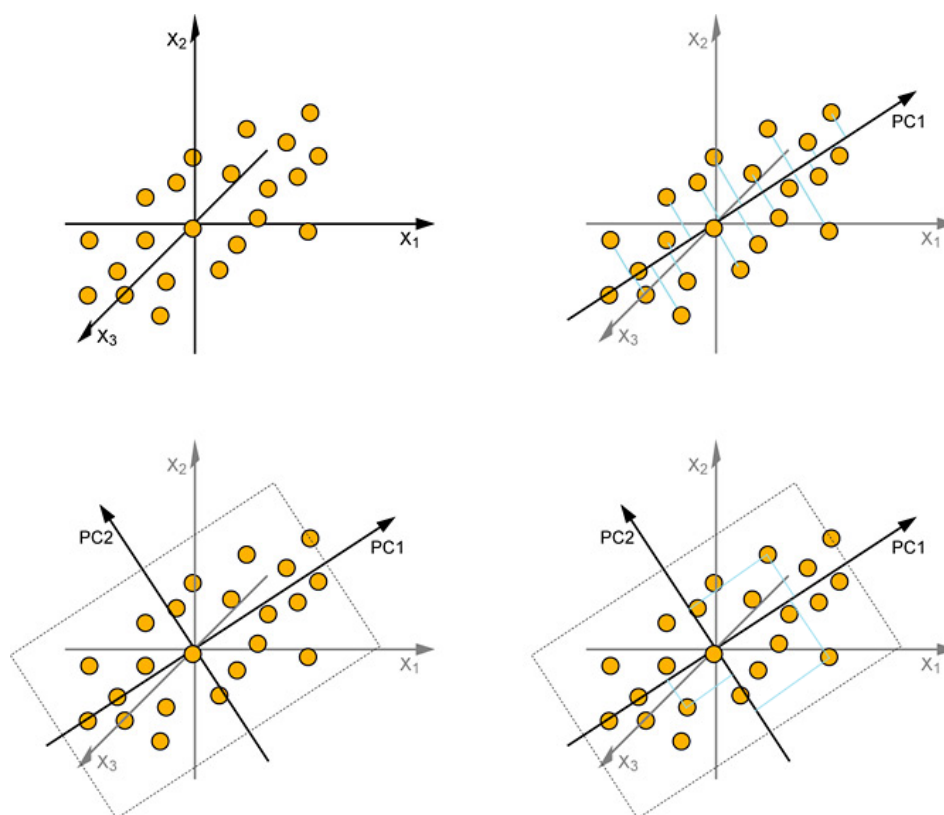
Figure 5.1: Principal component analysis [1]

in many cases the information necessary to distinguish classes is found in combinations of several principal components. [11]

5.2.2.2 Multiple linear regression

Multiple Linear Regression (*MLR*) is a classical method which combines a set of several X-Variables in linear combinations that correlate as closely as possible to the corresponding single **y**-vector [15]. Therefore, it is assumed that a regression vector **b** can be used to determine the property of the system y from the measured variables **x** (a row vector such as a spectra). Mathematically,

$$y = b_0 + b_1 x_1 + b_2 x_2 + \ldots + b_p x_p + f \tag{5.5}$$

Or in a compressed form

$$\mathbf{y} = \mathrm{X}\mathbf{b} + \mathbf{f} \tag{5.6}$$

The idea is to find the vector of regression coefficient **b** so that the error term **f** is the smallest possible. This can be done by using the least squares criterion on the squared error terms: find **b** so that $\mathbf{f}^T\mathbf{f}$ is minimized. This leads to the following equation [15]

$$\hat{\mathbf{b}} = \mathrm{X}^+\mathbf{y} \tag{5.7}$$

Where X^+ is the pseudo-inverse of X and, in MLR, is defined as

$$\mathrm{X}^+ = \left(\mathrm{X}^T\mathrm{X}\right)^{-1}\mathrm{X}^T \tag{5.8}$$

Unfortunately, this method often fails in practice. The most obvious cause is the collinearity of X, e.g. some columns of X (variables) are linear combinations of the other columns, since the matrix inversion will become unstable (dividing by zero). Another cause is when X contains fewer objects than variables (fewer rows than columns). For instance, the spectroscopy calibration is extremely *ill-conditioned* due to high degree of correlation between absorbances at nearby wavelength. It is also typical that there are fewer objects available than the number of wavelengths considered.

When Equation 5.7 is used with systems that produce nearly collinear data, the solution for **b** is unstable, i.e. small perturbations in the original data, possibly due to noise or experimental error, cause the method to produce wildly different results. While the calibrations may fit the data, they are typically not useful for predicting the properties of new samples.

5.2.2.3 Principal components regression

*P*rincipal *C*omponents *R*egression (*PCR*) allows to deal with the problem of ill-conditioned matrices. Instead of regressing the system properties, e.g. concentrations, on the original measured variables, e.g. spectra, the properties are regressed on the principal component scores of the measured variables. Therefore, PCA can be thought of as a *two-step procedure*: first a PCA is used to transform X, the resulting T-matrix fed the MLR algorithm.

Thus, X^+ is estimated as [42]

$$X^+ = P \left(T^T T \right)^{-1} T^T \tag{5.9}$$

As in PCA the number of principal components to retain in the model has to be determined. Since the aim of the regression model is to quantify the properties of interest for new samples, the number of PCs is chosen to optimize the predictive ability of the model. This is can be done either by cross-validation or by test set validation.

The total prediction error over all the test sets can be expressed as a function of the number of PCs and then used to determine the optimum number of PCs, i.e. the number of PCs which leads to the minimum predictor error. When all of the PCs are retained, the result is identical to that for MLR[5]. Therefore, it can be thought that the PCR model *converges* to the MLR model when the number of PCs used increased.

5.2.2.4 Partial Least Squares Regression (PLS-R)

*P*artial *L*east *S*quare (*PLS*) attempts to maximize *covariance* [42]. For a first approximation, PLS can be thought as two simultaneous PCA-analyzes, PCA of X and PCA of Y. The equivalent PCA equations are shown in Equations 5.10 and 5.11. Among other features, the PLS approach gives superior interpretation possibilities and same prediction results as PCR, but based on a smaller number of components.

---

[5]At least in the case of more samples than variables

$$X = \left(\sum_A TP^T \right) + E \qquad (5.10)$$

$$Y = \left(\sum_A UQ^T \right) + F \qquad (5.11)$$

Applying the NIPALS algorithm is one of the several ways to compute PLS model. The algorithm calculates the traditional scores T and loadings P, and an additional set of vectors known as weights, W. The addition of weights is required to maintain orthogonal scores.

The NIPALS algorithm can also be used when there is more than one predicted variables (PLS2), Y, and therefore scores U and loadings Q are also calculated for the Y-space. Finally, an *inner-relationship* regression coefficients vector, **b**, that relates the X and Y-space scores, has also to be determined. Using NIPALS the scores, weights, loadings and inner-coefficients are calculated sequentially as explained below. [42]

Prior to applying the algorithm to the X and Y matrices, the matrices must be centered and scaled.

Index initialization: i=1; $X_i = X$; $Y_i = Y$

i. For $\mathbf{u}_i$ choose any column of Y. It is often advantageous to choose the column with the greatest variance.

Of course, in case of univariate $\mathbf{y}$, $\mathbf{u}_i = \mathbf{y}$ (case of PLS1 algorithm).

ii. Calculate and normalized the loading weight vector $\mathbf{w}_i$ as follows:

$$\mathbf{w}_i = \frac{X_i^T \mathbf{u}_i}{\|X_i^T \mathbf{u}_i\|} \qquad (5.12)$$

iii. Calculate the coordinates of the score vector $\mathbf{t}_i$ as follows:

$$\mathbf{t}_i = X_i \mathbf{w}_i \qquad (5.13)$$

iv. Calculate and normalized the loading vector $\mathbf{q}_i$ as follows:

$$\mathbf{q}_i = \frac{Y_i^T \mathbf{t}_i}{\|Y_i^T \mathbf{t}_i\|} \qquad (5.14)$$

AALBORG UNIVERSITY ESBJERG

v. Calculate the coordinates of the score vector $\mathbf{u}_i$ as follows:

$$\mathbf{u}_i = \mathrm{Y}_i \mathbf{q}_i \tag{5.15}$$

vi. Check the convergence: if the convergence limit is ε, then proceed to Equation 5.17 when

$$|\mathbf{t}_i^{\mathrm{new}} - \mathbf{t}_i^{\mathrm{old}}| < \varepsilon \tag{5.16}$$

Otherwise, proceed to Equation 5.12 again.

If the Y-block is univariate, Equations 5.14 and 5.15 can be omitted, set $\mathbf{q}_i = 1$, and no iteration is required. [42]

vii. Calculate the coordinates of the loading vector $\mathbf{p}_i$ as follows:

$$\mathbf{p}_i = \frac{\mathrm{X}_i^T \mathbf{t}_i}{\|\mathbf{t}_i^T \mathbf{t}_i\|} \tag{5.17}$$

viii. Calculate the regression coefficient b for the inner relation:

$$b_i = \frac{\mathbf{u}_i^T \mathbf{t}_i}{\|\mathbf{t}_i^T \mathbf{t}_i\|} \tag{5.18}$$

ix. The X- and Y-block have to be updated as follows:

$$\mathrm{X}_{i+1} = \mathrm{X}_i - \mathbf{t}_i \mathbf{p}_i^T \tag{5.19}$$

$$\mathrm{Y}_{i+1} = \mathrm{Y}_i - b_i \mathbf{t}_i \mathbf{q}_i^T \tag{5.20}$$

By using the $\mathbf{p}$-vectors instead of the $\mathbf{w}$-vectors for updating X, the desired orthogonality for the $\mathbf{t}$-vectors is secured. [15]

x. It is now time to increase the iterator i

$$i = i + 1 = i + + \tag{5.21}$$

The score vectors $\mathbf{t}_a$ and the loading weights vectors $\mathbf{w}_a$ are orthogonal, while $\mathbf{p}_a$ loading vectors are not. $\mathbf{q}_a$ vectors are the **Y**-loadings which are the regression coefficient. Unlike MLR or PCR, in PLS[6], the regression coefficients $\mathbf{q}_a$ are found one at a time, which is also known as projection of latent structures. When the projection converts a single Y-variable, it is termed PLS1, while if it is the simultaneous modeling of two or more Y-variables, it is termed PLS2.

---

[6]PLS is also the abbreviation of the *partial least squares* due to the way of calculation of the regression coefficients.

In PLS, both P and W are important owing to the formal regression equation

$$Y = XB \tag{5.22}$$

Where B-matrix is calculated from:

$$B = W \left(P^T W\right)^{-1} Q^T \tag{5.23}$$

Where the W, P, and Q are calculated as above. This B-matrix is often used for practical prediction purposes.[15]

The important thing to remember is that PLS attempts to find factors which are correlated with Y while describing a large amount of the variation in X. This is in contrast with PCR, where the factors are selected solely on the amount of variation they explain in X.

5.2.2.5   Interpretation of PLS Models – PLS1 and PLS2

In principle PLS models are interpreted in much the same way as PCA and PCR. Plotting the X loadings weights (Y loadings) in the same plot allows to study the inter-variable relationships, also including the relationship between the X and Y-Variables.

PLS2 gives one set of X and Y scores and one set of X and Y loadings, which are *valid for all* of the Y-Variables simultaneously. Whereas, PLS1 gives one set of X and Y scores and one set of X and Y loadings *for each* Y-Variable.

On the other hand, PCR produces only one set of scores and loadings for each Y-Variable, even if there are several Y-Variables. PCR can model one Y-variable at a time.

5.3   Multivariate Calibration

Multivariate calibration is based on a set of matrices (X, Y). The Y-matrix contains the response/dependent variables i.e. parameters of interest, whereas X contains the corresponding independent variables, i.e. acoustic measurement.

Thus, the multivariate model for a set of matrices (X, Y) is simply a regression relationship of the empirical (X, Y) relations. After calibration, the model can be used for future prediction new Y-values.

Multivariate calibration always starts with a set of known measurements collected to form the Y-matrix. For each object in the Y-matrix we must have at disposition the corresponding object of X-matrix measured using the new technique to calibrate. The object in the Y-matrix are also measured with the method to replace. The matrices X and Y are respectively called the calibration set or training set.

The calibration set is of utmost importance in any multivariate calibration procedure. It must meet a number of requirements. The most important is that the calibration set is representative of the future population from which the new measurements are to be done, furthermore, the measuring conditions should be as similar as possible. [2]

Therefore, the calibration set has to span the X-space, as well as the Y-space, as widely and representatively as possible in the specific sense of future usage of the *final correctly validated* prediction model [2, 15].

5.4   Validation

The purpose of modeling is to produce model for future prediction of Y i.e. the variable of interest from unknown X measurements i.e. acoustic spectra.

In order to assess the robustness of the model, the prediction performance has to be tested. There are three main types of validation methods:

  i. leverage correction;
 ii. cross-validation;
iii. test set validation.

They are all designed to estimate a model predictive ability, in other words, the accuracy and precession associated with Y, Y_{pred}. Therefore, Y_{pred} is compared to the reference Y_{ref}. A good prediction accuracy is characterized by a small difference, called the prediction error and it is calculated for each objects.

$$\text{Prediction Error} = Y_{pred} - Y_{ref} \tag{5.24}$$

The square difference of all objects is summed, and the mean calculated, this gives the **R**esidual **V**alidation **V**ariance (**RVV**).

$$\text{Residual Validation Variance} = RVV = \frac{\sum\limits_{i=1}^{n} \left(\hat{y}_i^{\text{val}} - y_i^{\text{val}}\right)^2}{n} \tag{5.25}$$

where $\hat{y}^{\text{val}}$ is the predicted value based on data (X-Variables), y^{val} is the reference concentration determined by the analytical laboratory, and n is the number of reference samples. The residual validation variance can be minimized by eliminating outliers from the data set.

The square root of the residual variance is known as the **R**oot **M**ean **S**quare **E**rror of **P**rediction (**RMSEP**)

$$RMSEP = \sqrt{\frac{\sum\limits_{i=1}^{n} (\hat{y}_i^{\text{val}} - y_i^{\text{val}})^2}{n}} \tag{5.26}$$

The accuracy of a regression model is often represented in terms of the RMSEP with the same units as that of the reference Y value. A higher number of PC/PLSs component generally lower the difference, but only up to a point called the optimal number of components above which the difference starts increasing.

5.4.1 Test set validation

Test set validation constitutes the **best** approach to validate a model. The test set is not, in any way, associated with the calibration data set. Furthermore, ensuring that the samples of both sets are true representatives of the future population span increases the validity of validating a model.

In fact, the validation is based on the use of different data sets for calibration and validation. During the calibration step, calibration samples are used and then the calibrated model is used on the test samples, and the validation residual variance is computed form their prediction residuals. [15]

There is no clear cut limit to the number of samples of these set, it is purely a problem dependent issue. It is preferred that the test-set is extracted as a totally

separate sample set since it might include variations that may not have been present when the calibration set was built.

5.4.2   Cross-validation

Cross-validation consists essentially in an internal sampling of objects for validation purposes i.e. it only simulates a test set, and therefore will never be as realistic as test validation is. This validation technique can be used when it is not possible or desirable to extract more samples to perform a test set validation.

The principle behind cross validation can be explained as follow: *a model is made from part of the data set, while the rest is used for testing* [12]. Tow different approaches of cross validation are typically used: *full cross validation* and *segmented cross validation.*

As previously stated, cross validation provide only a simulation of test set, since a part of the calibration set is used as test set. Therefore, this approach is missing the random (TOS) sampling variations which can only be captured by extracting an independent test set.

5.4.2.1   Full cross validation

Full cross validation is also known as *leave one out cross validation*, it can be seen as a segmented cross validation with only one sample in each segment. This approach is used when the data set is extremely small [12].

Using full cross validation on large data sets might lead to over-optimistic results since the left out samples may on average lead to a significantly smaller sampling variance contribution. Furthermore, using full cross validation on a data set composed by replicates experiments results always in an artificial low validation variance owing to the validation of samples very similar to those left in the model. [12, 15]

The principle of full cross validation is depicted in Figure 5.2. A set of only 10 samples is used in this example, first the algorithm makes a model on samples 1-9 and uses 10 for validation, then a new model on samples 1-8+10 is computed using 9 for validation, etc. [48]
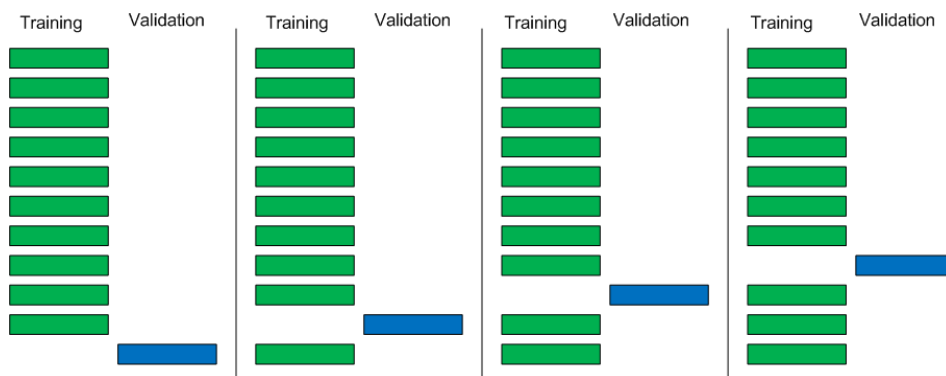
Figure 5.2: Full cross validation principle (only the first four of ten sub-models are shown here).

5.4.2.2 Segmented cross validation

Segmented cross validation can be put between full cross validation and test set validation. This approach is used when the training set is composed by a relative high number of samples.

The calibration set is divided into segments to simulate a test set. All the elements of the segments are left out and the remaining data are modeled, then the next segment is left out, and the first segment is included in the data to be modeled and so on. [15]

Selecting the optimal number of segments is based on the data set size. Nevertheless, two segments cross validation represents the best choice of all segmented options. [15]

5.4.3 Leverage corrected validation

Leverage corrected validation is initially used in modeling to save time owing to the fact that only one model is made to view the trends in the data set. It leads to *over-optimistic* estimates of the predictor error.

Therefore, the final validation must never be based on this method.

Part II

Laboratory scale reactor – Representativeness evaluation of the Applikon$^{\circledR}$ standard sampling system v.s. the ACABS' recurrent sampling loop

Chapter 6

Description of the Applikon® study

6.1 Aims of the study

This part of the thesis aims to contribute to the development and the improvement of the recurrent sampling loop mounted on the reactor, ending by evaluating the representativeness of the samples extracted from both recurrent sampling loop and Applikon® standard sampling system.

The first task is to redesign the recurrent sampling loop to be as much as technically possible in accordance with the Theory of Sampling, the second task is to find plastic particles with the following properties:

i. Density: $1.00 < \rho < 1.1 \ \frac{kg}{m^3}$;

ii. Size (largest dimension ℓ): $0.50 < \ell < 1.00 \ mm$;

The third task consists in evaluating the representativeness of the two sampling systems using simple model-systems composed by polymer pellets and water in different concentrations aiming at a lab- or pilot-scale trial on real (bio-)chemical system e.g. biogas fermentation.

Interest is also placed on the application of acoustic chemometrics to establish PLS prediction model quantifying key system parameters (liquid and solid).

6.2 Critical success factors

The most critical success factor is to find the proper plastic pellets. That task is far from easy people tried to find them by the past but they did not succeed. PoEM Research Group[1] is to be contacted in order to gather the address of polymer producers that might be able to produce them. A total a 35 chemical companies are to be contacted. If it turns to be impossible to find particles, a pilot study aiming to determine the clogging concentration of the plastic particles owned by the university is to be performed.

The deployment of the acoustic sensor is also an important factor. The accelerometer should be welded onto a metallic pipe to register as much vibrations as possible. The sensor can be advantageously placed in a bend of a pipe, since it will be able to *listen* to the particles hitting the pipe wall, giving better chance to record useful acoustic spectra.

When dealing with the model-system pellets/water the analytical grade of the analytes in the lot is always known and does not vary overtime. However, when dealing with real (bio-)chemical systems, the grade of the analytes vary over time owing to (bio-)chemical degradations and transformations occurring during the entire process, therefore leading to difficulties to quantify the true grade of the lot at a given time.

Other critical success factors can be pointed out as cleaning the system between two batches and the quantification of the sample content.

---

[1]Polymers and Engineering Materials – Esbjerg Institute of Technology – Aalborg University – Denmark

7

Chapter

Description of the reactor

Figure 7.1 shows the reactor equipped with the original adaptation of the ACABS' sampling loop and the Applikon® standard sampling system. The system is constituted by a peristaltic pump Ismatec MCP-Process IP-65 which circulates the reactor content into the recurrent loop, a Bio Controller Applikon® ADI-1010, a Bio Console Applikon® ADI-1025, and a Stirrer Motor Applikon® P-100.

The reactor body is made of glass and was specially designed to allow the deployment of the ACABS' recurrent sampling loop and to be used with standard Applikon® devices. It has a capacity of $5L$. The entire system is autoclavable.

As shown by the following analysis, the recurrent sampling loop deployment must be redesigned to be, as much as technically possible, in accordance with the Theory of Sampling.

7.1 Applikon® standard sampling system

The standard sampling system sold by Applikon® is constituted by a glass bottle mounted onto the head plate of the reactor and connected to a height-adjustable sample pipe (inner diameter: $10mm$). The samples are extracted with a syringe as shown in Figure 7.2.

According to Applikon®, the system guarantees that the samples extracted are representative of the reactor content. [8]

Figure 7.1: Laboratory scale reactor equipped with the original adaptation of the ACABS' sampling loop and the Applikon® standard sampling device – Picture courtesy of Ph.D. Student Carina J. Lomborg

Figure 7.2: Picture of Applikon® standard sampling system – Picture courtesy of Ph.D. Student Carina J. LOMBORG

In fact, the sampling system only extracts the sample around a given depth and location in the reactor. In other words, the lot particles do not have the same non-zero probability of selection depending where they are located in the medium. For instance if the pipe inlet is located near to the bottom of the reactor, the particles located at the top do not have the same non-zero probability of selection than the particles located at the bottom.

The samples can be extracted using either a grab sampling method or a composite sampling method. Nevertheless, the problem described above will affect the extracted samples and will produce a bias.

7.2 ACABS' recurrent sampling loop

The ACABS' recurrent sampling loop essentially transforms the three-dimensional reactor sampling issue into a one-dimensional pipeline sampling situation and circulate the content of the reactor from its bottom. When it is in steady state, it allows lot particles to have the same non-zero probability to end-up in the primary sample [31]. The system is depicted in Figure 7.3.

However, mounting a recurrent loop on a reactor does not, alone, ensure the sample extracted from to be representative of the reactor content. Indeed, the sampling ex-
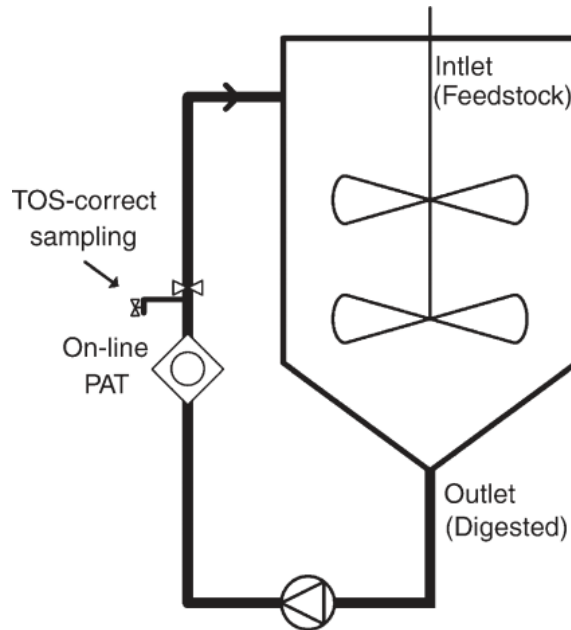
Figure 7.3: On-line PAT measurement and ACABS' recurrent sampling loop. Adapted in a modified form from [31]

traction device and method must be designed carefully in accordance to all the relevant principles of the Theory of Sampling.

Figure 7.4 shows the recurrent loop inlet. The *O-ring* is centered in the reactor, it has a diameter of $120mm$ and is located at $35mm$ height measured from the bottom of the reactor. It is composed by a stainless pipe of $10mm$ of inner-diameter and have 8 wholes of diameter $10mm$ located every $45°$ all around the top surface of the O-ring pipe.

Figure 7.4: Inlet of the recurrent loop placed at the bottom of the reactor – Picture courtesy of Ph.D. Student Carina J. LOMBORG

It cannot be deployed deeper in the reactor owing to its design and the height of the smallest nut available to maintain it at the bottom. Therefore, particles located

beneath the ring do not have the same probability of selection than particles located above it. A well mixed reactor should decrease the difference of probability between the particles allowing a better sample to be extracted.

Figure 7.5 shows the sampling valve of the original sampling loop whereas Figure 7.6 shows the schematic of its deployment. The pipe has an inner diameter of $9mm$ and an outer diameter of $10mm$.

Obviously, this configuration will not lead to structurally correct samples since only a fraction of the stream ends up in the primary sample. As Dr. Pierre Gy wrote [26, 27]: *The only probabilistic method for sampling a moving stream is: Take the whole of the stream a fraction of time shared between a number of increments of short duration.*

The original configuration will not lower the incorrect sampling error, but will most likely increase the increment delimitation error (IDE) and the increment extraction error (IEE). The sampling valve is, in fact, a simple clamp which cannot be easily manually operate.

Figure 7.5: Original sampling *valve* mounted on the recurrent loop – Picture courtesy of Ph.D. Student Carina J. LOMBORG
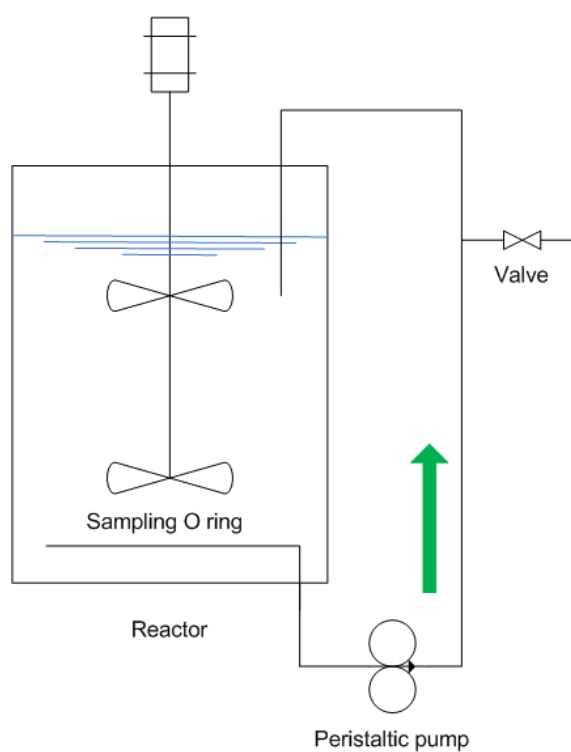
Figure 7.6: Schematic of the original recurrent sampling loop deployment.

Chapter 8

Rebuilding the system

8.1 Recurrent sampling loop

The recurrent sampling loop must be redesigned taking into account that the reactor must stay autoclavable, micro-organism friendly, and easy to sterilize. The biggest problem of the original loop is the sample extraction, therefore focus is placed on it.

To fulfill those three conditions the valve must not be in contact with the stream. Such valves exist on the market and are called a pinch valves [45]. Actually, when closed a pinch valve squeezes the pipe and stop the flow, thus only the pipe walls are in contact with the fluid, leading to a system easy to sterilize and micro-organism friendly. Furthermore, the pipe can be removed from the valve allowing the system to be autoclavable.

8.1.1 Sampling valves

The sampling valves will be electrically commanded and two configurations will be tried.

The first configuration uses a three-way pinch valve[1]. The valve tested is a Sirai S307-06-Z130A supporting pipes of outer diameter up to $9.5mm$. This was the largest pinch valve it was possible to find for laboratory scale use.

---

[1]A three-way valve is commonly made such that the flow coming in at one port can be directed to either the second port in one position or the third port in another position.
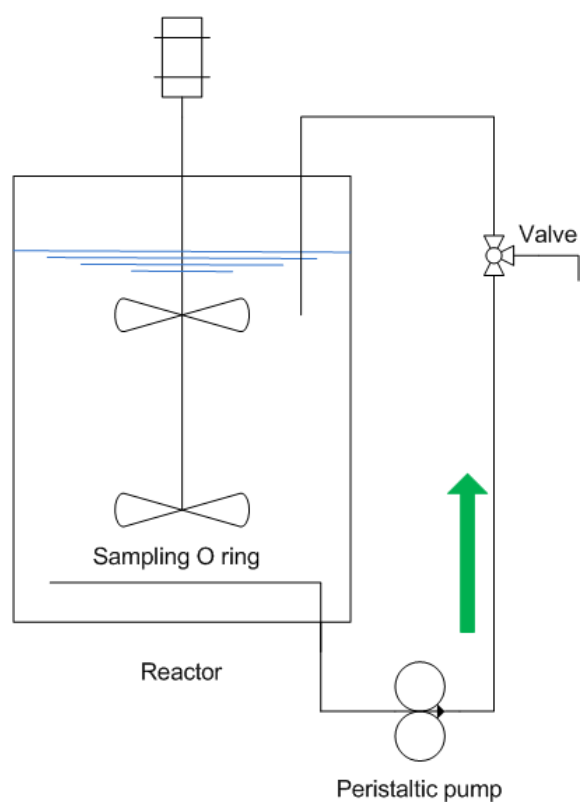
Figure 8.1: Schematic of the recurrent sampling loop using a three-way pinch valve electrically commanded.

The second configuration uses two two-way pinch valve. One is normally open (NO), which means that in absence of electrical signal the valve is open, and one is normally closed[2] (NC), which means that in absence of electrical signal the valve is closed. For obvious security reasons[3] the NC valve is to be mounted on the sampling outlet when the NO valve is to be mounted on the loop. Both valves are to be connected on the same switch allowing one valve to be open when the other is closed. The valves tested were Sirai S206-06-Z130A (NO) and S106-09-Z130A (NC). They have both the same characteristic as the three-way valve.
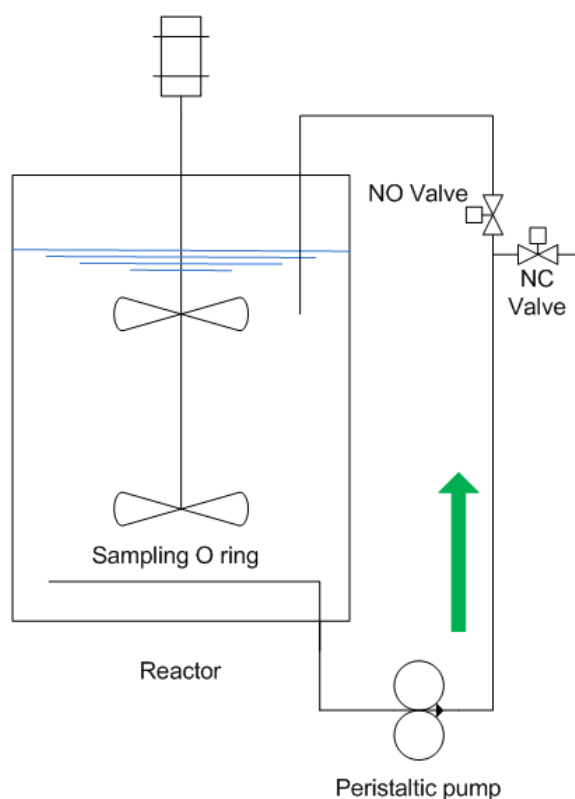
Figure 8.2: Schematic of the recurrent sampling loop using two two-way pinch valves electrically commanded.

8.1.2 Loop inlet and outlet

Acoustic chemometrics is to be used on the system to determine its dry matter content. A metallic structure is needed for the accelerometer to register most of the vibrations

---

[2]Two normally open valves could be used, but in that case proper electronic circuit is needed to create the normally closed function.

[3]And electric consumption reasons.

created by the particles. Therefore, the sensor is to be mounted on the inlet or outlet since they are in metal.

The new inlet and outlet are circled in red in Figure 8.3.
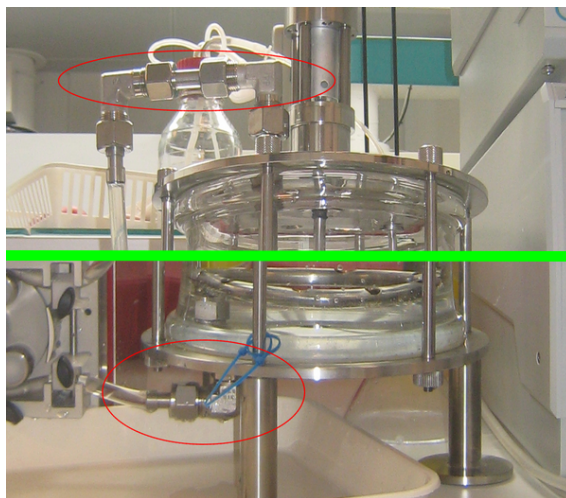
Figure 8.3: Metal inlet (bottom picture) and outlet (upper picture) allowing acoustic measurements.

8.2   System up-scaling

Up-scaling the reactor was the first emergency solution built in parallel to the other task.

The major issue of this part of the thesis is to find the proper plastic particles with the right size in order not to clog the system. In the past, Ph.D. Student Carina J. LOMBORG tried to find the particles during a few months search, but she did not succeed.

Up-scaling the system might solve the pellet size issue, since the pipes will also be up-scaled allowing standard pellets to be used. The idea was to stick as much as possible to an existing Applikon® system in order to use the materials at dispositions or order material from Applikon® to keep the systems interchangeable.

The new capacity of the reactor will be $20L$ which is the size of the largest auto-clavable lab-scale reactor existing in the Applikon® catalogue.

The reactor body will be a transparent plastic tube, allowing the present theoretical

study to be conducted[4].

Naturally, the experimental conditions are to be adapted for the up-scaled system. In particular, the tip speed[5] of the impeller must stay constant in both system, fixing all the stirring parameters. [47, 62]

---

[4]The system is not autoclavable, but in case of success, a glass body can be ordered making it autoclavable.

[5]The tip speed is the speed $[m/s]$ swept by the propeller tips.

Chapter 9

Sampling study

9.1 Experimental design

The experimental plans presented here use the plastic pellets owned by the university and it also includes the observations made during the pilot study.

9.1.1 5L Reactor

From a sampling point of view the diameter of the recurrent sampling loop pipe should be at least three times larger than largest dimension of the largest particles in the broth [26]. Since the inner diameter of the pipe is around $8 - 9mm$, the size of the particles should be less than $3mm$.

Some parameters are fixed for all experiments, e.g. the volume of the reactor, the number of impeller (2), the location of the sampling and acoustic equipments.

The key parameters of the design are cited below:

   i. Medium density;

  ii. Number of analyte;

 iii. Particles density;

 iv. Particles size;

v. Particles concentration;

vi. Sampling type (grab or composite);

vii. Stirring speed;

viii. Loop velocity;

ix. Impeller Type;

x. Aeration;

For each kind of impeller (rushton impeller and marine impeller) the following experimental design is to be performed (the design takes into account the issues discussed in the next chapter)

i. Medium density: 1.

ii. Number of analyte: 1.

iii. Particles concentration: $6g$ / $12g$ / $18g$.

iv. Stirring speed: $100RPM$ / $200RPM$ / $300RPM$.

v. Loop velocity: 50% / 75% / 100% of the maximum power of the pump.

vi. Sampling type: Grab and Composite of 3 and 5 increments extracted from both Applikon® system and recurrent loop.

vii. Replication factor: 10.

It was decided to perform a full factorial design, therefore, the experimental plan leads to 270 experiments. A randomized laboratory report is generated using The Unscrambler v9.2.

Between each replicate the system will be flushed and a new batch will be loaded.

9.1.2 $20L$ Reactor

The experimental design is similar, but the stirring speed must be recalculated as follow. [8]

The tip speed τ_i $[m/s]$ of the experimental condition i has to be determined. If N_i $[RPM]$ is the stirring speed and D_i $[m]$ the diameter of the impeller of the condition i, the tip speed is given by the relation

$$\tau_i = \frac{1}{60} N_i \pi D \tag{9.1}$$

Once the tip speed is known the new stirring speed can be calculated according to the size of the new impeller.

$$N_{\text{New}_i} = \frac{60 \tau_i}{\pi D} \tag{9.2}$$

Yet the power required for stirring must be calculated. According to [8], the required power per impeller of a stirrer motor in *non-aerated* media is given by the equation[1]

$$P = \rho \left(\frac{N}{60} \right)^3 D^5 N_p \tag{9.3}$$

Where P is the required power of the stirrer motor $[W]$, ρ is the density of the medium $[\frac{kg}{m^3}]$, N the stirrer speed $[rpm]$, D the impeller diameter $[m]$, and N_p the power number of the impeller type[2].

The require torque M is given in $[Nm]$ by the following equation

$$M = P \frac{60}{2\pi N} \tag{9.4}$$

The calculations presented above give a indication on how to adapt the experimental plans of the small reactor to the up-scaled. The plan is to be calculated when de diameter of the impellers will be known.

---

[1]Then mounted according to the given configuration, a second or third impeller on a shaft requires only 90% of the power of the first impeller. Therefore, for two impellers Equation 9.3 is multiplied by $1 + 0.90 = 1.90$ and for three impellers by 2.80.
    [2]Rushton impellers $N_p = 6$ – marine impellers $N_p = 1.5$. [8]

Chapter 10

Applikon® pilot study discussion

10.1 Clogging concentration

Since it was not possible to find the proper plastic pellets needed for the experiments, a the present pilot study was conducted to evaluate the clogging concentration when using the pellets owned by the university.

Those pellets have the right density, but their largest dimension is between $1.5mm$ and $3.0mm$ hence barely fulfilling the condition on the particle sizes regarding the inner diameter of the sampling pipes. Besides, when present in a too high concentration in the reactor they lead to the formation of clogs in the loop.

Figure 10.2 shows the reactor loaded with $3.0g$ (left) and $30.0g$ (right) of plastic pellets. The last concentration started to clog the pipes, therefore, higher concentration will not be tried during the sampling study.

The clogging concentration (0.60% dry matter) does not have the magnitude of the dry matter content of a biogas reactor, typically 5% to 10% [3, 4], but it was decided to have try with the particles and hope for the best.

It also revealed that the peristaltic pump shakes the metal pipes connected the plastic tubes. Those extra-vibrations must be taking into account when deploying the acoustic sensor. In fact, they can ruin the measurements by *masking* the vibrations of interest and thus jeopardize the chances to obtain a good model.
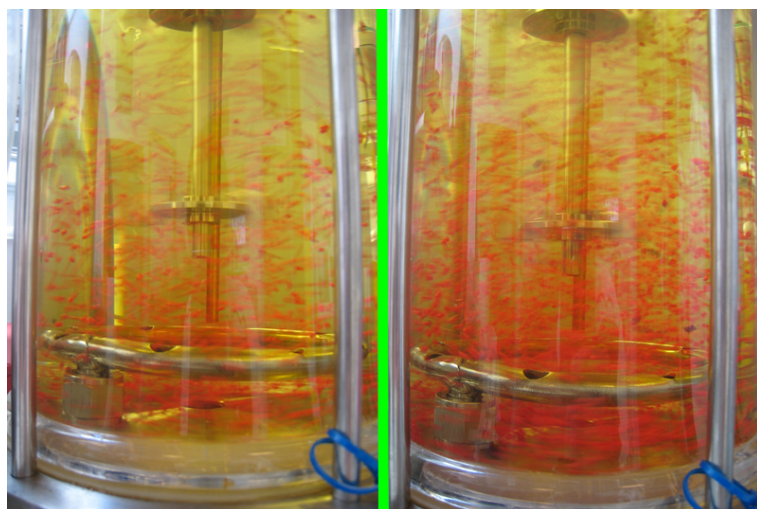
Figure 10.1: Reactor loaded with $3.0g$ (left) and $30.0g$ (right) of plastic pellets.
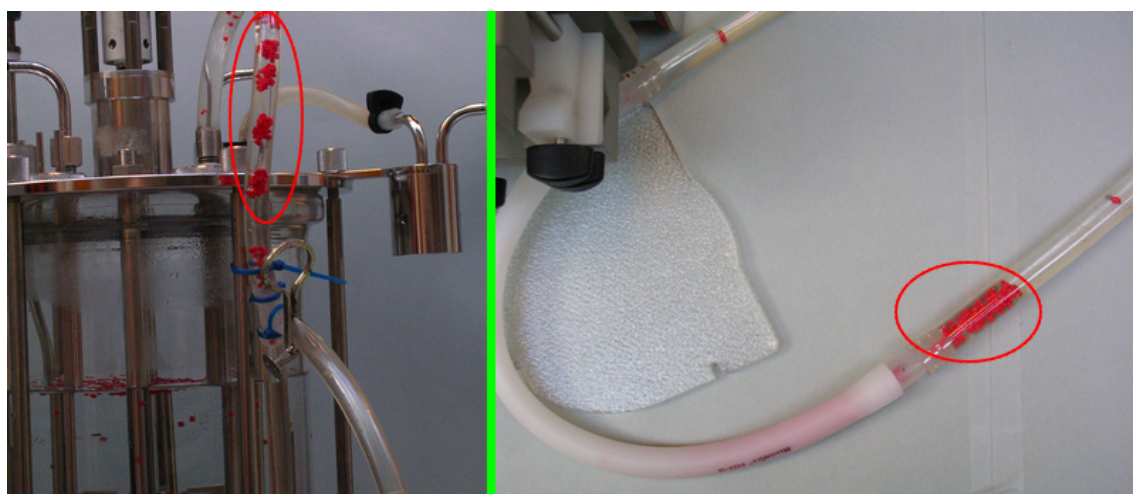
Figure 10.2: Clogs in the pipe – Picture courtesy of Ph.D. Student Carina J. LOMBORG

10.2   Valves behavior

The different valves were also analyzed. Figure 10.3 shows the normally open valve, the picture on the left shows the valve when open and that on the right when closed. The pipes fit and do not seem to be squeezed when the valve is open. The normally open valve should not introduce clogging problems.
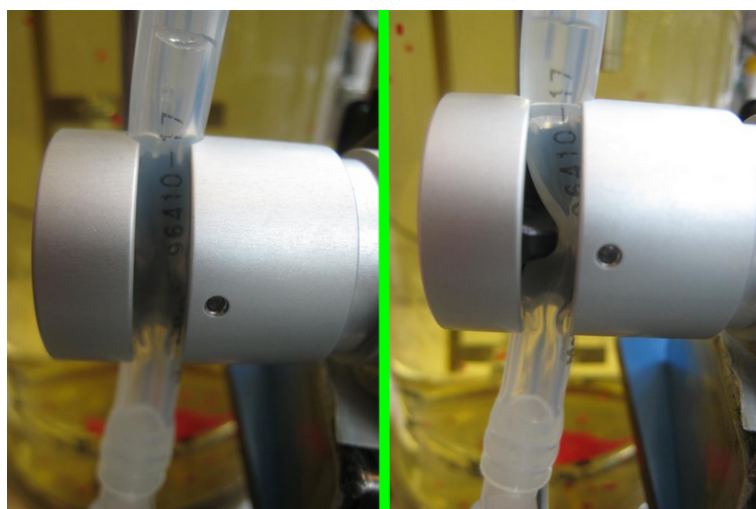
Figure 10.3: Normally open valve – Left picture shows the valve when open and the right when closed

Figure 10.4 shows the normally closed valve, the upper picture shows the valve when closed and that lower when open. In open position the valve squeezes the pipes. That might lead to clogging problems. A normally closed valve can always be replaced by a normally open if connected to proper electronic circuit.

Figure 10.5 shows the three-way valve. It can be noticed, on both pipes, the same issue than on the normally closed valve. Therefore the same pre-conclusion can be drawn.

The clogging concentration is more a trace concentration might be lowered owing to the risk of clogging presented by the normally closed valve.
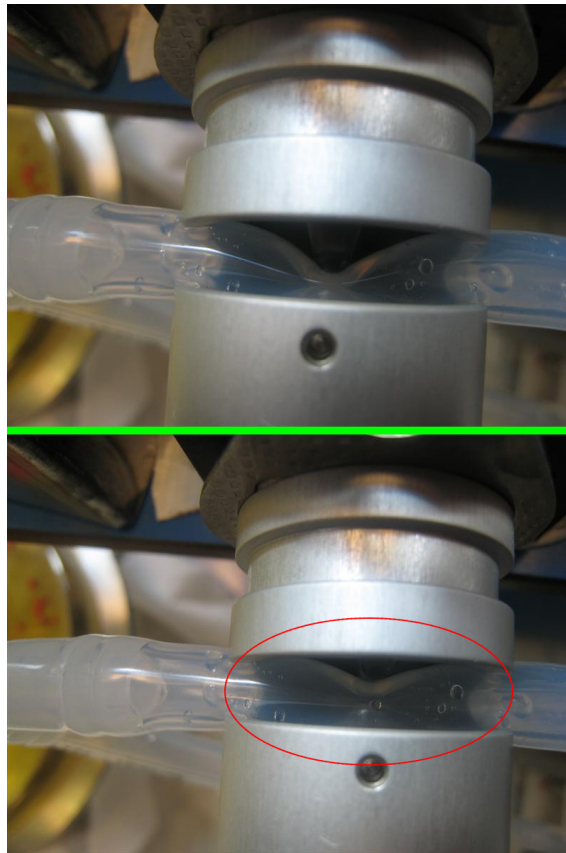
Figure 10.4: Normally closed valve – Upper picture shows the valve when closed and the lower when open
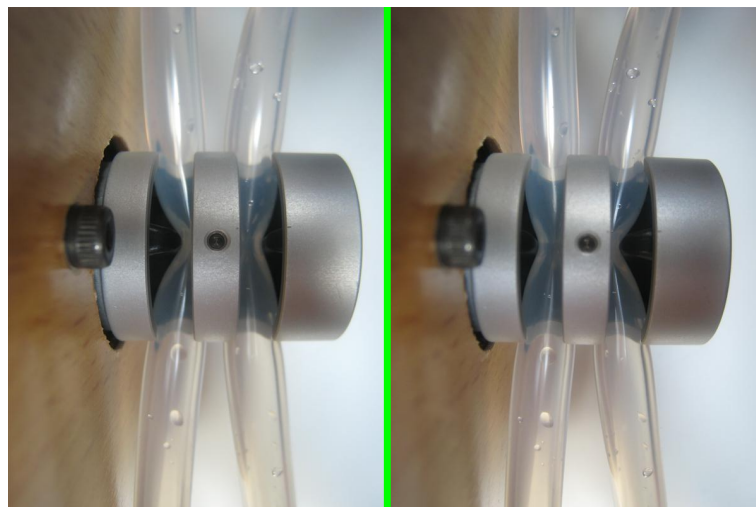
Figure 10.5: Three-way valve – Left picture shows the valve when the principal outlet is open and the right when it is closed

10.3 Unexpected events

10.3.1 Pellets issue

At the end of April 30 out of the 35 chemical companies contacted had replied, all saying that this was not possible to produce so small plastic particles or that they were not dealing with small quantities for special products i.e. if you order less than one ton we cannot help you.

It was decided to continue with the particles owned by the university. We all four sat at the table of the ACABS group room and started cutting them one by one with a razor blade. After one complete afternoon (5 hours i.e. 20 man hours), the quantity needed to perform 3.5 replicates[1] of the lowest concentration of pellets was cut i.e. $\pm 21.0g$. The idea was of course abandoned and a pilot study using the pellets was performed to know whether the system can handle them or not.

That was performed at the beginning of May and the reactor body for the $20L$ reactor was ordered.

10.3.2 Valves issue

Within the first month of the project two pinch valves were ordered according to the references of the catalogue, they were designed to handle a pipe of $10mm$. The delivery took six or eight weeks, and they arrived in the beginning of April.

However, the valves were to small. Apparently, the catalogue references did not correspond the to the reference encoded in the product data base.

We found another company which can deliver the valve we needed, the delivery took about 3 weeks, and we received them at the end of April.

10.3.3 Up-scaling issue

The first problem came from Applikon, it was not possible to order the top plate of the $20L$ reactor without ordering the reactor.

---

[1]According to the experimental plan $3240g$ of pellets is needed. 1t least $1kg$ of particles should be cut leading to ± 1030 man hours.

The second problem came from the non standards reactor body diameter, the company asked us if a pipe with standard diameter can be shipped instead, meaning that the top plate needed to be designed according to the dimensions of the pipes which were unknown.

The pipe was ordered at the beginning of May, in the middle of May we found out that the company had lost our order and we had to place it again.

The pipe finally arrived at the beginning of June but a *small* detail made it impossible to use ... The company sent us a pipe of $2m$ height (instead of 0.60m), in polycarbonate and the university does not have the equipment to cut it. The idea was thus abandoned. The impellers were to be ordered when we received the reactor body, but as the idea was dismissed, nothing was ordered from Applikon.

10.3.4 Clogging issue

In the mean time, in the middle of May, the experiments were started on the $5L$ system.

After the extractions of a few samples the pipes were blown away and the lab was flooded. The experiments were conducted again and the problem was identified – and the lab flooded again –, the normally closed valve squeezes the tube to much when in open position leading to a clog as shown in Figure 10.6.

It was decided to stop the experiments on the system, since time was running fast, and all the efforts put inside could not make it taking off. Instead a sampling study of the TENIRS system owned by the university was scheduled and started on the first of June[2].

---

[2]As the professor said: *Ah, it is nice to have an experiment go completely bust. Makes you need to think ...* And indeed after some thought, the alternative idea of evaluating the existing TENIRS system came up, which proved to be an excellent vehicle for this M.Sc. project.
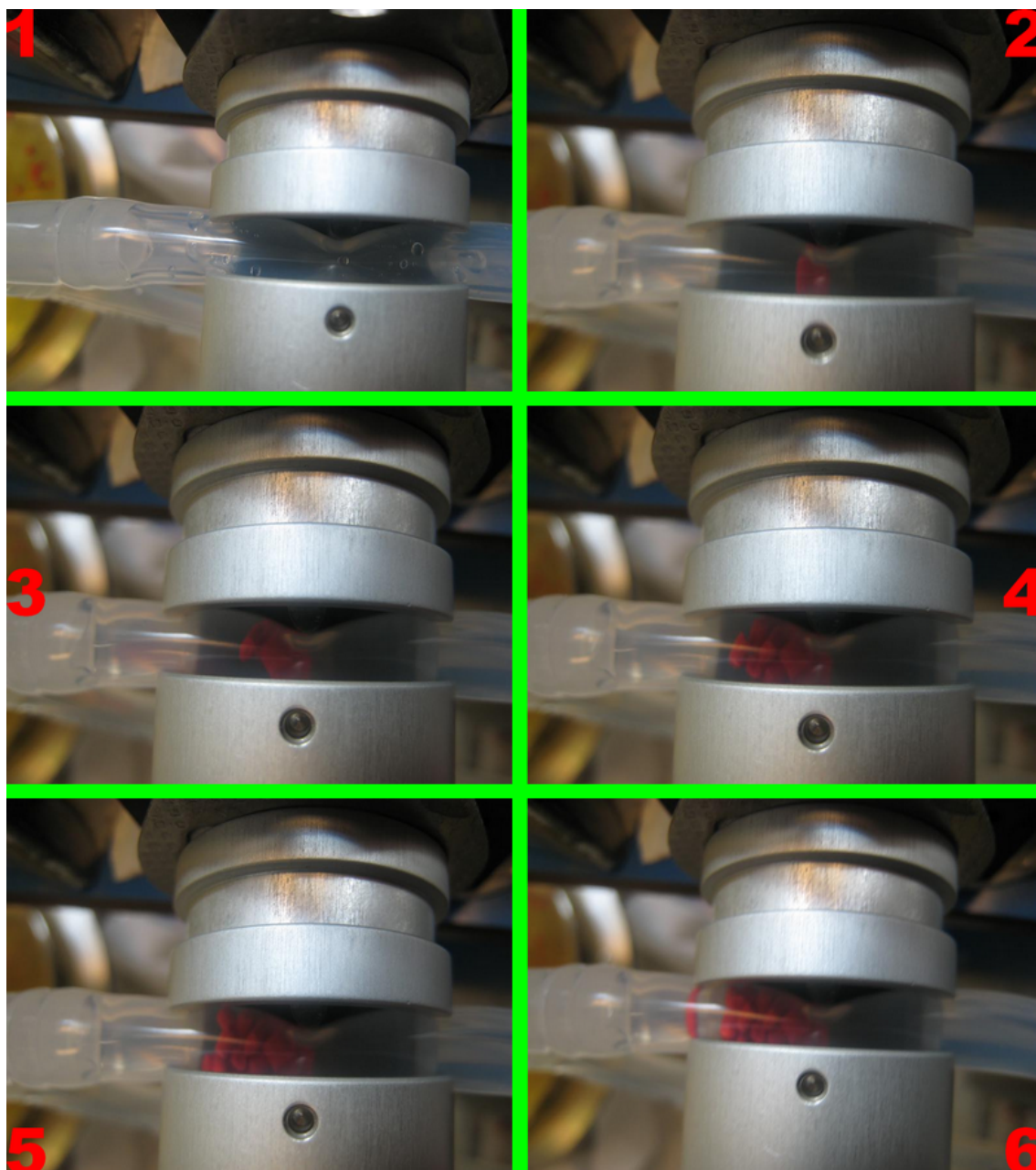
Figure 10.6: Progressive formation of the clog at the normally closed valve inlet.

Part III

TENIRS system −
Representativeness evaluation of
TENIRS sampling facility

Scopes of the TENIRS study

TENIRS stands for ***T****ransflexive* ***E****mbedded* ***N****ear* ***I****nfrared* ***S****ensor* system, this is a portable near infrared system developed at University of Kiel by the Institute of Agricultural Process Engineering (ILV) in collaboration with the manufacturer of spectroscopic solutions Carl Zeiss, Austria.

Aalborg University Esbjerg (AAUE) owns a prototype of this unit (see Figure 11.1). It has been used in different scientific studies [32–34] . The prototype is equipped with a pilot sampling device placed right after the TENIRS measuring cell. All the above studies mention that this sampling device is not completely designed in accordance with the theory of sampling, resulting in *slightly biased* samples, but none of them presents a quantification of this *slight bias*.

11.1   Aims of the study

This part of the thesis aims to evaluated the representativeness of the samples extracted with the TENIRS sampling device. The study starts by evaluating the representativeness of the TENIRS sampling device using simplistic model-systems composed by polymer pellets and water in different concentrations and ends by using a realistic model-systems composed by synthetic manure.

The third task consists in applying acoustic chemometrics to both kinds of model-systems to establish a model able to predict the dry matter content of the $1L$ bottle.
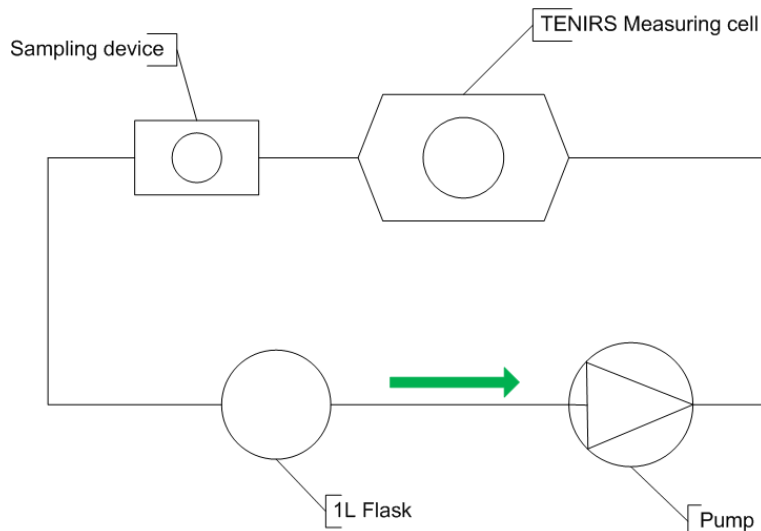
Figure 11.1: Schematic of the TENIRS loop owned by AAUE

11.2 Critical success factors

The most critical success factor common to each tasks is cleaning the loop. For the studies based on the model-systems polymer/water, it can be done by flushing with a few liters of water. When dealing with synthetic manure, more water is needed as the dry matter sticks to the pipe wall. The sampling device and the loop are to be cleaned between each experiments to limit the risk of cross contamination. Normally, the TENIRS is equipped with a valve allowing to switch from the $1L$ bottle to a large bucket of cleaning water. Unfortunately, the valve is broken had to be removed.

For the study based on the model-systems polymer/water, the second critical factor is the limited quantity of pellets owned by the university. In fact, the pellets need to be dried after each experiments. Drying the pellets ending up in the samples can be done within 5 hours where as drying the pellets remaining in the plastic bottle needs 24 hours. The experimental plans are to be switch from one to the other one the quantity of pellets is to low to continue the experimental work. The pellets from the lot are to be disposed in an aluminium box and put in the oven after the experiments. Two ovens are at disposition in the laboratory, their total capacity is 200 samples or 18 experiments.

For the study based on the synthetic manure, the second factor is the glycerol, the university owns liters of glycerol in different concentrations. Some are almost pure 99.9%w/w but most of them are aqueous solution with a concentration of glycerol varying from 50%w/w to 85%w/w. This information needs to be taken into account when preparing the batches, and the mass of water must be adjusted to have a total

mass of water in accordance with the experimental plan.

For the acoustic study the location of the sensor and the cleaning are of even importance. The sensor must be deployed to have its axis of sensitivity along the vibrations produced by the particles hitting the pipe wall. On the TENIRS system there is not many suitable locations, only one pipe is in metal, is located right after the pump. The accelerometer is to be deployed in the bend of this pipe.

The second critical success factor is the fixation of the sensor, according to [55], a steel stud should be welded or glued onto the pipe. A ceramic glue is to be used. The residual vibrations in the connecting wire can also be a problem, therefore the wires are to be taped on still surfaces before taking any measurements.

And last but not least, the noise and vibrations from the surroundings environment can also affect the measurements. Even though it is possible to treat the spectra afterwards to extract only the information of interest, the level of noise and vibrations should be limited as much as possible.

Description of the TENIRS system

12.1   The TENIRS circulation loop

The TENIRS system is constituted by an horizontal circulation loop shown in Figure 12.1. it includes a flow-through NIR measuring cell, a sampling device, an electric induction motor to ensure flow circulation, and a sample $1L$ bottle which contain the sampled material to circulate in the loop.

Figure 12.1: Front picture of the TENIRS loop.

The electric motor is controlled by a frequency convertor (Siemens Micromaster 420) allowing to set the angular velocity of the stirrer i.e. fixing the flow velocity to a desired level. The highest frequency applicable to the induction motor is $50Hz$ owing to its Delta connection to the grid.

12.2   The measuring cell

The measuring cell is made of polyoxymethylene (POM). This is a thermoplastic material with very good chemical, mechanical and thermal properties. It is acid-proof, presents a low coefficient of friction and shows good resistance to wear.

Figure 12.2 depicts the internal layout of the measuring cell as described in the studies. The inner-distance between the two silicate glass plates is equal to $3mm$. The broth[1] flow through the measuring cell and is irradiated with near-infrared light from the bottom of the cell, the near-infrared beam is reflected on a ceramic disc at the top of cell.
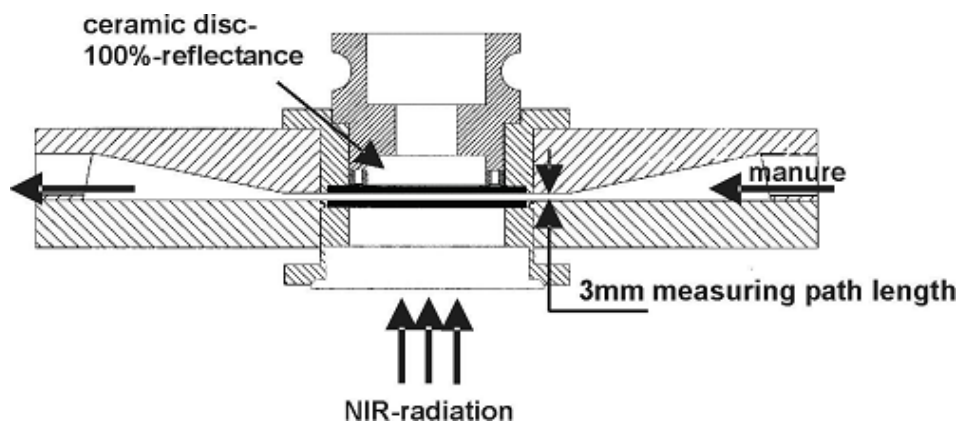
Figure 12.2: Flow-through measuring cell. [19, 32]

A quick look through the inlet of measuring cell created doubts on the actual path length between the glasses. In fact, the inner distance appeared to be higher than $3mm$. The cell was dismantled and a caliper was used to measure the inner distance (see Figure 12.3), which is equal to $6.5mm$. No adjustment of the height seems possible.

This is the first difference between the initial prototype presented by [19] and the prototype owned by AAUE.

Furthermore, according to [19] the measuring cell was designed to provide an uni-

---

[1]The TENIRS system was primarily designed to deal with liquid manure.
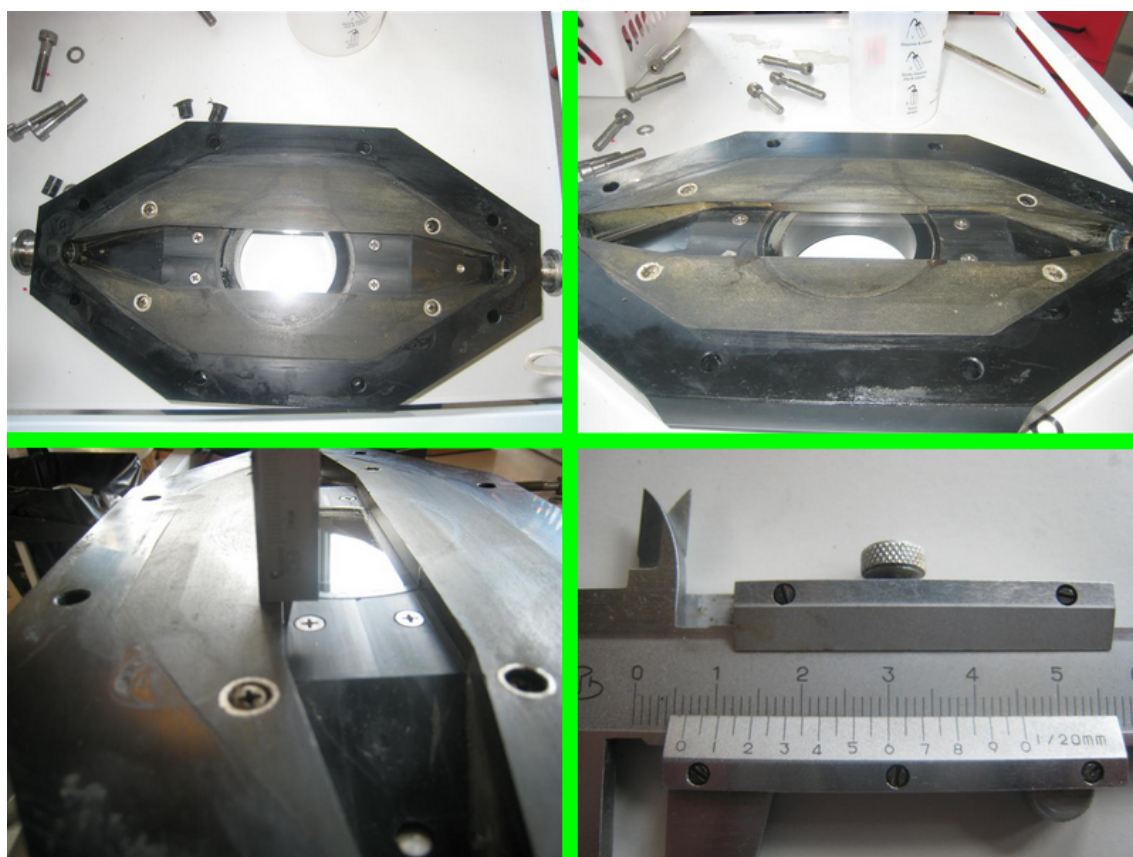
Figure 12.3: The dismantled TENIRS flow-through measuring cell.

formly distributed flow across the measuring window and to avoid separation with the manure, three built-in pins were placed at the in-let of the cell in order to create a turbulence zone and to generate remixing (see Figure 12.4). There were no turbulence pins to be observed upon dismantling the TENIRS flow-through cell (see Figure 12.3). According to the main author of [31–34], the path length between the glasses was increased and the built in pins removed to avoid clogging.
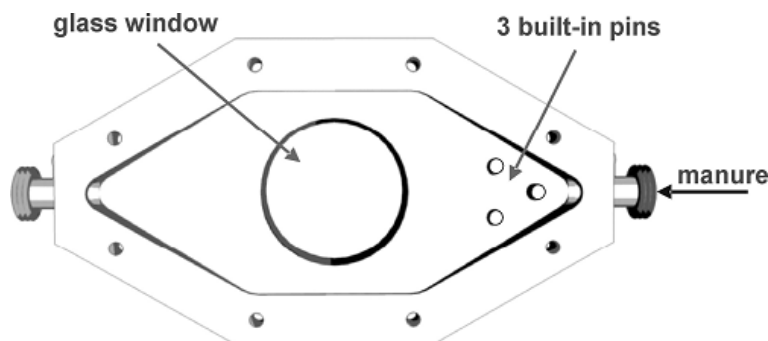
Figure 12.4: Flow-through measuring cell, interior view. [19]

12.3 The sampling device

Figure 12.5 shows the TENIRS sampling device, it consists in a $10mL$ bottle screwed in a holder placed at the *bottom* of the pipe. Samples are extracted by moving the stainless steel latch from side to side, opening and closing the aperture.
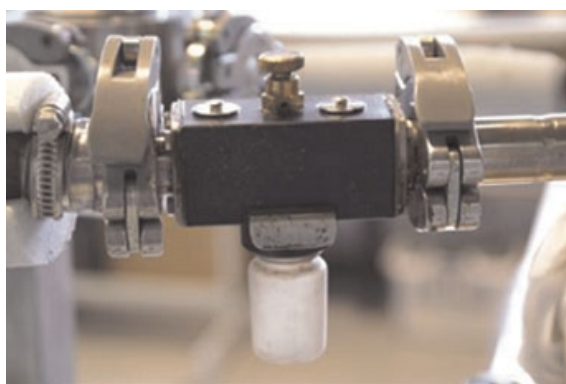
Figure 12.5: Prototype sampling device. [33, 34]

As mentioned in the different studies, the sampling device was not completely designed in accordance with the theory of sampling. Figure 12.5 reveals the first mistakes: the sample is extracted from an horizontal pipe, while it should always be extracted

from an up-stream vertically flowing piping system [26, 27]. The sampling valve is located at the bottom of the pipe, leading to an over representation of the heaviest and/or largest particles of the lot due to segregation.
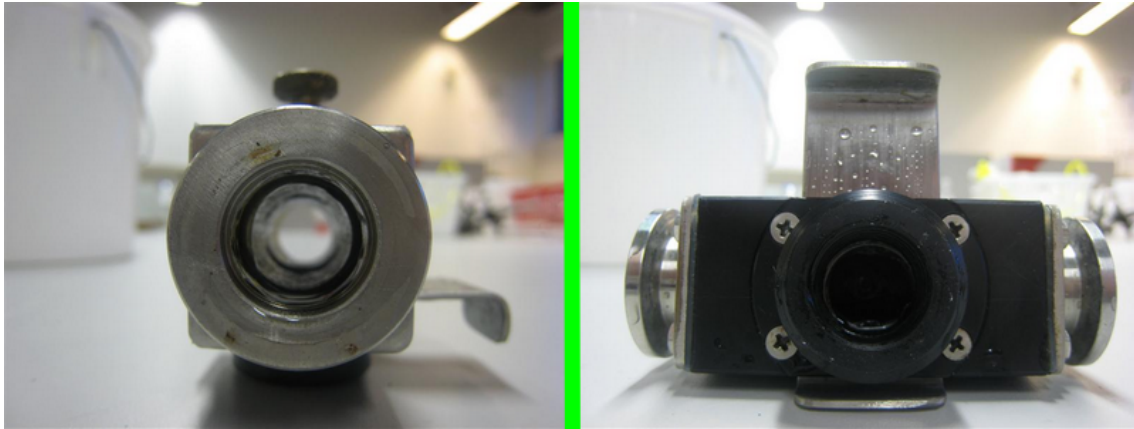
Figure 12.6: Closer view of the sampling device

Figure 12.6 shows a closer view of the sampling valve, revealing that only a part of the stream is extracted. In other words, the sampling device does not ensure a complete cross section of the stream to be extracted in the sample, constituting another mistake. According to Dr. Pierre Gy [26, 27]: *The only probabilistic method for sampling a moving stream is: Take the whole of the stream a fraction of time shared between a number of increments of short duration.* Sampling a fraction of the stream for the whole or for a fraction of the time does not lead to structurally correct samples and should never be practised [26, 27].

The valve can only be manually operated which does not allow to replicate the exact same sampling procedure over time, leading to variation in the mass of the extracted samples and in the duration of opening.

Figure 12.7 shows a cross-sectional picture of a sampling bottle. It reveals a potential problem when sampling multi-phase system containing solids. The part circled in red can act as a trap of particles leading to problems when emptying the sampling bottle for analysis.

From this analysis it can be concluded that the design of the TENIRS sampling device will not help to minimize the incorrect sampling errors. In fact, all three errors are present at different levels (IDE, IEE, IPE). Moreover, sample quality, representativeness or rather the lack hereof, seems to be highly problem-dependent, since a high velocity of the fluid in the loop may keep the particles in motion and counterbalance the effect of the gravity leading to a lower concentration of particles in the sample, whereas a low velocity leads to a higher concentration of particles – both with respect

Figure 12.7: Axial picture of a TENIRS sampling bottle.

to the actual, true, concentration in the circulating lot material, the composition of which is known in the evaluation studies.

Chapter **13**

Sampling study

The quality of a sample can be expressed in terms of its: [27]

i. Accuracy m_e^2 : defined as the absence of bias or systematic error. It is a property of the mean of the sampling errors and should be less than a low predefined acceptable value (very close to zero).

ii. Reproducibility σ_e^2 : defined as a low dispersion of repeated sample values about their mean. It is a property of the variance of the sampling errors and should be less than a low predefined acceptable value.

iii. Representativeness r_e^2 : defined as a synthesis of accuracy and reproducibility (see Equation 3.2). It is a property of the *mean square*, a combination of the mean *and* the variance of the sampling errors.

The procedure used hereafter is similar to that used by [32–34], 10 increments of $10mL$ are extracted during a period of 10 minutes and gathered to form a *composite sample* of $100mL$. Each increment can also be seen as a grab sample of $10mL$ and will therefore be analyzed independently. The composite sample made of those 10 increments is not representative of the lot because the increments are not free of sampling error, but this is the only way to build a composite sample using the TENIRS system as only a specific kind of bottles can be used and their volume is limited to $10mL$. As such it is a very good representation of all earlier uses of TENIRS [32–34].

113

13.1   Plastic pellets study

The model-systems are composed by water and two different kinds of plastic pellets added in different realistic quantities. The typical value of the dry matter content found in the feedstock used in anaerobic digestion (from 5.0% to 10.0% [3, 4]) is used as a basis to prepare the $1L$ bottle.

The plastic pellets have the same density, but two different masses: the red pellets are lighter and smaller than the yellows (see Figure 13.1). The mass of the red pellets is approximatively equal[1] $\pm 0.006g$ and the mass of the yellow pellets is ± 0.013. For the next developments, the term *heavy pellets* (HP) refers to the yellows and *light pellets* (LP) to the reds.

This simplistic model system, is believed to mimic the essentials of more complex real-world systems, especially with respect to the hydrodynamic behavior of multi-phases system.
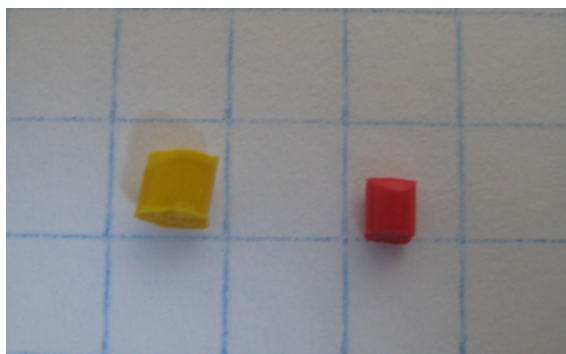
Figure 13.1: Picture of the plastic pellets used in the study.

13.1.1   Experimental conditions

After each extraction, the mass of the sampling bottle is recorded when it is full and when it is empty an dried, the plastic pellets are poured in a pyrex beaker and dried during 5 hours at $75°C$, their mass is recorded when dried using a Sartorius CP323S precision scale. Each experiment leads to a total of 11 beakers, 10 *so-called* increments and 1 containing the particles flushed out when cleaning the loop.

For each experimental condition defined below, the number of replicates is 5 i.e. 5 batches are prepared and the system is flushed with water between each replicate[2].

---

[1]Based on the measurements of the mass of 1, 5, 10, 20, 50, 75, 100 pellets.
[2]The preparation procedure of the batches can be found in Appendix G on page 197.

The cleaning is done by opening the loop and connecting it to a bucket of cleaning water, a sieve is placed at the outlet to catch the pellets remained in the system.

It is decided to perform a full factorial design, leading to a total of 110 experiments, for each experimental plan, a randomized laboratory report of the design is generated using The Unscrambler v9.2.

Light – red – pellets study. The experimental plan is as follow:

  i. Dry matter content: 5, 7.5, and 10% of the total mass;
 ii. Pump frequency: 10, 20, and 30 Hz;
iii. Replication factor: 5 (45 experiments).

Heavy – yellow – pellets study The experimental plan is as follow:

  i. Dry matter content: 5, 7.5, and 10% of the total mass;
 ii. Pump frequency: 10, 20, and 30 Hz;
iii. Replication factor: 5 (45 experiments).

Light and heavy – red and yellow – pellets study. The experimental plan is as follow:

  i. Dry matter content: 5% of the total mass;
 ii. Concentration of light/heavy pellets: 75/25 and 50/50 %
iii. Pump frequency: 20 and 30 Hz;
 iv. Replication factor: 5 (20 experiments).

13.2 Synthetic manure based study

The synthetic manure is composed by lignocellulosic fibers, rapeseed, glycerol and water in different amounts. To remain realistic and stay under the clogging concentration of the TENIRS system, the dry matter content is kept under 10% [3, 4]. Figure 13.2

shows a typical batch of synthetic manure. The solid constituents are allowed to swell for a period of 24 hours before experimentation in order to make this synthetic manure as realistic as possible.

Figure 13.2: Upper left: rapeseed. Lower left: lignocellulosic fibers. Right: a ready-to-use bottle of synthetic manure (dry matter = 10%).

For each experimental conditions defined below, the number of replicates is 3 i.e. 3 batches are prepared and the system is flushed with water between each replicate. Therefore, each experiments is performed with a new batch[3].

The laboratory routine used for this part is the same than that used for the study based on the plastic pellets.

13.2.1   Experimental conditions

The experimental plan for the synthetic manure based study is as follow:

---

[3]The preparation procedure of the batches can be found in Appendix G on page 197.

   i. Dry matter content: 2.5, 5.0, and 7.5% of the total mass;

  ii. Concentration of fibers/rapeseed: 25/75% of the total dry matter content;

 iii. Concentration of Glycerol: 5% of the total mass;

 iv. Pump frequency: 20 and 30 Hz;

  v. Replication factor: 3 (18 experiments).

It is decided to perform a full factorial design. A randomized laboratory report is generated using The Unscrambler v9.2.

Acoustic measurements

14.1 Sensor deployment

Acoustic chemometrics is used to establish models able to predict the dry mater content of the TENIRS bottles. It is performed by mounting a standard one-axis accelerometer[1] (DeltaTron, type 4396, Brüel & Kjær, Denmark) on the metal pipe right after the pump (see Figure 14.1).

This kind of accelerometer is able to measure acceleration along one axis, called the axis of sensibility, therefore its location must be carefully chosen in order to capture most of the vibrations along this axis.

The censor is screwed to a steel stud glued on the bend of the pipe. This location is chosen as there is only one metal pipe in the TENIRS system. Furthermore, located right after the pump and in the bend of the pipe ensure to have a turbulent flow of particles hitting the pipe wall i.e. creating informative vibrations in the pipe wall.

The wire connecting the sensor to the PSA100i is taped on the TENIRS and the table to avoid measuring vibrations due to any motion in the wire (see the lower right part of Figure 14.1). [55]

---

[1]The procedure for acquisition of acoustic spectra can be found in Appendix F on page 195.
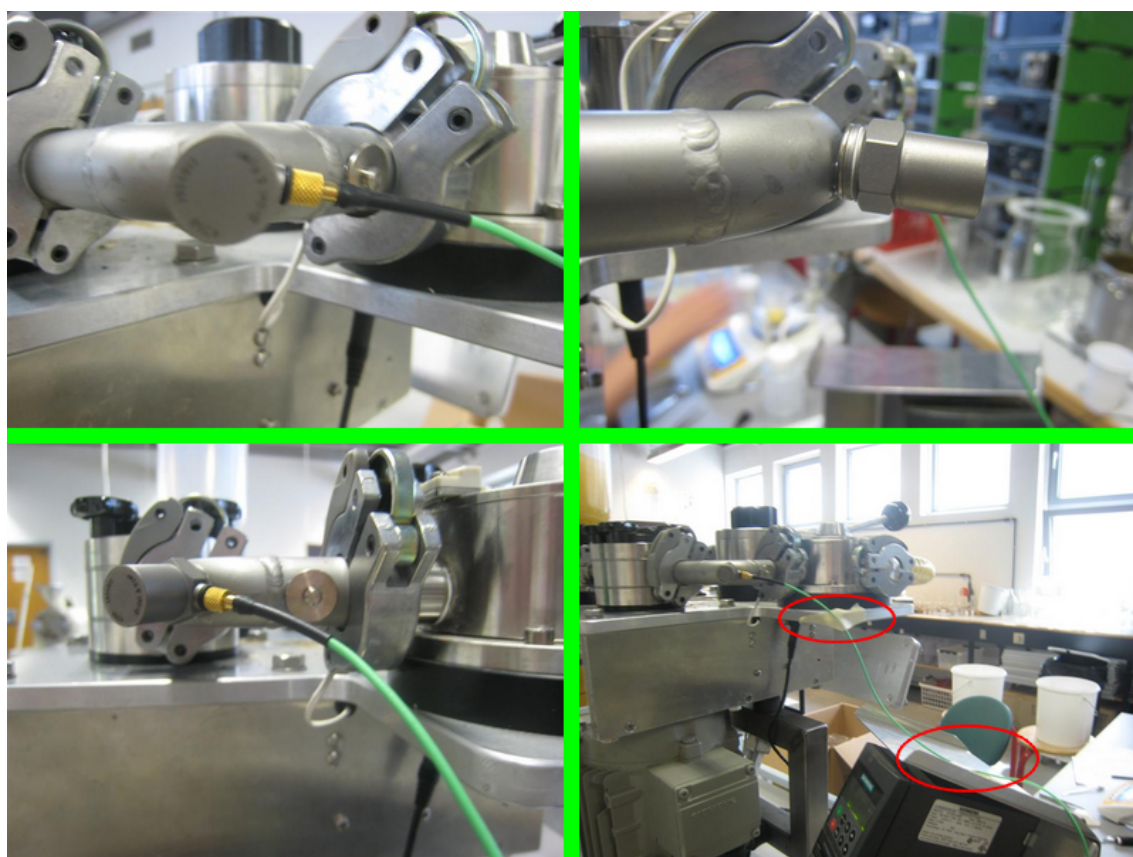
Figure 14.1: Acoustic sensor deployment on the TENIRS system.

14.2 Experimental conditions

Four series of spectra acquisitions are to be performed, one using exclusively the heavy (yellow) plastic pellets, one using exclusively the light (red) plastic pellets, one simultaneously using both kind of pellets, and the last one using the synthetic manure. Fast Fourier Transform spectra are calculated as the mean of 100 acquisition of time series. The TENIRS pump frequency is set on $40Hz$.

For each campaign of acquisitions a calibration set and a validation set i.e. test set [15] is acquired.

Between each batches the loop is flushed with cleaning water. Prior to measurements the loop is circulated at high speed and then the frequency is set on $40Hz$. After 5 minutes the TENIRS is considered to be in steady state and the acquisition is performed.

For each experimental plan a randomized laboratory experimental plan of the design is generated using The Unscrambler v9.2. A total of 160 acoustic spectra is to be acquired.

Light – red – pellets study.   The experimental plan is as follow:

 i. TENIRS pump frequency: $40Hz$.
 ii. Calibration Set – Dry matter concentration spanning from 0 to 15% by increments of 0.50%.
 iii. Validation Set – Dry matter concentration spanning from 1 to 15% by increments of 1.0%.
 iv. Number of spectra: 46.

Heavy – yellow – pellets study   The experimental plan is as follow:

 i. TENIRS pump frequency: $40Hz$
 ii. Calibration Set – Dry matter concentration spanning from 0 to 15% by increments of 0.50%.
 iii. Validation Set – Dry matter concentration spanning from 1 to 15% by increments of 1.0%.
 iv. Number of spectra: 46.

Light and heavy – red and yellow – pellets study. The experimental plan is as follow:

  i. TENIRS pump frequency: $40Hz$

 ii. Calibration Set and Validation Set – Dry matter concentration spanning from 5 to 10% by increments of 5.0%.

iii. Calibration Set – Yellow/Red concentration: $i/100 - i\%$ with i spanning from 0 to 100% by increments of 10.0%.

 iv. Validation Set – Yellow/Red concentration: $i/100 - i\%$ with i spanning from 0 to 100% by increments of 20.0%.

  v. Number of spectra: 51.

Synthetic manure study. The experimental plan is as follow:

  i. TENIRS pump frequency: $40Hz$

 ii. Calibration Set *and* Validation Set – Concentration of fibers/rapeseed: 25/75% of the total dry matter content.

iii. Calibration Set *and* Validation Set – Concentration of glycerol: 5% of the total batch mass.

 iv. *Calibration Set* – Dry matter concentration spanning from 0 to 10% by increments of 1%.

  v. *Validation Set* – Dry matter concentration spanning from 1.5 to 9.0% by increments of 1.5%.

 vi. Number of spectra: 17.

Chapter 15

Discussion

15.1 Pilot study

Prior to the sampling evaluation a pilot study was performed to point out as many problems as possible in order to adjust, if need be, the experimental procedure.

15.1.1 Plastic pellets experiments

Two of the problems revealed by the pre-study are shown in Figure 15.1. As we can see the sampling device introduces an increment extraction error (IEE), because particles are trapped between the sampling device body and the latch. The second problem was expected (see Figure 12.7), i.e. particles are trapped in the red circled part of the bottles, leading to problems when emptying them for subsequent analysis. In fact it is impossible to weight the entire content of the bottle reliably.

Therefore, the dry matter content determination is performed as follow: the bottle wall must by dried after extraction e.g. by using a paper towel, the full bottle must be weighted (m_b^f), emptied, cleaned, dried, and weighted empty (m_b^e). Equation 15.1 gives a good approximation of the total sample mass m_s.

$$m_s = m_b^f - m_b^e \qquad (15.1)$$

The clogging concentration was found to be equal to 15% of dry matter. The clog
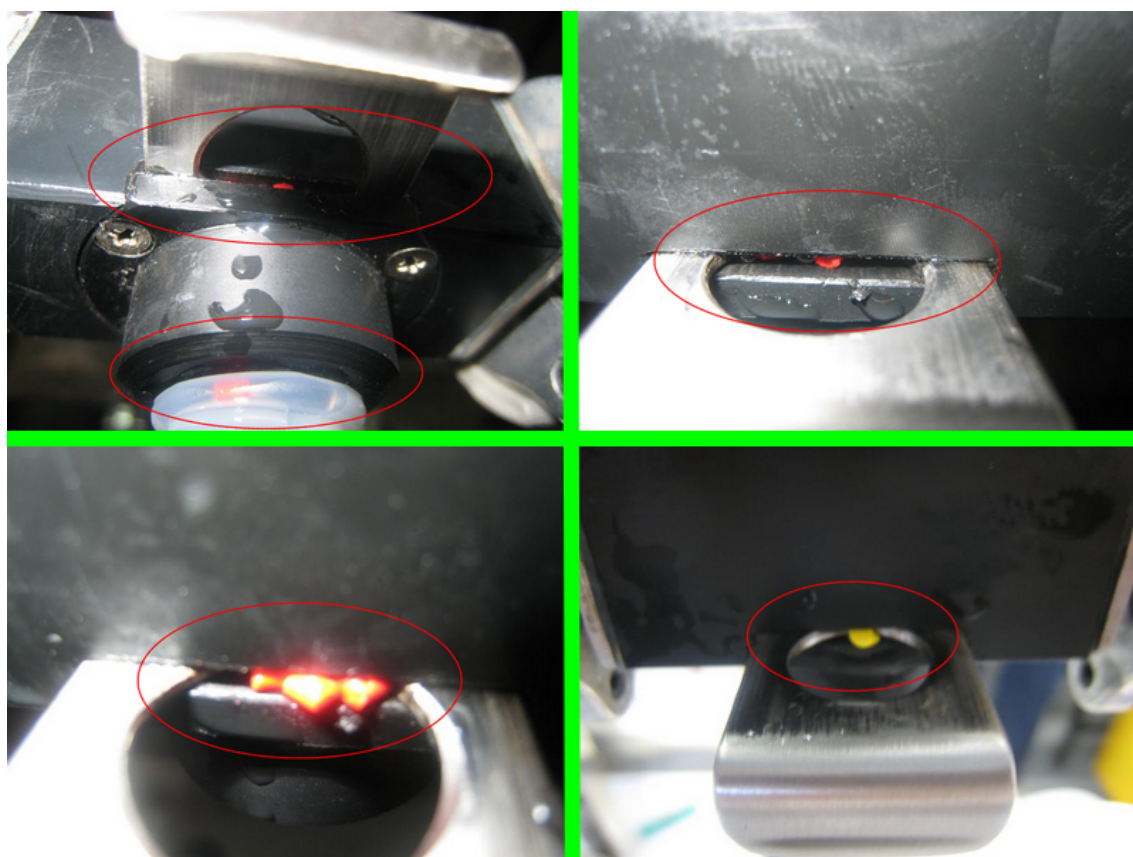
Figure 15.1: Increment extraction error (IEE) on the TENIRS sampling device.

is formed between the $1L$ bottle and the pump (see Figure 15.2).

Figure 15.2: Clogging concentration: 15% of dry matter.

As depicted in Figure 15.3, the plastic particles have a very clear tendency to segregate. The photos were taken at the outlet of the sampling device. The segregation decreases when the frequency increases.
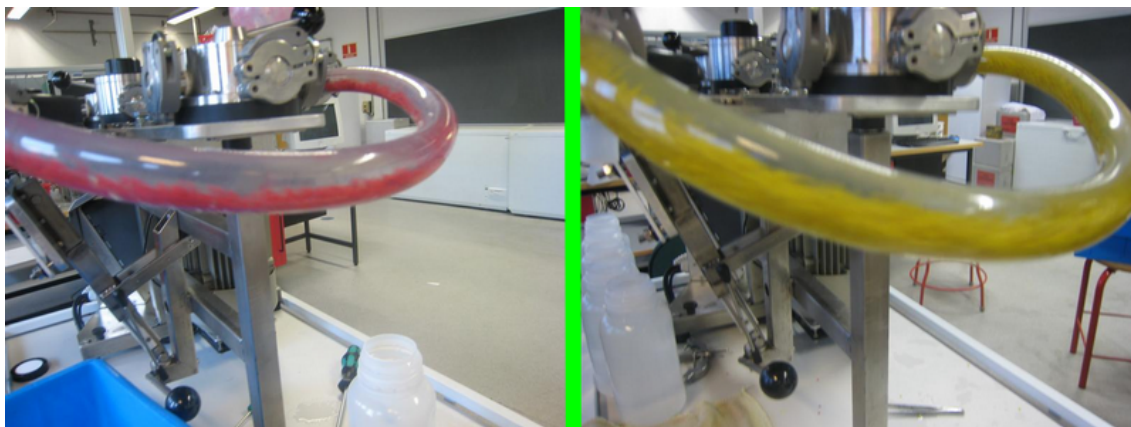
Figure 15.3: Segregation at the outlet of the sampling device.

The last problem pointed out by the pilot study is shown in 15.4. It was routinely observed that air bubbles could get caught up inside the top glass plate in the measuring cell, they could be flushed out by circulating the loop at high speed. They act as a damaging particle trap which most certainly leads to a significant sampling bias.
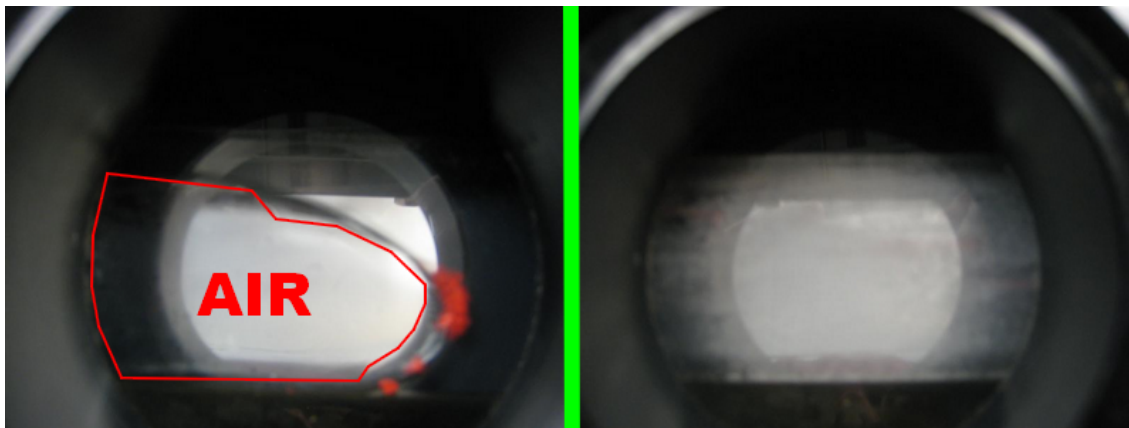
Figure 15.4: Left: photo of an air bubble intermittently located in the measuring cell. The bubble is acting as a damaging particle trap. Right: photo of the measuring cell in steady state

15.1.2 Synthetic manure based experiments

The above issues remain valid for the synthetic manure. The clogging concentration was here evaluated around 7.5% (see Figure 15.5). However, the experimental plan was not changed since it seems to be possible to use higher concentrations by starting the pump at high speed and then set the $1L$ bottle in circulation mode.

Figure 15.5: Clogging concentration: 7.5% of dry matter.

Increment extraction errors are still present as shown in Figure 15.6, however in the case of synthetic manure, not only particles are pushed out but also the fluid medium! Extracting chemicals containing acid might thus be directly armful!
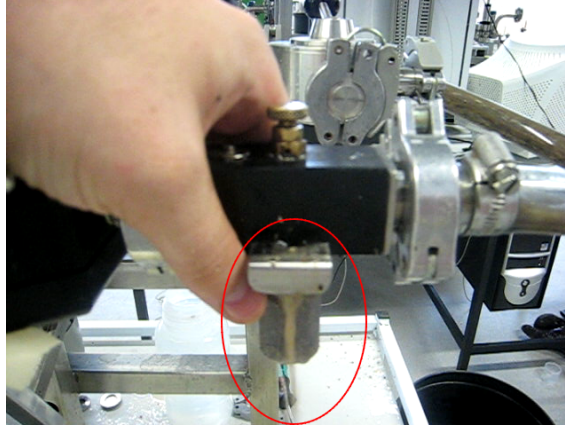
Figure 15.6: Several increment extraction errors (IEE) on the TENIRS sampling device.

15.2 Sampling study

The quality of a sampling device can be expressed in terms of its accuracy m_e^2, reproducibility σ_e^2, and representativeness r_e^2. They are calculated as follows:

$$e = \frac{a_S - a_L}{a_L} \tag{15.2}$$

Here e is the relative sampling error, a_S is the grade of the analyte in the sample and a_L the grade of the analyte in the lot. a_L is known – designed – and a_S is determined by the experiments. m_e is the average sampling error, σ_e^2 is its variance and the representativeness is defined by

$$r_e^2 = m_e^2 + \sigma_e^2 \tag{15.3}$$

A composite sample is made of ten $10mL$ increments extracted from the TENIRS loop, the relative sampling error on the composite sampling will thus be the sum of the errors of each increments. However, each increments are extracted using a non representative way as the sampling device is not in accordance with TOS. Therefore, the present composite sample cannot be considered as representative in the ultimate TOS fashion.

15.2.1   Bias

The bias is calculated as the average grade of the sample replicate minus the true known grade of the lot. The bias can also be expressed in percent of the true grade of the lot (Equation 15.2).

The bias presented in Figures 15.7–15.12 are the average bias of the individual increments and the average bias of the composite samples.

The magnitude of the bias of individual increments are close to that of the corresponding composite samples[1]. This is due to the size of the increments (the mass m_i of each increment is included in $[9.0; 11.0]$ and the average mass is equal to $[10.0 \pm 0.165]g$) and the lack of representativeness of the individual increments, i.e. as the individual increments are not representative of the true analytical grade of the lot, the composite sample will not be representative either.

15.2.1.1   Plastic pellets based experiments

Figures 15.7–15.11 present the biases for the experiments made with the model-systems polymer/water.

As delimited above, the average bias magnitudes of the composite samples and that of the individual increments are very close for each experiments.

It can be seen that the general trend is a decreasing bias from low frequencies to high frequencies i.e. from low circulation speeds to high. At a frequency between $20Hz$ and $30Hz$ the bias cross the abscise axis, effecting to a bias close to zero for this model-systems polymer/water and only for this specific, material-dependent circulation speed.

These relatively simplistic model-systems are believed to mimic the essentials of more complex real-world systems, especially with respect to the hydrodynamic behavior of multi-phases system. They give us a good illustration of the lack of quality of the sampling device.

The biases testify of the segregation taking place at the bottom of the pipe when the loop is circulated at low speed as many particles are trapped on the latch of the sampling device between two extractions. When circulated at high speed, the bias decreases as more particles remain in suspension in the flow.

---

[1] See Appendix E on page 191 for mathematical developments.

It can also be noticed from Figures 15.7 and 15.8 that, for the model-systems light and heavy pellets separately, the bias decreases not only with respect to the loop velocity but also with the concentration of polymer in the TENIRS bottle. When the dry matter content increases, the bias tend to decrease for all model-systems.
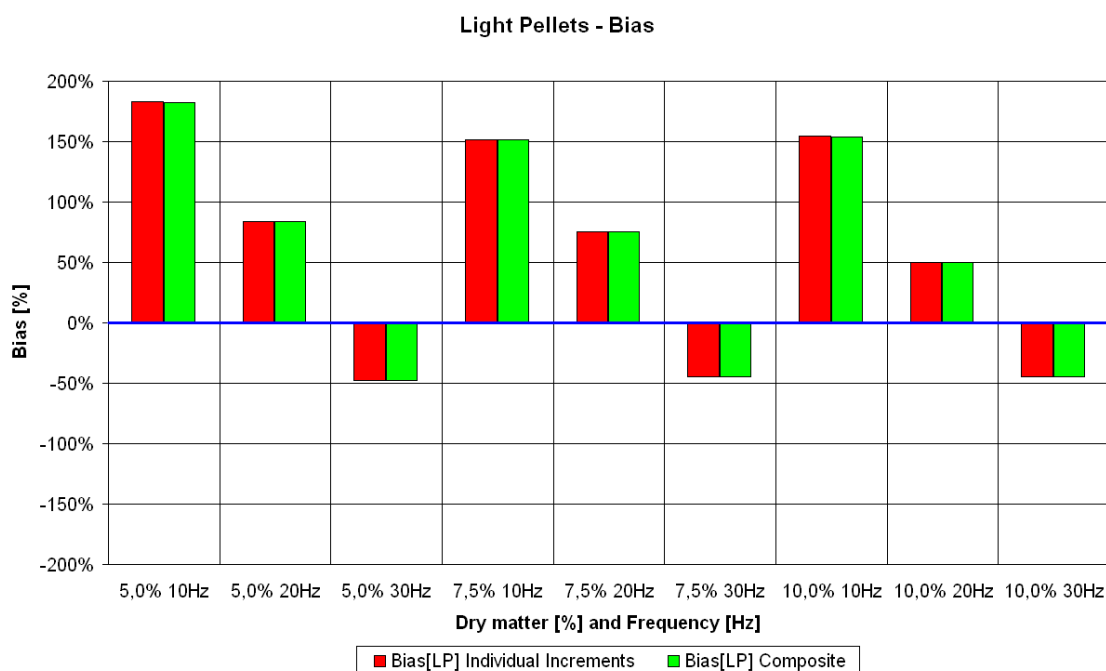
Figure 15.7: Model-systems made of light pellets – Bias of the individual increments and the composite samples
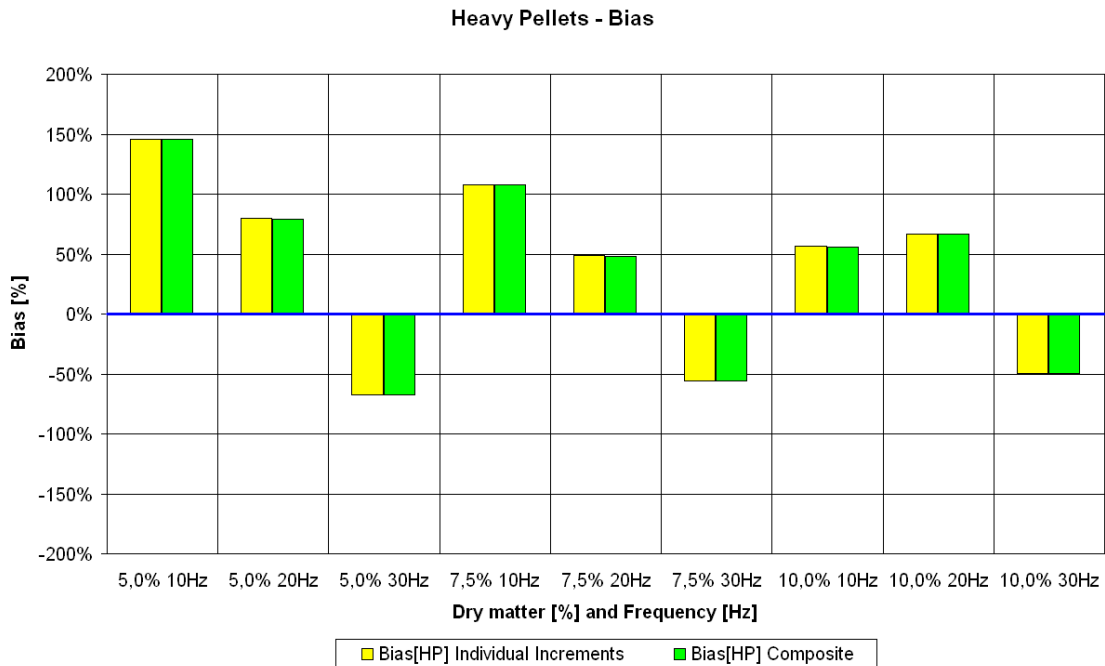
Figure 15.8: Model-systems made of heavy pellets – Bias of the individual increments and the composite samples

The interpretation is not so clear for the model-systems light and heavy pellets simultaneously, the total dry matter content was constant for all the experiments, only the ratio of light/heavy pellets changed. It can be concluded that at $20Hz$ the bias increases when the particles were in even proportions (see Figures 15.9–15.11). The biases of light pellets (as high as 175% – see Figure 15.9) are clearly higher than those of the heavy pellets (less than 50% – Figure 15.10). Whereas at $30Hz$ the tendency is in the other way, the biases of the heavy pellets (as low as -75% –Figure 15.10) are higher than those of the light pellets (as low as -50% – see Figure 15.9).
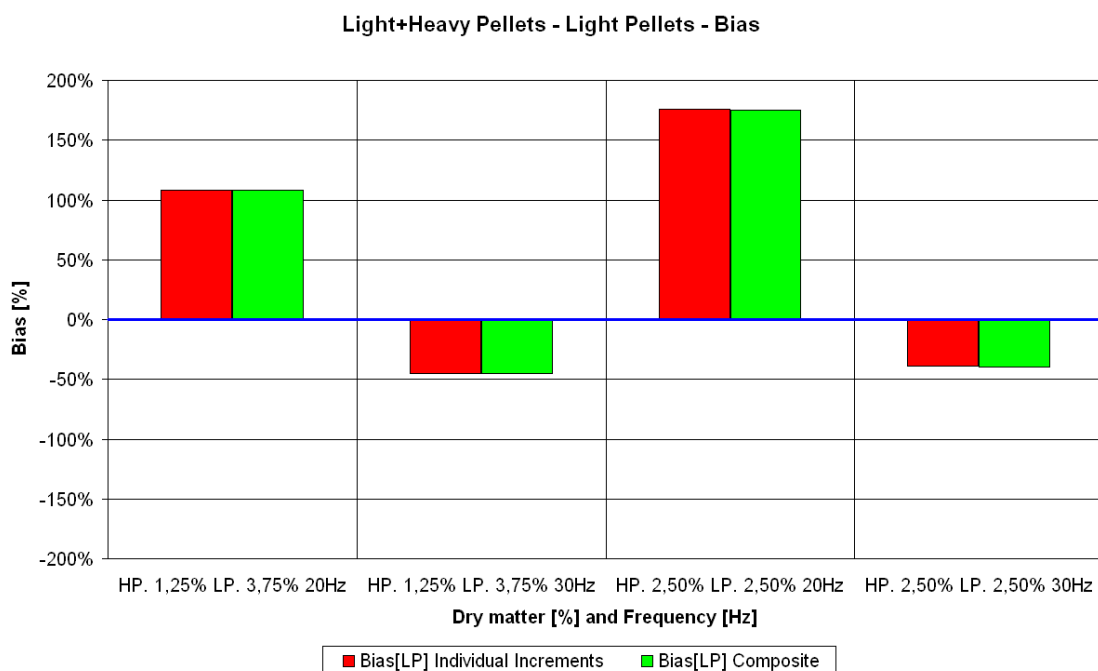
Figure 15.9: Model-systems made of light+heavy pellets – Bias for the light pellets of the individual increments and the composite samples
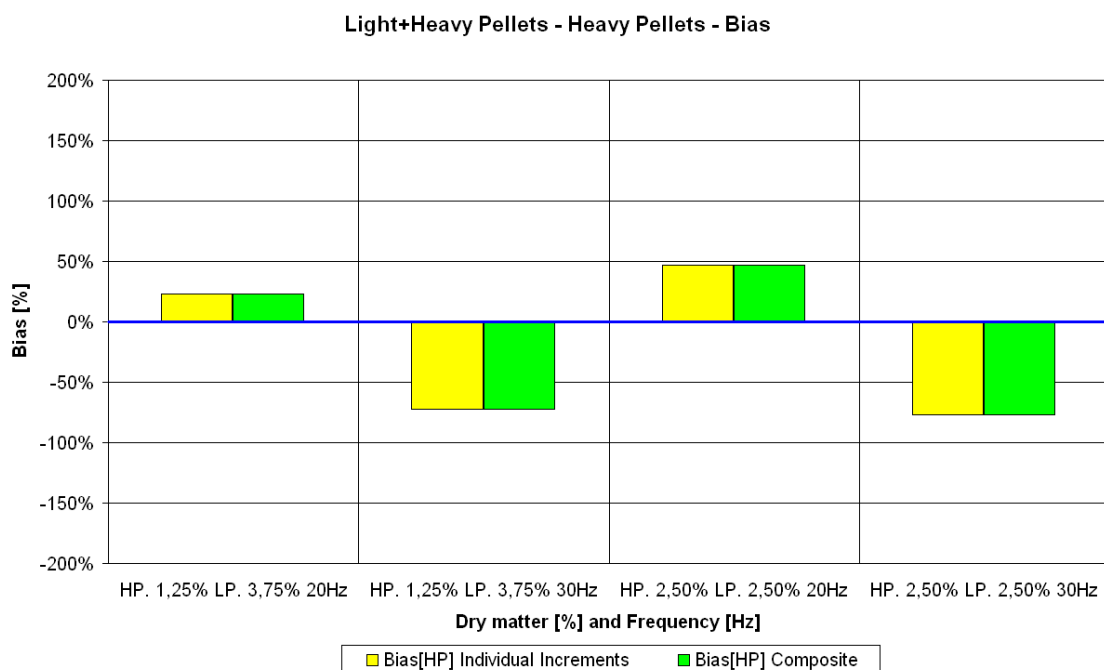
Figure 15.10: Model-systems made of light+heavy pellets – Bias for the heavy pellets of the individual increments and the composite samples

Figure 15.11 shows the bias with respect to the total dry matter of the model-systems light and heavy pellets simultaneously. These biases appear to be lower than those showed in Figures 15.9 and 15.10.
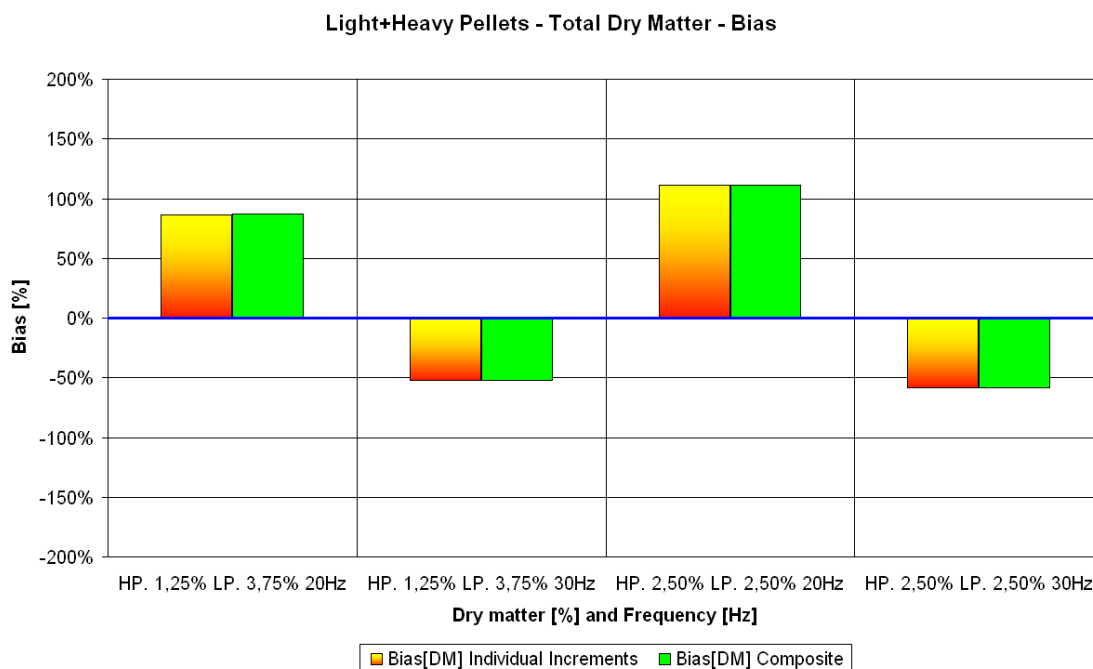
Figure 15.11: Model-systems made of light+heavy pellets – Bias for the total dry matter of the individual increments and the composite samples

15.2.1.2 Synthetic manure experiments

Figure 15.12 presents the biases for the experiments based on the synthetic manure. Once again, it can be seen that the bias decreases with respect to the frequency of the pump. Unlike the experiments based on the plastic pellets, the bias does not become negative at $30Hz$. The results are highly system- and frequency-dependents.

The synthetic manure is a simulate manure, its hydrodynamic behavior should not be taken as strictly identical to the behavior of real manure. Nevertheless, it is believed that it represents a good approximation. In fact the composition of the synthetic manure was suggested by colleagues used to deal with manure for a long time, one of them is the main author of [31–34].

The TENIRS samples are heavily biased at low frequency and low concentration (up to 320% for a dry matter content of 2.5% and a frequency of $20Hz$). When the concentration increases the bias gradually decreases (to 15% for a dry matter content

of 7.5% and a frequency of $30Hz$), this can be explained by the fact that the sampling valve more or less always extracts the same mass of dry matter whatever the grade of the lot!
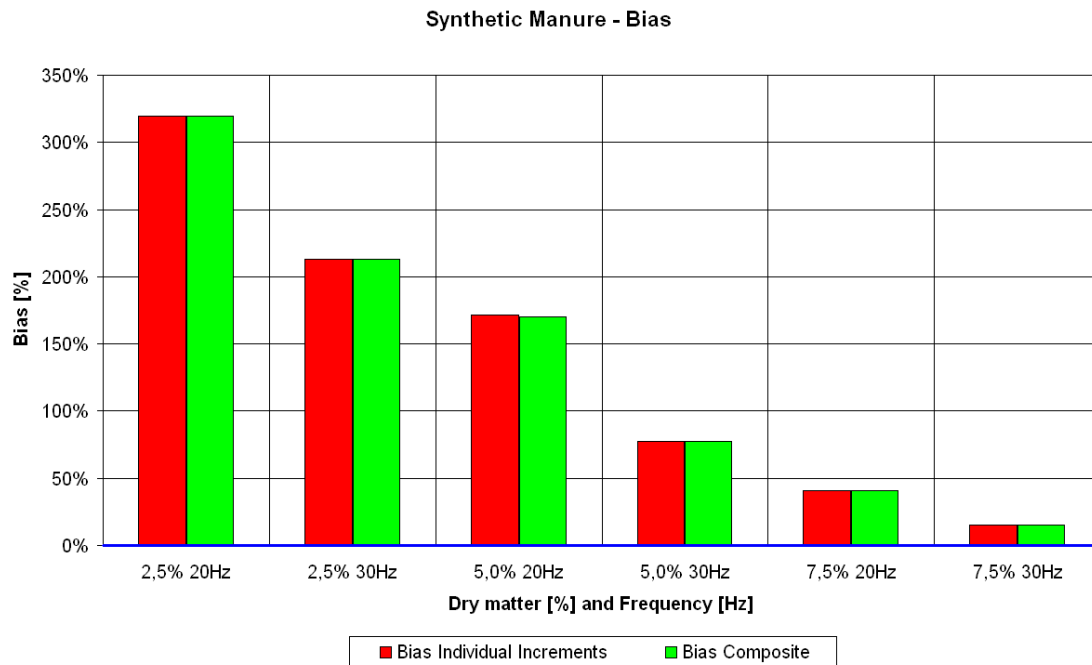
Figure 15.12: Model-systems made of synthetic manure – Bias of the individual increments and the composite samples

15.2.2 Representativeness

15.2.2.1 Plastic pellets based experiments

Figures 15.13–15.22 present the representativeness r^2, the accuracy m^2 and the reproducibility σ^2 of the sampling device for the experiments based on the plastic pellets.

From all of these it is possible to conclude that the TENIRS sampling device is functioning in a fashion which can be characterized as being *precisely wrong* i.e. its reproducibility σ^2 is very good and, in the cases of the composite samples, often close to zero, however it is not accurate at all!

Even though, the results are still heavily biased, the composite samples generally present a slightly better accuracy and reproducibility[2] than the individual increments,

---

[2]As would say Albert Einstein: Everything is relative!

allowing to conclude that composite sampling is *always* better than grab sampling even if the increments are extracted with a clumsy sampling device!

For the model-systems of light and heavy pellets separately (see Figures 15.13–15.16), the representativeness of the samples get slightly better when the dry matter content increases. When the circulation speed increases, the representativeness get significantly better. This can be explained as follows: more particles remain in suspension in the flow resulting in less particles trapped and caught by the TENIRS sapling device.

The reproducibility of the composite samples extracted at 20% from a lot containing 10% of light pellets is worse than the accuracy (see Figure 15.14). The only possible explanation is a problem during the extraction of the increments, in fact, the laboratory results show that the grades of nine out of the 10 increments are between three to five times lower than those of the other replicates. It believed that an air bubble was present somewhere in the TENIRS loop, trapping the particles i.e. decreasing the quantity of particles caught by the TENIRS sampling device.

Despite this obvious outliers, the reproducibilities of the composite samples are very good for both model-systems (see Figures 15.14 and 15.16) as they are close to zero.

As shown in Figures 15.13–15.16, the representativeness of the samples are material- and system-dependent since they are generally smaller for the model-systems of heavy pellets.

Light Pellets - Representativeness - Individual Increments
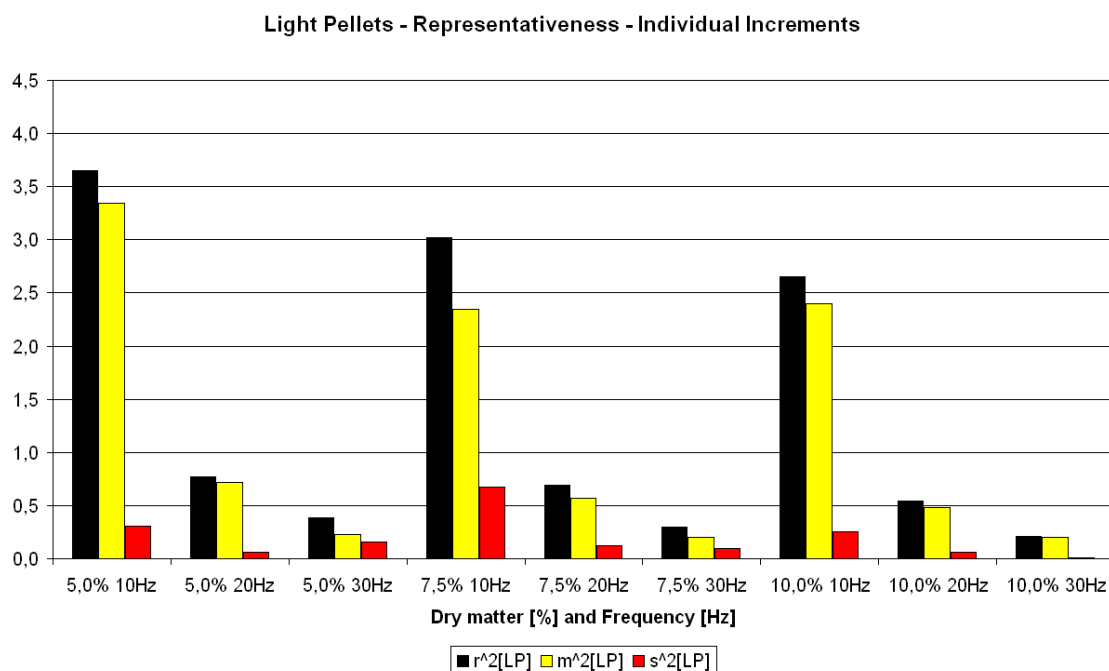
Figure 15.13: Model-systems made of light pellets – Representativeness of the individual increments.

Light Pellets - Representativeness - Composite Samples
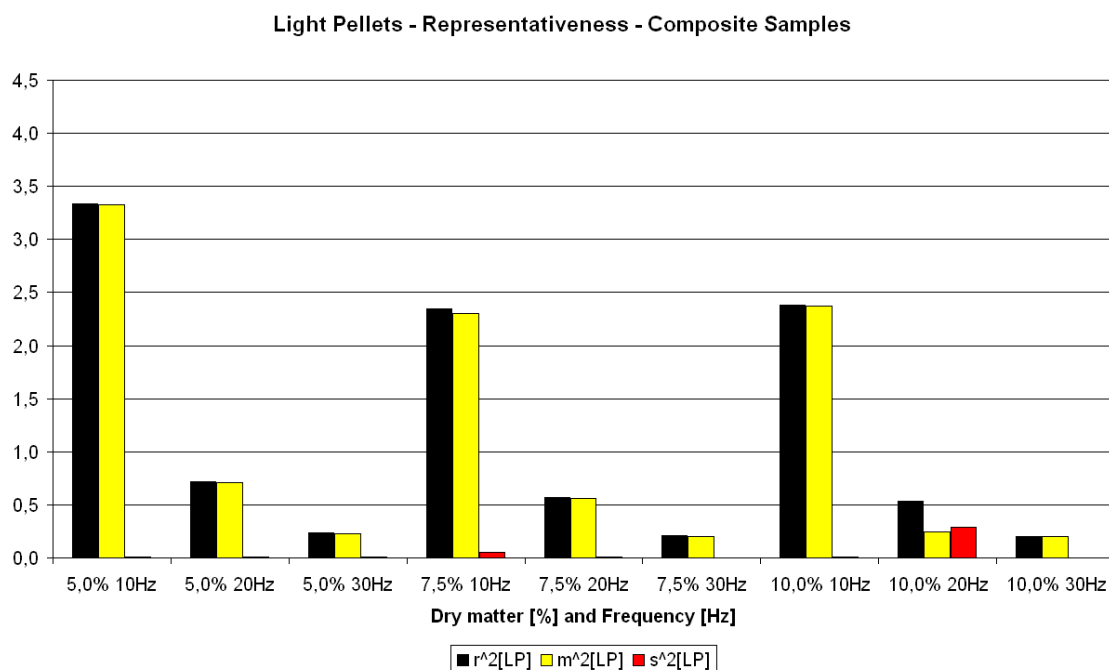
Figure 15.14: Model-systems made of light pellets – Representativeness of the composite samples.

Heavy Pellets - Representativeness - Individual Increments
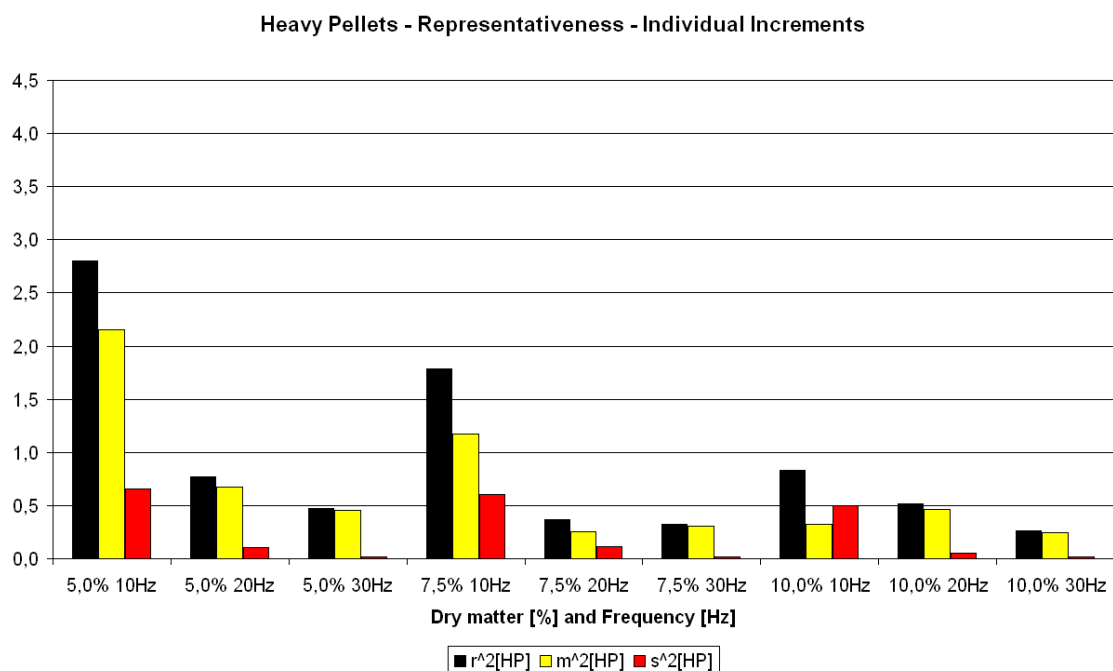
Figure 15.15: Model-systems made of heavy pellets – Representativeness of the individual increments.

Heavy Pellets - Representativeness - Composite Samples
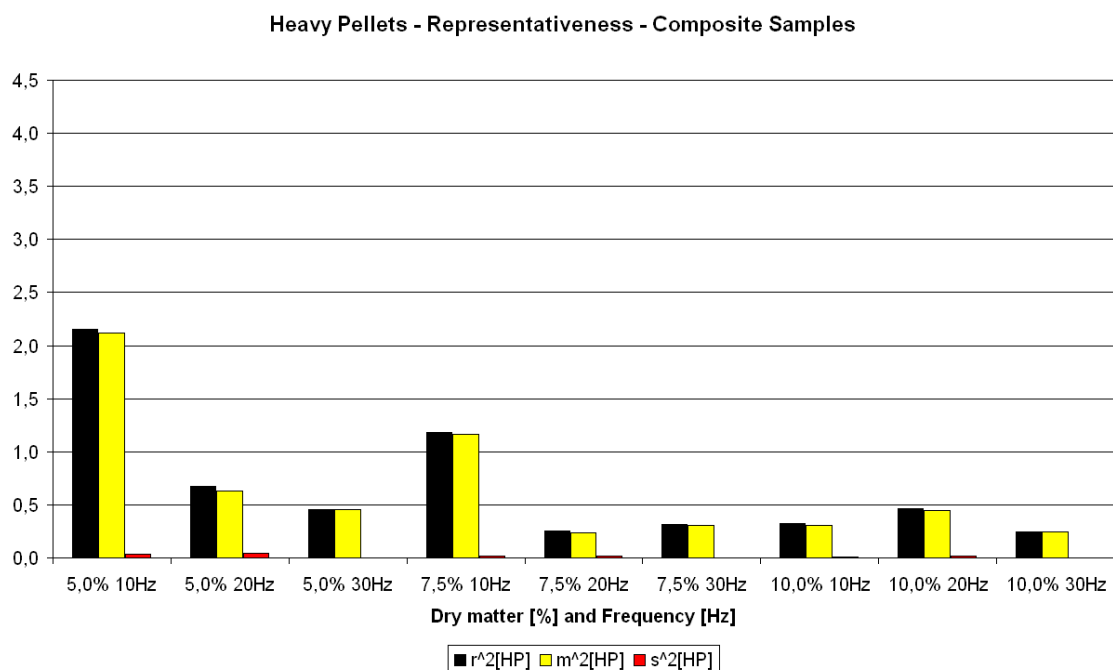
Figure 15.16: Model-systems made of heavy pellets – Representativeness of the composite samples.

Figures 15.17 and 15.18 show the representativeness for the samples regarding the concentration of light pellets for the model-systems of light and heavy pellets simultaneously. The reproducibility is good for both increments and composites, especially at $30Hz$. The accuracy is mainly responsible for the lack of representativeness which is particulary high at $20Hz$ when the concentration of pellets are even, this was expected regarding the biases commented above. The lacks of representativeness of the composite samples are lower than for the individual increments at $20Hz$ whereas they have the same order of magnitude at $30Hz$.
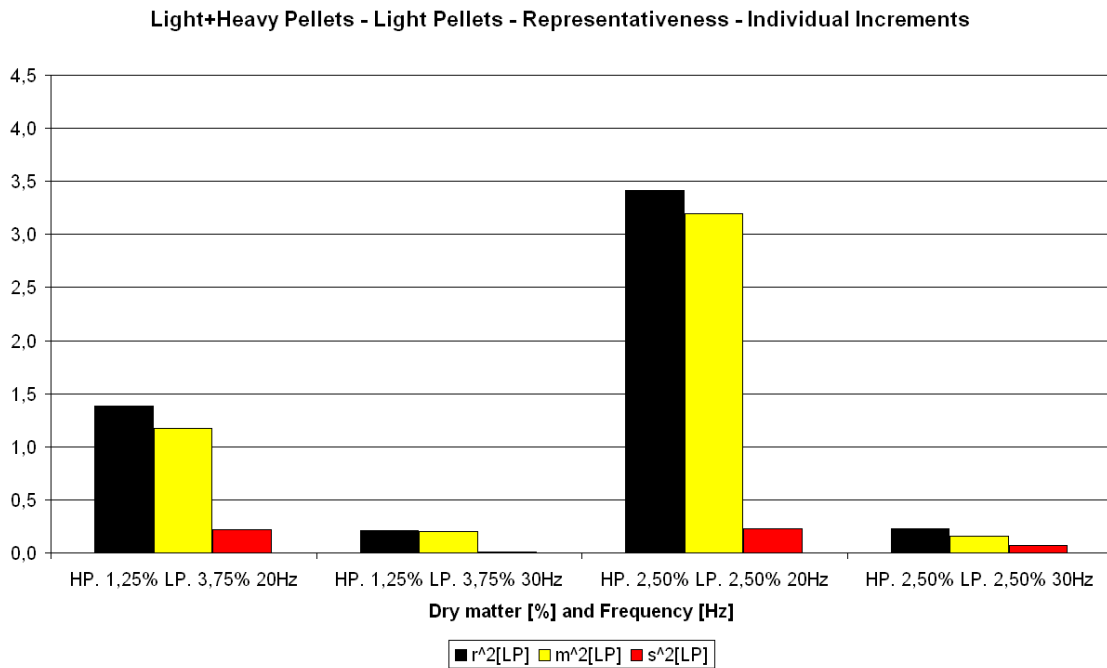
Figure 15.17: Model-systems made of light+heavy pellets – Representativeness for the light pellets of the individual increments.
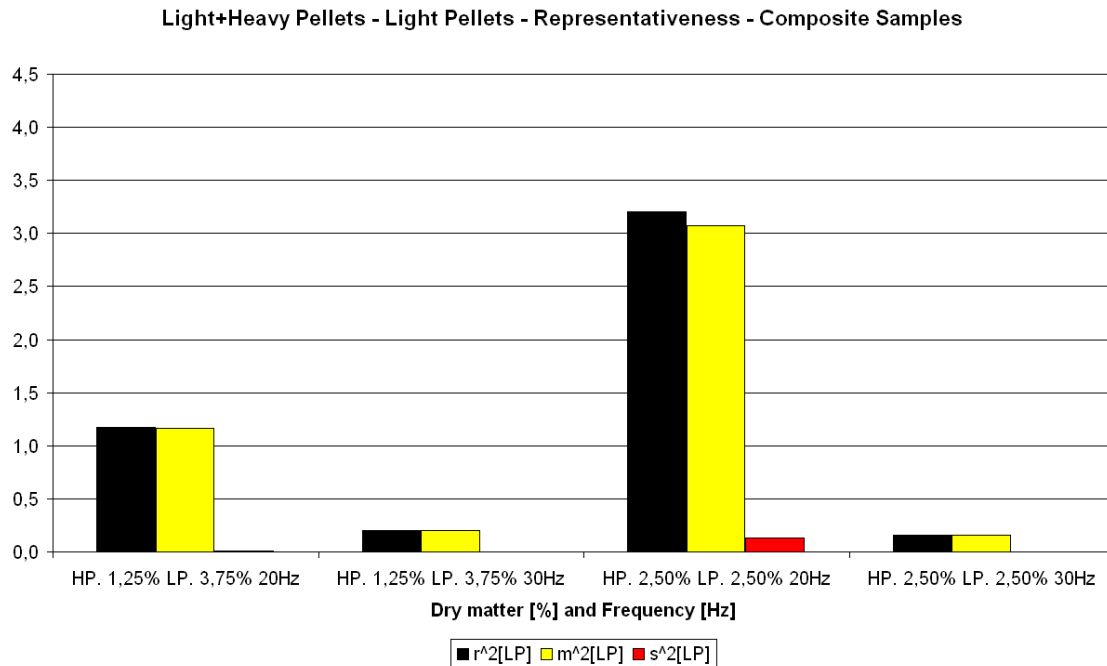
Figure 15.18: Model-systems made of light+heavy pellets – Representativeness for the light pellets of the composite samples.

Figures 15.19 and 15.20 show the representativeness for the samples regarding the concentration of heavy pellets for the model-systems of light and heavy pellets simultaneously. A high frequency ($30Hz$) leads to a higher lack of representativeness than a low one ($20Hz$). This observation is not in accordance with that made for the model-systems only based on the heavy pellets. Once again, it can be said that the behavior of the TENIRS sampling device is system- and material-dependent. The lacks of representativeness of the composite samples are lower than for the individual increments. It can be seen on Figure 15.20 that for the first concentration (1.25% of heavy particles and 3.75% of light particles) the composite samples are representative of the true concentration of heavy pellets in the lot, as r^2 is close to zero ($r^2 < 0.01$).
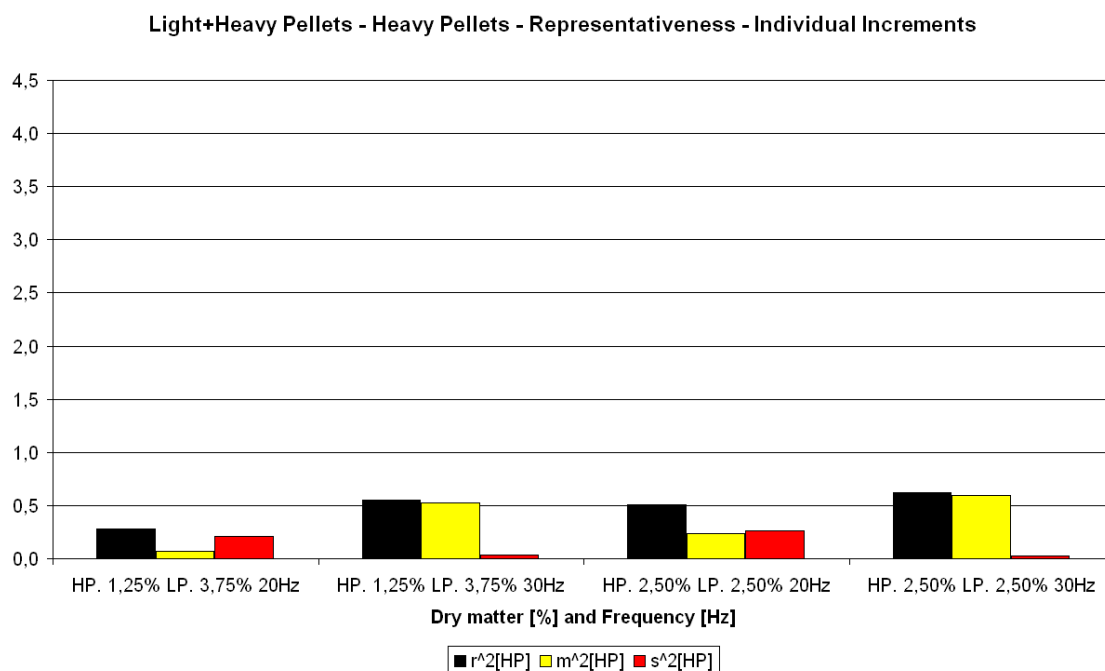
Figure 15.19: Model-systems made of light+heavy pellets – Representativeness for the heavy pellets of the individual increments.
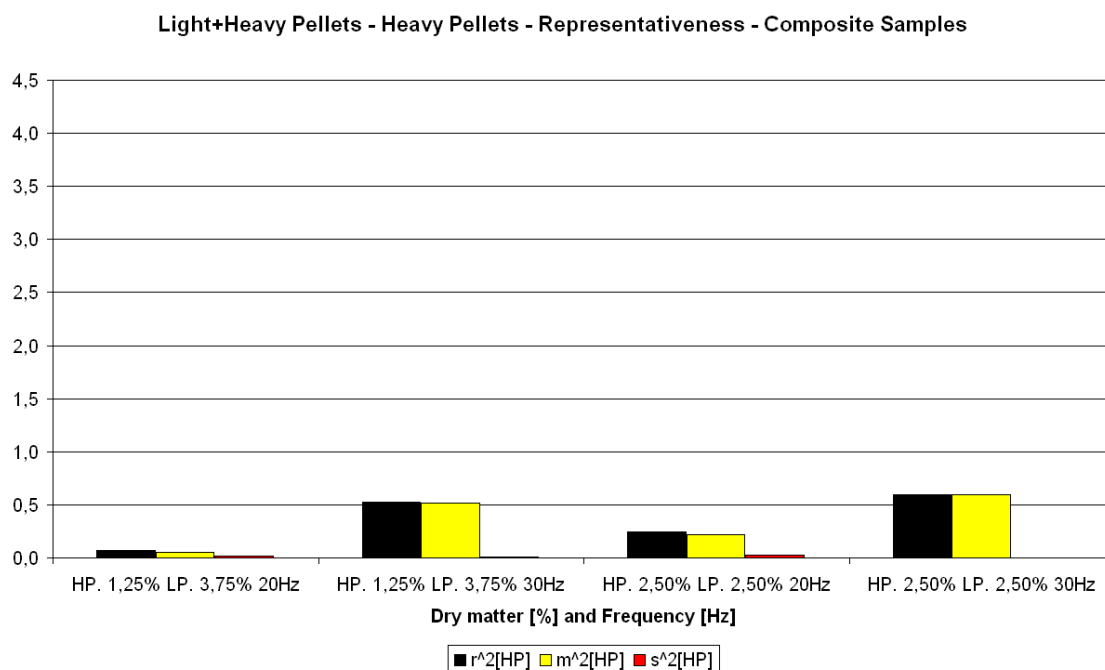
Figure 15.20: Model-systems made of light+heavy pellets – Representativeness for the heavy pellets of the composite samples.

Figures 15.21 and 15.22 show the representativeness for the samples regarding the concentration of dry matter for the model-systems of light and heavy pellets simultaneously. All the observations made for the individual concentrations of pellets remain valid for the total dry matter content.
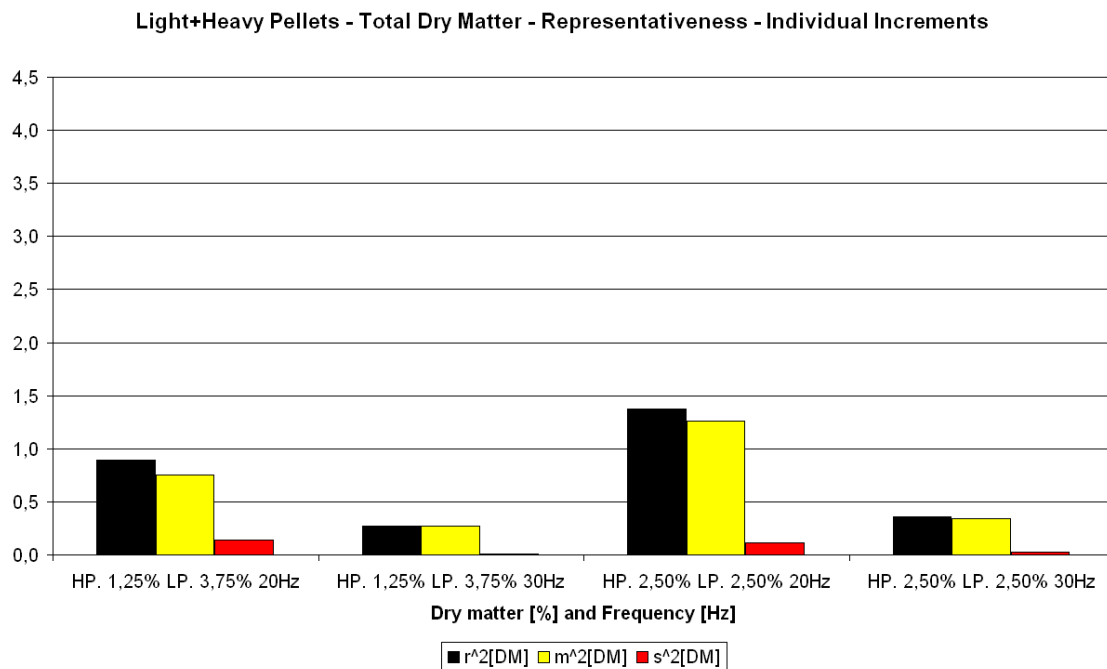
Figure 15.21: Model-systems made of light+heavy pellets – Representativeness for the total dry matter of the individual increments.

Light+Heavy Pellets - Total Dry Matter - Representativeness - Composite Samples
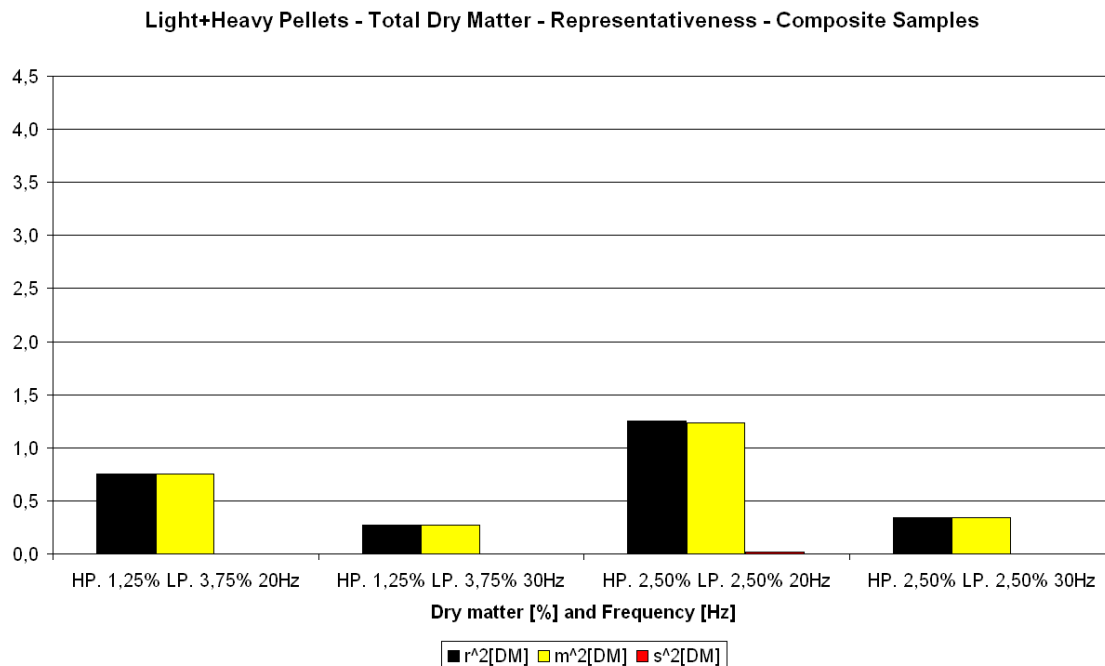
Figure 15.22: Model-systems made of light+heavy pellets – Representativeness for the total dry matter of the composite samples.

15.2.2.2 Synthetic manure based experiments

Figures 15.23 and 15.24 present the representativeness, the accuracy and the reproducibility of the sampling device for the experiments based on the synthetic manure.

Once again the TENIRS valve is *precisely wrong* and the composite samples only lead to slightly better results than the grab samples.

The representativeness for a concentration of dry matter of 7.5% must be considered with precaution as the system completely clogged for one of the replicate (the second) and for the last increment of the third replicate.

For both individual increments and composite samples, the lack of representativeness decreases when the loop velocity increases. It also notably decreases, at equal frequency, when the concentration of dry matter increases. The explanation given for the bias stays of course valid to explain this tendency.

Synthetic Manure - Representativeness - Individual Increments
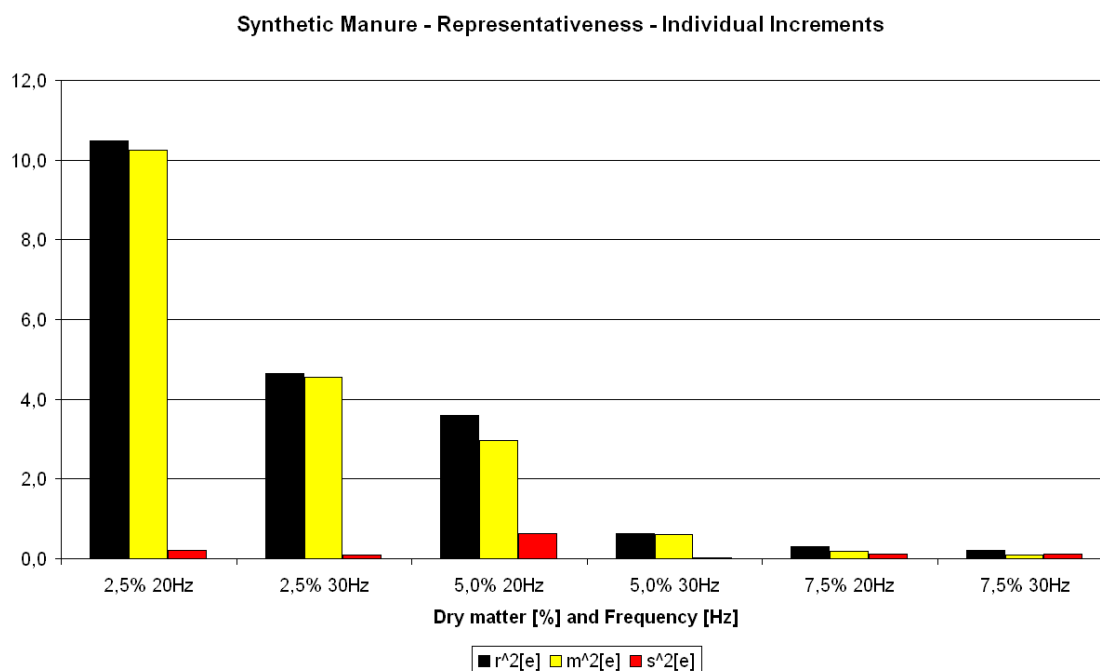
Figure 15.23: Model-systems made of synthetic manure – Representativeness of the individual increments.

Synthetic Manure - Representativeness - Composite Samples
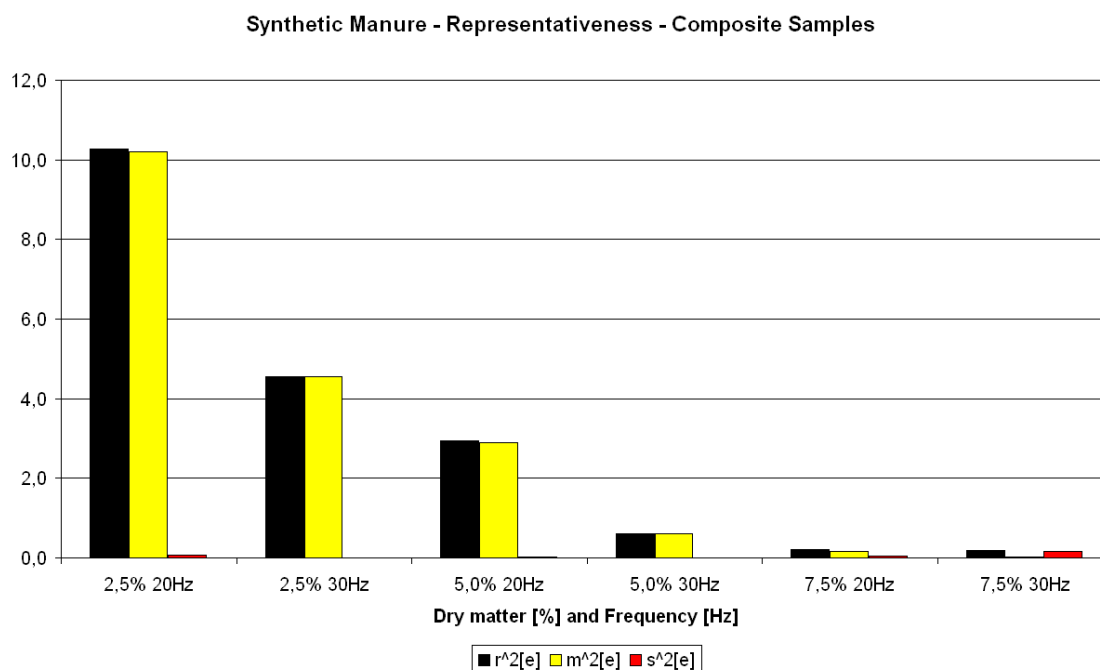
Figure 15.24: Model-systems made of synthetic manure – Representativeness of the composite samples.

15.3   Acoustic chemometrics

Acoustic chemometrics was used to predict the dry matter concentration on the model-systems based on the plastic pellets and the synthetic manure. The chemometrics modeling is presented in Appendix H on page 199. Table 15.1 gives an overview of the multivariate models obtained. For all models a calibration set and a bona fide test set was used in validation. Indeed test set validation is the only realistic validation and should always be preferred to cross validation. [15]

The Root-Mean-Square Error of Prediction RMSEP is given in % and is calculated as:

$$RMSEP[\%] = \frac{RMSEP}{\frac{y_{\max}^{\text{ref}} - y_{\min}^{\text{ref}}}{2}} \times 100 \tag{15.4}$$

System	# X-var	# PLS	RMSEP %	slope	r^2	#Outliers Cal	Val
Heavy	512	1	7.08	1.03	0.98	1	2
Light	512	1	7.43	0.95	0.98	0	1
Heavy in L+H	512	4	8.46	0.99	0.98	0	0
Light in L+H	512	4	11.58	1.02	0.96	0	0
DM in L+H	512	3	20.08	0.99	0.92	2	2
DM in SynMan	350	5	16.84	0.89	0.89	0	0

Table 15.1: Multivariate model overview based on acoustic spectra – All models were test set validated.

From table 15.1 the following observations can be drawn:

i. The overall results are highly satisfactory and gives good hope to apply acoustic chemometrics for determination of dry matter to the TENIRS system. They also validate the chosen deployment location of the sensor.

ii. Models determining the mass or the fraction mass of heavy pellets in the lot present a RMSEP of less than 9.0%. The model determining the mass of light pellets in the model-systems made of light pellets is also lower than 9.0%. When dealing with more complex material the percentages of RMSEP increase. However, the RMSEP of the synthetic manure is lower than that of the model-systems light and heavy pellets.

iii. For all the batches composed by red and yellow plastic pellets, only half of the X-variables are needed to described the system. The other 512 variables mainly lie on a flat line, and therefore almost did not carry information about the dry matter content of the batch.

iv. The number of PLS-components (1) needed to model the system composed by only the red or the yellow plastic pellets testifies of the simplicity of the system. These results are not surprising.

 v. The number of PLS-components (4, 4 and 3) to model the system composed by the red and the yellow plastic pellets testifies of the relative complexity of this system. However the system stay simplistic compared to synthetic manure or real manure.

vi. For the synthetic manure, the number of X-variables needed is lower, this might be explained by the fact that the dry matter content is not as heavy as the plastic pellets, therefore less vibrations (intensity and quantity) are produced in the pipe.

vii. For the synthetic manure the number of PLS components is 5 which is a readily accepted reflection of a – simulated – realistic system.

Part IV

Overall perspectives and conclusion

Chapter 16

Perspectives

16.1 Further development of acoustic chemometrics

The principle aims of acoustic chemometrics are to monitor the state of a process, and to monitor and characterize a product in a process. There are many ways: it can be by monitoring the manufacturing or product process or by monitoring the state of the production tools i.e. the state of a machine or wear and tear for maintenance purposes, or acoustic chemometrics can be used to monitor and characterize the raw material, intermediary or final product specification, it is also suitable to characterize multi-phase fluid systems and slurries.

The sensor deployment on a pipeline is a critical factor as it has to be located at a position of maximum impact in order to record better signals. Good knowledge of hydrodynamics and newtonian mechanics is beneficial to a correct deployment.

Moreover, since the sensor used only have one axis of sensibility i.e. it can only registered vibrations along one axis, only a part of the vibrations present in the pipe are recorded. In fact, when the particles hit the pipes wall they produce vibrations in three dimensional vibrations. The vibrations can be decomposed along the axis of accelerometer. Therefore, if the accelerometer is only sensible along one axis, only the projection of the vibration on this axis is recorded, leading to a biased view of the actual vibration.

Accelerometers allowing measurements on more than one axis exist. Typically they

can measure along two or three axis[1]. Hence, a 3-axis accelerometer should be able to record the entire vibration present at its deployment location.

It is therefore suggested to perform a pilot study using one-, two-, and three-axis accelerometers, deployed at the exact same optimal locations and with the exact same experimental design. Followed by one using the same accelerometers should be performed, but in this one, the accelerometers are to be deployed at the most unfavorable locations to assess which accelerometer is giving the best results.

According to the personal experience of the author [9], it is expected that the spectra based on the three axis accelerometer should lead to the best models.

16.2   Perspectives for the TENIRS system

16.2.1   Sampling evaluation and acoustic calibration based on real manure

The sampling was focused on plastic particles and synthetic manure. Real manure should be tested for dry matter and other physical/chemical components also. The samples must be extracted using a *correct* sampling facility.

Representative samples of manure extracted from a biogas plant, for example, can be used in the $1L$ bottles. The samples should be analyzed first to determine the exact dry matter content of the lot prior to start the experiments.

When determined, the dry matter of the $1L$ batches can be adjusted by dilution or addition of dry matter to it, remaining a completely realistic study.

16.2.2   Suggestions to improve the TENIRS loop

Even though the sampling design is not in accordance with the theory of sampling, the idea behind the TENIRS loop is judicious and very open to the necessary improvements. This section suggests some modest design modifications in the to improve the quality of the primary sample.

---

[1]Each axis produces a signal that must be recorded by the DAQ, therefore, a 3 channel DAQ must be used when dealing with three axis accelerometers.

16.2.2.1 Improvement of the sampling device

A step further to correct sampling is to replace the sampling device by a three-way valve placed on an up-stream vertically flowing pipe to ensure the entire flow to be sampled within a given time period (see Figure 16.1). Furthermore, the valve should electronically commanded to set up once for all the sampling protocol to be repeated for each new batch. The entire flow is to be kept as turbulent as possible in the entire loop.

The size of the sampling bottle should be increased to a sufficient size to hold the entire composite sample. The walls of the bottle has to be straight without particles trap and should be designed to be used in an oven (e.g. pyrex) in case of dry matter analysis, allowing the entire sample to be placed in the oven without need of pour it to another bottle.
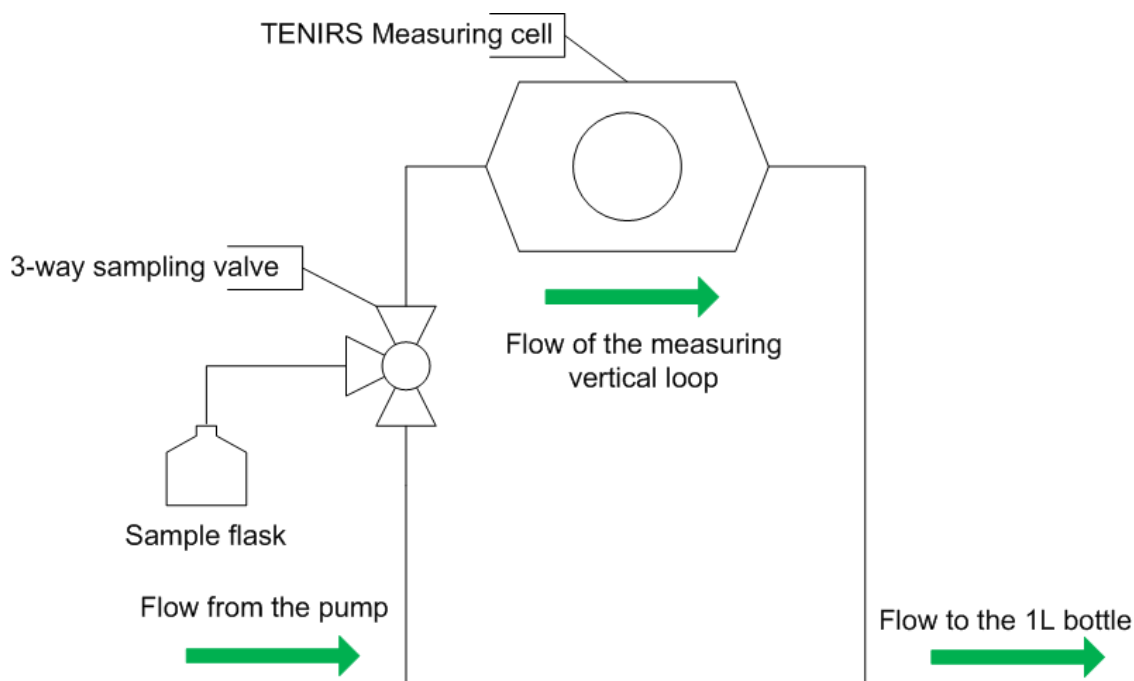
Figure 16.1: Suggested modification to be implemented on the TENIRS system.

16.2.2.2 Global redesign of the TENIRS loop

A complete automatic system is suggested in this section. All the improvements suggested above are to be implemented on the TENIRS prior to deploy an automatic system.

Once the $1L$ bottle screwed to the TENIRS loop, it should be automatically put in circulation position and the pump should started at the same time.

The frequency convertor should also be electronically commanded allowing to program the starting sequence at high speed for a given time period in order to help the system to get in steady state. Once in steady state the frequency can be decrease to reach the loop velocity desired for the trials.

The NIR spectrometer should be electronically trigger to start measuring when the loop is in steady state, once started sampling can be removed during the entire scanning period. In fact the sampling valve can be opened and closed many time during the NIR measurements.

Once the measurements done the bypass valve can be activated and fresh water can be run in the system to clean in when, in the meantime, the operator is setting up the new batch.

The whole point is to have a complete automatic system is to reproduce the exact same circulation, scanning, and sampling conditions for each samples.

Everything can be commanded using a Programmable Logic Controller (PLC) or using a LabView[2] based software.

The algorithm can be summarized by this list of items;

i. Screw the bottle to the TENIRS System and the sampling bottle and then press the start button;

ii. The system verify if the $1L$ liter bottle and the sampling bottle are present, if so;

iii. The bottle is set up in circulation position and the pump is started at high frequency f_1 for a time period of t_1 seconds;

iv. After t_1 seconds, the frequency of the pump is decreased to the operational frequency f_2 and the system is run for a time period of t_2 seconds;

v. After t_2 seconds, the NIR spectrometer is commanded to start measuring trough the flow cell for a time period of t_3 seconds;

vi. During the time period t_3 seconds the sampling valve is commanded to extract x increments every t_3/x seconds leading to a representative composite sample;

---

[2]LabView, National Instruments, Austin, Texas, The United States of America.

vii. After t_3 seconds, the $1L$ bottle is bypassed and the clean water is circulated in the loop during a time period of t_4 seconds;

viii. After t_4 seconds, the system is stopped and is waiting for further instructions.

All the different t_i and f_i can be settled by the operator to the optimal value. In case of connecting the TENIRS to a reactor as portative on-line measurement tool, the system should be notified and should not perform the test of the presence of the $1L$ bottle.

If other sensors are mounted on the loop, as acoustic sensor, the software should be able to deal with them and include them in the procedure. In case of a LabView software this can be really easy since it can be designed to acquire the acoustic spectra and calculate the FFT on the fly.

Therefore, the control software should include some extra routines or customizable routines to connect other sensors.

With a fully automatic system, reducing human intervention as much as possible, and all the recommendations previously mentioned integrated in the TENIRS loop, the TENIRS system should become a more reliable and powerful tool for TOS-correct process monitoring and calibration of on-line monitoring tools.

Chapter 17

Conclusion

In this master thesis, the representativeness of sampling system were tested and acoustic chemometrics was used to predict the dry matter content of a stream.

From the literature review the following conclusions can be drawn:

i. Extracting a sample representative of the analytical grade of the lot can only be done by mean of composite sampling using a correct sampling system designed in accordance with the theory of sampling.

ii. The theory of sampling presents a complete methodology for evaluating the total sampling error associated with both static and process sampling.

iii. Variographic analysis is revealed to be a powerful tool to identify the presence of patterns in the process data structure e.g. it may reveal trends in the variation, asses the periodicity of cycles, and determine optimal sampling frequency. It especially estimates the total 0-D sampling and analysis error as well.

iv. Acoustic chemometrics – passive method – is reported to be a powerful tool for potential quantification of physical parameters such as particle size distribution, flow velocity, concentration of solids, density, and viscosity. All depending on a full chemometrics multivariate calibration.

v. Acoustic-Resonance Spectrometry – active method – is predicted to be a powerful tool for quantifying physical properties of products.

vi. The feasibility, of both acoustic chemometrics and near infrared spectroscopy as monitoring and control tool of chemical processes, has been documented in several scientific studies.

Based on the practical work of this thesis, the following conclusions can be drawn:

i. It was not possible to find plastic particles small enough to be handled by the applikon system. The recurrent sampling loop was redesigned to be as much as technical possible in accordance to the theory of sampling. It should lead to the extraction of samples representative of the bio-reactor content.

ii. The actual sampling system mounted on the TENIRS system is *precisely wrong* i.e. it presents an apparent reproducibility but fatal accuracy.

iii. The experiments based on the light plastic pellets show an important bias: for the composite samples at low frequency ($10Hz$) up to $+182.4\%$, the bias decreases to $+84.1\%$ at $20Hz$ and becomes as low as -67.4% at $30Hz$. This tendency is the same for all the concentrations tested.

iv. The experiments based on the heavy plastic pellets show an important bias: for the composite samples at low frequency ($10Hz$) up to $+145.5\%$, the bias decreases to $+80.0\%$ at $20Hz$ and becomes as low as -55.0% at $30Hz$. This tendency is the same for all the concentrations tested.

v. The experiments based on the light+heavy plastic pellets show a bias more important for the light pellets than the heavy pellets, but the bias is still highly positive when the frequency converter is set to $20Hz$ and becomes negative when it is set on $30Hz$. This tendency is the same for all the concentrations tested.

vi. The experiments based on the synthetic manure show an important bias as high as 319.3% at $20Hz$.

vii. For all model-systems, the experiments show that the quality of the sampling is material- and system-dependent, depending on the concentration of dry matter and the velocity of the sampling loop, different bias were obtained. In fact the bias decreased with when the concentration of dry matter increased. For high concentrations of dry matter and high velocity of the loop the bias is artificially low owing to the design of the sampling instrument itself. (See Table 17.1)

viii. The bias and the representativeness of the composite samples are only slightly better than those of the corresponding grab samples but they have the same magnitude. Therefore, a representative sample can only be guarantee by applying the theory of sampling when designing the sampling device **and** by applying a sampling protocol in accordance to the theory of sampling.

ix. Cleaning of the TENIRS loop is an important task and should not be underestimated. Important cross contaminations can results from an insufficient cleaning. When dealing with the manure the cleaning is far from easy, and a large quantity of water must be used to flush the system. The flushing should be stopped when the water comes out as clear as it was when it came in the loop.

x. The TENIRS system should be redesigned to include a vertical sampling loop. The sampling facility should be mounted as close as possible to the measuring cell. A 3-way electronically commanded valve must be used.

xi. The ability of acoustic chemometrics to predict dry matter content of the $1L$ TENIRS bottle has been demonstrated, giving valuable indications that acoustic chemometrics is a powerful PAT modality, at least concerning physical Y-variables.

xii. The model based on the light plastic pellets shows a slope of 0.95 and a correlation coefficient r^2 of 0.98. The model was test set validated.

xiii. The model based on the heavy plastic pellets shows a slope of 1.03 and a correlation coefficient r^2 of 0.98. The model was test set validated.

xiv. The models based on the light+heavy plastic pellets show: for the quantification of heavy pellets a slope of 0.99 and a correlation coefficient r^2 of 0.98, for the quantification of light a slope of 1.02 and a correlation coefficient r^2 of 0.96, and for the quantification of dry mater a slope of 0.99 and a correlation coefficient r^2 of 0.92. The models were test set validated.

xv. The model based on the synthetic manure shows a slope of 0.89 and a correlation coefficient r^2 of 0.89. The model was test set validated.

It is not possible to extract representative samples using the TENIRS sampling device, as the representativeness is highly material- and system dependent. Each model-system (polymer/water and synthetic manure) lead to different conclusions regarding the bias and the representativeness of the sampling device. However, nearly all experiments show a very good reproducibility of biased samples: It can be concluded that this device is functioning in a fashion which can be characterized as being *precisely wrong* i.e. its reproducibility σ^2 is very good (and in the cases of the composite samples often close to zero), however its accuracy is abysmal!

It is claimed in studies [32–34] that samples obtained with the TENIRS sampler were *slightly biased as the device is not designed in total accordance with the theory of sampling*. These assessments must be declared as only marginally in touch with reality: The present evaluation demonstrates that the bias regarding dry matter concentration increases with respect to the complexity of the multi-phase system **and** decreases with respect to the circulation velocity: composite samples of synthetic manure – the most realistic model-systems evaluated – composed of 10 increments extracted at low speed ($20Hz$ i.e. 20% of the top circulation speed) can present a bias as high as 320% which indeed must be qualified as a *highly significant bias*, whereas composite samples of light pellets extracted in the same conditions reaches some 85%. At higher speed ($30Hz$ i.e. 60% of the top circulation speed), the bias observed for the synthetic manure was 15% while being significantly negative, -70% for model-systems based on the heavy model

system particles. These findings have severe implications regarding the necessity of redesigning the TENIRS reference sampling system completely.

Table 17.1 summarizes the bias measured.

System	Inc. bias [%]		Comp. bias [%]	
	Min	Max	Min	Max
Light	-47.7	182.8	-48.0	182.4
Heavy	-67.5	145.7	-67.4	145.5
Light in L+H	-45.0	175.7	-45.1	175.4
Heavy in L+H	-77.0	47.2	-77.0	46.8
DM in L+H	-58.1	111.4	-58.2	111.1
DM in SynMan	15.2	319.5	15.2	319.3

Table 17.1: Conclusion table relative to the bias generated by the TENIRS sampling facility for the individual increments (Inc. bias) and the composite samples (Comp. bias).

The work presented in this thesis shows that acoustic chemometrics is a powerful PAT modality concerning physical Y-variables. Dry matter content was substantiated in this work; there appear to be good reasons to expect a similar potential for e.g. density, viscosity . . . Much work on acoustic chemometrics on this type of applied biotechnological systems remains.

Bibliography

[1] Umetrics a.b. – Experts in Multivariate Data Analysis and Design of Experiments. http://www.umetrics.com/.

[2] Premus K. Ade and John F. Zuta. Acoustic Chemometrics Monitoring of Bedload Transportation Processes – A Norwegian Water Resources & Energy Directorate Flume Test Rig Simulation – Feasibility study towards deployment in Norwegian river systems. Master's thesis, Aalborg University, Esbjerg Institute of Technology, Denmark, 2006.

[3] Teodorita Al Seadi. *Good practice in quality management of AD residues from biogas production.* IEA Bioenergy, 2001. http://www.sdu.dk/bio/.

[4] Irini Angelidaki, Lars Ellegaard, Anders Hay Sørensen, and Jens Ejbye Schmidt. *Environmental Biotechnology.* Technical University of Denmark, Institute for Environment and Resources, Denmark, 2002. Notes for course no. 12133.

[5] Anonymous. *Guidance for Industry PAT – A Framework for Innovative Pharmaceutical Development, Manufacturing, and Quality Assurance.* U.S. Department of Health and Human Services, 2004. http://www.fda.gov/cder/OPS/PAT.htm.

[6] Katherine A. Bakeev, editor. *Process Analytical Technology.* Blackwell, 2005. ISBN 1-4051-2103-3.

[7] R.M. Belchamber, D. Betteridge, M.P. CoIlihs, T. Lilley, C.Z. Marczewski, and A.P. Wade. Quantitative study of acoustic emission from a model chemical process. *Analytical Chemistry*, 58:1873–1877, 1986.

[8] Applikon Biotechnology. Hardware & Installation Manual – Autoclavable Bio Reactor Systems 1-20 Liter, March 2004. http://www.applikon.com/.

[9] Ludovic Boland. Projet Ampacimon – Mesures sur pot vibrant. Technical report, Centre Spatial de Liège - Université de Liège, 2006. Confidential.

[10] Donald A. Burns and Emil W. Ciurczak, editors. *Handbook of Near-Infrared Analysis.* Taylor & Francis Group, LLC, 2008. ISBN 0-8493-7393-X.

[11] Eigil Dåbakk. *Near infrared spectrometry – a potential method for environmental monitoring of aquatic systems.* PhD thesis, Research Group for Chemometrics - Department of Organic Chemistry - Umeå University, 1999. ISBN 91-7191-678-4.

[12] Casper Kierulf Dahl. *Theory of Sampling Contributions to Multivariate Image Analysis with a Special Focus one Image Analytical Sampling.* PhD thesis, Aalborg University Esbjerg. Analytical Chemistry, Applied Chemometrics, Applied Biotechnology; Bio-energy & Sampling Research Group - ACABS, 2008. ISBN 978-87-7606-021-3.

[13] Adams Douglas. *The Hitch-hiker's Guide to the Galaxy.* Pan Books: London, 1979. ISBN 0517226952.

[14] K.H. Esbensen, B. Hope, T.T. Lied, M. Halstensen, T. Gravermoen, and K. Sundberg. Acoustic chemometrics for fluid flow quantifications – II: A small constriction will go a long way. *Journal of Chemometrics*, 13:209–236, 1999.

[15] Kim H. Esbensen. *Multivariate Data Analysis – in practice.* Camo Software AS, 2002.

[16] Kim H. Esbensen, Maths Halstensen, Thorbjørn Tønnesen Lied, Arild Saudland, Jørild Svalestuen, Sunil de Silva, and Bjørn Hope. Acoustic chemometrics – from noise to information. *Chemometrics and Intelligent Laboratory Systems*, 44:61–76, 1998.

[17] Kim H. Esbensen, Premus K. Ade, John F. Zuta, Jim Bogen, and Møen Knut. Acoustic chemometrics of complex natural systems: flume test rig feasibility studies for monitoring river bed-load sediment transportation processes. *J. Chemometrics*, 21:459–473, 2007. doi: 10.1002/cem.1076.

[18] Kim H. Esbensen, Hans Henrik Friis-Petersen, Lars Petersen, Jens Bo Holm-Nielsen, and Peter P. Mortensen. Representative process sampling – in practice: Variographic analysis and estimation of total sampling errors (TSE). *Chemometrics and Intelligent Laboratory Systems*, 88:41–59, 2007. doi: 10.1016/j.chemolab.2006.09.011.

[19] ACABS Research Group Aalborg University Esbjerg, editor. *Baltic Biorefinery Symposium*, 2005. Aalborg University Esbjerg. Proceeding.

[20] Christian Gruber and Willy Benoit. *Mécanique générale.* Presses polytechniques et universitaires romandes, 1998. ISBN 2-88074-305-2.

[21] Pierre Gy. Sampling of discrete materials – a new introduction to the theory of sampling I. Qualitative approach. *Chemometrics and Intelligent Laboratory Systems*, 74:7–24, 2004. doi: doi:10.1016/j.chemolab.2004.05.012.

[22] Pierre Gy. Sampling of discrete materials II. Quantitative approach – sampling of zero-dimensional objects. *Chemometrics and Intelligent Laboratory Systems*, 74: 25–38, 2004. doi: doi:10.1016/j.chemolab.2004.05.015.

[23] Pierre Gy. Sampling of discrete materials III. Quantitative approach – sampling of one-dimensional objects. *Chemometrics and Intelligent Laboratory Systems*, 74: 39–47, 2004. doi: doi:10.1016/j.chemolab.2004.05.011.

[24] Pierre Gy. Part IV: 50 years of sampling theory – a personal history. *Chemometrics and Intelligent Laboratory Systems*, 74:49–60, 2004. doi: doi:10.1016/j.chemolab. 2004.05.014.

[25] Pierre Gy. Part V: Annotated literature compilation of Pierre Gy. *Chemometrics and Intelligent Laboratory Systems*, 74:61–70, 2004. doi: doi:10.1016/j.chemolab. 2004.05.010.

[26] Pierre Gy. *Hétérogénéité, échantillonnage, homogénéisation*. Masson, 1988. ISBN 2-225-81313-2.

[27] Pierre Gy. *Sampling for Analytical Purposes*. Wiley, 1998. ISBN 0-471-97956-2.

[28] M. Halstensen and K.H. Esbensen. New developments in acoustic chemometric prediction of particle size distribution – the problem is the solution. *Journal of Chemometrics*, 14:463–481, 2000.

[29] Maths Halstensen. *Experimental Multivariage Sensor Technology and Development of System Prototype for Industrial Multi-phase Characterisation*. PhD thesis, Norwegian University of Science and Technology, 2001. ISBN 82-471-5381-5.

[30] Maths Halstensen, Peter de Bakker, and Kim H. Esbensen. Acoustic chemometric monitoring of an industrial granulation production process – a PAT feasibility study. *Chemometrics and Intelligent Laboratory Systems*, 84:88–97, 2006. doi: 10.1016/j.chemolab.2006.05.012.

[31] Jens Bo Holm-Nielsen, Casper K. Dahl, and Kim H. Esbensen. Representative sampling for process analytical characterization of heterogeneous bioslurry systems- - a reference study of sampling issues in PAT. *Elsevier - Chemometrics and intelligent laboratory systems*, 83:114–126, March 2006. doi: 10.1016/j. chemolab.2006.02.002.

[32] Jens Bo Holm-Nielsen, Helga Andree, Harald Lindorfer, and Kim H. Esbensen. Transflexive embedded near infrared monitoring for key process intermediates in anaerobic digestion/biogas production. *Journal of Near Infrared Spectroscopy*, 15: 123–135, 2007. doi: 10.1255/jnirs.719.

[33] Jens Bo Holm-Nielsen, Carina Juel Lomborg, Piotr Oleskowicz-Popiel, and Kim H. Esbensen. On-line Near Infrared monitoring of glycerol-boosted anaerobic digestion processes – evaluation of Process Analytical Technologies. *Biofuels and Environmental Biotechnology*, 99:302–313, 2007. doi: 10.1002/bit.21571.

[34] Jens Bo Holm-Nielsen, Karina J. Larsen, Helene Møller, Henrik B. Møller, Stephen Njoku, Ludovic Boland, Michael Madsen, and Kim H. Esbensen. Process Analytical Technology – Monitoring of Biogas Processes at Meso- and Full-Scale Biogas Plants. *Article submitted in May 2008 to Journal of Biotechnology and Bioengineering, Wiley Periodicals, Inc.*, 2008.

[35] R. Hou, A. Hunt, and R.A. Williams. Acoustic monitoring of pipeline flows: particulate slurries. *Powder Technology*, 109:30–36, 1999. doi: 10.1016/S0032-5910(99) 00051-0.

[36] Jun Huang, Sivert Ose, Sunil de Silva, and Kim H. Esbensen. Non-invasive monitoring of powder breakage during pneumatic transportation using acoustic chemometrics. *Powder Technology*, 129:130–138, 2003.

[37] J. Michael Jacob. *Advanced AC Electronics: Principles & Applications*. Delmar Learning, 2003. ISBN 076682330-X.

[38] B.H. Junker and H.Y. Wang. Bioprocess Monitoring and Computer Control: Key Roots of the Current PAT Initiative. *Biotechnology and Bioengineering - Wiley InterScience*, 95:226–261, 2006. doi: 10.1002/bit.21087.

[39] Karl Heinz Koch. *Process Analytical Chemistry – Control, Optimization, Quality, Economy*. Springer, 1999. ISBN 3-540 65337-6.

[40] Andriy Kupyna, Reidar Barfod Schüllera, Elling-Olav Rukkea, and Tomas Isaksson. Acoustic chemometrics on liquid flow: Shift in the frequency spectra and its relationship to the physical properties of the liquid and the pipe. *Chemometrics and Intelligent Laboratory Systems*, 91:151–163, 2008. doi: 10.1016/j.chemolab. 2007.10.010.

[41] Michael Madsen. Full-scale anaerobic digestion monitoring using on-line acoustic chemometrics, near infrared spectroscopy, and recurrent loop process sampling – a Process Analytical Chemometrics (PAC) feasibility study. Master's thesis, Aalborg University, Esbjerg Institute of Technology, Denmark, 2007.

[42] F. McLennan and B. Kowalski, editors. *Process Analytical Chemistry*. Blackie Acamedic & Professional, 1995. ISBN 0-7514-0038-6.

[43] Joseph Medendorp and Robert A. Lodder. Acoustic-Resonance Spectrometry as a Process Analytical Technology for Rapid and Accurate Tablet Identification. *AAPS PharmSciTech*, 7:1–9, 2006. doi: 10.1208/pt070125.

[44] P.P. Mortensen. *Process Analytical Chemistry – Opportunities and problems for bio-industrial implementation.* PhD thesis, Aalborg University, Esbjerg Institut of Technology, Denmark, 2006. ISBN 87-92855-10-1.

[45] Brian Nesbitt, editor. *Handbook of Valves and Actuators.* Elsevier B.V., 2008.

[46] Isaac Newton. *Philosophiæ Naturalis Principia Mathematica.* S. Pepys, 1687. ISBN 0674664752.

[47] Jens Nielsen, John Villadsen, and Gunnard Liden. *Bioreaction Engineering Principles.* Kluwer Academic / Plenum Publishers, 2003.

[48] Lars Petersen. *Pierre Gy's Theory of Sampling (TOS) – in practice : Laboratory and Industrial Didactics including A first foray into image analytical sampling.* PhD thesis, Aalborg University Esbjerg. Analytical Chemistry, Applied Chemometrics, Applied Biotechnology; Bio-energy & Sampling Research Group - ACABS, 2005.

[49] Lars Petersen and Kim H. Esbensen. Representative process sampling for reliable data analysis – a tutorial. *Journal of Chemometrics*, 19:625–647, 2005.

[50] Lars Petersen, Penti Minkkinen, and Kim H. Esbensen. Representative sampling for reliable data analysis: Theory of Sampling. *Elsevier - Chemometrics and intelligent laboratory systems*, 77:261–277, 2004. doi: 10.1016/j.chemolab.2004.09.013.

[51] P.F. Pind, I. Angelidaki, and B.K. Ahring. A new VFA sensor technique for anaerobic reactor systems. *Biotechnology and Bioengineering*, 82:54–61, 2003.

[52] Francis F. Pitard. *Pierre Gy's Sampling Theory and Sampling Practice – Heterogeneity, Sampling Correctness, and Statistical Process Control.* CRC Press, 1993. ISBN 0-8493-8917-8.

[53] R.B. Randall. *Frequency Analysis.* Brüel & Kjær, 1987. ISBN 87-87355-07-8.

[54] Matthew Scarff, S. Alison Arnold, Linda M. Harvey, and Brian McNeil. Near Infrared Spectroscopy for Bioprocess Monitoring and Control: Current Status and Future Trends. *Biotechnology*, 26:17–39, 2006. doi: 10.1080/07388550500513677.

[55] Mark Serridge and Torben R. Licht. *Piezoelectric Accelerometers and Vibration Preamplifiers – Theory and Application Handbook.* Brüel & Kjær, 1987.

[56] H. W. Siesler. NIR-Instrumentation, 2002. http://www.nir-spektroskopie.de/.

[57] Erik Skibsted. *PAT and Beyond.* PhD thesis, Universiteit van Amsterdam, 2005.

[58] Douglas A. Skoog, F. James Holler, and Timothy A. Nieman. *Principles of In-strumental Analysis.* Thomson Learning, 1998. ISBN 0-03-002078-6.

[59] Patricia L. Smith. *A Primer for Sampling Solids, Liquids, and Gases – Based on the Seven Sampling Errors of Pierre Gy.* ASA SIAM, 2001.

[60] D. H. Titterton and J. L. LinkWeston. *Strapdown inertial navigation technology.* American Institute of Aeronautics & Ast, 2004. ISBN 1563476932.

[61] Phil Williams and Karl Norris, editors. *Near-Infrared Technology in the Agricultural and Food Industries.* American Association of Cereal Chemists, Inc., 2001. ISBN 1-891127-24-1.

[62] Marko Zlokarnik. *Scale-up in Chemical Engineering.* Wiley-VCH, 2006. ISBN 3-527-31421-0.

Part V

Appendices

Appendix A

The Gy's Formula

Equation below expresses the Gy's formula

$$\sigma^2(FSE) = Cd^3 \left(\frac{1}{M_S} - \frac{1}{M_L} \right) = cfg\beta d^3 \left(\frac{1}{M_S} - \frac{1}{M_L} \right) \qquad (A.1)$$

Where

c is a dimensionless parameter called the *constitutional parameter* of specific gravity expressed in $\frac{g}{cm^3}$. It can vary from a fraction of unity to several million. The constitution parameter can be calculated as follow:

$$c = \frac{\left(1 - \frac{a_L}{\alpha} \right)^2}{\frac{a_L}{\alpha}} \rho_c + \left(1 - \frac{a_L}{\alpha} \right) \rho_m \qquad (A.2)$$

where a_L is the average concentration of the lot; α is the concentration of the critical particles (particles of interest); ρ_c is the density of the critical particles; ρ_m is the density of the matrix.

f is a dimensionless factor called *particle shape factor*. It describes the deviation from the ideal shape of a square. A square will have $f = 1$, a sphere $f = 0.52$ and a almost flat disc $f = 0.1$.

g is a dimensionless factor called *size distribution factor*. It describes the span of particles sizes in the lot. The following rules of thumb can be formulated: if

all particles have the same size, then $g = 1$, if $1 < \frac{d}{d_{0.05}} < 2$ then $g = 0.75$; if $2 < \frac{d}{d_{0.05}} < 4$ then $g = 0.5$; if $\frac{d}{d_{0.05}} > 4$ then $g = 0.25$.

β is a dimensionless factor called *liberation factor*. It describes the degree of liberation of the critical component from the matrix. Totally liberated particles means $\beta = 1$ and totaly incorporated particles means $\beta = 0$. Otherwise β can be calculated from:

$$\beta = \sqrt{\frac{L}{d}} \tag{A.3}$$

where L is the liberation size.

d is the *top particle size*, defined as the square-mesh screen that retains 5% of the material[1].

Obviously, the FSE estimate is better if we can determine all these parameters. However this can be really difficult in practice, thus some default parameter value may be used.

Finally,

$$\sigma^2(FSE) = \left[\frac{\left(1 - \frac{a_L}{\alpha}\right)^2}{\frac{a_L}{\alpha}} \rho_c + \left(1 - \frac{a_L}{\alpha}\right) \rho_m \right] fg \left(\sqrt{\frac{L}{d}}\right) d^3 \left(\frac{1}{M_S} - \frac{1}{M_L}\right) \tag{A.4}$$

Appendix based on [18, 27, 31, 48–50].

---

[1]Dimension of length expressed in *cm*.

Appendix B

Accelerometer

Vibration problems associated with structures which are more delicate and intricate, and machines which are faster and more complex as raised in importance since the recent years. Therefore, there has been a requirement for a greater understanding of the causes of the causes of vibration and dynamic response of structures to vibratory forces.

During the last few years the technology became more and more cheap allowing accelerometer to be included in many different devices such as cell phones, numeric camera, video game console, etc.

Piezoelectric accelerometer is the best choice for vibration transducer. The large range of high performance measuring equipment now available can fully utilize the very wide frequency range and dynamic range offered by such vibration transducer. [55]

This kind of accelerometer is widely accepted as the best available transducer for the absolute measurement of vibration. This is a direct results of these properties:

i. Usable over very wide frequency ranges.

ii. Excellent linearity over a very wide dynamic range.

iii. Acceleration signal can be electronically integrated to provide velocity and displacement data.

iv. Vibration measurements are possible in a wide range of environmental conditions while still maintaining excellent accuracy.

v. Self-generating so no external power supply is required.

vi. No moving parts therefore extremely durable.

vii. Extremely compact plus a high sensitivity to mass ratio.

B.1 Basic definitions

B.1.1 Quantification of vibration levels

There are several ways of quantifying the vibration amplitudes of a signal in the time domain. The actual measurement units may differ from an application to another. Therefore, the descriptor described in Figure B.1 are widely used.
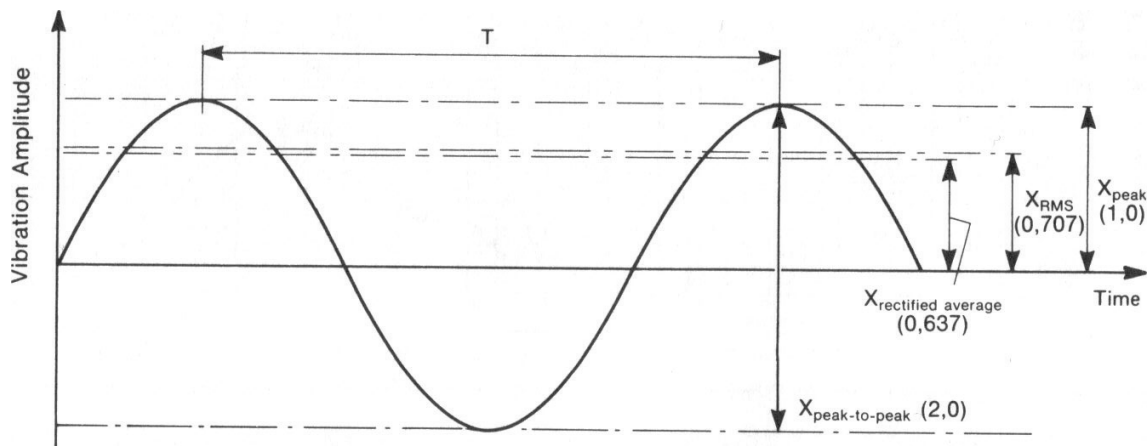
Figure B.1: Simple harmonic vibration. [55]

Figure B.1 depicts the simples form of vibration. It is represented by a particle oscillating about a reference position where exactly equal conditions of motion are encountered at fixed time intervals called period, T, of vibration.

It can be shown that the shape and period of the vibration remain the same when displacement, velocity or acceleration amplitude is chosen to represent the motion. Only the relative phases are different.

The amplitude of vibration, as shown in Figure B.1, can be described by using the following descriptors: [55]

i. **RMS (Root Mean Square) Level:** Provides the most useful description of

vibration levels. The square root of the integrated time-averaged squared function is related to the vibration energy and thus the vibration's damage potential. The RMS value a sine wave[1] is $\frac{1}{\sqrt{2}}$ times the value of the peak level.

ii. **Peak Level:** Defines the maximum level which is measured and is useful in the measurement of short duration shocks. Nevertheless, no account is taken of the time history of the vibration.

iii. **Peak-to-Peak:** Although of some use in describing vibration displacement, this descriptor is mostly never used.

iv. **Average Level:** Takes the time history of the vibration into account but there is no useful relationship between the average level and any physical quantity.

v. **Crest Factor:** Defines the ration of the peak value of a signal to the RMS value. As the vibration becomes more impulsive or more random, the cres factor increases. Therefore, by monitoring the growth of the crest factor, it is possible to predict a breakdown or element fault.

B.1.1.1 Linear amplitude and frequency scales

Linear amplitude and frequency scales are used in vibration measurements when a high resolution is needed. A linear frequency scale helps to separate closely spaced frequency components. The linear frequency scale gives the further advantage that equally spaced harmonic components of a vibration signa are easily recognized. [55]

B.1.1.2 Logarithmic amplitude and frequency scales

Piezoelectric accelerometers are able to perform accurate vibration measurements over extremely wide dynamic and frequency ranges. Hence, to obtain convenient interpretation of results the following are often required: [55]

i. An amplitude scale which can accommodate vibration amplitudes from the lowest detectable amplitudes up to shock amplitudes, and which can also simplify the comparison of vibration amplitudes.

ii. A frequency scale with the same percentage resolution over the whole width of the recording chart.

Those two requirements can be met using the following:

---

[1]And only of a sine wave!

A decibel scale Although more commonly associated with acoustic measurements the decibel (dB) is equally useful in vibration measurements. It is defined as follow

$$N(dB) = 10 \log \left(\frac{a^2}{a_{\text{ref}}^2} \right) = 20 \log \left(\frac{a}{a_{\text{ref}}} \right) \tag{B.1}$$

Where N is the number of decibel, a the measured vibration amplitude, and a_{ref} the reference amplitude.

A logarithmic frequency scale Sometimes, frequency is plotted on a logarithmic scale. This kind of scale has the effect of expanding the lower frequency ranges and compressing the higher frequency ranges. The result is equal relative resolution over the frequency axis, and the size of the scale is kept to reasonable proportions. Therefore, a logarithmic frequency scale is used to cover a wide frequency scale. [55]

B.2   Physical principle behind

B.2.1   Operation of an accelerometer

Figure B.2 depicts a simplified model of a piezoelectric accelerometer showing only the mechanical parts. The active elements of the accelerometer are the piezoelectric elements. These act as springs connecting the base of the accelerometer to the seismic masses via the rigid triangular center post.

When the accelerometer is vibrated a force, equal to the product of the acceleration of a seismic mass and its mass, acts on each piezoelectric element. The piezoelectric elements produce a charge proportional to the applied force. The seismic masses are constant and consequently the element produce a charge which is proportional to the acceleration of the seismic masses. [55]

Since the seismic masses accelerate with the same magnitude and phase than the accelerometer base over a wide frequency range, the output of the accelerometer is proportional to the acceleration of the base and therefore to the acceleration of the surface onto which the piezoelectric accelerometer is mounted.
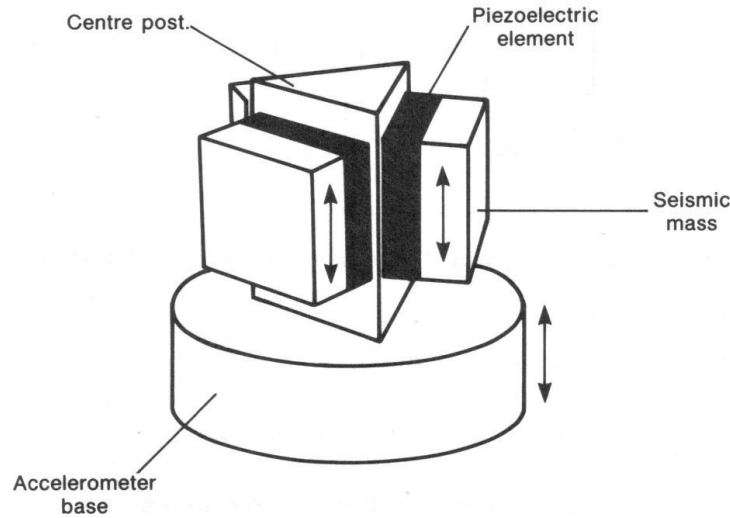
AALBORG UNIVERSITY ESBJERG

Figure B.2: Schematic of a piezoelectric accelerometer. [55]

B.2.2 Analytical treatment of accelerometer operation

The developments presented in this section were established for a one-axis accelerometer but can be applied to a two- or three-axis accelerometer without major changes.

Figure B.3 shows a simplified model of the accelerometer previously described and referenced to an inertial system. The two masses are unsupported and connected by an ideal spring. Damping is neglected in this model because most of the accelerometer available on the market have a very low damping factors.

In order to well understand the mathematical development present in this section, it is needed to define the parameters and variables of the equations.

m_s is the total seismic mass, m_b is the mass of the accelerometer base, x_s is the displacement of the seismic mass, x_b is the displacement of the accelerometer base, L is the distance between the seismic mass and the base when the accelerometer is at rest in the inertial system, k is the equivalent stiffness of the piezoelectric elements, F_e is the harmonic excitation force, F_0 is the amplitude of excitation force, ω is the excitation frequency and is equal to $2\pi f$, ω_n is the natural resonance frequency of the accelerometer, ω_m is the mounted resonance frequency of the accelerometer, f_m is the mounted resonance frequency of the accelerometer, and f is the excitation frequency. All those variables and parameters have to be expressed in the international standard system of unit. [55]

From Figure B.3 the following equations can be written

AALBORG UNIVERSITY ESBJERG
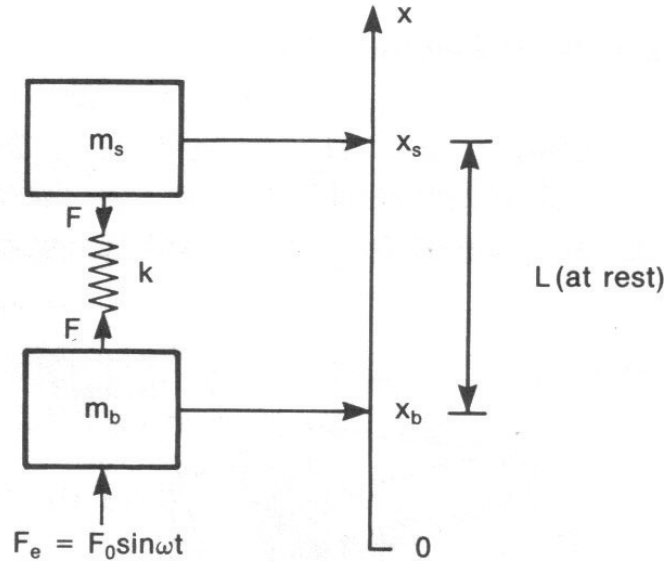
Figure B.3: Simplified model of an accelerometer. [55]

i. The string force:

$$F = k(x_s - x_b - L) \tag{B.2}$$

ii. Force on the base[2]:

$$m_b \ddot{x}_b = F + F_e \tag{B.3}$$

iii. Force on the seismic masses

$$m_s \ddot{x}_s = -F \tag{B.4}$$

Therefore, the equation of the motion for the model can be found

$$\ddot{x}_s - \ddot{x}_b = -\frac{F}{m_s} - \frac{F + F_e}{m_b} = \frac{k}{\mu}(x_s - x_b - L) - \frac{F_e}{m_b} \tag{B.5}$$

---

[2]In Newtonian mechanic, $\dot{x}$ and $\ddot{x}$ are defined as follows

$$\frac{d}{dt}x(t) = \dot{x}(t) = \dot{x}$$
$$\frac{d^2}{dt^2}x(t) = \ddot{x}(t) = \ddot{x}$$

or

$$\mu\ddot{r} = -kr - \frac{\mu}{m_b}F_0\sin\omega t \tag{B.6}$$

Where

$$\frac{1}{\mu} = \frac{1}{m_s} + \frac{1}{m_b} \tag{B.7}$$

or

$$\mu = \frac{m_s m_b}{m_s + m_b} \tag{B.8}$$

μ is often referred to as the *reduced mass* and r is the relative displacement of the seismic mass to the base

$$r = x_s - x_b - L \tag{B.9}$$

B.2.2.1 Free vibration

When the accelerometer is in a free hanging position and is not being excited by external forces ($F_e = 0$) the equation for its *free* vibration reduces to

$$\mu\ddot{r} = -kr \tag{B.10}$$

This simple differential equation can be solved[3] by assuming that the displacement of m_s relative to m_b varies harmonically with an amplitude R, therefore

$$r = R\sin\omega t \tag{B.11}$$
$$\dot{r} = R\omega\cos t \tag{B.12}$$
$$\ddot{r} = -R\omega^2\sin t \tag{B.13}$$

---

[3]Using the full mathematical theory about differential equations will lead to the same results. But will complicated the calculations.

Hence

$$-\mu R \omega^2 \sin \omega t = -kR \sin \omega t \qquad \text{(B.14)}$$

Therefore, the resonance frequency of the accelerometer, ω_n, can be written as follows

$$\omega_n^2 = \frac{k}{\mu} \qquad \text{(B.15)}$$

or if we use Equation B.7 in Equation B.15

$$\omega_n^2 = k \left(\frac{1}{m_s} + \frac{1}{m_b} \right) \qquad \text{(B.16)}$$

From Equation B.16 it is possible to calculate the natural frequency of the seismic mass-spring system. In fact, if the accelerometer is mounted with perfect rigidity onto the structure which is heavier than the total weight of the accelerometer then m_b becomes much larger than m_s and the resonance frequency of the accelerometer becomes lower. Taken to the limit, of the accelerometer is mounted on an *infinitely* heavy structure $(m_b \to \infty)$, the previous equation reduces to

$$\omega_m^2 = \frac{k}{m_s} \qquad \text{(B.17)}$$

Equation B.17 expresses the natural frequency of the seismic mass-spring system and is defined as the *mounted* resonance frequency, ω_m, of the accelerometer. It is a property of the accelerometer and is used to define the useful operating frequency range of an accelerometer.

Obviously, it is impossible, in practice, to mount the accelerometer on an infinitely heavy and stiff structure. Therefore, the resonance frequency when mounted will change and will split up in two and the lowest resonance frequency will be lower than the mounted resonance frequency. [55]

B.2.2.2   Forced vibration

The forced vibration of the accelerometer must be examined since it that we are interested in. The *applied* force on the accelerometer must be included in the analysis along with the natural resonance frequency, ω_n, define by Equation B.16. For this analysis any kind of applied force can be used, however, in order to keep the calculations easy a sinusoidal force will be applied. Therefore Equation B.5 becomes

$$\ddot{r} + \omega_n^2 r + \frac{F_0}{m_b} \sin \omega t = 0 \tag{B.18}$$

if we assume that the displacement of the masses vary sinusoidally[4] then

$$-\omega^2 R \sin \omega t + \omega_n^2 R \sin \omega t + \frac{F_0}{m_b} \sin \omega t = 0 \tag{B.19}$$

and thus,

$$R(\omega_n^2 - \omega^2) + \frac{F_0}{m_b} = 0 \tag{B.20}$$

or

$$R = -\frac{F_0}{m_b(\omega_n^2 - \omega^2)} \tag{B.21}$$

At a frequency well below the natural resonance frequency of the accelerometer ($\omega_n \gg \omega$) the displacement (R_0) is expressed by

$$R_0 = -\frac{F_0}{m_b \omega_n^2} \tag{B.22}$$

B.2.3   Frequency range

The ratio A of the displacement at low frequency, R_0 expressed by Equation B.22, to the actual displacement, R expressed by Equation B.21, can be expressed after rearranging

---

[4]Which can be seen, with a little training, from the equation form

AALBORG UNIVERSITY ESBJERG

the expression

$$A = \frac{R}{R_0} = \frac{1}{1 - \left(\dfrac{\omega}{\omega_n}\right)^2} \tag{B.23}$$

Equation B.23 shows that the displacement between the base and the seismic masses increases when the forcing frequency becomes comparable to the natural resonance frequency of the accelerometer. Therefore the force on the piezoelectric elements and the electrical output also increase.

As shown in Figure B.4, the upper frequency limit is hence equal to to natural resonance frequency of the accelerometer. However the useful frequency ranges cannot included the peak of the frequency response, therefore they will be limited to $0.3 f_m$.
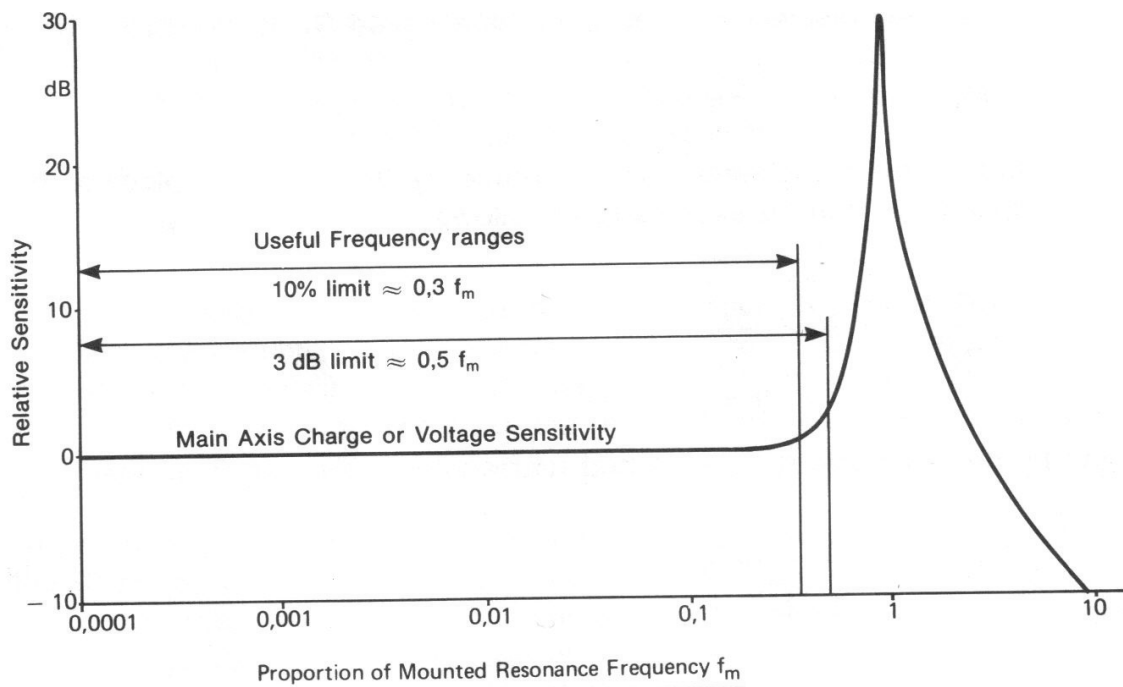

Figure B.4: Relative sensitivity of an accelerometer vs. frequency. [55]

As the accelerometer is not able to produce true DC response, the piezoelectric elements will only produce a charge when acted upon by dynamic forces. The actual low frequency limit is determined by the preamplifier which determines the rate at which the charge leaks away from the accelerometer.

B.2.4 Piezoelectric materials

A piezoelectric material can develop an electrical charge when subjected to a force. It can be made of intrinsic piezoelectric mono-crystals such as quartz and Rochelle salt, or artificially polarized ferroelectric ceramics.

The process by which the ceramics are polarized is analogous to the process by which a piece of iron can be magnetized by a magnetic field. A high voltage surge is applied across two ends of the material. the domains within the molecular structure of the material become aligned in such a way that an external force causes deformations of the domains and charges of opposite polarity to form on opposite ends of the material. Figure B.5 depicts the piezoelectric effect[5]. [55]

As stated before, when a piezoelectric accelerometer is vibrated forces proportional to the applied acceleration act on the piezoelectric elements and the charge generated by them is picked up by the contact.
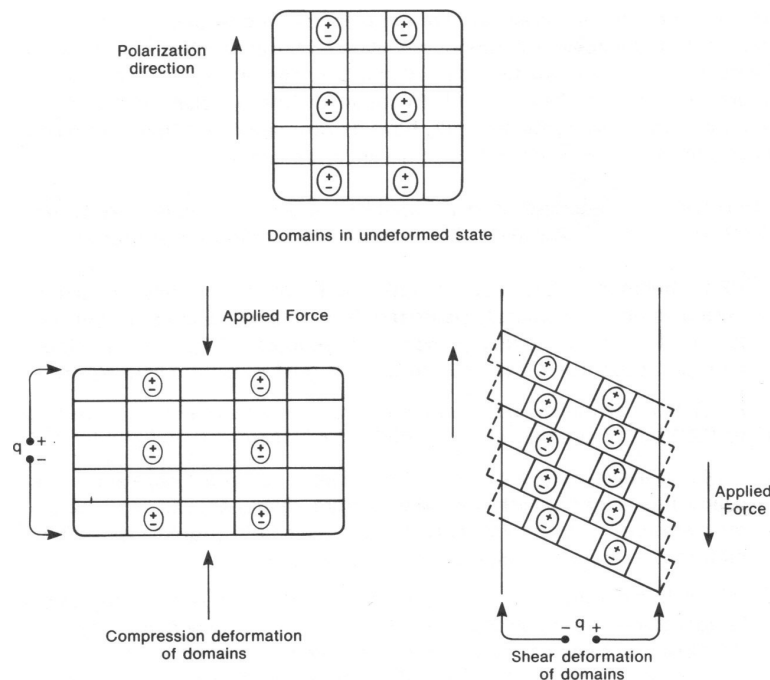

Figure B.5: Simple model of the piezoelectric effect within an artificially polarized ceramic. The charge q is collected between the indicated surfaces. [55]

The piezoelectric element can undergo both compression and shear deformation as shown in Figure B.5. In both cases a charge is developed along the surface on which the forces act. [55]

---

[5]The sensitivity of piezoelectric material is given in pC/N

B.3   Accelerometer performance in practice

In order to obtain accurate vibration measurements it is important to be aware of the problems linked to the environment in which the accelerometer is placed.

Figure B.6 illustrates the many different extraneous inputs which may be present during a vibration analysis. In most cases, piezoelectric accelerometers are designed to minimize the contribution of all these external phenomena to ensure that the output is only related to the vibration input.
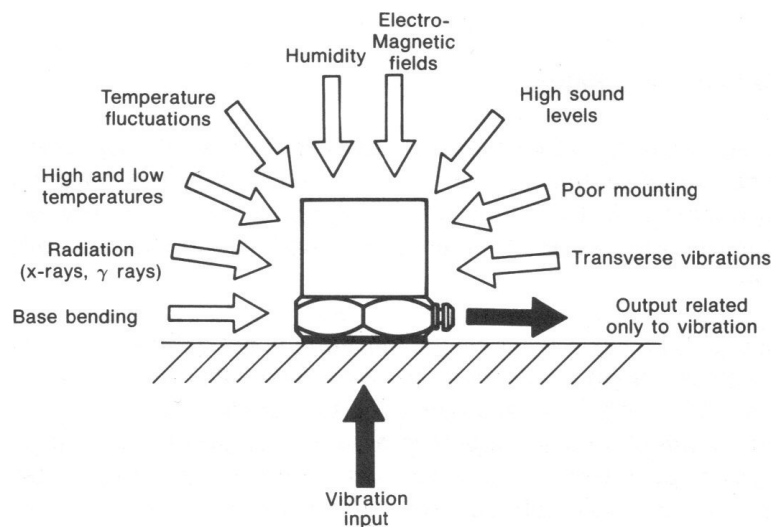

Figure B.6: Selection of the many extraneous inputs which can result in non-vibration related outputs in a poorly designed vibration transducer. [55]

Two general areas have to be considered:

1. The environment (noise, temperature, humidity, radiation, electromagnetic fields, etc.). In fact, a vibration transducer which is totally immune to environmental effects does not exist. Nonetheless, it is possible to find accelerometer which offer excellent performance in extreme environments.

2. Mounting. In fact, the mounting technique used can alter the frequency response and dynamic ranges of the accelerometer mass as well as its mounting location.

B.4 Applications

Piezoelectric accelerometers are mostly used for vibration testing, machine health monitoring and fault diagnosis, structural analysis, human vibration measurement, acoustic chemometrics, etc.

However, nowadays accelerometers are used in different kind of electronics devices such as cell phones, cameras, video game consoles, etc.

Appendix based on [9, 20, 46, 55, 60].

Fourier analysis

The mathematical basis of frequency analysis is the fourier transform which takes different form depending on the type of signal analyzed. However, all have in common that the signal is assumed to be composed of a number of sinusoidal and co-sinusoidal components at various frequencies, each with an amplitude A and initial phase ϕ.

C.1 Fourier series

If $g(t)$ is a period function of period T i.e.

$$g(t) = g(t + nT) \quad n \in \mathbb{N} \tag{C.1}$$

According to Fourier's theorem using complex exponentials[1], $g(t)$ can be represented represented as a sum of sinusoidal components at equally spaced frequencies kf_1 where $f_1 = 1/T$ and k is an integer[2].

---

[1]This is an application of Euler's equation

$$e^{\jmath\theta t} = \cos(\theta t) + \jmath\sin(\theta t)$$

Where $\jmath$ is the imaginary unit.

[2]Including zero and negative values.

$$g(t) = \sum_{k=-\infty}^{\infty} G[f_k]e^{j2\pi f_k t} \tag{C.2}$$

Where Fourier coefficients $G[f_k]$ are given

$$G[f_k] = \frac{1}{T}\int_{-\frac{T}{2}}^{\frac{T}{2}} g(t)e^{-j2\pi f_k t}dt \tag{C.3}$$

Where $f_k = kf_1$ and the square brackets are used to emphasize that the domain of this function is a discrete set of frequencies.

At this stage it is important to notice that if the function $g(t)$ is real-valued, then each component at frequency f_k must be matched by a component at $-f_k$ which has equal amplitude but opposite phase. Therefore the imaginary parts at all frequencies will always be canceled and the resultant will always be real.

The relationship concerning the distribution with frequency of the power content of the signal can be now established. The instantaneous power of the time signal $g(t)$ is equal to $\{g(t)\}^2$ and the mean power over one period is given by integrating the instantaneous value over one period and dividing by the periodic time.

$$P_{\text{mean}} = \frac{1}{T}\int_0^T \{g(t)\}^2 \, dt \tag{C.4}$$

For typical sinusoidal component $A_k\cos(2\pi f_k t + \phi_k)$ this results in

$$\begin{aligned}
P_{\text{mean}} &= \frac{1}{T}\int_0^T A_k^2\cos^2(2\pi f_k t + \phi_k)dt \tag{C.5}\\
&= \frac{A_k^2}{T}\int_0^T \frac{1}{2}\left(1 - \cos 2(2\pi f_k t + \phi_k)\right)dt \tag{C.6}\\
&= \frac{A_k^2}{T} \tag{C.7}
\end{aligned}$$

The spectrum of squared amplitudes is known as the *power spectrum*, and this is often the most useful part of the entire spectra. Nonetheless, the initial phase infirmation is lost, and it is not possible to re-synthesize the original time signal from the power spectrum. [53]

C.2 Fourier transform

All the previous results apply to periodic signal but it is possible to extend Equation C.3 to a more general case by letting $T \to \infty$. In this case, the spacing $1/T$ between the harmonics tends to zero and $G[f]$ becomes a continuous function of f

$$G[f] = \int_{-\infty}^{\infty} g(t)e^{-j2\pi ft}dt \tag{C.8}$$

The latest equation, known as the forward *transform* can be combined to Equation C.2 to give

$$g(t) = \int_{-\infty}^{\infty} G[f]e^{j2\pi ft}df \tag{C.9}$$

which is known as the *inverse transformation*.

Together they form the so-called *Fourier Transform Pair*. The only difference between them is the sign of the exponent of the exponential.

C.3 Sampled time functions

Another form of Fourier Transform pair applies to sample functions, or functions which are represented by a sequence of values at discrete equi-spaced points in time. This case is really important in digital processing of data.

It can be seen that this situation is the reverse of au Fourier transform pair, it happens that the spectrum becomes periodic, with a period equal to the sampling frequency $F_s = 1/\Delta t$.

The Fourier transform equation becomes

$$G[f] = \sum_{n=-\infty}^{\infty} g(t_n)e^{-j2\pi ft_n} \tag{C.10}$$

$$g(t_n) = \frac{1}{F_s} \int_{-\frac{f_s}{2}}^{\frac{f_s}{2}} G[f]e^{j2\pi f t_n} df \tag{C.11}$$

Where $t_n = n\Delta t$ represents the time corresponding to the nth time sample.

C.4   Discrete Fourier Transform (DFT)

It occurs when the function are sampled in both time and frequency domain. Owing to the sampling, it is evident that both time signal and frequency spectrum are implicitly periodic.

The forward transform takes the form of

$$G[k] = \frac{1}{N} \sum_{n=0}^{N-1} g(n)e^{-j\frac{2\pi kn}{N}} \tag{C.12}$$

while the inverse transform takes the form of

$$g[n] = \sum_{k=0}^{N-1} G[k]e^{j\frac{2\pi kn}{N}} \tag{C.13}$$

Owing to the infinite continuous integral of Equations C.8 and C.9 have been replaced by finite sums; known as $\boldsymbol{Discrete\ Fourier\ Transform\ (DFT)}$, much better to digital computations.

Hence, obtaining N frequency components from N time samples requires N^2 complex multiplication. A calculation procedure known as the $\boldsymbol{Fast\ Fourier\ Transform}$ ($\boldsymbol{FFT}$) algorithm can lead to the same result with a number of complex multiplication of the order of $N\log_2 N$.

C.5 Aliasing

The misinterpretation of high frequencies (above half the sampling frequency according to Shannon's sampling theorem) as lower frequencies is called *aliasing*. This is one of the pitfalls to avoid when digitizing continuous signals.

Considering these two practical cases may help to understand this problem

i. The cartwheels in western films often appear to run backwards, i.e. negative frequency, or too slowly forwards owing to the sampling involved in filming.

ii. The stroboscope is in fact an aliasing device which is designed to represent high frequencies as low ones, even zero frequency when the picture is frozen.

Figure C.1 shows the aliasing effect while sampling a sinusoidal signal, it can be noticed that the period of the output waveform is much longer (slower) than that of the input waveform, and the two waveform shapes are different.

It should be understood that the Nyquist frequency is an absolute maximum frequency limit for an ADC, and does not represent the highest practical frequency measurable. To be safe, it should not be expected that an ADC can successfully resolve any frequency greater than one-fifth to one-tenth of its sample frequency.
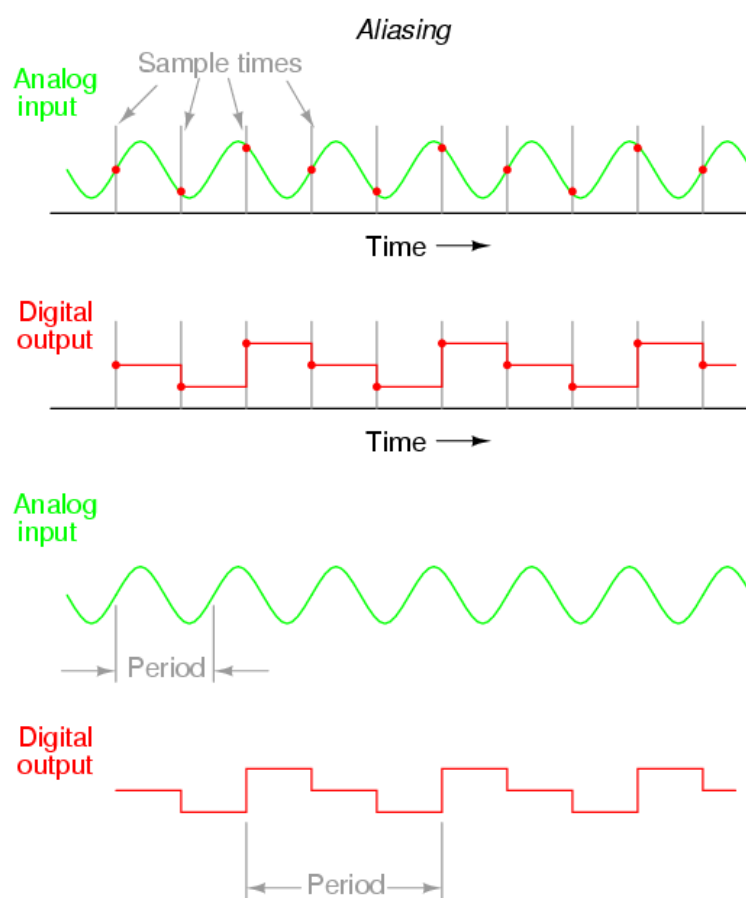
Appendix based on [37, 53, 55].

Figure C.1: Illustration of aliasing effect [Anonymous]

Low pass filters

A low-pass filter is a filter that passes low-frequency signals but attenuates/reduces the amplitude of signals with frequencies higher than the cutoff frequency. The actual amount of attenuation for each frequency varies from filter to filter. It is sometimes called a high-cut filter, or treble cut filter when used in audio applications.

The concept of a low-pass filter exists in many different forms, including electronic circuits (like a hiss filter used in audio), digital algorithms for smoothing sets of data, acoustic barriers, blurring of images, etc.

A low-pass filter can be made of RC, LR, operational amplifier, and RLC circuit. However, this appendix only describes the principles of a RC, (passive) and an operational amplifier[1] based (active) low-pass filter. Applying the same principles to the other circuits will lead to the same conclusions.

D.1   RC circuit based low-pass filter

Figure D.1 depicts a low pass RC filter for voltage signals. Signal V_out retains unattenuated only frequencies below the cut-off frequency of the filter set by its RC time constant $\tau = RC$.

---

[1]An op-amp is a DC-coupled high-gain electronic voltage amplifier with differential inputs and, usually, a single output. Its output is controlled either by negative feedback, which largely determines the magnitude of the output voltage gain, or by positive feedback, which facilitates regenerative gain and oscillation. High input impedance at the input terminals and low output impedance are important typical characteristics. [37]
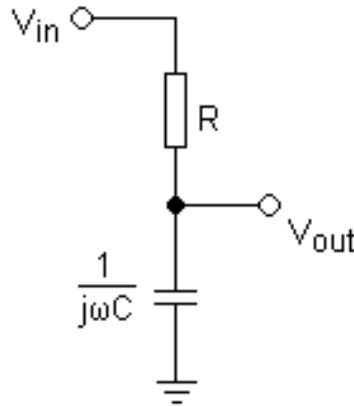
Figure D.1: A low-pass electronic filter realized by an RC circuit.

A RC low-pass filter consists of a resistor in series with a load, and a capacitor in parallel with the load. The capacitor exhibits reactance, and blocks low-frequency signals, causing them to go through the load instead. At higher frequencies the reactance drops, and the capacitor effectively functions as a short circuit.

A capacitor is a charge storage device. Its capacitance is defined as the quantity of charge stored ar a unit voltage across the capacitor. Its reactance is defined as follow

$$X_C = \frac{1}{\jmath\omega C} = \frac{-\jmath}{2\pi\nu C} \tag{D.1}$$

Where ν is the frequency, ω the pulsation, and C the capacitance.

Therefore, when the frequency is high, X_C tends towards to zero and the capacitor functions as a short circuit. However, when the frequency is low, X_C tends towards to infinity and blocks the current.

The following equations are valid for an ideal capacitor.

$$V = \frac{q}{C} \tag{D.2}$$

$$I = \frac{dq}{dt} \tag{D.3}$$

$$I = C\frac{dV}{dt} \tag{D.4}$$

where V is the voltage, I the current, q the charge.

Using Ohm's law it is possible to write the following equation to define the circuit.

$$I = \frac{dq}{dt} = \frac{V}{R} + C\frac{dV}{dt} \tag{D.5}$$

If the currents and voltages are assumed to be harmonic functions, the following can be derived.

$$V = \frac{q}{\left(1 + \frac{1}{\jmath\omega RC}\right)C} = \frac{q}{\left(1 + \frac{1}{\jmath\omega\tau}\right)C} \tag{D.6}$$

$$= \frac{q\left(1 + \jmath\frac{1}{\omega RC}\right)}{\left(1 + \frac{1}{\omega^2\tau^2}\right)C} \tag{D.7}$$

The cut-off frequency is defined as the frequency for which $\omega\tau = 1$, therefore

$$\nu_c = \frac{1}{2\pi RC} = \frac{1}{2\pi\tau} \tag{D.8}$$

All the frequencies lower than n_c will passed through the filter when the higher will be reduces by the filter.

D.2 Operational amplifier based low-pass filter

This kind of low-pass filter is basically the same except that it include a operational amplifier, often called an op-amp.

In this case, the cut-off frequency is defined by the resistance and the capacitor present in the negative feedback loop (Figure D.2).

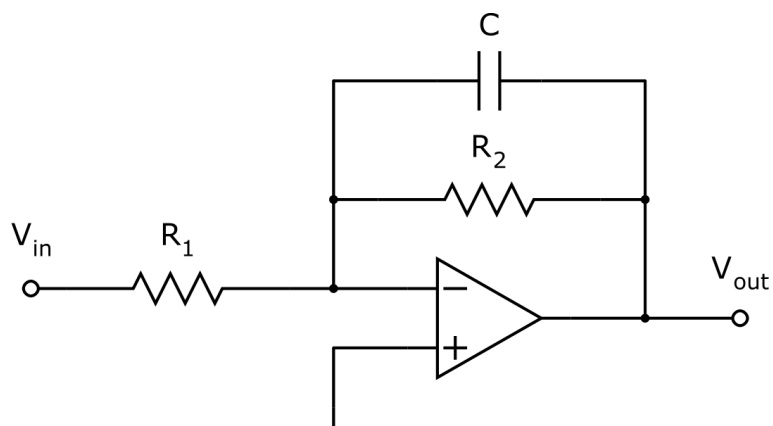$$\nu_c = \frac{1}{2\pi R_2 C} \tag{D.9}$$

Figure D.2: An operational amplifier based active low-pass filter.

Appendix based on [9, 37, 55].

Appendix E

Mathematical approximation of the bias

The mass m_{ij} of each increment is included in $[9.0; 11.0]$ and the average mass is equal to $[10.0 \pm 0.165]g$.

The mass m_C of the composite samples made of N increments is defined by

$$m_C = \sum_{i=1}^{N} m_{ij} \tag{E.1}$$

Where i is the running number for the individual increments and j the running number for the replicates.

The mass of the analyte m_{aC} in the composite samples is defined by

$$m_{aC_j} = \sum_{i=1}^{N} m_{a_{ij}} \tag{E.2}$$

The grade of the each increments and the grade of the composite samples are defined by

$$a_{ij} = \frac{m_{a_{ij}}}{m_{ij}} \tag{E.3}$$

$$a_{C_j} = \frac{m_{aC_j}}{m_{C_j}} = \frac{\sum\limits_{i=1}^{N} m_{a_{ij}}}{\sum\limits_{i=1}^{N} m_{ij}} \tag{E.4}$$

Since the average increment mass is centered on $[10.0 \pm 0.165]g$, it can be approximated to be equal to 10, therefore $m_{ij} \approx m$ and Equation E.4 becomes:

$$a_{C_j} = \frac{\sum\limits_{i=1}^{N} m_{a_{ij}}}{\sum\limits_{i=1}^{N} m_{ij}} \approx \frac{\sum\limits_{i=1}^{N} m_{a_{ij}}}{N \times m} = \frac{1}{N} \sum\limits_{i=1}^{N} \frac{m_{a_{ij}}}{m} \tag{E.5}$$

$$\approx \frac{1}{N} \sum\limits_{i=1}^{N} a_{ij} = \overline{a_{ij}} \tag{E.6}$$

Which is the average analytical grade of the individual increments.

The relative sampling error e_{C_j} of the composite samples of replicate j is therefore approximated by

$$e_{C_j} \approx \frac{\overline{a_{ij}} - a_L}{a_L} \tag{E.7}$$

Whereas the bias of the individual component is defined as

$$m_{e_{ij}} = \overline{e_{ij}} = \frac{1}{N} \sum\limits_{i=1}^{N} e_{ij} = \frac{1}{N} \sum\limits_{i=1}^{N} \frac{a_{ij} - a_L}{a_L} \tag{E.8}$$

$$= \frac{1}{N} \times \frac{1}{a_L} \sum\limits_{i=1}^{N} (a_{ij} - a_L) = \frac{1}{N} \times \frac{1}{a_L} \left(\sum\limits_{i=1}^{N} a_{ij} - \sum\limits_{i=1}^{N} a_L \right) \tag{E.9}$$

$$= \frac{1}{N} \times \frac{1}{a_L} \left(\sum\limits_{i=1}^{N} a_{ij} - N a_L \right) = \left(\frac{1}{N} \sum\limits_{i=1}^{N} a_{ij} \right) \times \frac{1}{a_L} - 1 \tag{E.10}$$

$$= \frac{\overline{a_{ij}} - a_L}{a_L} \approx e_{C_j} \tag{E.11}$$

Therefore, since the bias of the composite samples is defined as

$$m_{e_C} = \overline{e_{C_j}} \qquad \text{(E.12)}$$

and taking into account that the TENIRS sampling valve has a high degree of reproducibility (see Section 15.2.2 on page 133), each e_C is centered around the same average value, the average bias of the composite samples is close to the average bias of the individual increments. Furthermore, as the individual increments are not representative of the true analytical grade of the lot, the composite sample will not be representative either.

Settings for acquisition of acoustic spectra

The aim of the acoustic measurements was to illustrate the feasibility of applying acoustic chemometrics for on-line determination of the concentration of dry mater in bio-slurry.

Device	Remark
Process analyzer	PSA100i, Process Signature Analyser, Detect A/S, Porsgrunn, Norway
Accelerometer	DeltaTron general purpose piezoelectric accelerometer, insulated base, Brüel & Kjær part no. 4396
Other device	Remark
Software	APM_setup version 2.0.3, release 09.09.2005
Signal cable, accelerometer	75Ω 1,2 m coaxial with BNC connector and miniature coaxial plug, single shielded
Signal cable, computer	RS232 Sub-D, 9 leads, 15 m, female-female, null modem cable

Table F.1: Method parameters for acquisition of acoustic spectra

Parameter	
Number of axis	1
Temperature range, operation	$-50°C$ to $+125°C$
Weight	$18.2g$
Height	$23.7mm$
Spanner size	$15.0mm$
Sensitivity, axial	$10mVm^{-1}s^2$
Acoustic sensitivity, typical	$2mN$ or $0.002ms^{-2}$
Measuring range, typical ($T < 100°C$)	$750ms^{-2}$
Frequency range, typical	$1 - 14000Hz$
Temperature range, environment	$-50°C$ to $+125°C$

Table F.2: Characteristics for the applied accelerometer

Dialog box	Parameter	Value
I/O	Port	Select the computer port to which the cable is connected.
	Input Channel	Tick the box Activated to active the channel you when to listen to. Tick also $0 - 20mA$.
Data format	FFT	Tick the boxes: Show chart; Save to file; Automatic.
		Samples in chart: 1024
FFT	Number of average FFT meas	100
	LP Filter	15
	Gain 1	15
	Gain 2	4

Table F.3: Software parameters for acoustic measurements

Appendix G

TENIRS – Batch preparation

The below procedure of batch preparation is used for the sampling study and the acoustic measurements.

G.1 Plastic pellets based batch

   i. Tare a precision scale with a clean beaker;

  ii. Add plastic pellets to the beaker until reaching the desired mass;

 iii. Tare a scale with a clean $1L$ TENIRS bottle;

 iv. Pour the pellets inside;

  v. Adjust the mass to $1kg$ using water;

 vi. Add one drop of anti-foam (tween-80) to lower the surface tension of the water.

G.2 Synthetic manure based batch

   i. Crush (macerate) the lignocellulosic fibers into a powder to avoid clogging;

  ii. Pass the rapeseed through a sieves to remove all extraneous fibers and agglomerate of seeds;

 iii. Tare a precision scale with a clean beaker;

 iv. Add rapeseed to the beaker until reaching the desired mass;

  v. Tare a scale with a clean $1L$ TENIRS bottle;

    vi. Pour in the designed rapeseed masse;

   vii. Tare a precision scale with a clean beaker;

  viii. Add lignocellulosic fibers to the beaker until reaching the desired mass;

    ix. Pour the lignocellulosic fibers in the TENIRS bottle;

    x. Pour the desired quantity of glycerol (according to its concentration) in the TENIRS bottle;

   xi. Adjust the mass to $1kg$ using water;

  xii. Add one drop of anti-foam (tween-80) to lower the surface tension of the water.

Appendix H

Acoustic models

This appendix documents the multivariate model for dry matter based on acoustic spectra.

For the PLS-1 regression all X-variables (the spectra) were scaled (multiplied by the inverse standard deviation) and centered in order to equalize the variances of the X-variables. The total solids concentrations (y-data) were also scaled and centered.

H.1 Model based on model-systems made of heavy pellets

The acoustic spectra is made of 1024 variables (X-variables) and is presented in Figure H.1.

It can be seen from the spectra that the last 512 X-variables – highest frequencies – lie approximatively on a flat line. Therefore, the spectra is reduced to the first 512 variables as shown in Figure H.2

Prior to start modeling it must be said that 3 samples are expected to be outliers due to manipulation problems in the laboratory.

Figure H.3 shows the first model based on the reduced acoustic spectra. One PLS component is needed to model the mass of pellets in the batch. The model is test set validated. The slope $s = 0.92$, the correlation coefficient $r^2 = 0.91$ and the RMSE is
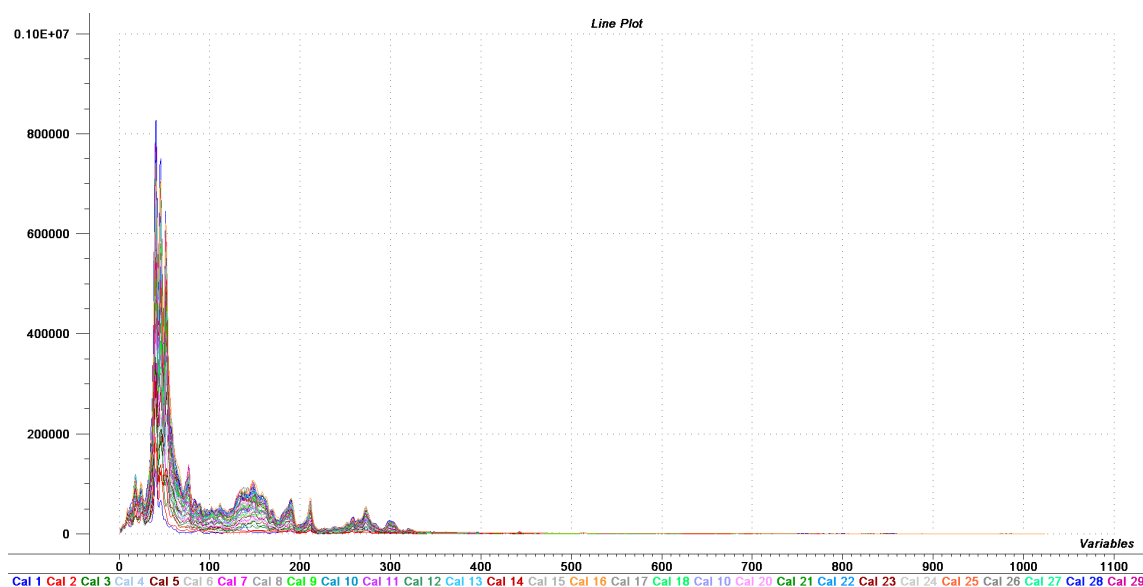
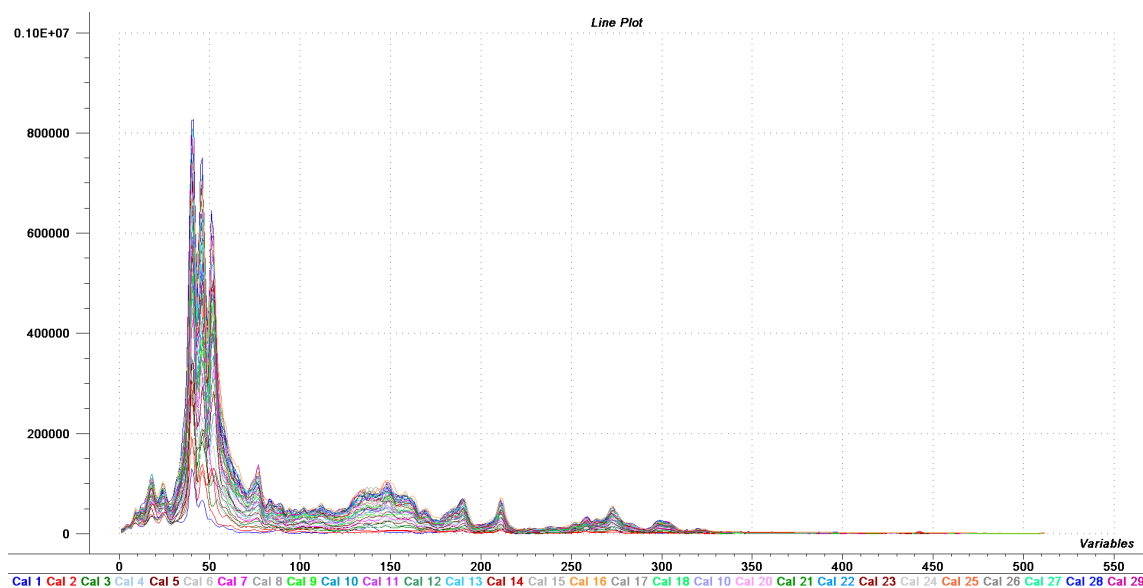Figure H.1: Complete acoustic spectra for model-systems made of heavy pellets.

Figure H.2: Reduced (512 first variables) acoustic spectra for model-systems made of heavy pellets.

AALBORG UNIVERSITY ESBJERG

low which hope to have a good model.

As expected three samples three samples seem to be outliers (samples 2, 42, and 44). A new model excluding them is computed.
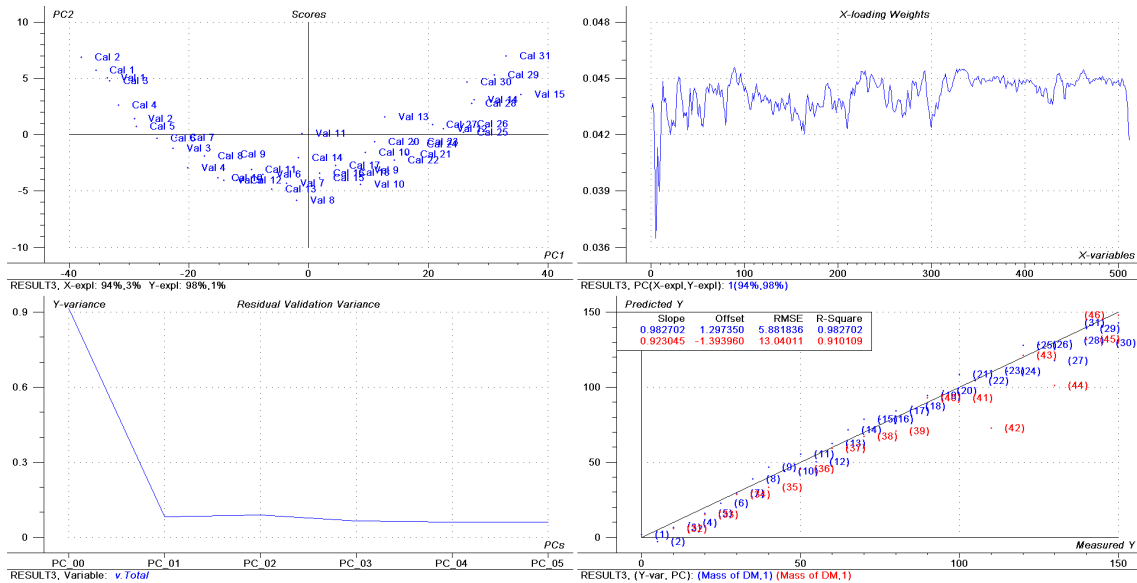

Figure H.3: First model based on the reduced acoustic spectra for model-systems made of heavy pellets – Model based on the reduced acoustic spectra – Test set validation.

Figure H.4 shows the final model obtained for the heavy pellets. The slope $s = 1.03$, the correlation coefficient $r^2 = 0.98$, the Residual Validation Variance $RVV = 0.02$, Root Mean Square Error of Prediction $RMSEP = 5.31$, and the bias is -3.93. The system is of course simplistic since it is only composed by heavy pellets.
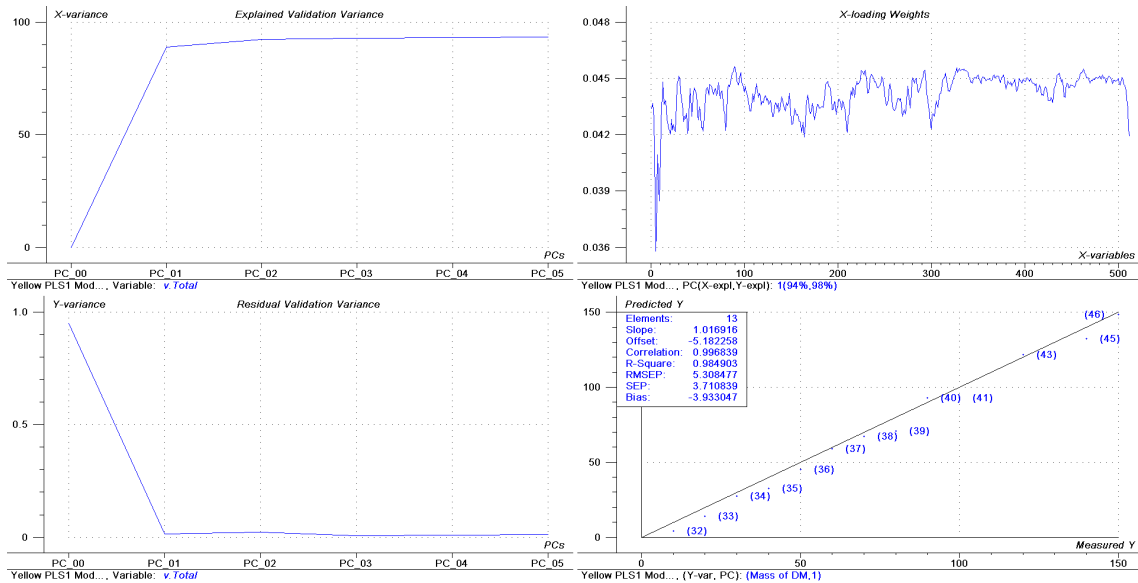
Figure H.4: Final model based on the reduced acoustic spectra for model-systems made of heavy pellets – Samples 2, 42, and 44 are excluded – Model based on the reduced acoustic spectra – Test set validation.

H.2 Model based on model-systems made of light pellets

The acoustic spectra is made of 1024 variables (X–variables) and is presented in Figure H.5.

The same observation regarding the last 512 X-variables can be made. Therefore, the spectra is reduced to the first 512 variables as shown in Figure H.6

Figure H.7 shows the first model based on the reduced acoustic spectra. One PLS component is needed to model the mass of pellets in the batch. The model is test set validated. The slope $s = 0.98$, the correlation coefficient $r^2 = 0.96$ and the RMSE is low which leave great hopes to have a good model.

By analyzing the score plots, sample 43 is revealed to be an outliers. Figure H.8 shows the final model obtained for the light pellets. The slope $s = 0.95$, the correlation coefficient $r^2 = 0.98$, the Residual Validation Variance $RVV = 0.01$, Root Mean Square Error of Prediction $RMSEP = 5.57$, and the bias is 0.46. Once a again it must be said that the system is simplistic since it is only composed by light pellets. However, this gives good hopes for the next models.
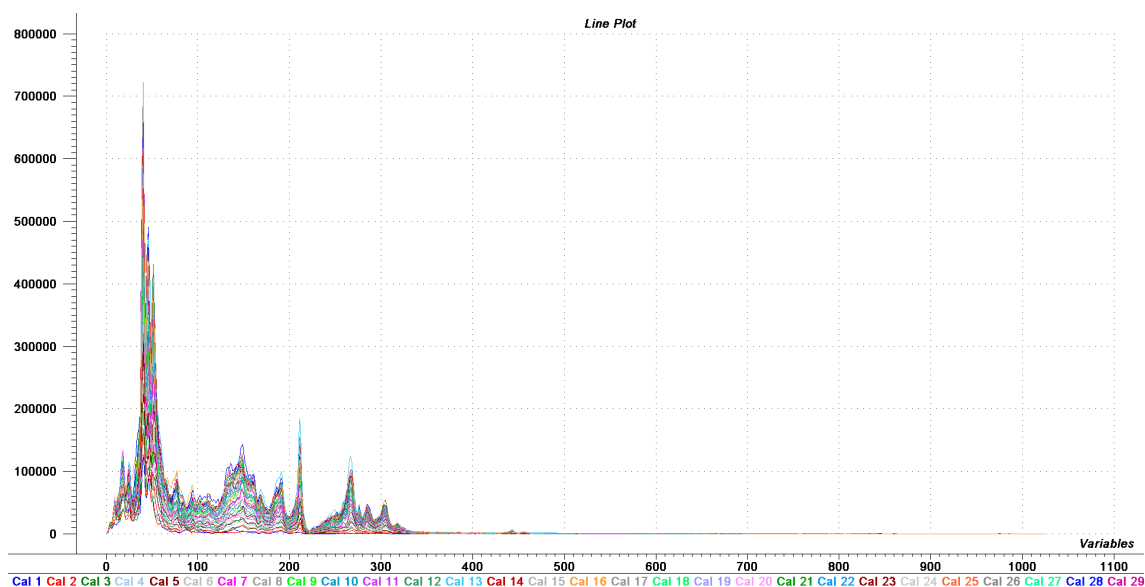
Figure H.5: Complete acoustic spectra for model-systems made of light pellets.
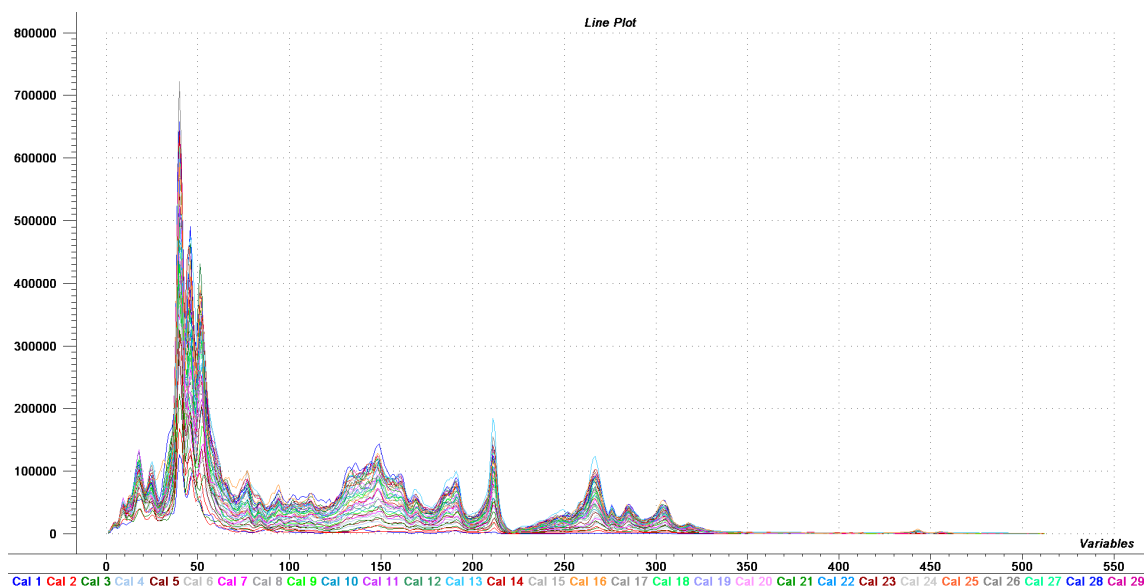

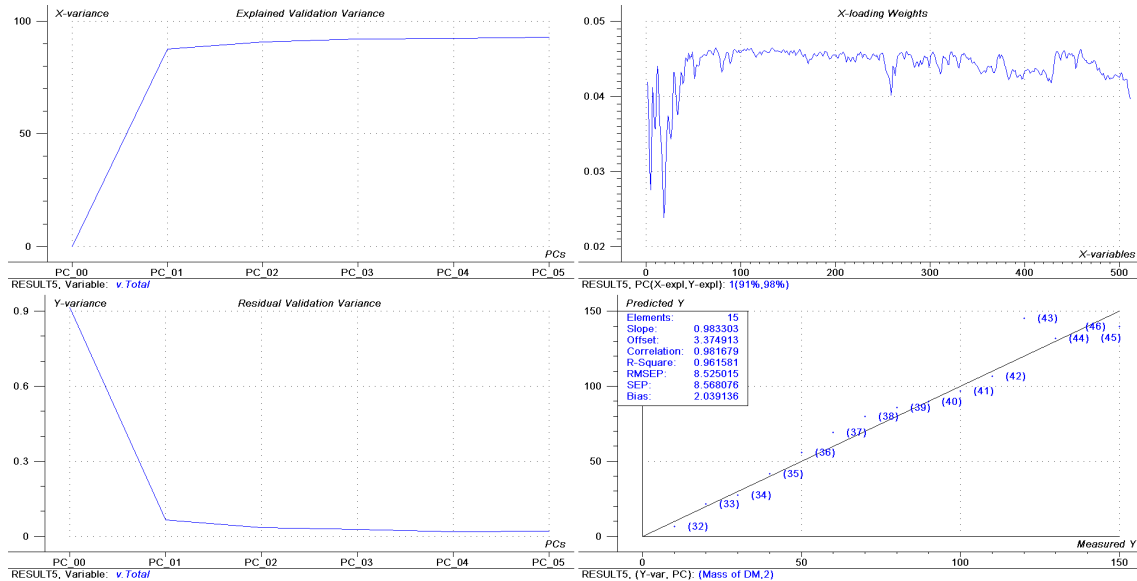Figure H.6: Reduced (512 first variables) acoustic spectra for model-systems made of light pellets.

Figure H.7: First model based on the reduced acoustic spectra for model-systems made of light pellets – Model based on the reduced acoustic spectra – Test set validation.
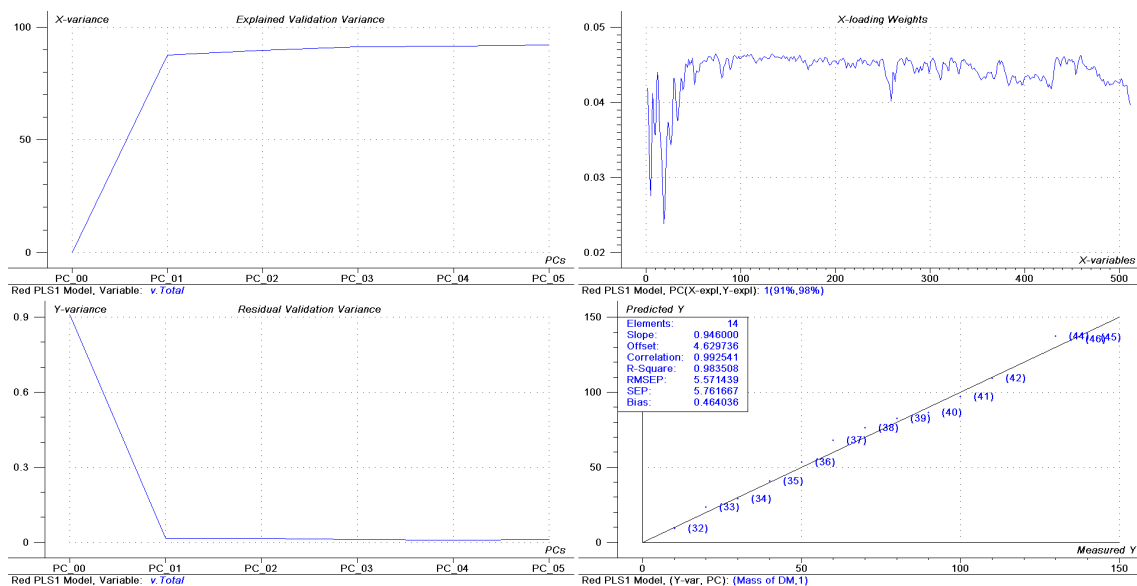

Figure H.8: Final model based on the reduced acoustic spectra for model-systems made of light pellets – Samples 43 is excluded – Model based on the reduced acoustic spectra – Test set validation.

H.3 Model based on model-systems made of light and heavy pellets

The models based on the light and heavy pellets are quite good which perhaps give high hopes for the model based on the mixture of both. Once again it must be said that the system is very simple compare to manure or synthetic manure.

The acoustic spectra is made of 1024 variables (X-variables) and is presented in Figure H.9.
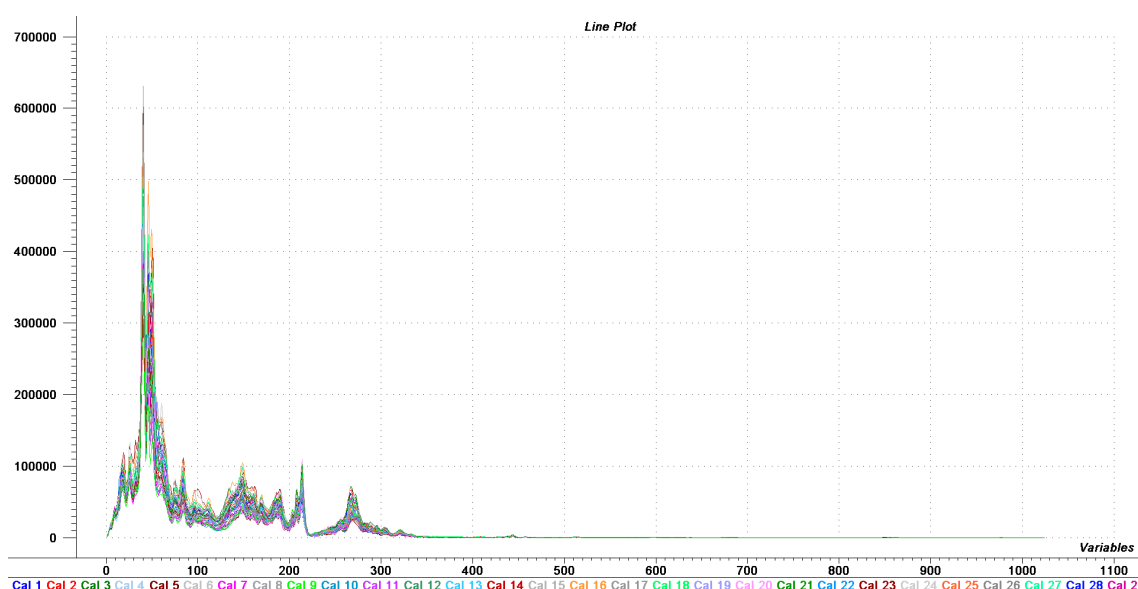

Figure H.9: Complete acoustic spectra for model-systems made of light and heavy pellets.

For the reasons already defined, the spectra is reduced to the first 512 variables as shown in Figure H.10
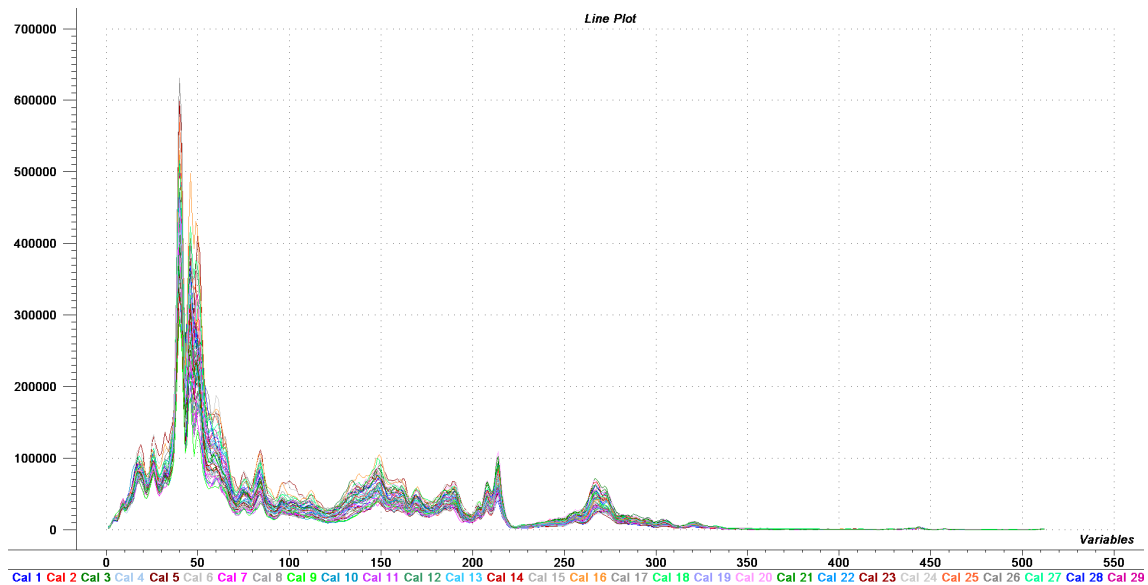
Figure H.10: Reduced (512 first variables) acoustic spectra for model-systems made of light and heavy pellets.

H.3.1 PLS1 Model to predict the mass fraction of heavy pellets

Figure H.11 shows the final model quantifying the content of heavy pellets content in model-systems made of light and heavy pellets. Four PLS component are required to model the broth. The slope $s = 0.99$, the correlation coefficient $r^2 = 0.98$, the Residual Validation Variance $RVV = 0.02$, Root Mean Square Error of Prediction $RMSEP = 4.23$, and the bias is 0.41. No samples are excluded.
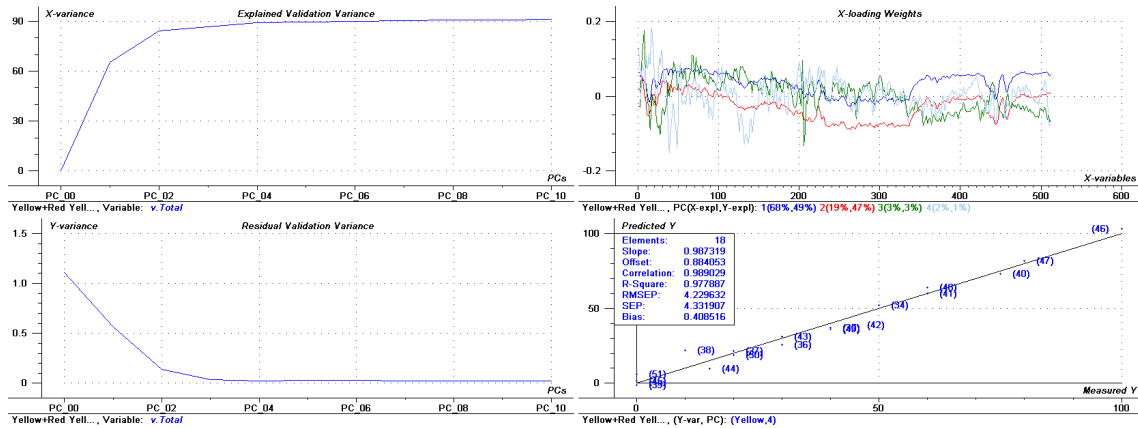
Figure H.11: Final model determining the quantity of heavy pellets for model-systems made of light and heavy pellets – No samples are excluded – Model based on the reduced acoustic spectra – Test set validation.

H.3.2 PLS1 Model to predict the mass fraction of light pellets

Figure H.12 shows the final model quantifying the content of light pellets content in model-systems made of light and heavy pellets. Four PLS component are required to model the broth. The slope $s = 1.02$, the correlation coefficient $r^2 = 0.96$, the Residual Validation Variance $RVV = 0.04$, Root Mean Square Error of Prediction $RMSEP = 5.79$, and the bias is 0.50. No samples are excluded.
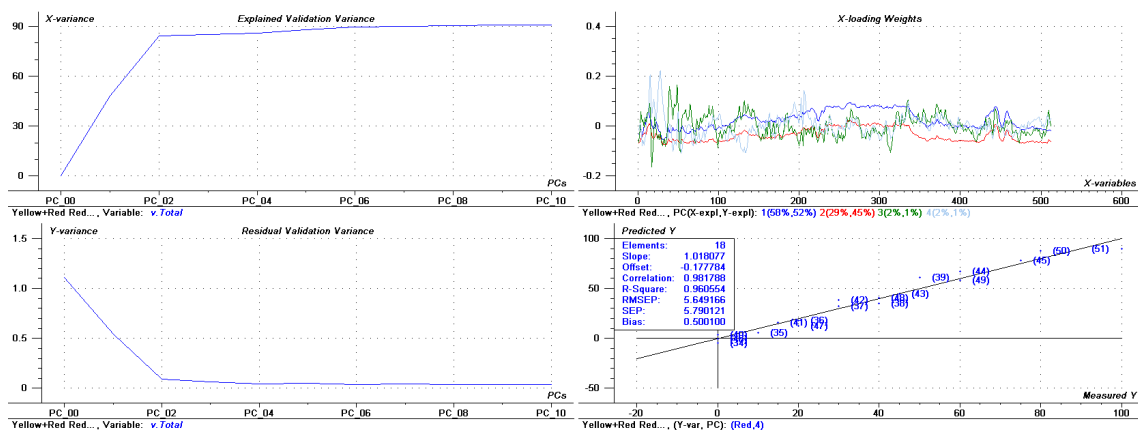

Figure H.12: Final model determining the quantity of light pellets for model-systems made of light and heavy pellets – No samples are excluded – Model based on the reduced acoustic spectra – Test set validation.

H.3.3   PLS1 Model to predict the mass of dry matter

Figure H.13 shows the final model quantifying the content of dry matter pellets content in model-systems made of light and heavy pellets. Three PLS component are required to model the broth. The slope $s = 0.99$, the correlation coefficient $r^2 = 0.92$, the Residual Validation Variance $RVV = 0.06$, Root Mean Square Error of Prediction $RMSEP = 5.20$, and the bias is 1.39. Samples 23, 24, 46, and 48 are excluded.
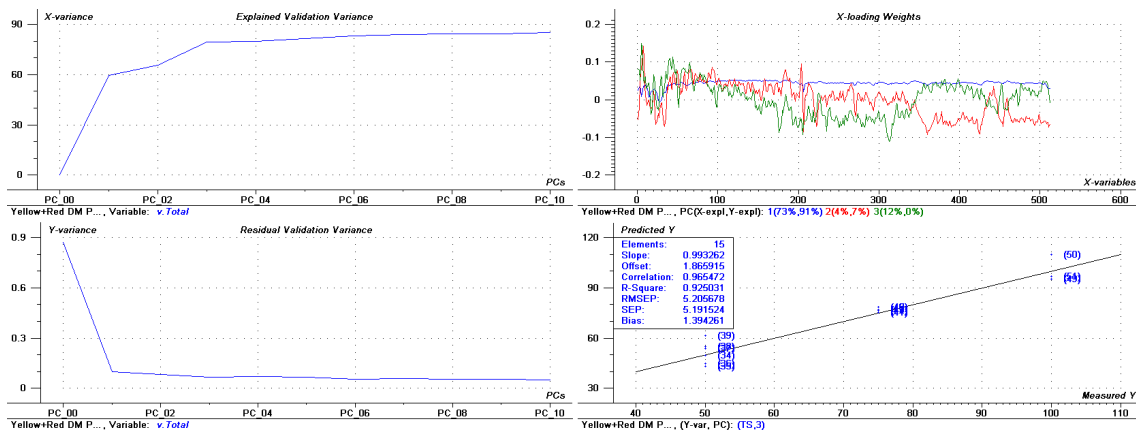

Figure H.13: Final model determining the quantity of dry matter pellets for model-systems made of light and heavy pellets – Samples 23, 24, 46, and 48 are excluded. – Model based on the reduced acoustic spectra – Test set validation.

H.4   Model based on batches made of synthetic manure

The acoustic spectra is made of 1024 variables (X-variables) and is presented in Figure H.14.

It can be seen from the spectra that the last 512 variables lie approximatively on a flat line. However, unlike the model based on the plastic pellets, sequential reductions of the spectra showed that the model is getting significantly better after when keeping only the first 350 variables (Figure H.15).

Model based on complete acoustic spectra is showed in Figure H.16 whereas model based on the first 350 variables is showed in Figure H.17.

The X-Y outliers plot were inspected for outliers, even though some points could be considered as outliers, removing them did not improve the model. Therefore the
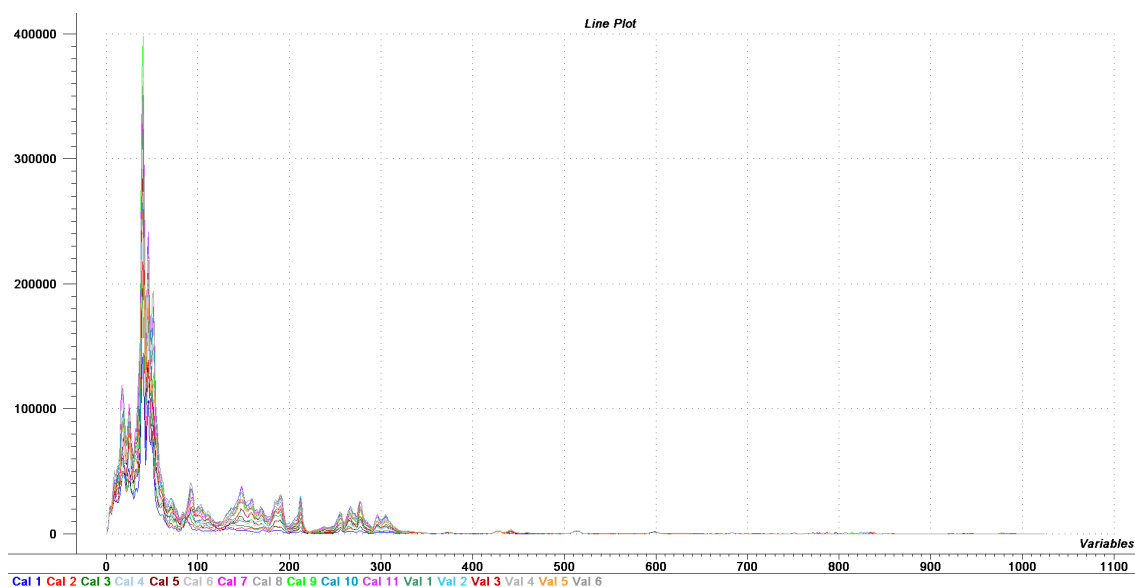
Figure H.14: Complete acoustic spectra for batches made of synthetic manure.
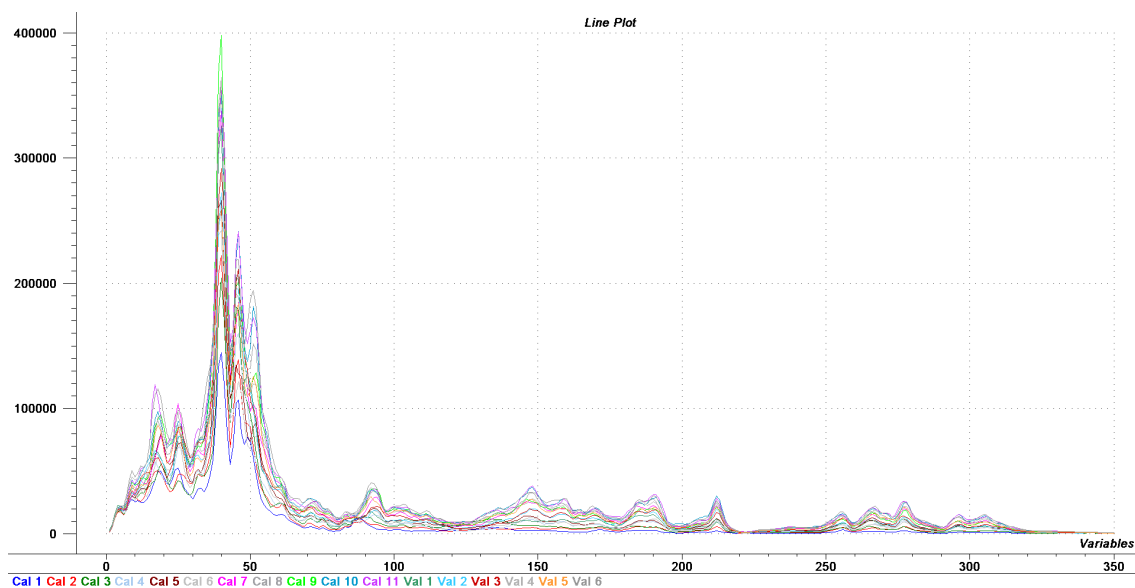

Figure H.15: Reduced (350 first variables) acoustic spectra for batches made of synthetic manure.
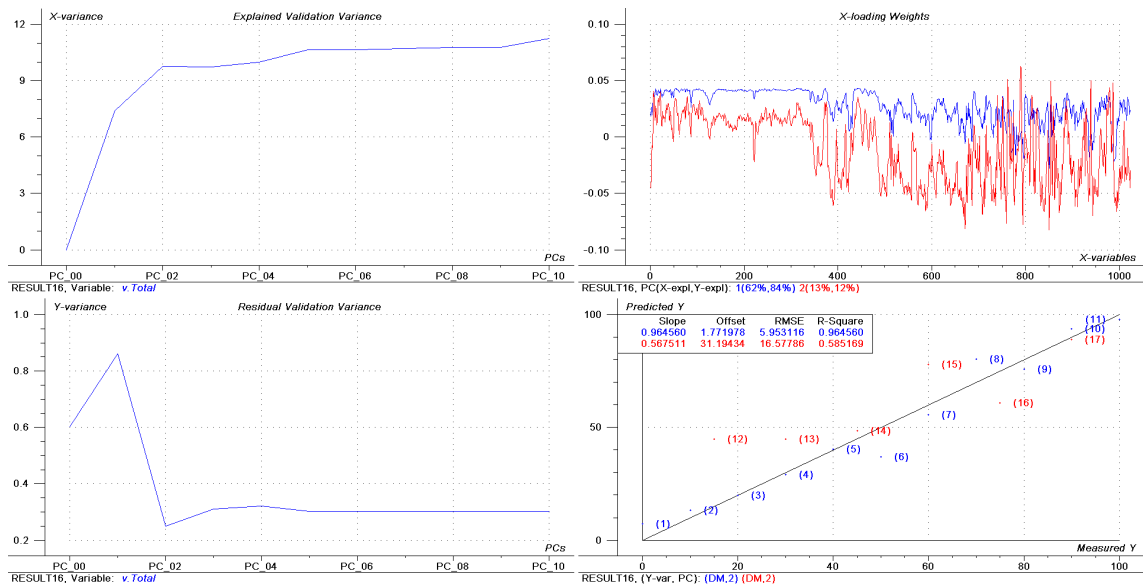
Figure H.16: Model predicting the dry matter content of the synthetic manure – Model based on the *complete* acoustic spectra – Test set validation.
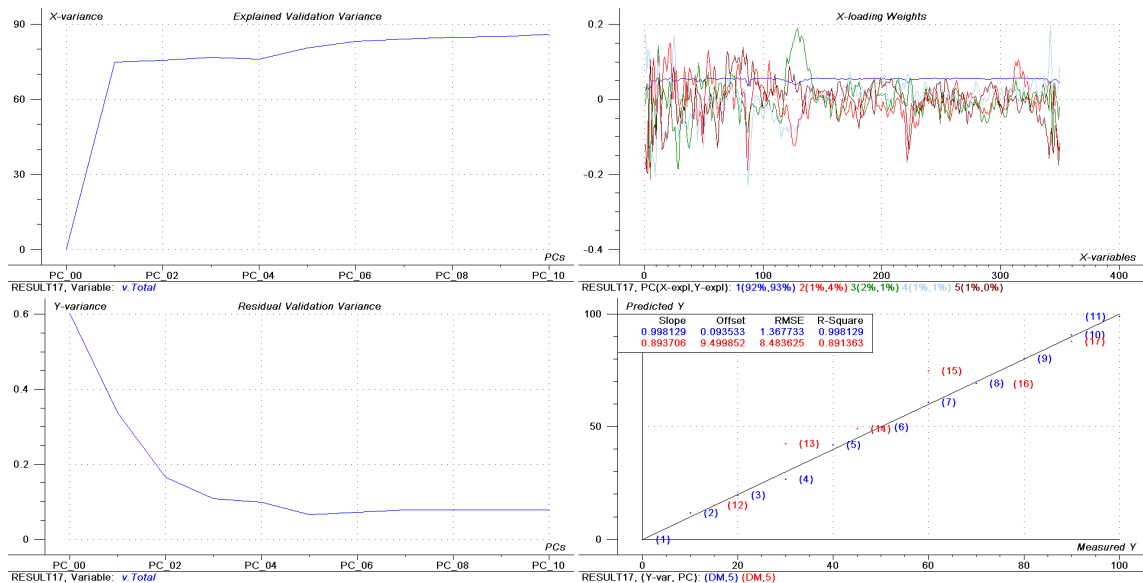

Figure H.17: Model predicting the dry matter content of the synthetic manure – Model based on the *first 350 variables* acoustic spectra – Test set validation.

model presented in Figure H.18 is considered to be the final model to determine the dry matter content in the synthetic manure.

Five PLS component are required to model the broth. The slope $s = 0.89$, the correlation coefficient $r^2 = 0.89$, the Residual Validation Variance $RVV = 0.06$, Root Mean Square Error of Prediction $RMSEP = 8.42$, and the bias is 3.91. Which is fully acceptable for such complicated system. No samples are excluded
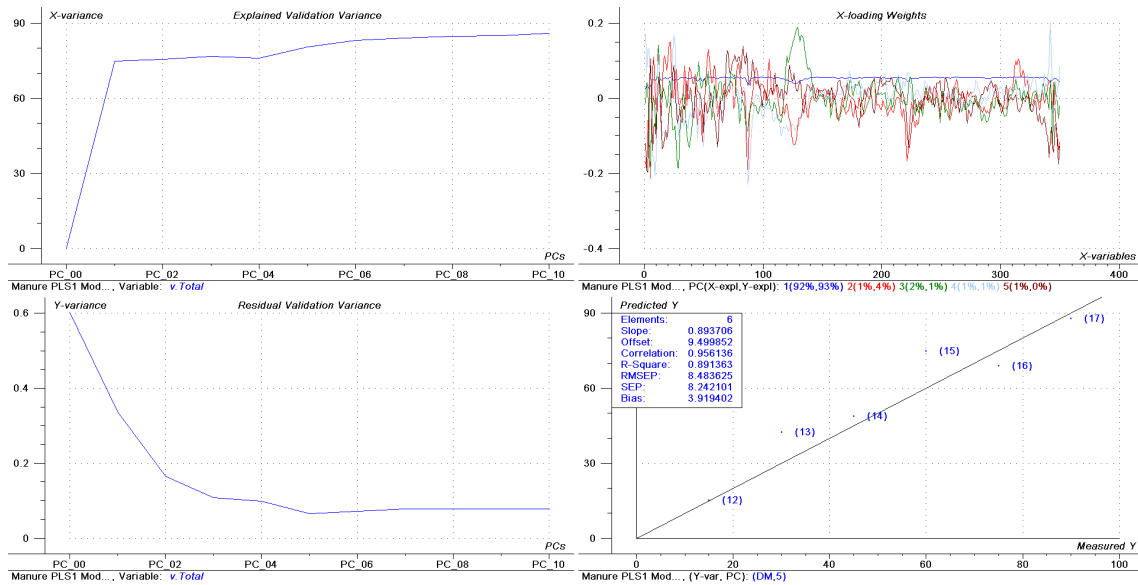
Figure H.18: Final model predicting the dry matter content of the synthetic manure – Model based on the first 350 variables acoustic spectra – No samples are excluded – Test set validation.

This model is a valuable indication that acoustic chemometrics is a powerful PAT modality, at least concerning physical Y-variables. Several a.c. studies [14, 16, 28, 30, 35] have strongly enclosed a.c. also for a variety of chemical and physical variables.

I

Data sheet – DeltaTron from Brüel & Kjær

Product Data

DeltaTron® Range

Miniature Accelerometer Types 4394, 4397
Accelerometer Types 4395, 4396, 4398, 4399
Charge Converter Type 2646
Power Supply ZG 0328

USES:

❍ Shock and vibration measurement

❍ Vibration analysis

❍ Vibration monitoring

❍ Vibration test control

❍ Product and quality control

❍ Charge converter for conventional accelerometers

❍ Adaptor for Brüel & Kjær analyzer inputs

❍ Accelerometers with:

  – Integral preamplifiers
    – All-welded construction
    – Delta Shear® Uni-Gain design
    – Plain or Insulated base
    – Low sensitivity to all extraneous environments
    – Individual standard-traceable calibration

FEATURES:

❍ All DeltaTron® products operate on constant-current line-drive principles

DeltaTron® is the generic name for the new family of accelerometers and signal conditioning products from Brüel & Kjær. The DeltaTron® name identifies products that are designed to operate on a constant-current power supply and to give output signals in the form of voltage modulation on the power supply line.

The DeltaTron® range described in this Data Sheet comprises:

❍ Piezoelectric accelerometers with integral preamplifiers.

❍ Charge converter for use with conventional accelerometers.

❍ Power supply/adaptor for use with Brüel & Kjær Signal Analyzers and other instruments with 7-pin microphone inputs.

All DeltaTron® accelerometers are individually calibrated and a calibration chart showing the individually measured frequency response curve is provided with each accelerometer.

In addition to the products described in this Data Sheet, Brüel & Kjær also supply DeltaTron® accelerometers for permanent industrial installations, a comprehensive range of Delta Shear® piezoelectric accelerometers and a wide range of signal conditioning amplifiers. Details of these products are given in their respective Product Data sheets.

4394
2646
4395
4396
4397
4398
4399

Brüel & Kjær

DeltaTron® Accelerometers

The DeltaTron® accelerometers described here are constructed to the proven Brüel & Kjær Delta Shear® design with the addition of an integral preamplifier. They require an external constant-current, power supply and operate as voltage sources.

DeltaTron® accelerometers operate over a frequency range from below 1 Hz to approximately half the resonance frequency of the accelerometer assembly. All are supplied with individual calibration charts which give individually measured frequency response curves (see Fig. 1).

Design and Construction

PZ 23 lead zirconate titanate, piezoelectric elements are used in the accelerometers, whose housings are all-welded. The accelerometers are available as types, with a plain base (no insulation), or as types with an insulated base.

On the insulated types the mounting bases are insulated by high-quality ceramic discs bonded between base and housing. Both base and housing are made of titanium, making the accelerometers very corrosion resistant.

The built-in preamplifier is a charge converter made using thick film technology. It comprises a low-noise MOS Field Effect Transistor as its input stage and a bipolar transistor to give low output impedance. A single-pole filter at the input extends the accelerometer's usable frequency range to approximately 50% of the mounted resonance frequency. Special efforts have been made to minimise interference from RF (radio frequency) electromagnetic fields.

Characteristics

Uni-Gain Sensitivity
The Brüel & Kjær Uni-Gain designation applies to all DeltaTron® accelerometers. This means that the accelerometer sensitivity is adjusted during manufacture to within 2% of either 1 or 10 mV/ms^{-2}.

Frequency response
The upper frequency limits given in the specifications are the frequencies where the deviation from the reference sensitivity is less than 10%. It is approximately 50% of the mounted resonance frequency. This assumes that the accelerometer is correctly mounted onto the test structure – a poor mounting can have a marked effect on the mounted resonance frequency.

The lower frequency limits and phase response are determined by the built-in preamplifiers. The lower frequency limits are given in the specifications for deviations from reference sensitivity of less than 10%.

The low damping of Brüel & Kjær accelerometers leads to the single, well-defined resonance peak shown on the frequency response curves.

The individually measured frequency response curves with absolute values of amplitude and phase are given on the calibration chart for the major part of the frequency range. At low and high frequencies, the curves given are typical (Fig. 1).
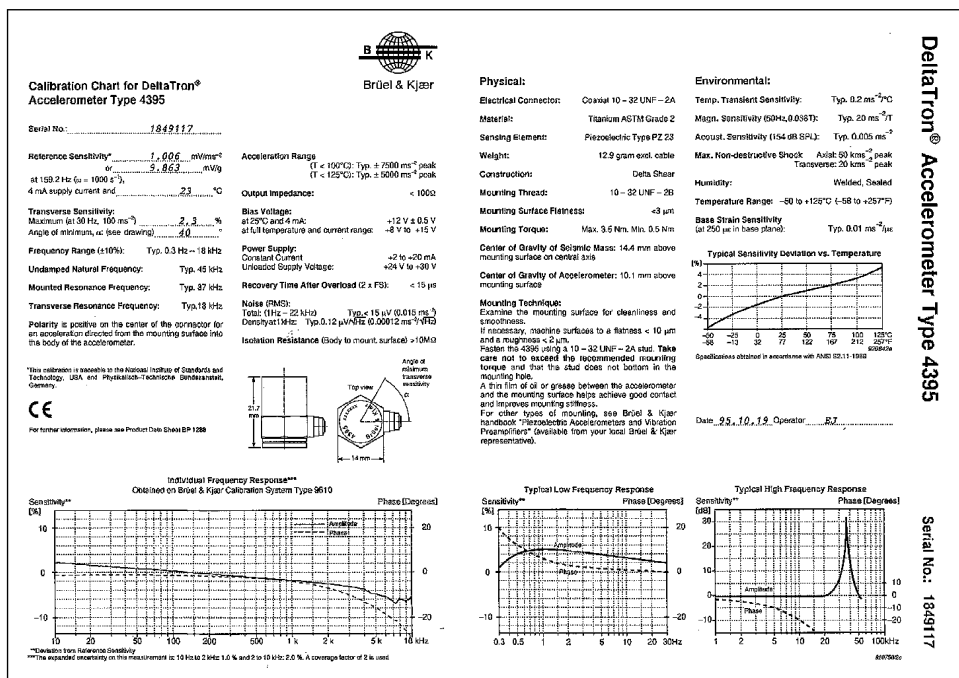

Fig.1 Example of the calibration chart supplied with Brüel & Kjær DeltaTron® accelerometers

Transverse Sensitivity

All piezoelectric accelerometers are slightly sensitive to acceleration that is perpendicular to their main sensitivity axis. This transverse sensitivity is measured during the factory calibration process using a 30 Hz and 100 ms^{-2} excitation, and is given as a percentage of the corresponding main axis sensitivity.

The direction of minimum transverse sensitivity is indicated on the calibration chart of each DeltaTron® accelerometer.

Transverse Resonance Frequency

Typical values for the transverse resonance frequency are obtained by mounting an accelerometer on the side of a steel cube attached to a Calibration Exciter Type 4290.

Dynamic Range

The dynamic range of an accelerometer is the range over which its electrical output is directly proportional to the acceleration applied to its base.

Upper Limit

In general, the smaller the accelerometer, the higher the vibration level at which it can be used. The upper limit depends on the type of vibration to which the accelerometer is subjected and is determined by the prestressing of the piezoelectric elements as well as by the mechanical strength of the element.

The acceleration ranges given in the specifications are determined by the measuring limits of the integral preamplifiers. For transporting and handling, the maximum non-destructive shock is given.

When short duration transient signals are measured, care must be taken to avoid ringing effects due to the high-frequency resonance of the accelerometer. As a general rule, the duration of a half sine shock pulse should be greater than $5/f_R$ for an amplitude error of less than 10%, where f_R is the mounted resonance frequency of the accelerometer.

Lower Limit

The lower limit is imposed by the noise level of the integral preamplifier, which has been constructed to give very low noise levels, and by the environment in which the measurements are made.

A discussion of the effect of environmental influences, can be found in the Brüel & Kjær handbook "Piezoelectric Accelerometers and Vibration Preamplifiers".

Electrical Impedance

All DeltaTron® accelerometers have integral preamplifiers and can be regarded as voltage sources. The output impedance is specified as typically less than 100 Ω. With a supply current of >4 mA output impedance is typically <30 Ω.

Environment

Temperature

DeltaTron® accelerometers are specified to an operating temperature range of −50°C to +125°C. Throughout this range, the sensitivity of the accelerometers has a small temperature dependence, details of this are given in the individual calibration charts (see Fig. 1).

Temperature Transients

All piezoelectric accelerometers have slight sensitivity to temperature fluctuations. This effect may be significant when low frequency, low level accelerations are being measured.

The procedure for measuring temperature transient sensitivity is described in the Brüel & Kjær handbook "Piezoelectric Accelerometers and Vibration Preamplifiers".

Humidity

DeltaTron® accelerometers have all-welded titanium housings to give them a high resistance to the majority of corrosive agents found in industry. The low impedance of the preamplifier gives it a low sensitivity to humidity on the output terminal and allows the accelerometers to be used without protection in conditions where there is small amounts of condensation.

Where heavy condensation is encountered, the use of moisture impervious cables and sealing will permit operation. Suitable sealants are Dow Cornings RTV 738 or similar compounds.

Sound Pressure

The acoustic sensitivity is low, and for most vibration measurements it can be neglected. The vibration signal from the structure-under-test is normally much greater than the signal due to acoustic sensitivity.

Acoustic sensitivity is specified as an equivalent acceleration caused by a 154 dB sound pressure level in the frequency range 2 Hz to 100 Hz, but the specified value is normally valid outside this range.

Electromagnetic Compatibility (EMC)

Susceptibility of DeltaTron® accelerometers to radio-frequency electromagnetic radiation is also low.

The accelerometers are certified (C€) to Standards EN 50081−1 and EN 50082−2 for emission and immunity, respectively.

EN 50081−1 covers:
- Radiated emission from 30 to 1000 MHz
- Conducted emission from 0.15 to 30 MHz.

EN 50082−2 covers the effects of:
- Radio frequency fields from 20 to 1000 MHz at a field strength of 3 and 10 V/m with an amplitude modulation of 80%
- Electrostatic discharge at 4 and 8 kV
- Transient bursts at 1 kV
- Magnetic fields from 50 Hz to 20 kHz with a strength of 30 A/m at 50 Hz

Base Strains

These can be introduced into an accelerometer by distortion of the surface to which it is attached.

Base strain sensitivity, which is minimised by the Delta Shear® construction, is specified in ms^{-2}/με.

Mounting

DeltaTron® accelerometers can be mounted with their main sensitivity axis aligned in any direction.

Recommended Mounting Technique

Fig. 2 shows the recommended mounting method for DeltaTron® accelerometers. Steel Stud YS 8321 is a flanged M3 stud which is used with Accelerometer Type 4394. It is available in sets of 25 as order number UA 1221. For the uninsulated miniature accelerometer Type 4397 steel stud YQ 2003 is used. For types 4395, 4396, 4398 and 4399, steel stud YQ 2962 is used. The accelerometers are screwed, using the stud, onto a clean metal surface meeting the requirements specified in Fig. 3. The optimum torque for tightening the M3 studs is between 0.2 Nm (1.8 lbf.-in) and 0.6 Nm (5.3 lbf.-in). For 10−32 UNF studs, the corresponding values are 0.5 Nm (4.4 lbf.-in) and 3.5 Nm (31 lbf.-in). To avoid possible damage to the ceramic disc, it is important that the maximum torque is not exceeded.

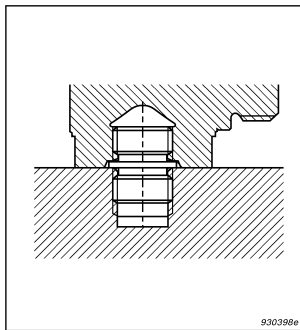It should be noted when using the recommended technique, that if the

3

Fig. 2 Recommended mounting technique for Type 4394, using a steel stud YS 8321 (YQ 2003 for uninsulated base, Type 4397)
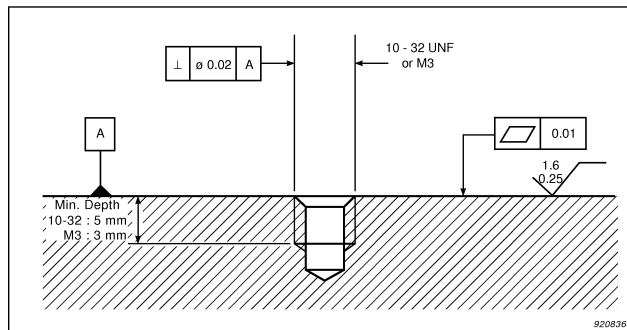

Fig. 3 Recommended tolerances for the mounting surfaces. Dimensions and symbols in accordance with ISO 1101

mounting surface is not perfectly smooth, the application of a thin layer of silicon grease to the base of the accelerometer before screwing it down on the mounting surface will improve the mounting stiffness.

Alternative Mounting Techniques
The section entitled Standard Accessories lists the mounting accessories that are supplied with individual accelerometers.

When mounting techniques other than the recommended one are used, the mounted resonance frequency of the accelerometer will probably be lowered. Most alternative mounting techniques are described in the Brüel & Kjær "Piezoelectric Accelerometers and Vibration Preamplifiers" handbook, where their effects on the frequency response are illustrated.

Connecting Cables

For direct connection to DeltaTron® accelerometers, miniature, double-screened low-noise, single-core, coaxial cables are available. These are a standard 1.2 m long, Teflon-insulated, cables that are supplied fitted with miniature coaxial plugs.

Types 4394 and 4397 require an M3 connector and is supplied with Cable AO 1381 which is fitted with one M3 and one 10−32 UNF connector. Types 4395, 4396, 4398 and 4399 are supplied with Cable AO 1382 which is fitted with two 10−32 UNF connectors. DeltaTron® Charge Converter Type 2646 is supplied without a cable, but AO 0406, a 5 m cable fitted with 10−32 UNF connectors and supplied with a 10−32 UNF to BNC adaptor, is available as an accessory. As an alternative, an AO 1382 cable

can be used. Additional cable lengths and connectors can be ordered.

Note, however, that for many, non-critical applications, lower quality cables or twisted pairs can be used. However, when such cables are used, the EMC certification is not valid.

Details of the accelerometer connections and recommended plug clearances are given in the section entitled Accelerometer Dimensions.

Maximum Cable Length
The maximum output voltage of a DeltaTron® accelerometer depends on the supply current at which it is operating, and on the capacitive load due to the connecting cable.

Fig. 4 shows typical curves for maximum output levels with supply currents of 2 and 20 mA (for distortion ≤1%). The maximum cable length in metres (L) is given by:

$$L = 75000 \times \frac{I_s}{f \times V_o \times C_m}$$

where:
I_s = supply current [mA]
f = frequency [kHz]
V_o = *output voltage* [V_{peak}]
C_m = *cable capacitance* [pF/m]

If the supply current is less than 4 mA, the power consumption of the built-in preamplifier becomes significant and this formula cannot be applied.

Calibration

Factory Calibration
All Brüel & Kjær Accelerometers are thoroughly checked and examined at each stage of manufacture and assembly. Every accelerometer under-

goes an extensive calibration procedure and artificial ageing process to ensure completely predictable performance and stable operation. Accurate numerical details of the calibration are reported on the calibration chart supplied with each transducer (see Fig. 1).

At Brüel & Kjær, piezoelectric accelerometers are calibrated by back-to-back comparison with a primary reference standard accelerometer which is regularly calibrated by laser interferometry at the Danish Primary Laboratory of Acoustics and by both the American National Institute of Standards and Technology and the German Physikalisch−Technische Bundesanstalt. The overall accuracy of the back-to-back comparison is 2% with a 99.9% confidence level (1.6% for a 99% confidence level), while for the interferometry method the accuracy is better than ±0.6% with a 99% confidence level.

Subsequent Calibration
Regular calibration of accelerometers helps maintain confidence in the measurements taken and indicates whether accelerometers have been damaged. Brüel & Kjær manufacture a range of equipment for frequency response, sensitivity and system calibrations, details of which are available in separate Product Data Sheets.

Individual Accelerometers

Dimensions and specifications for the accelerometers can be found in the schemes given towards the end of this Data Sheet.

**Miniature Accelerometer
Type 4394 and 4397**
These accelerometers are suitable for measurements on lightweight structures where relatively high-level, high-frequency vibrations are encountered.

**Shock and Vibration Accelerometer
Type 4395 and 4398**
Type 4395 and 4398 accelerometers are designed for the measurement of relatively high levels of continuous vibration and mechanical shock up to $7\,500\,\mathrm{ms}^{-2}$.

**General Purpose Accelerometer
Type 4396 and 4399**
These accelerometers are intended to be used for general purpose vibration measurements.

Charge Converter Type 2646

Charge Converter Type 2646 is a signal conditioner designed for use with standard piezoelectric accelerometers or other piezoelectric transducers. It requires an external, constant-current power supply, and its function is to convert a charge input to a voltage-modulation of the constant-current power supply lines.

Type 2646 is also designed to withstand severe environments so that it can be mounted directly onto transducers with 10 – 32 UNF top connectors, or located in close proximity to transducers with side connectors.

For miniature size and low weight, Type 2646 has thick film electronics that are double sealed in a silicone elastomer compound and contained in a titanium housing. Type 2646 is supplied without a cable, however there is a space in the case for storing a cable. Cables AO 0406 and AO 1382 are available as accessories.

Full specifications are given on the last page of this Data Sheet, and the

Fig. 4 Typical curves for maximum output level of DeltaTron® accelerometers, showing maximum capacitive load over the recommended current supply range

extensive range of accelerometers that are suitable for use with Type 2646 are described in the Brüel & Kjær Data Sheet "Piezoelectric Accelerometers" (BP 0196).

Power Supply Adaptor ZG 0328

The Power Supply Adaptor ZG 0328 is designed to connect directly into the 7-pin microphone (preamplifier) socket that is provided on many Brüel & Kjær instruments (except Types 2230 to 2235). The function of ZG 0328 is to adapt the socket for direct use with DeltaTron® accelerometers.

From the power available in the microphone socket, ZG 0328 provides the constant-current drive for the accelerometer and the signal input to the microphone socket.

How to Order Accelerometers

Accelerometers are available as standard or as a **Set**.

As standard an accelerometer is supplied with a cable and mounting studs (for example Order No. **4395**).

An **Accelerometer Set** (suffix S after the type number) consists of a single accelerometer complete with cable and accessories in a case.

A complete list of the accessories supplied with each set or standard version, is given in the section on Standard Accessories. Additional accessories are available on separate order.
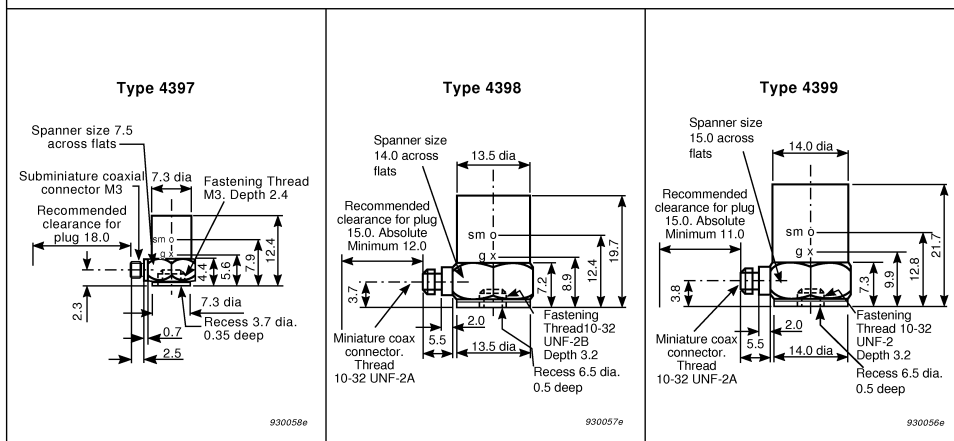
5

**Accelerometer Dimensions
Insulated Base**

Shown full scale
All dimensions in mm

Type 4394 · Type 4395 · Type 4396
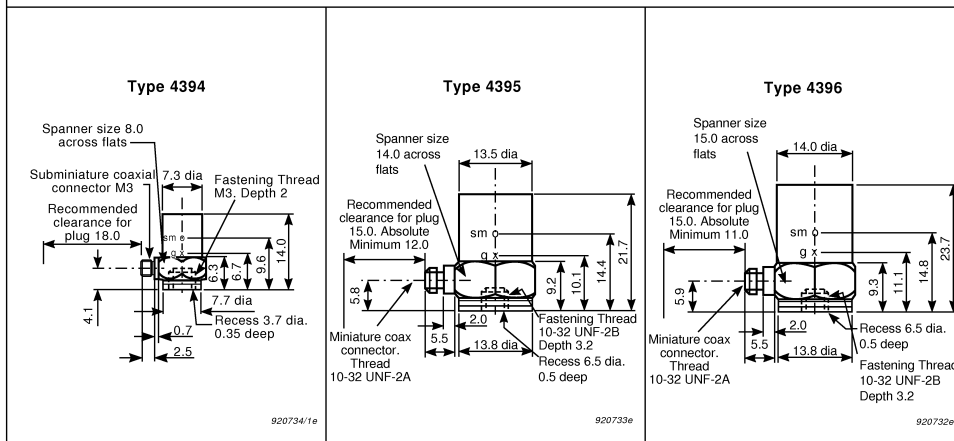
**Accelerometer Dimensions
Uninsulated Base**

Shown full scale
All dimensions in mm

Type 4397 · Type 4398 · Type 4399

6

Standard Accessories

B&K Part Number	Standard Accessories	4394		4395		4396		4397		4398		4399	
		S		S		S		S		S		S	
AO 1381	Teflon low-noise cable, double screened AC 0104 ($\varnothing$ 1.6 mm). Fitted with one 10–32 UNF and one M3 connector. Length 1.2 m	1	1					1	1				
AO 1382	Teflon low-noise cable, double screened AC 0104 ($\varnothing$ 1.6 mm). Fitted with two 10–32 UNF connectors. Length 1.2 m			1	1	1	1			1	1	1	1
JJ 0032	Extension connector for cables fitted with 10–32 UNF connectors	3		3		3		3		3		3	
JP 0145	10–32 UNF to BNC adaptor	1		1		1		1		1		1	
YS 8321	Steel stud M3/M3 (UA 1221 is a set of 25 of these studs)	3	3										
YQ 2003	Steel Stud M3, 5 mm long							3	3				
YQ 2960	10–32 UNF threaded steel stud. Length 0.5 in.			2		2				2		2	
YQ 2962	10–32 UNF threaded steel stud. Length 0.3 in.			3	1	3	1			3	1	3	1
YM 0414	10–32 UNF nut			1		1				1		1	
QA 0041	Tap for M3 thread	1						1					
QA 0029	Tap for 10–32 UNF thread			1		1				1		1	
DB 0757	Cement stud M3. Diameter 8 mm	1						1					
DB 0756	Cement stud 10–32 UNF. Diameter 14 mm			1		1				1		1	
QA 0042	Hexagonal key for M3 studs	1						1					
QA 0013	Hexagonal key for 10–32 UNF studs			1		1				1		1	
YJ 0216	Beeswax for mounting	1		1		1		1		1		1	
UA 0642	Mounting magnet with 10–32 UNF stud			1		1				1		1	
YO 0073	25 × adhesive mounting disc. Diameter 5.5 mm	1						1					
QS 0007	Tube of cyanoacrylate adhesive	1						1					
BC 0200	Individual calibration chart	1	1	1	1	1	1	1	1	1	1	1	1
	Accessory set included with S version	UA 1218		UA 1219		UA 1219		UA 1218		UA 1219		UA 1219	

Table 1 The accelerometers can be ordered as standard version (for example: Order No. 4395) or as an "S" version (for example: Order No. 4395 S). This table gives details about which accessories are supplied with accelerometers in the standard version and which are supplied with the "S" version

7

## Additional Accessories Available
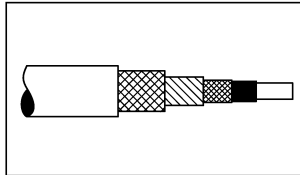
AC 0104. Teflon insulated double screened low-noise cable (illustrated).
AC 0005. Teflon insulated super low-noise cable.
AC 0200. Reinforced double screened version of AC 0005.
AC 0208. PVC coated cable
The EMC certification (CE) is only valid for AC 0104.

AO 0406. Teflon insulated double screened cable AC 0104 fitted with 10−32 UNF connectors and supplied with a 10−32 UNF to BNC adaptor (JP 0145). Length 5 m.
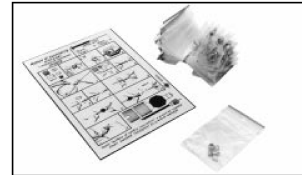
UA 0130. Set of 25 plugs JP 0012 for cable AC 0104 and AC 0005.
UA 0730. Set of 25 plugs JP 0056 for cable AC 0200. For mounting the plugs, the assembly tool QA 0035 is required.
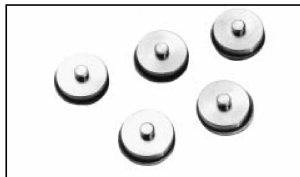
UA 0643. Set of 5 10−32 UNF mounting magnets UA 0642. Includes PTFE self adhesive discs for electrical insulation.
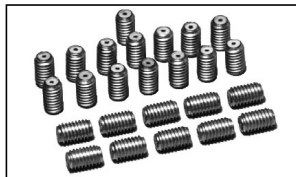
UA 0186. Set of 25 extension connectors JJ 0032 for miniature cables with plugs JP 0012 and JP 0056.

UA 0553. Set of 5 electrically insulated Mechanical Filters UA 0559, plus a tommy bar for mounting.

JP 0145. 10−32 UNF to BNC adaptor for connection of cables with miniature coaxial plugs JP 0012 and JP 0056.

QA 0035. Assembly tool for mounting miniature plugs on accelerometer cables.
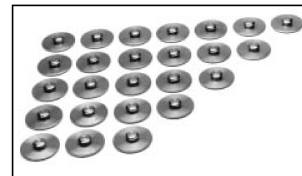
UA 0866. Set of 25 10−32 UNF cement studs DB 0756.
UA 0867. Set of 25 M3 cement studs DB 0757.

UA 1221. Set of 25 steel studs YS 8321.

UA 0125. Set of 10 insulating studs YP 0150, 10 steel studs YQ 2960, 10 nuts YM 0414, 10 mica washers YO 0534 plus 10−32 UNF tap and hexagonal key for 10−32 UNF studs.

8

Accelerometer Specifications
Insulated Base

Dynamic		Type 4394	Type 4395	Type 4396
Mounted Resonance Frequency, typical	kHz	52	37	28
Transverse Resonance Frequency, typical	kHz	15	13	9

Electrical

Case Insulation to Ground	MΩ	>10		

Environmental

Base Strain Sensitivity, typical	ms^{-2}(g)/με	0.005 (0.0005)	0.01 (0.001)	0.005 (0.0005)

Physical

Weight	gram (oz)	2.9 (0.10)	12.9 (0.46)	18.2 (0.64)
Height	mm (in)	14.0 (0.55)	21.7 (0.85)	23.7 (0.93)
Spanner Size	mm (in)	8.0 (0.31)	14.0 (0.55)	15.0 (0.59)

Accelerometer Specifications
Uninsulated Base

Dynamic		Type 4397	Type 4398	Type 4399
Mounted Resonance Frequency, typical	kHz	53	38	29
Transverse Resonance Frequency, typical	kHz	17	14	10

Environmental

Base Strain Sensitivity, typical	ms^{-2}(g)/με	0.005 (0.0005)	0.02 (0.002)	0.01 (0.001)

Physical

Weight	gram (oz.)	2.4 (0.09)	11.8 (0.42)	17.1 (0.60)
Height	mm (in)	12.4 (0.49)	19.7 (0.77)	21.7 (0.85)
Spanner Size	mm (in)	7.5 (0.30)	14.0 (0.55)	15.0 (0.59)
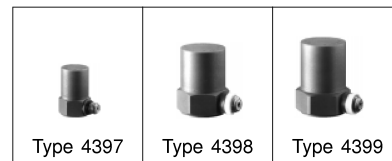
Common Specifications for Both Types of Accelerometers

Dynamic			Type 4394 Type 4397	Type 4395 Type 4398	Type 4396 Type 4399
Sensitivity (axial) at 159.2 Hz, 100 ms^{-2} (10.2 g), 25°C (77°F), 4 mA		mV/ms^{-2} (/g)	1.00 (9.807) ±2%		10.0 (98.07) ±2%
Measuring Range (peak), typical	temperature <100°C (212°F)	ms^{-2} (g)	±7500 (765)		±750 (76)
	temperature <125°C (257°F)	ms^{-2} (g)	±5000 (510)		±500 (51)
Frequency Range (±10%), typical.*		Hz	1 to 25000	0.3 to 18000	1 to 14000
Maximum Transverse Response		%	<4		

*Note: The frequency range from 10 kHz to 10 kHz is measured individually and shown on the calibration chart supplied. The expanded uncertainty on this measurement is: 1.0% from 10 Hz to 2 kHz and 2.0% from 2 kHz to 10 kHz at 2σ (i.e. expanded uncertainty using a coverage factor of 2)

9

Common Specifications for Both Types of Accelerometers (Cont.)

Electrical

Constant Current Supply	temperature <100°C (212°F)	mA	+2 to +20		
	temperature <125°C (257°F)	mA	+2 to +10	+2 to +20	
Supply Voltage, unloaded	for full specification	V DC	+24 to +30		
	minimum (reduced specification)	V DC	+18		
Output Impedance		Ω	<100		
Bias Voltage	at 25°C (77°F), 4 mA	V	12 ±0.5		
	full temperature and current range	V	8 to 15		
Residual Noise, typical	from 1 to 22000 Hz	μV	<25	<15	<40
	equivalent acceleration	ms^{-2} (g)	<0.025 (0.0026)	<0.015 (0.0015)	<0.004 (0.0004)
Polarity (acceleration directed from base into body)			Positive		
Recovery time from Overload (2×maximum level)		μs	<20	<15	<25

Environmental

Maximum Non-destructive Shock (peak)	Axial	ms^{-2} (g)	100000 (10200)	50000 (5100)	20000 (2040)
	Transverse	ms^{-2} (g)	50000 (5100)	20000 (2040)	10000 (1020)
Temperature Range		°C (°F)	−50 to +125 (−58 to +257)		
Humidity			Welded, sealed		
Temperature Transient Sensitivity, typical		ms^{-2}/°C (g/°F)	2 (0.1)	0.2 (0.01)	0.1 (0.006)
Magnetic Sensitivity (50 Hz, 0.038 T), typical		ms^{-2}(g)/T	10 (1)	20 (2)	5 (0.5)
Acoustic Sensitivity (154 dB SPL), typical		ms^{-2} (g)	0.01 (0.001)	0.005 (0.0005)	0.002 (0.0002)

Physical

Construction		Delta Shear	
Piezoelectric Material		PZ 23	
Case Material	Titanium	ASTM Gr. 2	
Connector	Coaxial	M3 miniature	10−32 UNF
Mounting Thread	Tapped center-hole	M3	10−32 UNF
Mounting Torque	Nm (lb.in)	0.2 to 0.6 (1.8 to 5.3)	0.5 to 3.5 (4.4 to 31)

Compliance with Standards

CE	CE-mark indicates compliance with: EMC Directive
Safety	EN 61010−1 and IEC 1010−1: Safety requirements for electrical equipment for measurement, control and laboratory use.
EMC Emission	EN 50081−1: Generic emission standard. Part 1: Residential, commercial and light industry. EN 50081−2: Generic emission standard. Part 2: Industrial environment. CISPR 22: Radio disturbance characteristics of information technology equipment. Class B Limits. FCC Class B limits
EMC Immunity	EN 50082−1: Generic immunity standard. Part 1: Residential, commercial and light industry. EN 50082−2: Generic immunity standard. Part 2: Industrial environment. **Note:** The above is guaranteed using accessories listed in this Product Data sheet only.
Temperature	IEC 68−2−1 & IEC 68−2−2: Environmental Testing. Cold and Dry Heat. Operating Temperature: −50 to +125°C (−58 to +257°F)
Humidity	IEC 68−2−3: 90% RH (non-condensing at 40°C (104°F))

10

Specifications for DeltaTron® Charge Converter Type 2646

Charge Input

INPUT CONNECTOR:
10–32 UNF coaxial. Used for direct attachment of 2646 to an accelerometer that has a top mounted connector. Also accepts a miniature accelerometer cable for side-by-side mounting with an accelerometer

MAXIMUM SINUSOIDAL INPUT:
7.5×10^3 pC peak at temperatures between -50 and $+100°C$ (-58 and $+212°C$), decreasing to 5×10^3 pC at $+125°C$ ($257°F$)

INPUT CAPACITANCE: >200 nF

Amplifier Response

SENSITIVITY:
1 mV/pC ±1% at 25°C (77°F) with a constant current of 4 mA

FREQUENCY RANGE:
0.3 Hz to 100 kHz (−10% limits)

NOISE RMS (referred to input terminated with a transducer capacitance of 1 nF):
Inherent, lin. 1 Hz to 22 kHz: $<15 \times 10^{-3}$ pC

Density at 10 Hz: 0.80×10^{-3} pC/√Hz
           100 Hz: 0.28×10^{-3} pC/√Hz
           1 kHz: 0.12×10^{-3} pC/√Hz
           10 kHz: 0.05×10^{-3} pC/√Hz

Electromagnetic: 5 pC/T (50 Hz, 0.038 T)
RECOVERY TIME ($2 \times$ FS): $<15 \mu s$

Output

OUTPUT CONNECTOR:
10–32 UNF coaxial. Used for both signal output and power input through a single coaxial cable

PHASE (output referred to input): Inverted
OUTPUT IMPEDANCE: <100 Ω

Power Supply

CONSTANT CURRENT: +2 to +20 mA
UNLOADED SUPPLY VOLTAGE:
+24 to +30 V (minimum: +18 V with reduced specification)

BIAS VOLTAGE:
+12 ±0.5 V at 4 mA and 25°C. For full temperature and current range, the bias voltage range is +8 to +15 V

Environmental

TEMPERATURE RANGE:
−50 to +125°C (−58 to +257°F). Sensitivity temperature coefficient is within ±0.03%/°C (±0.016%/°F)

HUMIDITY:
0 to 90% RH (non-condensing) without extra sealing

VIBRATION INDUCED NOISE:
1×10^{-3} pC/ms^{-2} (0.01 pC/g)

MAXIMUM PHYSICAL SHOCK:
50 kms^{-2} (5100 g) peak

MAXIMUM INPUT WITHOUT DAMAGE:
50000 pC

CASE MATERIAL: Titanium ASTM Gr. 2

Dimensions and Weight

Diameter: 13.5 mm (0.53 in)
Height: 16.0 mm (0.64 in)
Weight: 5.3 g (0.19 oz.)

Note: All values are typical at 25°C (77°F), unless measurement uncertainty is specified

COMPLIANCE WITH STANDARDS:

CE	CE-mark indicates compliance with: EMC Directive.
Safety	EN 61010−1 and IEC 1010: Safety requirements for electrical equipment for measurement, control and laboratory use.
EMC Emission	EN 50081−1: Generic emission standard. Part 1: Residential, commercial and light industry. EN 50081−2: Generic emission standard. Part 2: Industrial environment. CISPR 22: Radio disturbance characteristics of information technology equipment. Class B Limits. FCC Rules, Part 15: Class B limits.
EMC Immunity	EN 50082−1: Generic immunity standard. Part 1: Residential, commercial and light industry. EN 50082−2: Generic immunity standard. Part 2: Industrial environment. **Note 1:** The above is guaranteed using accessories listed in this Product Data sheet only. **Note 2:** Sensitivity to RF common-mode, injected to signal line (in accordance with EN 50082−2): <70 μV (13 dB), with the converter connected directly to the accelerometer <900 μV (35 dB), with a cable between the converter and the accelerometer
Temperature	IEC 68−2−1 & IEC 68−2−2: Environmental Testing. Cold and Dry Heat. Operating Temperature: −50 to +125°C (−58 to +257°F)
Humidity	IEC 68−2−3: Damp Heat: 90% RH (non-condensing at 40°C (104°F))

Ordering Information

Type 2646	DeltaTron® Charge Converter
Includes the following accessories:	
JJ 0032:	Cable Extension Connector (10–32 UNF)
2 × YJ 0606:	O–Ring

Specifications for DeltaTron® Power Supply ZG 0328

	COMPLIANCE WITH STANDARDS:	
CE	CE-mark indicates compliance with: EMC Directive.	
Safety	EN 61010−1 and IEC 1010−1: Safety requirements for electrical equipment for measurement, control and laboratory use.	
EMC Emission	EN 50081−1: Generic emission standard. Part 1: Residential, commercial and light industry. EN 50081−2: Generic emission standard. Part 2: Industrial environment. CISPR 22: Radio disturbance characteristics of information technology equipment. Class B Limits. FCC Rules, Part 15: Class B limits.	
EMC Immunity	EN 50082−1: Generic immunity standard. Part 1: Residential, commercial and light industry. EN 50082−2: Generic immunity standard. Part 2: Industrial environment. **Note 1:** The above is guaranteed using accessories listed in this Product Data sheet only. **Note 2:** Sensitivity to magnetic fields (30 A/m, 50 Hz): 80 nA	
Temperature	IEC 68−2−1 & IEC 68−2−2: Environmental Testing. Cold and Dry Heat. Operating Temperature: -10 to +55˚C (+14 to +131˚F) Storage Temperature: -25 to +70˚C (+13 to +158˚F)	
Humidity	IEC 68−2−3: Damp Heat: 90% RH (non-condensing at 40°C (104°F))	
Mechanical	Non-operating IEC 68−2−6: Vibration: 0.3 mm, 20 m/s^2, 10−500 Hz IEC 68−2−27: Shock: 1000 m/s^2 IEC 68−2−29: Bump: 4000 bumps at 400 m/s^2	

SHORT-CIRCUIT CURRENT: $3 \pm 0.9 \text{ mA}$
UNLOADED SUPPLY VOLTAGE: 27 V
DYNAMIC IMPEDANCE: $> 100 \text{ k}\Omega$
NOISE RMS (inherent, Lin. 1 Hz to 22 kHz): $< 50 \text{ nA}$
OUTPUT: Transducer signal connected to pin 4 of the microphone socket
TRANSDUCER CONNECTOR: BNC
SUPPLY CONNECTOR: Standard Brüel & Kjær 7-pin microphone plug

Environmental
TEMPERATURE RANGE: −10 to +55˚C (+14 to +131˚F)
HUMIDITY: 0 to 90% RH (non-condensing)
CASE MATERIAL: Nickel-coated Brass

Dimensions and Weight
Diameter: 26.5 mm (1.04 in.)
Length: 52.5 mm (2.07 in.)
Weight: 48.5 g (1.707 oz.)

Note: All values are typical at 25°C (77°F), unless measurement uncertainty is specified.

Ordering Information

ZG 0328 DeltaTron® Power Supply
Includes the following accessories:
JP 0145:   10−32 UNF to BNC adaptor

Brüel & Kjær reserves the right to change specifications and accessories without notice

Brüel & Kjær